FATIGUE BEHAVIOR AND MODULUS GROWTH OF CEMENTITIOUSLY STABILIZED PAVEMENT LAYERS

by

TIRUPAN MANDAL

A thesis submitted in partial fulfillment

of the requirements for the degree of

MASTER OF SCIENCE

(CIVIL AND ENVIRONMENTAL ENGINEERING)

at the

UNIVERSITY OF WISCONSIN-MADISON

FALL 2012

FATIGUE BEHAVIOR AND MODULUS GROWTH OF CEMENTITIOUSLY STABILIZED PAVEMENT LAYERS

Tirupan Mandal **9066280265**

Student Name Campus ID Number

Approved:

Signature	Date	Signature	Date
Tuncer B. Edil, PE		James M. Tinjum, PE	
Professor		Assistant Professor	

EXECUTIVE SUMMARY

The objective of National Cooperative Highway Research Program (NCHRP) Project 04-36 was to recommend laboratory procedures to measure performance-related characteristics of pavement layers stabilized with cement, lime, and fly ash and to provide validated distress models to be incorporated into the Mechanistic-Empirical Pavement Design Guide (MEPDG). The objective of this specific study was to identify a procedure for determining the fatigue behavior of cementitiously stabilized materials (CSM) and modulus growth with time. A laboratory based, third-point flexural beam test and a non-destructive ultrasonic pulse velocity test were developed and applied to cementitiously stabilized materials. Ultrasonic pulse velocity measurements were conducted to assess non-destructively the flexural strength and flexural modulus of base and subgrade soil stabilized with cement, fly ash, and lime.

The host materials selected for this study are classified as gravel (GM), sand (SP), silt (ML), and clay (CL) based on the Unified Soil Classification System (USCS). The host materials were stabilized with four binders: cement, Class C fly ash, lime-Class F fly ash, and lime. Laboratory tests to monitor the fatigue behavior of CSMs involved flexural strength, flexural modulus, and fatigue cracking tests. These tests were performed using a third-point flexural beam test for all CSMs. Prismatic molds of dimensions 102 mm × 102 mm × 400 mm were used to fabricate the beam specimens. Different curing procedures were applied to different mixtures depending on the binder. Cement-stabilized mixtures (gravel, sand, silt, and clay) were cured in the moist room (100% relative humidity, 23 °C) for 28 d

(ASTM D558). Fly ash-stabilized mixtures (sand, silt, and gravel), clay-lime and silt-lime-Class F fly ash were sealed with plastic wrap and cured in an oven set to 40 °C (ASTM C593) for 7 d. Nine different mixtures were studied. The effect of density, binder content, and curing time was also studied. Additionally, modulus growth tests were conducted on these specimens. Resilient modulus tests were performed in general accordance with NCHRP 1-28A on lightly stabilized materials and flexural modulus tests were performed on heavily stabilized soils. Cylindrical specimens were prepared for the resilient modulus tests.

An ultrasonic velocity test system "PUNDIT (Portable Ultrasonic Nondestructive Digital Indicating Tester)-Plus" manufactured by CNSFARNELL was used to measure the propagation speed of a pulse of ultrasonic longitudinal stress waves. The beam and cylindrical specimens were tested by the direct transmission of the pulse of ultrasonic longitudinal stress waves. P-wave velocity (or constrained modulus) of the CSMs was studied using the ultrasonic pulse velocity test. The ultrasound velocity tests were used to assess nondestructively the flexural strength and modulus as well as modulus growth.

Results from the flexural strength tests showed clay-cement and silt-fly ash to have the highest and the lowest flexural strength among these nine mixtures, respectively. For the three class C fly ash stabilized soils (sand-fly ash, gravel-fly ash and silt-fly ash), the sand-fly ash specimen had the highest flexural strength, while the silt-fly ash specimen had the lowest flexural strength. The flexural strength was found to decrease when the specimens were under-compacted and to increase when the binder content and curing period increased.

The flexural modulus test results indicate that determination of flexural modulus should be done at a stress level of 30% to obtain consistent results. Among the nine mixtures,

the highest and the lowest flexural modulus for the 30% stress level (i.e., applied stress divided by flexural strength) was observed for the clay-cement and the silt-fly ash specimens, respectively. The non-plastic silt-fly ash specimens were the weakest mixture. For the fly ash-stabilized soils, the gravel-fly ash had the highest flexural modulus. The flexural modulus was found to increase with binder content for all stress levels. A linear relationship was developed between the flexural strength and flexural modulus. Also, a relationship between the unconfined compressive strength and flexural strength was found.

In general, the fatigue life ranged between 1 and 75,537 cycles in this study. The modulus kept degrading as the fatigue test continued, whereas the displacement increased. The fatigue life for different mixtures ranged from 44% to 64% of the initial modulus. The specimens compacted to a reduced dry density showed a lesser fatigue life than the specimens compacted to the target dry density. The sand-cement specimens with higher binder content did not perform well as compared to the sand-cement specimens with lower binder content. The fatigue life of sand-cement (6% binder) was greater than the fatigue life of sand-cement (8% binder) at the same stress level. For the gravel-cement specimens, there was not much improvement in the fatigue life with increase in binder content, but the silt-fly ash specimens performed better with increased binder.

A stress-based fatigue model was developed using two parameters – stress ratio (SR) and fatigue life (N) that resulted in a good fit for estimating the fatigue life. The R^2 values for the different specimens ranged between 0.70 and 0.95. The fatigue data from this study fitted very well to the MEPDG fatigue model, and also to most of the concrete fatigue models with varying degrees of success (R^2 ranged between 0.50 and 1.00). An attempt to develop a

strain-based model using the initial strain (which is calculated from the fatigue test data) was also made. The model was a good fit (R^2 = 0.79) for only the sand-fly ash mixture. The strain-based fatigue data was not found to be a suitable fit in this study.

Results from the ultrasonic pulse velocity tests showed that with decrease in density of the specimens, constrained modulus and P-wave velocity decreases, whereas, with increase in binder content and curing time of the specimens, the constrained modulus and P-wave velocity increases. A relationship was found between the flexural strength and P-wave velocity (or constrained modulus) as well as between the flexural modulus and P-wave velocity (or constrained modulus). Flexural modulus as measured in beam tests was found to increase with time. Resilient modulus did not follow the same trend of increase probably due to the selected method that proved to be destructive. This might be due to the testing of the same specimen at different curing periods, which may have damaged the specimens. The ultrasonic pulse velocity tests showed a clear trend of increasing stiffness (constrained modulus) with time for all mixtures.

This study showed that the developed third-point flexural beam test is appropriate for all combinations of binder and soil mixtures; i.e., lightly and heavily cementitiously stabilized materials. A stress-based fatigue model using two parameters, stress ratio (SR) and fatigue life, represent the fatigue behavior satisfactorily. A strain-based model was not suitable for all mixtures. The ultrasonic pulse velocity test proved to be a convenient non-destructive method for estimation of the flexural strength and flexural modulus. Furthermore, the ultrasonic velocity test allows for a convenient procedure to study modulus growth with time.

ACKNOWLEDGMENT

I would like to express my sincere thanks and deep sense of gratitude to my advisors, Professors Tuncer Edil and James Tinjum for their encouraging support and constant guidance throughout the project. I would also like to thank Professors Hussain Bahia and Dante Fratta for their support and advice throughout my time at the University of Wisconsin. Also, thanks to my project partners Dr. Ahmet Gokce, Zhipeng Su, and Jeff Casmer at University of Wisconsin-Madison, and Professor Haifang Wen, Professor Balasingam Muhunthan, and Jingan Wang at Washington State University, for their contributions for this research project.

I would also like to thank everyone affiliated with the Geological Engineering program at UW-Madison. Xiaodong (Buff) Wang for helping me out with my tests and helping me trouble shoot any problems I ran into. I would also like to thank Bill Lang for teaching me the laboratory skills I needed to know to in the structures lab.

I would especially like to thank all the other undergraduate and graduate students in the Geological Engineering program at the University of Wisconsin, especially Stacy Oszuscik and Erik Friede for helping me preparing my specimens. I also appreciate Andrew Keene for his help and input for the research. I would also like to thank to all of my friends in the GLE group and especially for: Ryan Shedivy, Steve Schubert, and Ali Soleimanbeigi for helping me with this project.

TABLE OF CONTENTS

LIST OF TABLES

LIST OF FIGURES

CHAPTER 1 – INTRODUCTION

Growth in the construction and rehabilitation of the roadway systems in the United States (US) increases the consumption of natural materials and energy (Lee et al. 2010). According to the Federal Highway Administration's (FHWA) Office of Highway Policy Information, there were approximately 208 million licensed drivers and approximately 248 million registered motor vehicles in the US in 2008. With the increase of vehicles, the demands for better roads have increased steadily. To relieve pressure on an already stressed transportation system, government agencies in the US have constructed new roads at a rate of approximately 13,000 lane miles per year. This rate of construction activity places significant strain on the availability and quality of natural aggregates and soils used in highway construction.

The development of high capacity roads depends on two main criteria: (i) the improvement of the geometric design which ensures proper slopes and curves of the roads and (ii) the improvement of the pavement design which ensures smoother and comfortable roads. Therefore, many government agencies have begun stabilizing lower quality aggregates and subgrade as a means of constructing roads where high quality aggregate sources are limited.

The concept of soil stabilization has been around for thousands of years, dating to the time where lime or pozzolans were used as additives. In modern times, stabilization regained acceptance during the 1960's and 70's due to general shortages of aggregates and petroleum resources. Use of stabilization techniques will increase as global demand for raw materials, fuel, and infrastructure increase.

Soil stabilization is the practice of improving the engineering properties of soil used for pavement base course, subbase course, and subgrade by the use of additives or binders which are mixed into the soil to effect the desired improvement. The addition of such binders transforms unbound material layers to bound layers, which are sometimes referred to as chemically or cementitiously stabilized layers (CSL).

While a great amount of research has been conducted on the properties of stabilized soil and aggregate, there is a significant lack of research relating the properties to the performance of pavements in which they are used. The American Association of State Highway and Transportation Officials (AASHTO) Interim Mechanistic-Empirical Pavement Design Guide Manual of Practice (MEPDG) provides a methodology for the analysis and performance prediction of pavements incorporating such layers. However, the characterization in CSL properties over time and their distress models have not been adequately addressed in MEPDG (Wen et al., 2010).

The objectives of this study were to identify a procedure for determining the fatigue life of CSL using the flexural beam test; and to validate and develop fatigue cracking models to be incorporated in the MEPDG. A laboratory based, dynamic, and non-destructive testing method using ultrasonic pulse velocity was developed for application to cementitiously stabilized materials. Ultrasonic pulse velocity measurements were conducted to evaluate the effect of flexural strength and flexural modulus on base and subgrade soil with cement, fly ash, and lime stabilization. This thesis describes the findings of this study and is part of a broader investigation of CSL for NCHRP Project 04-36, *Characterization of Cementitiously Stabilized Layers for Use in Pavement Design and Analysis.*

Background information is provided in Chapter 2. Chapter 3 describes materials and methods. Results and analysis are presented in Chapter 4. Fatigue modeling is provided in Chapter 5. Chapter 6 presents the results of the ultrasonic wave tests. Chapter 7 presents the modulus growth tests. Conclusions are discussed in Chapter 8.

CHAPTER 2 – BACKGROUND

2.1 STABILIZATION OF ROADWAY BASE/SUBGRADE

Stabilization of subgrade or subbase/base is the process of physical and chemical alteration of the material to enhance their engineering properties in roadway structure. Stabilization can be achieved with a variety of chemical additives or binders including lime, self-cementing fly ash and portland cement, calcium or sodium chloride, viscoelastic materials such as bitumen, and by-products such as lime-kiln dust and cement-kiln dust. The process may include the blending of materials to achieve a desired gradation or the mixing of commercially available additives that may alter the gradation, texture or plasticity, or act as a binder for cementation of the soil (Department of Army, Navy, and Air Force, 1994).

The stabilization mechanism may vary widely from the formation of new compounds binding the finer soil particles to the coating of particle surfaces by the additive to limit the moisture sensitivity. Therefore, a basic understanding of the stabilization mechanisms involved with each additive is required before selecting an effective stabilizer suited for a specific application (Little and Nair, 2009).

A survey was conducted by Washington State University in 2009 which reported that 28 State Department of Transportation (DOT) use stabilization for subgrade, subbase, or base materials in pavement construction. The most commonly used additives were Portland cement, lime, and Class C fly ash (Wen et al., 2010).

2.1.1 Materials Blended with Cement

Portland cement is the most common binder used in soil stabilization. When cement is mixed with water, hydration processes take place, which allows the cement to bond with the soil materials and produce a strong mix. According to the Portland Cement Association (PCA), the typical 7-day UCS of soil-cement falls between 2.1 MPa to 5.5 MPa for cement contents between 3% and 10% (PCA, 2011). The use of soil-cement in highway construction has steadily increased through the years to the point where the current annual output corresponds to several thousand miles of equivalent two-lane roadway (Mitchell, 1970). Due to the cementitious material, as well as the calcium hydroxide (lime) formed, portland cement may be successful in stabilizing both granular and fine-grained soils.

Nussbaum and Childs (1975) studied the fatigue behavior of concrete slabs on cement-treated subbases. Pavement sections in 0.76-m-deep concrete containers with inside dimensions approximately 1.2 m x 4.8 m were constructed. Concrete slabs of various thicknesses directly on a clay subgrade or on cement treated subbase was cast. Comparison of the slab responses to fatigue loading to that of theory was found to be in good agreement. Nussbaum and Childs (1975) also found that the load carrying capacity of cement-treated subbases were 26% greater than predicted by theory and 71% greater than the values for similar pavements without subbases. Molenaar and Pu (2008) developed a field fatigue relationship to predict the fatigue cracking in cement-treated sand bases, which are used often in Netherlands. The relationship was based on an extensive analysis of a data base, which contained performance of pavements with a cement-treated base. Finite element analysis was done to analyze the stress conditions near cracks and determined the effect of load transfer. An endurance limit for these types

of materials was developed. In the case when load transfer across transverse cracks was guaranteed, a strain value of 50 μm/m was taken as such a limit; whereas, when the load transfer across transverse cracks was assumed to be poor, this limit was 41μm/m.

Paige-Green and Netterberg (2004) studied the impact on compaction and strength characteristics of seven different cements on two materials typically used as stabilized layers. Modified AASHTO compaction procedures with 2-4 hour compaction delay, with the addition of 3% cement by weight was used. Paige-Green and Netterberg (2004) found a decrease in the maximum dry density (MDD) and increase the optimum moisture content (OMC) compared to the natural unstabilized materials. Decrease in dry density ranged from 1 to 4% and increases in OMC ranged from 1.0% to 2.8%. Unconfined compressive strength (UCS) test results showed a range of 2.0 MPa to 3.4 MPa after 7-day curing.

Chai et al. (2005) did a case study of a trial section along the North-South Expressway in Malaysia, where the Falling Weight Deflectometer (FWD) was adopted to determine the *in situ* stiffness of the cement-stabilized road base. The material stiffness of the cement stabilized layer using FWD was analyzed. Chai et al. (2005) monitored the improvement in the stiffness of the stabilized base layer, and tested the samples during the trial. FWD was found useful for the structural assessment of the cement-stabilized base layer. The results from the FWD were used to verify the assumed design parameters for the pavement. Using the FWD, an empirical relationship between the deflection and the stiffness modulus of the pavement foundation was proposed.

Sariosseiri and Muhunthan (2008) studied the use of portland cement in the modification and stabilization of soils in Washington. Cement was added in percentages of 2.5%, 5.0%, 7.5%, and 10.0% by dry weight of the soils. Laboratory tests to determine

the drying rate of the soil, Atterberg limits, compaction characteristics, unconfined compressive strength, and consolidated-undrained triaxial behavior were performed. The results showed significant improvement in drying rate, workability, unconfined compressive strength, and shear strength. The improvement was dependent on the type of soil. The results of undrained triaxial tests showed that while cement treatment improved shear strength significantly, the type of failure behavior varied greatly. Sariosseiri and Muhunthan (2008) found that the non-treated, 5%, and 10% cement-treated soils displayed ductile, planar, and splitting type of failure, respectively. Treated soils with 10% cement content split during failure, with a rapid rise in pore pressure that equaled the confining pressure thus resulting in zero effective pressure at failure.

Batioja (2011) studied on the classification of the pavement materials sampled from a failed road in Huaquillas, Ecuador. The optimum cement content required to stabilize a blend of the moisture-susceptible base material and recycled asphalt pavement (RAP) and recommended a flexible pavement design adequate for the conditions at the site was investigated.

Hou et al. (2011) measured the fracture toughness of cement-treated aggregate using three-point bending method. Four specimen curing periods (14 d, 28 d, 60 d and 90 d) and four different cement contents (4%, 5%, 6% and 7%) were used in the study. Beam specimens of size 100×100×515-mm were prepared for this purpose. The results indicated that the fracture toughness of cement treated aggregate increased with the increase of specimen curing period. Also, with an increase of cement content, the fracture toughness of the cement treated aggregate tended to decrease.

2.1.2 Materials Blended with Lime

According to the National Lime Association (NLA), lime can be used to treat soils in order to improve their workability and load-bearing characteristics in a number of situations. Lime can also be used to modify most fine-grained soils. The strength gained in lime-stabilized soil is due to long-term pozzolonic reactions. The most important factors to control during soil-lime construction are pulverization and scarification, lime content, uniformity of mixing, time sequence of operations, compaction and curing (Department of Army, Navy and Air Force, 1994). Doty and Alexander (1978) found that the 7-day curing strength of lime stabilized soils at 38 $^{\circ}$C to be roughly equivalent to the 28-day curing strength at 23 $^{\circ}$C.

Laguros (1965) studied the stabilizing effects of hydrated lime and chemical additives on a montmorillonitic clayey soil from Texas. Laguros (1965) conducted various tests like compressive strength, durability, consistency, consolidation, and permeability on the lime-stabilized soil and found that the strength imrovement from the addition of lime to the soil was substantial. Consoli et al. (2009) studied the influence of the amount of lime, the porosity and the moisture content on the strength of a lime-treated sandy lean clay soil. A number of UCS tests were conducted for this study. The results showed that the UCS increased linearly with the increase in the lime content as well as with the reduction in porosity of the compacted mixture.

Osinubi and Nwaiwu (2006) studied the effects of compaction delays on properties of lime-stabilized lateritic soil using two-way analysis of variance and multiple regression analysis. Osinubi and Nwaiwu (2006) found that the reductions in MDD and OMC associated with compaction delays were statistically significant at the 5% level,

regardless of the compactive effort employed. Also, the effects of compaction delays on UCS were statistically significant for different compactions, lime contents, and curing.

Swanson and Thompson (1967) performed flexural beam tests on soil-lime mixtures. The flexural fatigue response of four different soil-lime mixtures was evaluated. The soils selected for the study represented typical reactive soils from Illinois. Beam specimens of 50x50x178-mm dimensions were prepared and subjected to cyclic loading until failure. The stress ratio (SR) vs. the log of the number of cycles (N) to failure was plotted to create a series of S-N curves. The S-N curves of the four soil-lime mixtures were found to be similar to those for the portland cement and lime-fly ash aggregate mixtures.

Gnanendran and Piratheepan (2010) studied the use of indirect diametrical tensile (IDT) testing with internal displacement measurement for determining stiffness and fatigue life of a granular base material lightly stabilized with slag-lime cementitious binder. Laboratory investigation for predicting the fatigue life of granular material stabilized lightly with 3-5% slag lime was carried out. A fatigue model based on the experimental results for determining the fatigue life using the static or dynamic stiffness modulus and maximum tensile strain was proposed, which was used in mechanistic-empirical pavement design involving such materials.

2.1.3 Materials Blended with Fly ash

Fly ash is a byproduct of coal combustion and comprises of fine particles that rise with the flue gases. Fly ash is most commonly used as a high-performance substitute for portland cement or as clinker for portland cement production. Geotechnical applications of fly ash include soil stabilization, road base, structural fill, embankments, and mine

reclamation. Addition of self-cementing fly ash improves the compressive strength and shearing strength of the soil. When fly ash and soil are mixed and compacted immediately, the fly ash causes the mixture to have a higher dry unit weight, by filling in voids with ash particles (ACAA, 2011).

Two types of fly ash are commonly used: Class C and Class F. Class C fly ash is often a high-calcium fly ash with carbon content less than 2%; whereas, Class F fly ash is generally a low-calcium fly ash with carbon contents less than 5% but sometimes as high as 10%. There are also self-cementing fly ashes that cannot be classified as Class C or F (i.e., with high carbon content but also high calcium content) (Basham et. al, 2007).

Class F fly ash cannot be used alone in soil stabilization applications as it is not self-cementing. An activator such as portland cement or lime must be added to produce cementitious products (i.e., pozzolan-stabilized mixtures). Lime and fly ash bases exhibit many of the same properties as soil-cement bases with potential for less shrinkage cracking. The nature of lime-fly ash and lime-cement-fly ash stabilization is similar to that for lime only (Department of Army, Navy and Air Force, 1994).

Shirazi (1999) studied the performance of lime- and fly ash-stabilized base as an alternative to soil-cement-stabilized base for flexible pavement systems on reconstructed highways in Louisiana. Lime and Class C fly ash test sections were installed on two Louisiana highway reconstruction projects in the northwestern part of the state. For each project, two 0.4-km test sections with different percentages of lime and fly ash were constructed. The remainder of each project was constructed with 8% soil-cement base by volume. On both projects, the first test section used 2% lime and 4% fly ash by weight for stabilization and the second test section used 3% lime and 6% fly ash. Test specimens were molded in the field during construction by using stabilized base material taken from

the roadway immediately before compaction. Shirazi (1999) also prepared laboratory test specimens with materials taken from, but not mixed at, the construction sites. Both field and laboratory samples were tested in unconfined compression at 7, 28, and 56 days. Shirazi (1999) found that the overall UCS of lime and fly ash was 30% lower than that of soil cement; but, the soil-cement-stabilized control sections cracked earlier and more extensively than the lime and fly ash test sections.

Arora and Aydilek (2005) studied the use of Class F fly ash amended soil–cement or soil–lime as base layers in highways. Tests on soil–fly ash mixtures prepared with cement and lime as activators were performed. UCS, California bearing ratio (CBR), and resilient modulus tests were conducted on these specimens. The required base thicknesses were calculated using the laboratory-based strength parameters. The results showed that the strength of a mixture is highly dependent on the curing period, compactive energy, cement content, and water content at compaction. Lime treatment did not provide sufficient strength for designing the mixtures as highway bases.

Phanikumar and Sharma (2007) studied the effect of fly ash on the volume change of two different types of clay, one a highly plastic expansive clay and the other a non-expansive clay, also of high plasticity. The effect of fly ash content on free swell index (FSI), swell potential, and swelling pressure of expansive clays were studied. The FSI decreased on addition of fly ash, as evidenced by the tests done on two highly swelling clays. Swell potential and swelling pressure also decreased significantly with decreasing fly ash content. For the type of fly ash and expansive clays used, 20% fly ash content reduced FSI, swell potential, and swelling pressure as determined by the free swell method by about 50%.

Edil et al. (2006), Zha et al. (2008), and Tastan et al. (2010) studied the effectiveness of fly ash-stabilized soils. Edil et al. (2006) studied the effectiveness of self-cementing fly ash for stabilization of soft fine-grained soils. CBR and resilient modulus tests were conducted on the mixtures. The CBR of soil-fly ash mixtures were observed to generally increase with fly ash content and decreased with increasing compaction water content. There was no increase in resilient modulus for a soil stabilized with 10% fly ash; however, the resilient modulus increased by 30% when the fly ash content was 18% and strength gain higher in wetter and more plastic fine-grained soil. The resilient modulus grew modestly between 7 and 14 days and an additional increase of 20 to 40% between 14 and 56 days.

Zha et al. (2008) evaluated the potential use and the effectiveness of expansive soils stabilization using fly ash and fly ash-lime as admixtures. The results showed that the plasticity index, activity, free swell, swell potential, swelling pressure, and axial shrinkage percent decreased with an increase in fly ash or fly ash-lime content. With the increase of the curing time for the treated soil, the swell potential and swelling pressure decreased. Soils treated immediately with fly ash showed no significant change in the unconfined compressive strength. However, after curing the fly ash treated soils for 7 days, the UCS increased significantly. Tastan et al. (2011) studied the effectiveness of fly ash use in the stabilization of organic soils and the factors that likely affect the degree of stabilization. UCS and resilient modulus tests on organic soil–fly ash mixtures and untreated soil specimens were performed.

Tastan et al. (2011) found that the increase in the strength and stiffness were attributed primarily to cementing caused by pozzolanic reactions, although the reduction in water content resulting from the addition of dry fly ash solid also contributes to

strength gain. The pozzolonic effect appeared to diminish as the water content decreased. Also, for most of the soil–fly ash mixtures tested, unconfined compressive strength and resilient modulus increased as the fly ash percentage was increased.

2.2 FATIGUE CRACKING

Fatigue cracking is one of the major load-related distresses experienced in pavements and it occurs when a pavement layer is subjected to repeated loading under passing traffic. Pavement fatigue is a form of structural failure. According to studies conducted in South Africa, there are two types of fatigue failure for CSL, bottom tension and top compression (crushing). The repeated tensile stress/strain at bottom of CSL induces bottom tension fatigue. When the CSL thickness is relatively thin, the repeated tensile stress/strain at the bottom of CSL induces bottom tension fatigue of CSL, which causes alligator cracking and rutting in hot mix asphalt (HMA) layer. The top compression fatigue occurs as a result of repeated compressive stress/strain at the top of CSL. The current MEPDG only considers bottom tension fatigue (Wen et al., 2009). Three important parameters are typically considered for fatigue cracking:

1. Flexural strength (or modulus of rupture)
2. Flexural modulus
3. Fatigue

2.2.1 Flexural Strength

Flexural strength (or modulus of rupture) is a key parameter in the analysis of fatigue of CSL. Tensile strength affects the development of shrinkage cracking in CSL. Fracture and failure of cement-stabilized aggregate base course is mainly caused by the flexural stress and strain produced on the bottom of the base course (Figure 2.1). To

evaluate the crack resistance of cement-stabilized aggregate base course reasonably, flexural strength and flexural modulus of elasticity are two important performance parameters of cement stabilized aggregate (Zhang et al., 2009). Flexural strength can be determined from a standard procedure like ASTM D1635, where a constant load rate is applied until the specimen fails. The flexural test assumes the applicability of the beam-bending theory and that the material has the same elastic modulus in compression and tension (Otte, 1978)

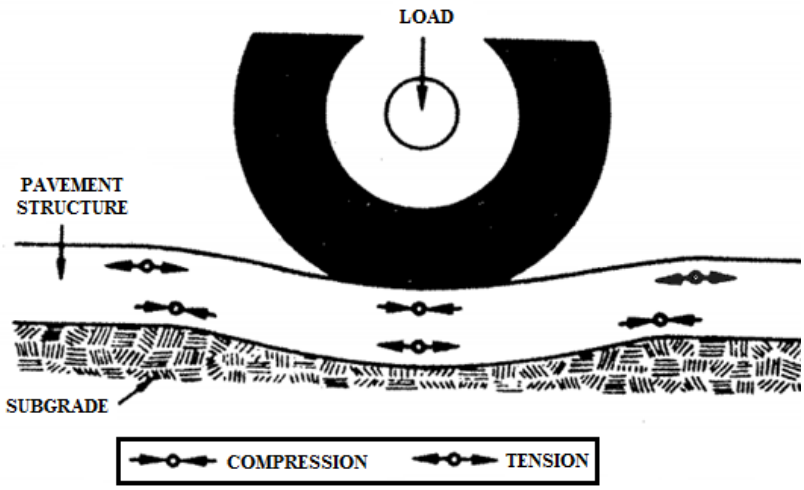

Figure 2.1 Repeated Tension Cracks in the Surface Layer causes Cracking

Zhang et al. (2010), Paul and Gnanendran (2011), and Zhang and Wei (2011) studied the flexural strength properties of cement-stabilized soils. Zhang et al. (2010) studied the flexural properties of cement-stabilized macadam reinforced with polypropylene fiber. Four different cement contents (4%, 5%, 6%, and 7%) were used in their study. A series of beam specimens with the size of 100×100×400-mm were prepared to determine the flexural strength and flexural modulus of elasticity. The beam molds for the preparation of beam specimens were made of steel molds, which were designed referring to the manufacture principle of cylinder specimens in the Chinese Standard. The

mixes were mixed in the mixing plant and all the specimens were prepared by compacting at their respective maximum dry density and optimum moisture content. The compacting and stripping of the specimens were both carried out by pressure testing machine. Before being stripped, the specimens were covered by plastic sheets and allowed to stand for 4-5 hours. After stripping, the specimens sealed in plastic sheets were cured at 100% relative humidity and controlled temperature (21 ± 2) ºC. The flexural strength and flexural modulus of elasticity of cement-stabilized macadam was measured by means of four-point loading method. The results indicated that the flexural strength and flexural elastic modulus increased with the increase in specimen curing period. Also, with the increase in cement content, there was a tendency to increase both in the flexural strength and flexural elastic modulus.

Paul and Gnanendran (2011) studied the effect of loading rate on the flexural properties of lightly stabilized granular materials. Flexural beam specimens of dimension 285x76x76-mm were prepared according to ASTM D1632. The beam samples were prepared from a typical granular material stabilized lightly with 1.5% cement-fly ash and moisture at OMC. The specimens were cured for 7 days and tested by monotonic third-point load testing at different loading rates ranging from 0.01 to 1.2 mm/min. A pair of video extensometer to measure the mid-span vertical deflection of the beam was used. Paul and Gnanendran (2011) used this device to compute the net deflection by tracking two gauge marks attached to the specimen. The experimental results showed that the loading rate had a significant influence on the modulus of rupture and flexural modulus of lightly stabilized material.

Zhang and Wei (2011) studied the effect of the curing period and cement content on flexural strength and flexural modulus of elasticity of cement-stabilized aggregate.

Four curing periods (7 days, 14 days, 28 days and 60 days) and four different cement contents (4%, 5%, 6% and 7%) were studied. The beam preparation was same as that of Zhang et al. (2010). The results showed that the flexural strength and flexural modulus of elasticity of cement-stabilized aggregate increased with an increase in curing time. And, with the increase of cement content, both the flexural strength and flexural modulus of elasticity of cement-stabilized aggregate increased.

2.2.2 Flexural Modulus and Fatigue

Modulus of CSL is critical for pavement analysis to determine stress/strain and thus, performance prediction. Low modulus of CSL may lead to high levels of tensile stress at the bottom of the surface layer and, subsequently, bottom tension fatigue cracking. However, HMA pavement with a very stiff base is prone to top-down cracking (ARA, 2004) and rutting in the HMA layer (Meng, 2004). In general, high modulus is due from high additive content, which also may cause high shrinkage rates. Therefore, the modulus of CSL has to be characterized for pavement design and analysis.

According to AASHTO T 321, the fatigue life (N) is defined as the total number of load repetitions that cause a 50 percent decrease in initial stiffness. The objective of a fatigue test is, generally speaking, to determine the fatigue life and/or the danger point; i.e., the location of a test piece subjected to a prescribed sequence of stress amplitudes (Weibull, 1961). The stress condition of the semi-rigid base transforms from compressive to tensile along the depth when subjects to traffic loads, which conforms to the beam bending theory assumed in bending test. Therefore, repeated flexural bending test simulates the response of semi-rigid materials base subjects to traffic loads well (Judycki,

1997). There is no standard test procedure for determining the flexural modulus and the fatigue of a stabilized material.

Flexural fatigue testing is typically used for determining fatigue characteristics of bound materials that undergo repetitive bending in transportation infrastructure, such as concrete, asphalt, and cement-stabilized soils. Fatigue and resilient response of materials in the track are important aspects for determining required maintenance frequency and life cycle of bound layers (Huang, 2004).

Several researchers (Pretorius 1970, Otte 1978, Raad 1982, Litwinowicz and Brandon 1994, Sobhan and Mashnad 2003, Midgley and Yeo 2008, Casmer 2011, Li and Dong 2011, and Wang et al. 2011) have studied the fatigue behavior of cement-stabilized soils. Pretorius (1970) studied the shrinkage and fatigue cracking of pavements which consisted of a soil-cement base and an asphalt concrete layer resting on a silty-clay subgrade. Properties such as strength, elastic properties, fatigue, shrinkage, and creep of the materials were studied. Fatigue behavior of the materials was similar to that of the concrete and in close agreement with previously reported soil-cement fatigue results. The strain history studies were concluded to be appropriate for the fatigue damage studies.

Otte (1978) studied the structural design procedure for cement-treated pavement layers. Otte (1978) was the first to study the behavior of cemented materials as pavement layers in South Africa. Otte (1978) established a correlation between the UCS of a cemented material and its elastic modulus; and defined a parameter 'ε_b' (breaking strain) as the strain recorded at the first occurrence of a flexural-tension crack.

Raad (1982) developed a mechanistic model for strength and fatigue of cement-treated soils using the Griffith failure theory for the purpose of understanding the

structural behavior of cement-treated bases in pavement. Results of repeated load triaxial tests on clayey gravel soil-cement were used to define the fatigue failure criteria for cement-treated soils. The analytical fatigue model developed was used to derive a cumulative damage hypothesis. According to this hypothesis, fatigue behavior under compound loading depended on the sequence and magnitude of applied loads and the curing age of the cement-treated soil.

Litwinowicz and Brandon (1994) studied fatigue testing on cement treated materials. Both, large-scale tests and laboratory tests were conducted. Eighteen specimens were tested in repeat load flexure and five specimens monotonically to determine the stress, strain and modulus of the specimens. These specimens were sourced from untrafficked areas of the Accelerated Loading Facility (ALF) Mulgrave Trial. Litwinowicz and Brandon (1994) also prepared laboratory compacted specimens which were compacted at the field conditions with 3% cement content and statically compacted to a target of 100% modified maximum dry density. Litwinowicz and Brandon (1994) compared the laboratory test data with the field performance of the Mulgrave test pavement, AUSTROADS and other published fatigue relationships. The results showed that beam flexure fatigue testing of ALF field-sourced and laboratory-compacted specimens to be a powerful technique for predicting pavement life. Independent strain and deflection measurements correlated closely to the laboratory-compacted specimens but differed by up to a factor of 3 for field specimens. Also, flexural strength was found to be relatively unaffected, but stiffness values were significantly lower for the field specimens.

Sobhan and Mashnad (2003) conducted a laboratory investigation to evaluate the fatigue behavior of a pavement foundation material containing cement stabilized

reclaimed crushed aggregate. Class C fly ash, and waste-plastic strip (high density polyethylene, HDPE) were used as reinforcement. The objectives of the study were to evaluate the flexural fatigue behavior of the new composite, and to evaluate the accumulation of fatigue damage in the material. The results indicated that the fatigue resistance of this material was similar to other traditional stabilized pavement materials. The dynamic elastic modulus remained approximately constant (degraded slowly) for most specimens up to the end of fatigue life. The fatigue damage was computed using a dissipated energy approach. The damage accumulation in the material approximately followed Miner's rule for cumulative damage.

Midgley and Yeo (2008) conducted research for Austroads (AP-T101-08) entitled 'Influence of Vertical Loading on the Performance of Unbound and Cemented Materials'. Investigation of a number of parameters was done which influenced the performance of unbound pavements with thin bituminous surfacing and pavements containing cemented materials. Laboratory testing of two cemented materials were conducted which were subsequently tested under full scale loading using the ALF. Midgley and Yeo (2008) found flexural beam test to be practical and useful for strength, modulus and fatigue testing of bound cemented materials. The study indicated that the number of cycles of load to half the initial modulus was a suitable definition for the fatigue life of laboratory samples. The results from Midgley and Yeo (2008) showed that shortly after the cycles to half the initial modulus was reached, the flexural beam specimens typically ruptured. Midgley and Yeo (2008) defined the initial modulus as the mean modulus for the first 50 cycles of the fatigue test and the initial strain as the mean strain during the first 50 cycles of the fatigue test.

Li and Dong (2011) studied the performance of pavement stabilized with recycled cement mixture in the base course. Fatigue performance variation of the mixture under three different levels of recycled aggregate component by the value of splitting tensile strength was studied. Li and Dong (2011) developed the logarithmic form of a single S-N curve to fit the experimental results. The results from Li and Dong (2011) were a good reference for design and application of recycled aggregate mixture in the base as well as construct quality control.

Casmer (2011) studied the fatigue cracking of cementitiously stabilized pavement layers through large-scale model experiments (LSME). LSME tests on silt-cement (4% by weight) pavement layers of approximately 1m x 1m and 0.2 m thick was conducted. The surface and subgrade deflections were measured, and the stabilized layer for fatigue cracking was monitored. LSME tests on recycled pavement materials (RPM) was also conducted which was stabilized with 3% cement and silt cement (8% by weight) placed on expanded polystyrene (EPS). The geometry of these stabilized layers was changed to approximately 1 m x 2 m and 0.1-m thick. The results from the silt-cement (8% by weight) LSMEs were used to for validation of the fatigue model incorporated into MEPDG. The regression coefficients (k_1 and k_2) were first calibrated using laboratory beam fatigue tests. The tensile stress at the bottom of the stabilized layer in the LSME was determined from the finite element program MichPAVE, simulating the LSME setup. The results from Casmer (2011) showed that the deformational performance of stabilized layers was not affected by fatigue cracking in the LSME. Fatigue behavior of stabilized layers was controlled by stress conditions and material defects.

Wang et al. (2011) studied the fatigue damage characters of the soil-cement under dynamic load. Experiments on soil-cement specimens using an electric hydraulic servo

fatigue testing machine were conducted and the ultrasonic velocity of soil-cement under dynamic loading was measured. The results showed that the ultrasonic wave velocity through the cemented soil samples free surface obviously attenuated as the cycles of the dynamic loading increased. Based on the damage variable defined by the ultrasonic wave velocity, an equation for accumulated fatigue damage was established. The fatigue damage of soil-cement under dynamic loading could be divided into three stages: the initial rapid decay of the initial state, stability decay, and rapid damage close to the destruction. The results from Wang et al. (2011) provided an important reference for non-destructive testing of soil-cement under dynamic loading.

Bhattacharya and Pandey (1986), Pranshoo (2010), and Yu et al. (2011) studied the fatigue behaviour of lightly-stabilized soil mixtures. Bhattacharya and Pandey (1986) studied the dynamic modulus and the flexural fatigue strengths of the lime-soil mixtures. Tests on four different types of laterite soils compacted at three dry densities – light, medium and heavy were carried out. Bhattacharya and Pandey (1986) established a relationship between stress ratio and the logarithm of the number of the stress cycles to failure. Heavily compacted lime-soil specimens were found to have a considerable higher dynamic modulus and fatigue life than those having standard Proctor compaction.

Pranshoo (2010) studied the behavior of cementitiously stabilized subgrade soils under tension and fatigue failure. Beam specimens of dimensions 381x64x51 – mm were prepared for determining the flexural properties. The fatigue life tests conducted on beam specimens showed that the mean fatigue life of silty clay (P-soil) beams stabilized with 6% lime was greater than 2 million cycles. On the other hand, beams of silty clay stabilized with 6% lime failed at a relatively low N value (approximately 50). The 6% lime and 10% CKD-stabilized beams of lean clay (V-soil) exhibited mean fatigue life of

1,430,000 and 965,000, respectively. Pranshoo (2010) proposed a strain-based model for predicting fatigue life of cementitiously stabilized soil and compared with the existing model in the literature.

Yu et al. (2011) studied the fatigue behavior of lime-fly ash treated aggregate (LFTA) using the four-point bending beam model. The maximum deflection and maximum tensile strain among different compacted beam specimens of size 50 mm x 63 mm x 380-mm was observed, and a fatigue equation for LFTA using the S-N curves for fatigue failure was established, which is shown below:

$$\log N = -13.178\,(\sigma/S) + 14.394 \qquad (2.2)$$

where N is flexural fatigue life, σ is flexural tensile stress, and S is flexural tensile strength of the specimen.

Adhikari and You (2010) evaluated the fatigue behavior of asphalt pavement using a beam fatigue apparatus. Four-point bending beam fatigue testing was used for a typical Michigan Asphalt mixture under various loading frequencies (10.0 Hz, 5.0 Hz, 1.0 Hz, 0.5 Hz, and 0.1Hz) and test temperatures (21.3 °C, 13 °C, and 4 °C). The different fatigue prediction models (Asphalt Institute Model and Shell Model) were evaluated over wide ranges of laboratory testing conditions. Adhikari and You (2010) also found a strong linear correlation between compression modulus and flexural stiffness, with the flexural stiffness about 30% lower than the compression modulus.

Fatigue behavior of concrete slabs was studied by Shoban and Krizek 1998, Roesler et al. 2004, and Roesler et al. 2005. Shoban and Krizek (1998) studied the resilient and fatigue damage in stabilized, recycled, aggregate base course. Cyclic load-deformation data were recorded continuously during the entire fatigue life until fracture

to determine the magnitude and variation of cumulative plastic strain and dynamic elastic modulus as a function of the number of loading cycles. The extent of fatigue damage was calculated as a fatigue damage index, which was based on the cumulative energy dissipated during cyclic loading. Beam specimens containing 4% cement, 4% fly ash, and 92% recycled aggregate were prepared; the fiber reinforced specimens contained an additional 4% hooked-end steel fibers. The resulting resilient modulus in flexure varied between about 2.75 GPa and 10.4 GPa, and the degradation of the dynamic elastic modulus did not exceed 25% of the initial modulus. Also, Miner's Rule of linear summation of damage was applicable to unreinforced material but not to fiber-reinforced material.

Miner's rule is one of the most widely used cumulative damage models for failures caused by fatigue. It was popularized by M. A. Miner in 1945. It states that if there are *k* different stress levels and the average number of cycles to failure at the *i*th stress, S_i, is N_i, then the damage fraction, C (ReliaSoft Corporation, 2007), expressed as:

$$\sum_{i=1}^{k} \frac{n_i}{N_i} = C \tag{2.1}$$

where n_i is number of cycles accumulated at stress S_i, and C is fraction of life consumed by exposure to the cycles at the different stress levels. In general, when the damage fraction reaches 1, failure occurs.

Roesler et al. (2004) studied the resistance of concrete slabs to fatigue cracking under several stress ratios, stress ranges, and two different load pulse types (single and triple dual tandem). Slab fatigue testing by Roesler et al. (2004) confirmed previous research findings that concrete slabs exhibited a greater fatigue resistance than predicted

by concrete beam fatigue curves. The main reason for this discrepancy was the inaccuracy in characterizing the slab's static strength using a beam flexural strength test. For this testing program, the slab's flexural strength was approximately 2.8 times higher than the beam flexural strength. The slab fatigue curve developed for this study was also significantly different than previous slab fatigue curves when using beam strength in the stress ratio calculation. The slab fatigue curves were found to be dependent on slab geometry and boundary conditions and thus had no unique slab fatigue curve using the traditional S-N curves approach to concrete fatigue. For high-cycle fatigue tests (>100,000 cycles) using the single pulse, the stress range affected the number of repetitions to failure for a given stress ratio. However, for the low-cycle fatigue tests, the high-stress ratio dominated the failure of the slab and the effect of stress range was not distinguishable. The high-stress ratio caused progressive changes to the slab's support conditions, thereby making the impact of stress range on fatigue difficult to assess. Test results between single and triple dual tandem pulses matched better when the triple dual tandem cycle was counted as three equivalent single pulses. For the edge-loaded slabs, cracking did not initiate at the free edge of the slab but initiated behind the load platen on the bottom of the slab in most cases.

Roesler et al. (2005) conducted large-scale concrete slab tests in the laboratory to evaluate the effect of multiple wheel gears on the fatigue resistance of concrete slabs. Monotonic and cyclic loading tests on sixteen fully-supported slabs were performed. The effects of peak stress ratio, stress range, and stress pulse type on the fatigue resistance of concrete slabs were addressed in the study. For low cycle fatigue, stress range was not a significant factor while the applied peak stress controlled the number of repetitions to failure. For high cycle fatigue, peak stress and stress range affected the number of cycles

to failure. Roesler et al. (2005) developed S-N curves of the fatigue results and showed that the number of repetitions to failure for the tridem pulses was not equivalent to the single pulse repetitions to failure for the same pulse duration, peak stress, and stress range.

Sobhan and Das (2007) investigated on the fatigue durability, endurance limit, and damage accumulation process in recycled crushed concrete aggregate stabilized with cement–fly ash mixtures. The results showed that around 2 million cycles fatigue endurance limit for the stabilized recycled aggregate was nearly 53% of the static modulus of rupture. This indicated that the fatigue strength of the material was quite similar to or better than other traditional cementitious composites. The accumulated permanent deformation and the expended fatigue life were related by a nonlinear power law, and the fatigue damage in this material approximately followed the Miner's rule for cumulative damage.

2.2.3 Fatigue Cracking Models

The fatigue life (N) of a cemented layer is due to tension along the bottom and is usually considered to be a function of either the applied stresses (σ_t), the applied tensile strain (ε_t), or as the ratio of these responses to the breaking stress (σ_b) or the breaking strain (ε_b) of the material (Wen et al., 2009). The general relationship is typically shown as:

$$\log N = f_n \left[\frac{\sigma_t}{\sigma_b} \text{ or } \frac{\varepsilon_t}{\varepsilon_b}\right] \tag{2.3}$$

Figure 2.2 shows the general load stress distribution in a pavement layer. Many studies (Packard 1973, Darter 1977, Freeme et al. 1982, Foxworthy 1985, Pell 1987,

Thompson 1987, Darter 1990, Thompson and Barenberg 1992, Jameson et al. 1992, Corte 1996, Li and Dong 2011, and Yu et al. 2011) have been done on the fatigue behavior of pavements; and researchers have developed models which are used to predict the fatigue life of these pavements. The fatigue models are mainly developed in terms of stress (or stress ratio) or the strain (or strain ratio) of the specimens.

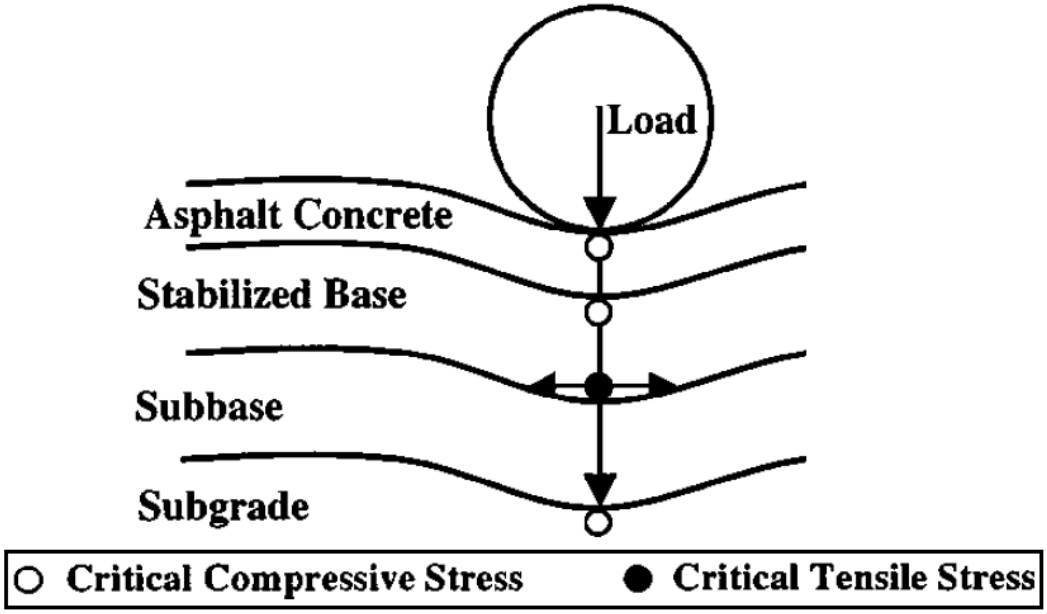

Figure 2.2 Load Stress Distributions in a Pavement (from Sobhan and Mashnad (2003))

The stress ratio (SR) is the ratio of the total tensile bending stress experienced by the pavement layer (or specimen), to the specimen modulus of rupture.

$$SR = \sigma / MR \tag{2.4}$$

where σ is Total tensile stress due to traffic and environmental load at critical location and MR is modulus of rupture

The MR is typically obtained from the third-point loading configuration of beams, after curing. The strain ratio is the ratio of initial strain (ε_i) (from the fatigue test) to the breaking strain (ε_b) (from the monotonic loading tests).

Smith and Roesler (2003) reviewed and summarized some of the common fatigue models which are used in concrete airfield pavement designs. All these models are in terms of the SR. The models and fatigue life equations are presented in Table 2.1. Carpenter (2006) studied the fatigue performance of HMA mixture for designing the pavement containing asphalt concrete (AC). Some of the fatigue models described in his report related to stress and strain of the specimens are shown in Table 2.2. Midgley and Yeo (2008) summarized fatigue models for cement-stabilized pavement layers in their report for Austroads (AP-T102-08). The models presented in their report are in terms of stress and strain ratio. These models and fatigue life equations are presented in Table 2.3.

In 1996, AASHTO began development of a new design guide through NCHRP Project 1-37A. After eight years of development, the Mechanistic Empirical Pavement Design Guide was released. This new design guide uses mechanistic-empirical numerical models to predict pavement performance over the service life (AASHTO, 2004).

Table 2.1 Concrete Fatigue Models

Model Name	Equation	Reference
Darter Fatigue Model	$\log N = 2.13 \left[\frac{MR}{\sigma}\right]^{1.2}$	Darter (1990)
Foxworthy Fatigue Model	$\log N = 1.323 \frac{MR}{\sigma} + 0.588$	Foxworthy (1985)
NCHRP Project 1-26 Fatigue Model	$\log N = 2.8127\left[\frac{\sigma}{MR}\right]^{-1.2214}$	Thompson and Barenberg (1992)
PCA Fatigue Model	$\log N = 11.810 - 12.165 \frac{\sigma}{MR}$	Packard (1973)
FHWA Zero-Maintenance Fatigue Model	$\log N = 17.61 - 17.61 \frac{\sigma}{MR}$	Darter (1977)

The MEPDG fatigue model only considers fatigue for chemically stabilized material used in flexible pavements. The fatigue cracking model incorporated in the MEPDG is currently uncalibrated and is shown in Equation 2.5:

$$\log N = \left[\frac{k_1 \beta_{c1} - \left[\frac{\sigma_t}{MR}\right]}{k_2 \beta_{c2}}\right] \tag{2.5}$$

where k_1 and k_2 are regression coefficients and β_{c1} and β_{c2} are field calibration factors. As the fatigue cracking model has not been field calibrated due to the complexity of carrying out such a field test, the MEPDG recommends the field calibration factors, β_{c1} and β_{c2} be defined as unity (ARA Inc., 2004). Also, the regression coefficients, k_1 and k_2, have not been defined for different types of CSL. Analysis of CSL using the MEPDG model is conducted within a predefined analysis period of one to four weeks (ARA Inc., 2004). The result from Equation 2.5 is used to predict the accumulated damage during an analysis period based on Miner's law (Miner, 1945).

Fatigue damage leads to a reduction in modulus of the CSL, thus affecting pavement response (Yeo et al., 2002). The MEPDG accounts for the modulus reduction by calculating a new modulus for each analysis period given the associated damage index, D_i, using:

$$E_{CSM}(t) = E_{CSM}(\min) + \frac{(E_{CSM}(\max) - E_{CSM}(\min))}{1 + e^{(-4+14D)}} \tag{2.6}$$

where $E_{CSM}(t)$ is the new CSL modulus at damage level D, $E_{CSM}(\max)$ the maximum CSL modulus for an intact layer, and $E_{CSM}(\min)$ the minimum CSL modulus after total layer destruction (Casmer, 2011). All modulus terms in Equation 2.6 are in pounds per square inch (psi).

Table 2.2 Asphalt Fatigue Models

Equation	Parameters in the equation	Reference
$N = K1 \left[\frac{1}{\varepsilon_0}\right]^{K2}$	K1 and K2 = fitting coefficients to the data; ε_o = tensile strain	Pell (1987)
$N = K1 \left[\frac{1}{\varepsilon_0}\right]^{K2} E^b$	b = fitting coefficients to the data; E = dynamic stiffness modulus of the HMA	Bonnaure et al. (1980) and Finn et al. (1977)
$N = K \left[\frac{1}{\varepsilon_{AC}}\right]^{n}$	K, n = factors due to composition and properties of the AC	Thompson (1987)
$N = 18.4\ (C)(4.325E\text{-}3)(\varepsilon_o)^{-3.291}(E)^{0.854}$	C = function of volume of voids and asphalt	Asphalt Institute (1982)
$N = 4.91 \times 10^{-13}\ (0.86\ V_b + 1.08)^{5.0}\ (1/\varepsilon)^{5.0}\ (1/S_{mix})^{1.8}$	V_b = volume of asphalt in the mixture, S_{mix} = dynamic modulus of the asphalt mixture	Dijk and Visser (1977)
$N = 4.92 \times 10^{-14}\ (1/\varepsilon)^{4.76}$	ε = initial strain	Verstraeten et al. (1977 and 1982)
$N = \beta_{f1}\ k_1\ (\varepsilon_t)^{-\beta f2k2}\ (E)^{-\beta f3k3}$	k_1, k_2, k_3 and β_{f1}, β_{f2}, β_{f3} = regression/calibration coefficients	El-Basyouny and Witzcak (2005)

Table 2.3 Cement Stabilized Fatigue Models

Model Name	Equation	Parameters in the equation	Reference
Strain Based Models			
South Africa Department of Transportation Model	$\log N = 9.1\left[1 - \frac{d_s \varepsilon_t}{\varepsilon_b}\right]$	d_s = factor to account for shrinkage crack induced stress concentration	Freeme et al. (1982)
Australian Model	$\log N = 18 \log \frac{C}{\varepsilon_t}$	C = constant, E = modulus of the cemented material	NAASRA (1987)
Australian Model	$\log N = 12 \log \left[\frac{E^{\frac{113000}{0.804}} + 191}{\varepsilon_t}\right]$	E = modulus of the cemented material	Austroads (2004)
Australian Model	$\log N = 8 \log \left[\frac{35000}{\varepsilon_t E^{0.45}}\right]$	E = modulus of the cemented material	Jameson et al. (1992)
Stress Based Models			
French Model	$\log N = \frac{1}{B}\left[\frac{d_s \sigma_t}{\sigma_b}\right]$	B = regression constant	Corte (1996)
USA Model	$\log N = \frac{1}{0.0825\,\beta_{c2}}\left[0.972\beta_{c1} - \frac{\sigma_t}{\sigma_b}\right]$	β_{c1}, β_{c2} = calibration coefficients	AASHTO (2006)

2.3 RESILIENT MODULUS

Resilient modulus (M_r) is a measure of material stiffness and provides a mean to analyze stiffness of materials under different conditions, such as moisture, density, and stress level. The M_r is a key input in NCHRP 1-37 (mechanistic-based pavement design approach), which is being evaluated for adoption by numerous state highway agencies (Pan et al., 2006).

Resilient modulus (M_r) is defined as the ratio of the cyclic deviator stress to the resilient (recoverable) strain, expressed as:

$$M_r = \left({}^{\sigma_d}/_{\varepsilon_r} \right) \tag{2.7}$$

where ε_r is recoverable elastic strain, and σ_d is applied deviator stress

The M_r of subgrade and subbase soils are very important properties in the analysis and design of a flexible pavement system (Kim et al., 2001). The design of roadway pavement relies on proper characterization of the load-deformation response of the pavement layers (Tian et al., 1998). Base and subgrade deforms when subjected to repeated loads from moving vehicular traffic. The M_r defines the nonlinear elastic response of pavement geomaterials, such as unbound aggregate base and subbase, under repeated traffic loading (Pan et al., 2006).

Achampong (1996) studied two synthetic soils of CL and CH, which were blended in the laboratory. The effects of deviator stress, molding moisture content, curing period, and soil type on the resilient modulus of lime and cement stabilized CL and CH soils were investigated. Achampong (1996) found that the M_r values increased with increasing lime and

cement content, and extended curing period but decreased with increasing deviator stress. Moisture variations around optimum had significant effect on the unstabilized soils but insignificant effect on the M_r of CL and CH soils when the lime contents exceeded 4%. Multiple regression analyses and test of M_r values of the unstabilized and stabilized CL and CH soils indicated that all of the factors investigated were significant. A model of nonlinear M_r to account for the effects of the stabilizer contents was proposed. Achampong (1996) also found that improved M_r of stabilized subgrade soils increased the fatigue life of the asphalt concrete pavements.

2.4 ULTRASONIC PULSE VELOCITY TESTS ON SOILS

Ultrasonic pulse velocity testing is a nondestructive testing technique, which sends sound waves ranging in frequency from 20 kHz to 1 GHz through the specimen. By measuring the travel time through the specimen, the p-wave or shear wave velocity and related dynamic properties of the material can be determined. Many studies have been conducted using the ultrasonic pulse velocity tests for quality control and defect detection in the civil infrastructure. This method is quick and non-destructive for applications in soils.

Yesiller et al. (2001) conducted tests to evaluate the feasibility of using ultrasonic testing in stabilized mixtures. Ultrasonic testing consisted of determining p-wave velocities of stabilized mixtures. Tests were conducted on a high plasticity clay stabilized with lime, cement, and fly ash and a Class F fly ash stabilized with lime and cement. UCS tests were used to determine compressive strength and modulus of the mixtures immediately after sample preparation and after 7-day and 28-day curing periods. Ultrasonic tests were conducted on the compaction and compression test specimens and correlations were made

between the test results. Variation of velocity with water content demonstrated a similar trend as the variation of dry density with water content for the soil. Yesiller et al. (2001) found that velocity increased with increasing density for both soil and fly ash. For compression characteristics, velocity increased with increasing modulus for both soil and fly ash. The results showed that the velocity was well correlated to the UCS of fly ash samples.

Leong et al. (2003) evaluated an ultrasonic test system in determining compression and shear wave velocities. Aluminum, mild steel, stainless steel, nylon, granite, residual soil, and kaolin specimens were tested to establish reliable procedures for determination of the wave travel time. The effect of the acoustic coupling agent, signal processing techniques, and the effect of length over diameter (L/D) and length over wave length (L/λ) on the P-wave and shear wave velocities were investigated. Leong et al. (2003) found that increasing the confining pressure increased the wave velocities and reduced attenuation. Additionally, a general trend of a decreasing Poisson's ratio with increasing void ratio was observed.

Williams and Nazarian (2007) conducted tests to justify the potential use of seismic modulus testing method to conduct QA/QC of base and subgrade layers. A procedure for relating high strain modulus, M_r, and low strain seismic modulus was provided. The results showed good correlation between M_r and seismic modulus both in cohesive soil and granular soil. The finding was enhanced by two specific site including one clayed subgrade and another for a granular base material.

Toohey and Money (2011) studied the seismic modulus growth of lime-stabilized soil (LSS) during curing using free-free resonance testing. Tests on 3 stabilized soils were conducted for 28 days. Toohey and Money (2011) measured E and G growth ranged from

250% to 900% during curing for the soils. The modulus values and growth in modulus were significantly influenced by mineralogy and soil processing. Toohey and Money (2011) found that the growth in seismic modulus for each soil exhibited a power law relationship with curing time. The 28-day modulus was estimated within 8% error for two soils using early curing modulus data, that is, through 7 days. Seismic modulus was found to correlate linearly with UCS throughout curing. The proportionality of E and UCS remained constant during curing for each soil beyond day 3.

CHAPTER 3 - MATERIALS AND METHODS

3.1 TEST MATERIALS

The host materials selected for this study are classified as gravel (GM), sand (SP), silt (ML), and clay (CL) based on the Unified Soil Classification System (USCS). The gravel was procured from a quarry in Jefferson County, Wisconsin, owned by Evenson Construction Company. Wisconsin DOT testing indicated the gravel at this quarry does not meet specifications for use without stabilization. In particular, the gravel does not meet the criteria for the freeze-thaw maximum of 18 (AASHTO T-103). Sand was procured locally from Capital Sand and Gravel in Cross Plains, Wisconsin. Commercially, the product is known as 'torpedo' sand. The silt and clay were obtained from the Dane County Public Works Landfill on USH 12 in Madison, Wisconsin. Silt was brought to the landfill during construction excavation for a project on the University of Wisconsin-Madison campus, while the clay was part of a remnant stockpile from the landfill's clay liner construction (Casmer, 2011). Figure 3.1 shows the four kinds of soils used.

A summary of the index properties and compaction properties of these four host materials are shown in Table 3.1. The particle size distribution curves, determined using ASTM D6913, are shown in Figure 3.2. According to USCS (ASTM D2487) the gravel is classified as GM, the sand as SP, the silt as ML, and the clay as CL. The clay had a liquid limit (LL) of 39 and a plastic limit (PL) of 19. The remaining materials are non-plastic (NP), although the silt had a LL of 18.

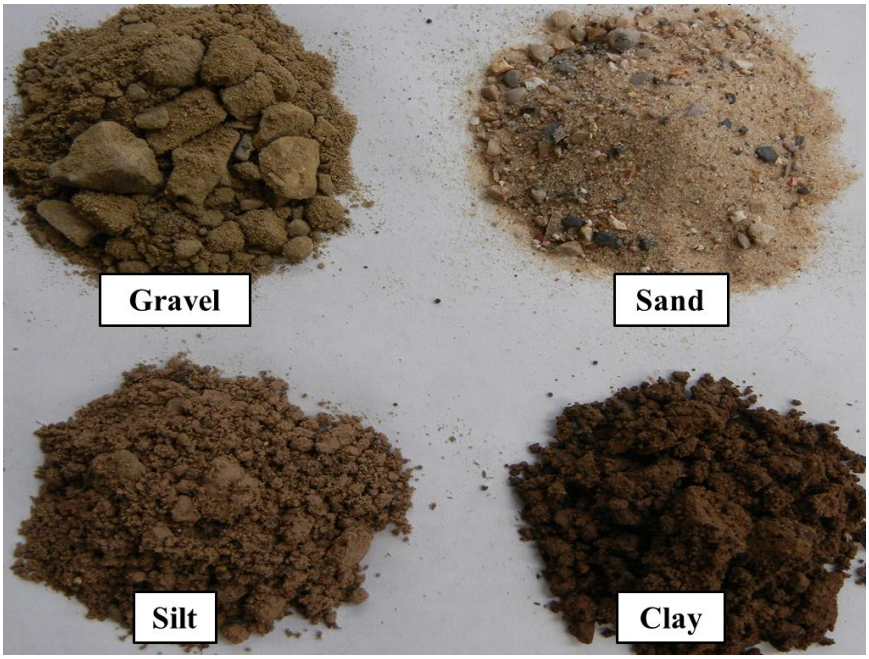

Figure 3.1 Host Soils

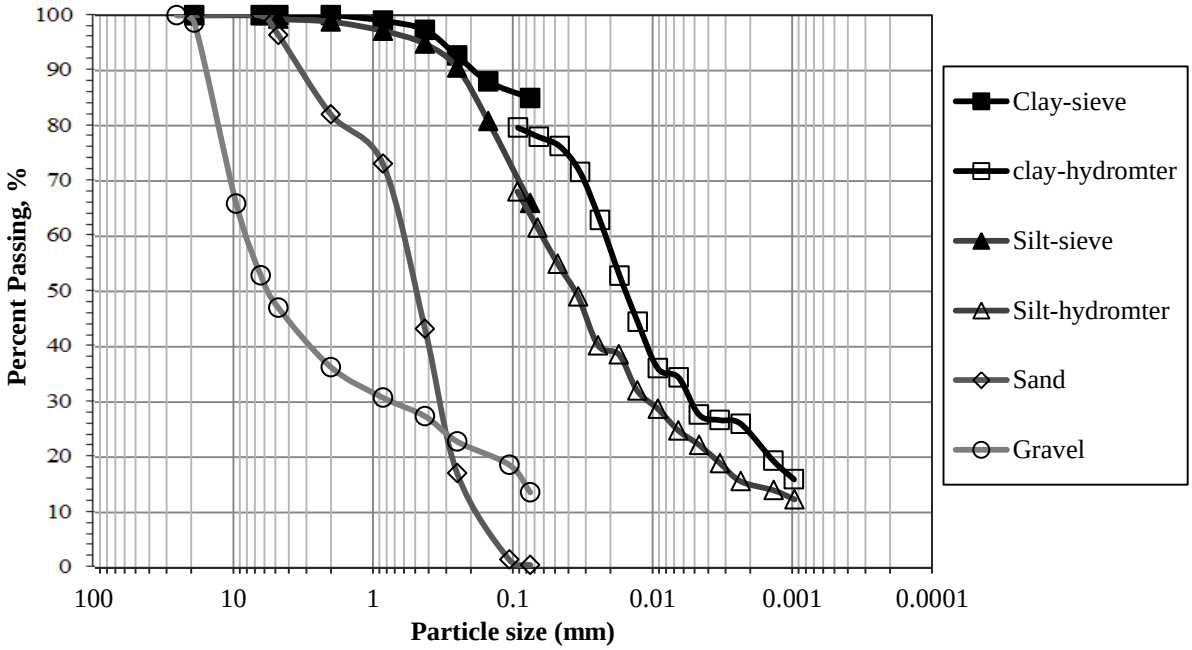

Figure 3.2 Particle Size Distributions for Gravel, Sand, Silt, and Clay

Table 3.1 Index Properties for Gravel, Sand, Silt, and Clay

Sample	D_{50} (mm)	C_u	C_c	G_s	ω_{opt} (%)	γ_{dmax} (kN/m^3)	LL (%)	PL (%)	Gravel Content (%)	Sand Content (%)	Fines Content (%)	USCS Symbol	AASHTO Symbol
Gravel	3.5	110.0	1.3	-	7.0	22.0	NP	NP	45.4	40.5	14.1	GM	A-1-a
Sand	0.5	2.8	0.83	2.69	11.0	18.7	NP	NP	2.1	97.8	0.1	SP	A-1-b
Silt	0.01	15.0	6.7	2.72	10.5	19.4	18	NP	3.0	37.0	60.0	ML	A-4
Clay	0.015	33.3	2.1	2.62	16.0	16.9	39	19	2.0	18.0	80.0	CL	A-6

D_{50} = median particle size, C_u = coefficient of uniformity, C_c = coefficient of curvature, G_s = specific gravity, ω_{opt} = optimum water content, γ_{dmax} = maximum dry unit weight, LL = liquid limit, PL = plastic limit, NP = nonplastic

Note: Particle size analysis conducted following ASTM D6913, G_s determined by ASTM D854, γ, γ_{dmax} and ω_{opt} determined by ASTM D698 except for gravel determined by ASTM D1557, USCS classification by ASTM D2487, AASHTO classification by ASTM D3282, and Atterberg limits by ASTM D431

Compaction tests were performed for each soil at standard compactive effort following ASTM D698 except for the gravel, where modified compactive effort was used per ASTM D1557. The compaction curves in Figure 3.3 shows that the gravel is insensitive to water content, while the bell-shaped curves of the silt and clay indicate their maximum dry unit weights are sensitive to water content. The curve for sand shows optimum moisture content between 10 and 12%. Optimum water contents and maximum dry unit weights of the soils are summarized in Table 3.2.

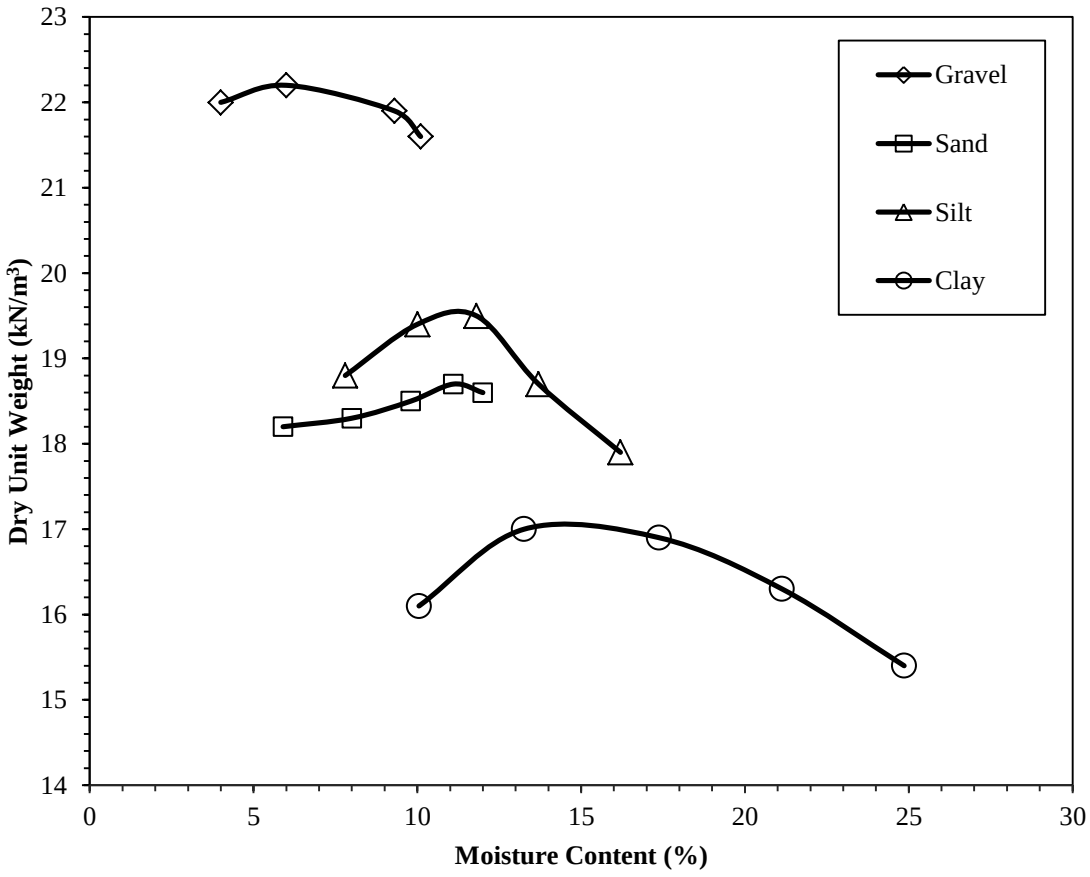

Figure 3.3 Compaction Curves for Gravel, Sand, Silt, and Clay

Table 3.2 Optimum Moisture Contents and Maximum Dry Unit Weights for Native Soils

Materials	Optimum Moisture Content (%)	Maximum Dry Unit Weight (kN/m^3)
Gravel	7.0	22.1
Sand	11.0	18.7
Silt	10.5	19.4
Clay	14.5	16.9

3.2 BINDERS

The host materials were stabilized with four binders: cement, Class C fly ash, Class F fly ash, and lime (Figure 3.4). A total of nine mix combinations were selected based on survey results from various DOTs (Wen et al., 2010). The mix combinations and mix design results shown in Table 3.3 were determined at Washington State University from the appropriate standards (Wen et al., 2011). Each mix combination was compacted to maximum density at the optimum moisture content for three binder contents. The specimens were cured for 7 days following appropriate curing method and then subjected to UCS testing. The minimum binder content to achieve a specified strength was selected for each mix combination.

Table 3.3 Final Mix Design, Maximum Dry Density and Optimum Moisture Content of Stabilized Mixtures

	Clay			Silt			Sand			Gravel		
	BC (%)	OMC (%)	MDUW (kN/m^3)	BC (%)	OMC (%)	MDUW (kN/m^3)	BC (%)	OMC (%)	MDUW (kN/m^3)	BC (%)	OMC (%)	MDUW (kN/m^3)
No additive	N/A	19.12	16.88	N/A	10.39	19.44	N/A	7.15	18.13	N/A	7.74	21.77
Cement	12	17.98	16.22	8	11.12	18.84	6	8.67	19.26	3	6.23	22.01
Lime (Lime-Class F fly ash*)	6	19.35	16.47	4/12*	12.44	18.59	x			x		
Fly ash	x			13	10.04	19.05	13	19.05	21.25	13	7.38	21.89

BC = Additive content, OMC = Optimum Moisture Content, MDUW = Maximum Dry Unit Weight

Note: *Lime-Class F fly ash (Wen et al., 2011)

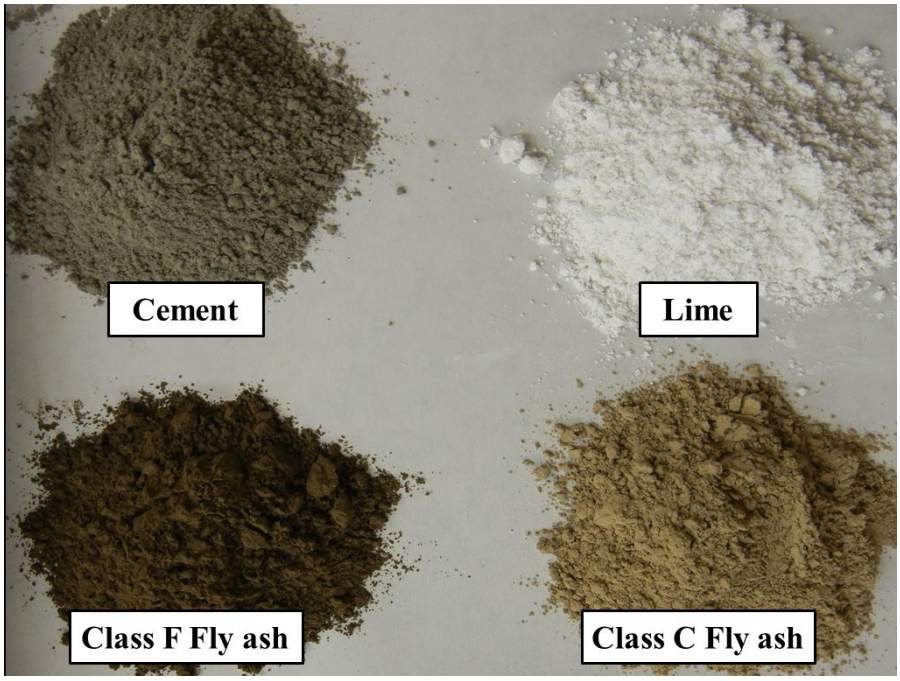

Figure 3.4 Binders

Type I Portland cement was used to stabilize each of the host materials for this study. The cement was manufactured by Lafarge and purchased from a local supplier in 21.3-kg bags. As per PCA, cement-stabilized soils should have a 7-d UCS of at least 2.1 MPa based on ASTM D1633 (PCA, 1992). Based on these recommendations, cement content suitable for stabilizing gravel, sand, silt, and clay were determined to be 3%, 6%, 8%, and 12%, respectively (Figure 3.5).

Class C fly ash was used to stabilize each host material with the exception of the clay. The fly ash was obtained from the Oak Creek Power Plant in Oak Creek, Wisconsin. The power plant pulverizes coal prior to combustion to produce electricity using four boiler units. Fly ash is removed from the system with electrostatic precipitators. The FHWA recommends fly ash stabilized soils to have at least a 7-d UCS of 2.8 MPa based on ASTM D1633

(FHWA, 2003). Three Class C fly ash contents (10%, 13% and 16%) were used as trial contents for silt, sand, and gravel. The sand-fly ash was the only mix combination to exceed this criterion at 13% fly ash by weight. The MEPDG also recommends fly ash-stabilized soils have at least a 7-d UCS of 1.4 MPa based on ASTM C593 (ARA Inc., 2004). Gravel-fly ash met this criterion using 13% fly ash. Silt-fly ash failed to meet either recommendation; therefore, the fly-ash content (13%) yielding the highest strength was chosen (Figure 3.6).

Lime was also used to stabilize clay for this study. High-calcium hydrated lime was purchased from a local supplier in 22.7-kg bags, which was manufactured by Western Lime Corporation. National Lime Association (NLA) standards recommend that lime-stabilized soils have a UCS of at least 0.5 MPa after 7-d curing at 40 °C based on ASTM D5102 (NLA, 2006); and at least 2% lime should be used to stabilize clay based on the minimum pH of 12.49 as shown in Figure 3.7. Clay-lime specimens met this recommendation at 6% lime by weight (Figure 3.8).

Silt-lime did not meet the 7-d UCS as recommended by NLA. Hence, Class F fly ash was combined with lime to stabilize silt. Class F fly ash is similar to Class C fly ash, but lacks sufficient calcium to be self-cementing. Lime provides the necessary calcium content to produce a cementing reaction when mixed with water (American Coal Ash Association, 2008). Class F fly ash was processed from the Elm Road Generating Station at the Oak Creek power plant. MEPDG recommends soil-lime-fly ash specimens to have a 7-d UCS of at least 1.4 MPa based on ASTM C593 (ARA Inc., 2004). 4% lime and 12% Class F fly ash by weight met this recommendation (Figure 3.9).

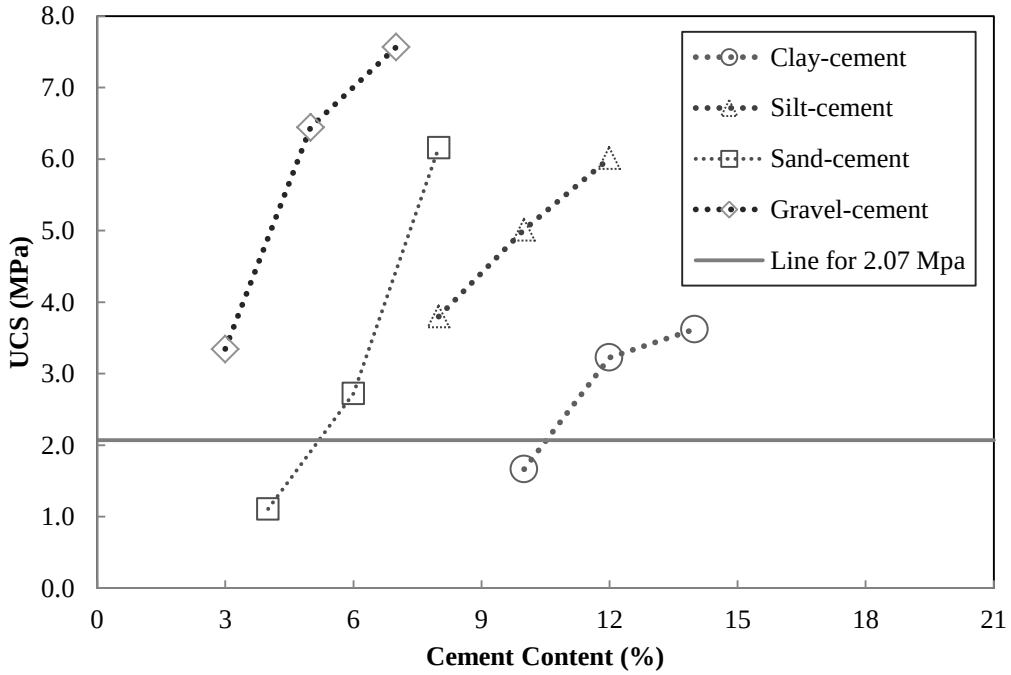

Figure 3.5 Results of UCS after 7-d Curing for Cement-Stabilized Soils

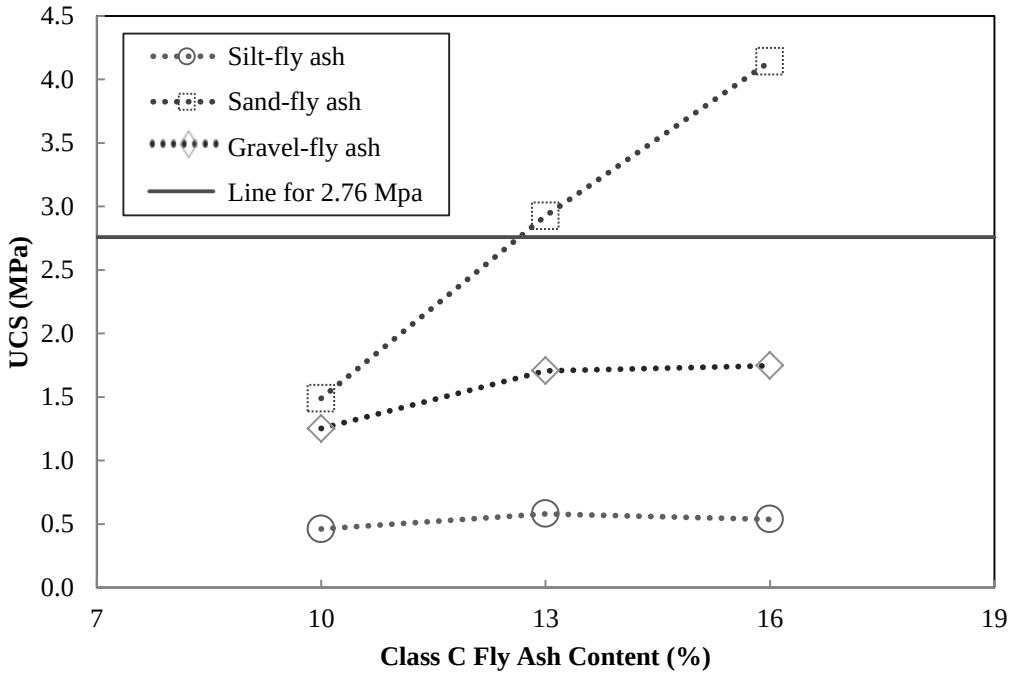

Figure 3.6 Results of UCS after 7-day Curing for Class C Fly ash-Stabilized Soils

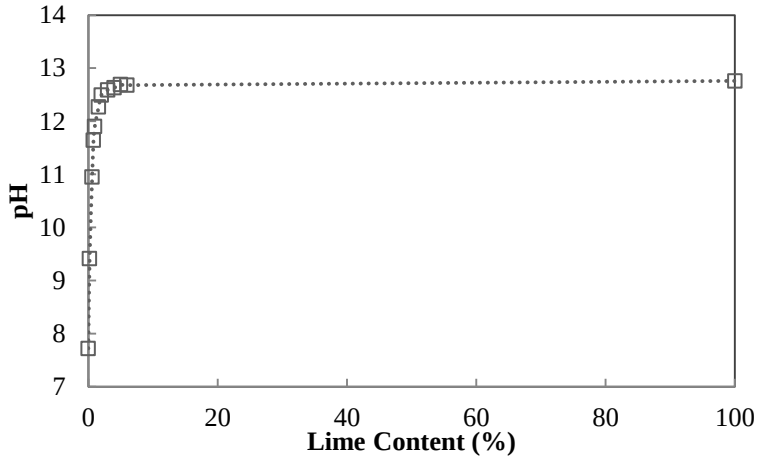

Figure 3.7 pH Value vs. Lime Content

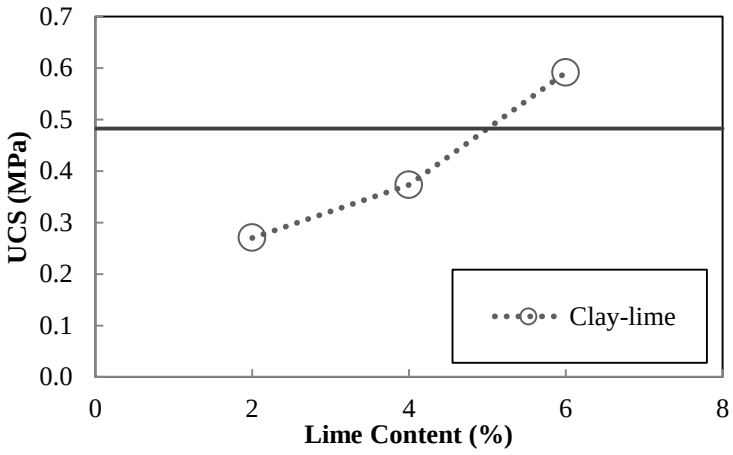

Figure 3.8 Results of UCS after 7-d Curing for Clay-Lime Mix

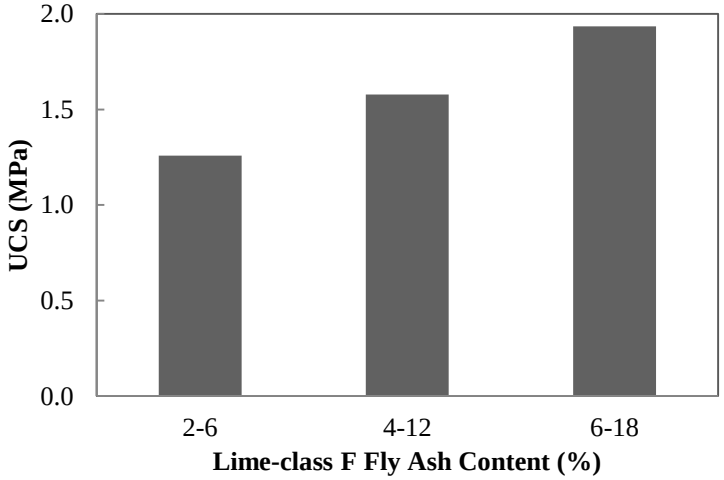

Figure 3.9 Results of UCS after 7-d Curing for Silt-Lime-Class F Fly ash

3.3 TEST PROCEDURES

3.3.1 Specimen Preparation

Beam specimens were prepared for flexural strength, flexural modulus and fatigue tests. Prismatic molds of dimensions 102 mm × 102 mm × 400 mm (as shown in Figure 3.10) were used to fabricate the specimens. Figure 3.11(a) shows the rammer used for compacting the beam specimens and Figure 3.11(b) shows the different weights used in the rammer for standard and modified compaction of beam specimens. For resilient modulus tests, PVC molds of 102-mm diameter and a height of 152 mm were used. For stabilized gravel specimens used in resilient modulus tests, bigger PVC molds (152-mm diameter and a height of 305 mm) were used for preparing the specimens. Particles larger than 25 mm were removed prior to compaction. The specimens were prepared in conjunction with the appropriate hammer weight, drop height, and compaction effort.

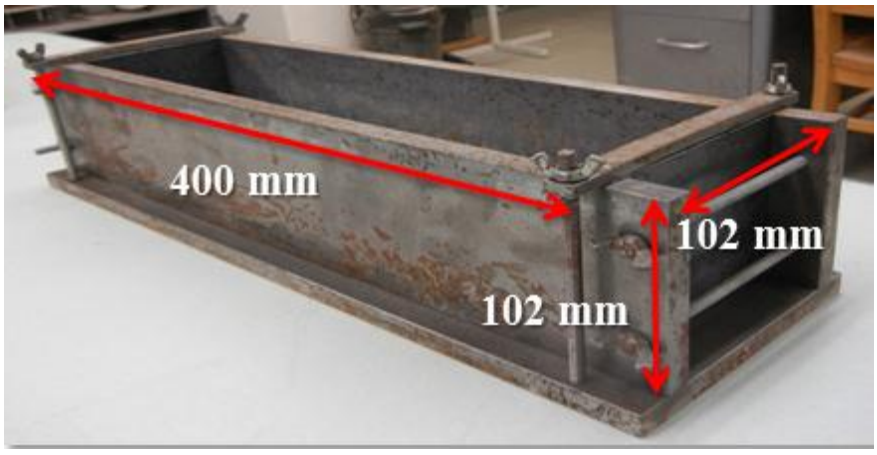

Figure 3.10 Prismatic Beam Molds

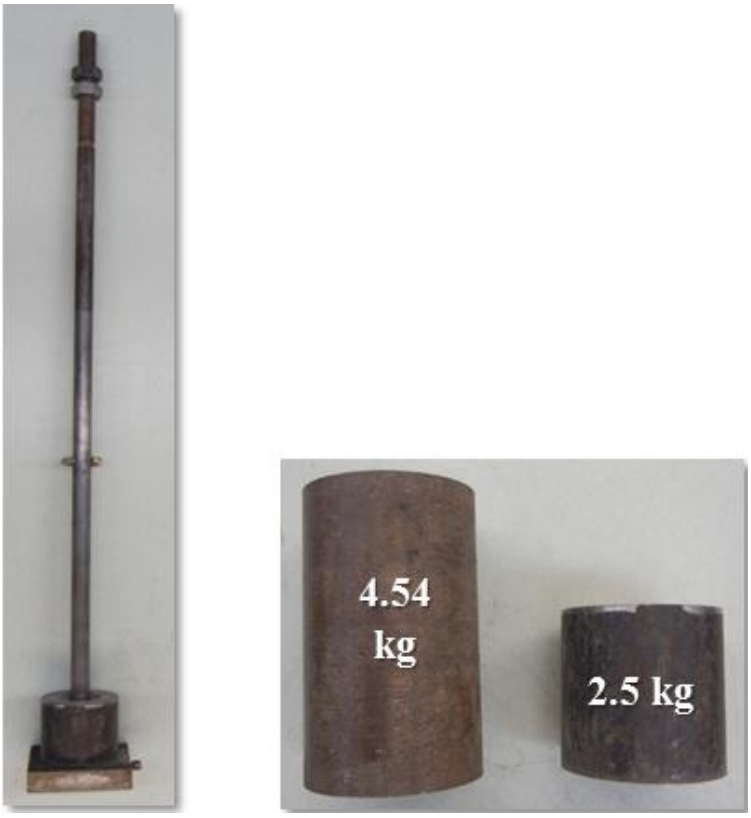

(a) Rammer **(b)** Weights for rammer (enlarged)

Figure 3.11 Rammer used for Compacting Beam Specimens

Specimens were prepared as follows:

1. Moisture content of soil was measured and the soil was blended with the required percentage by weight of binders (according to Table 3.3) until the mixture has uniform color throughout.
2. The soil-cement/ soil-fly ash/ soil-lime mixture was moistened with water to the reach the desired optimum moisture content and blended until uniform; the mixtures were compacted immediately except for clay-lime, which was tightly covered in plastic and allowed to mellow 24 h before compaction.

3. The specimens were compacted in three equal layers in the mold to achieve the maximum dry unit weight. The surface between layers was scarified to a depth of 0.6 mm to ensure a good bond. The gravel stabilized specimens were compacted with modified compaction effort according to AASHTO T180, "Standard Method of Test for Moisture-Density Relations of Soils Using a 4.54 kg Rammer and a 457 mm drop." The sand, silt and clay stabilized specimens were compacted with standard compaction effort according to AASHTO T 99, "Standard Method of Test for Moisture-Density Relations of Soils Using a 2.5 kg Rammer and a 305 mm drop."
4. The beam specimens were cured in the molds for 2 d and covered to prevent moisture evaporation at 23 °C and then were taken to corresponding curing facilities depending on the binder types. The cylindrical specimens were taken directly to the curing facilities after compaction.

Different curing procedures were applied to different mixtures depending on the binder. Cement stabilized mixtures (gravel, sand, silt, and clay) were cured in the moist room (100% relative humidity, 23 °C) for 28 d (ASTM D558). Fly ash stabilized mixtures (sand, silt, and gravel), clay-lime and silt-lime-Class F fly ash were sealed with plastic wrap and cured in an oven set to 40 °C (ASTM C593) for 7 d. Figure 3.12 shows the prepared beam specimens and Figure 3.13 shows the prepared cylindrical specimens.

(a) Gravel – cement beam specimen

(b) Gravel – class C fly ash beam specimen

(c) Sand – cement beam specimen

(d) Sand – class C fly ash beam specimen

(e) Silt – cement beam specimen

(f) Silt – class C fly ash beam specimen

Figure 3.12 Prepared Beam Specimens for Flexural Beam Tests (Size: 400 mm x 100 mm x 100 mm) **(Contd.)**

(g) Clay – cement beam specimen

(h) Clay – lime beam specimen

(i) Silt – lime - class F fly ash beam specimen

Figure 3.12 Prepared Beam Specimens for Flexural Beam Tests (Size: 400 mm x 100 mm x 100 mm)

(a) Silt – Class C Fly ash

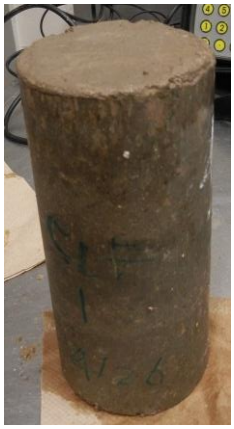

(b) Silt – Lime – Class F Fly ash

(c) Clay – Lime

(d) Gravel – Class C Fly ash

Figure 3.13 Prepared Cylindrical Specimens for Resilient Modulus Tests

(Size: **a**, **b**, **c** - diameter 102 mm, height 152 mm; **d** - diameter 152 mm, height 305 mm)

3.3.2 Flexural Strength

Flexural strength tests of the specimens were performed within 30 min of removal from the moisture room/oven. The Australian Austroads test procedure for flexural beam test was followed for conducting the flexural beam strength tests (Midgley and Yeo, 2008). The schematic of the setup for the flexural beam test is shown in Figure 3.14. The nominal dimensions of the beam samples were 100 mm high by 100 mm wide by 400 mm long. The beam supports were set 300 mm apart to achieve a span to depth ratio of 3. The beam specimens were tested by a 25-kN MTS Systems Model 244.12 servo-hydraulic machine. A constant loading was applied at a rate of 690 kPa/min ± 39 kPa/min until the specimen failed. The laboratory testing setup is shown in Figure 3.15.

The load positions were at third-points along the sample. The vertical beam displacement was measured using two linear variable differential transformers (LVDTs) at the mid-point of the beam to provide an estimate of the strain at break (Figure 3.16). The beam deflection data was sampled at a frequency of 100 Hz, together with the applied load. After the specimen failed, the peak load and approximate location of the break point were recorded using a LABVIEW program. Testing was conducted under normal laboratory environment conditions at 23 ºC. Flexural strength is expressed in the terms of the modulus of rupture as shown in Equation 3.1.

$$R = PL/bd^2 \tag{3.1}$$

where R is modulus of rupture (kPa), P is maximum applied load (N),

L = span length (mm), and b, d = average width and depth of specimen (mm)

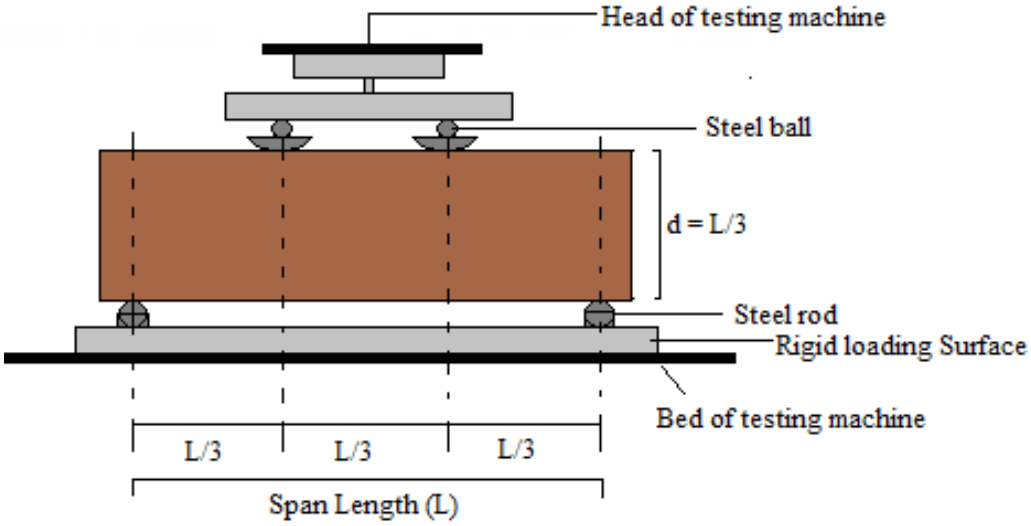

Figure 3.14 Diagrammatic View of Setup for Flexural Strength Test

Figure 3.15 Laboratory Setup for Flexural Strength Test

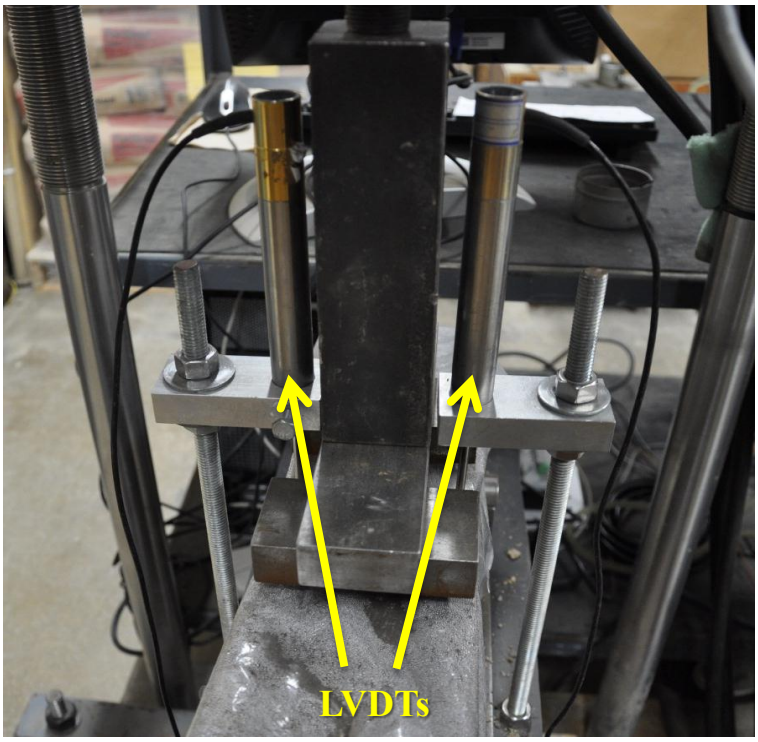

Figure 3.16 Position of LVDTs for Measuring Deflection of Beam Specimens

3.3.3 Flexural Modulus

The same setup for flexural strength (Chapter 3.3.2) was followed to conduct the flexural modulus test. The flexural modulus test was conducted with a pulse period of 1 Hz. Cyclic haversine load pulses of 250-ms duration and 750-ms as rest period was applied for each cycle. A contact load, which was more than 22 N but less than 45 N, was applied to the specimen.

As per the Austroads report (Midgley and Yeo, 2008), the loading for the flexural modulus test should be up to 40% of the estimated ultimate breaking load of the specimen. Three different stress levels (20%, 30% and 40%) were chosen for this study to observe the effect on the flexural modulus based on the beams which were tested for strength. The cyclic haversine loading was applied for 100 load pulses. The maximum force applied to the specimen and the peak displacement for the haversine load pulses applied for each pulse cycle was recorded using a LABVIEW program. The first 50

cycles were considered pre-conditioning. The data from the second 50 consecutive cycles were used to calculate the flexural modulus of the specimen using Equation 3.2. Average of the second 50 cycles was considered as the flexural modulus of the specimen.

$$S_{max} = \frac{23\ P\ L^3}{108\ b\ d^3\ \delta h} \text{ x } 1000 \tag{3.2}$$

where S_{max} is flexural modulus (MPa) and δh is peak mid-span displacement (mm)

3.3.4 Fatigue

The fatigue test was initiated immediately after the modulus test on the same specimen (provided no fatigue damage has occurred in the specimen). The same setup as explained in Chapter 3.3.2 was followed to conduct the fatigue test. The peak magnitude of the haversine load pulses was increased to a value in the range of 45% to 95% of the breaking load (based on the beams which were tested for strength). The fatigue test was conducted with a haversine pulse width of 250-ms duration with 250-ms rest between pulses for a total 500-ms pulse period (2 Hz frequency). A contact load, which was more than 22 N but less than 45 N, was applied to the specimen. The haversine loading pulse was applied until the beam specimen failed. The maximum force applied to the specimen and the peak displacement for the haversine load pulses applied for each pulse cycle was recorded using a LABVIEW program.

According to Austroads fatigue test protocol (Midgley and Yeo, 2008), the initial modulus of the specimen is defined as the average modulus determined from the first 50 load pulses applied to the specimen during the fatigue test. The fatigue life was defined as the number of pulses applied to the specimen to reduce the specimen modulus to half of the initial modulus or failure of specimen.

3.3.5 Resilient Modulus

Resilient modulus tests were performed in general accordance with NCHRP 1-28A on lightly stabilized materials (gravel – Class C fly ash, silt – Class C fly ash, silt – lime – Class F fly ash and clay – lime). The objective of the resilient modulus tests was to monitor modulus growth with time. Thus, only 2 load sequences were applied to the specimens. The loading sequence involved conditioning of the specimens in the first sequence followed by the expected in situ stresses for subbase/base course layer used to calculate the summary resilient modulus (SRM) (shown in Table 3.4). For base/subbase, SRM corresponds to the resilient modulus at a confining pressure of 103 kPa and cyclic stress of 35 kPa, as suggested by Section 10.3.3.9 of NCHRP 1-28A. SRM is a primary pavement design variable used directly in the mechanistic-empirical pavement design. The layer coefficient is also determined using SRM, which is a required input in the older AASHTO pavement design (Tian et al., 1998). The application of only partial loading sequence (only the 2nd load sequence was applied in subsequent times) was assumed to not damage the specimen significantly, thus allowing the use of resilient modulus tests as a non-destructive test on the same specimen.

Table 3.4 Loading Sequence for Resilient Modulus Test

Sequence	Confining Pressure (kPa)	Contact Stress (kPa)	Cyclic Stress (kPa)	Number of Cycles
1	103	21	207	1000
2	35	7	103	100

All resilient modulus tests were conducted with both internal and external LVDTs. The schematic of the setup for the resilient modulus test is shown in Figure 3.17. Clamps for the internal LVDTs were built in accordance with NCHRP 1-28A specifications. Internal LVDTs were placed at quarter points of the specimen to measure

the deformations over the half-length of the specimen (Figure 3.18); whereas external LVDTs measured deformations of the entire specimen length (Figure 3.19).

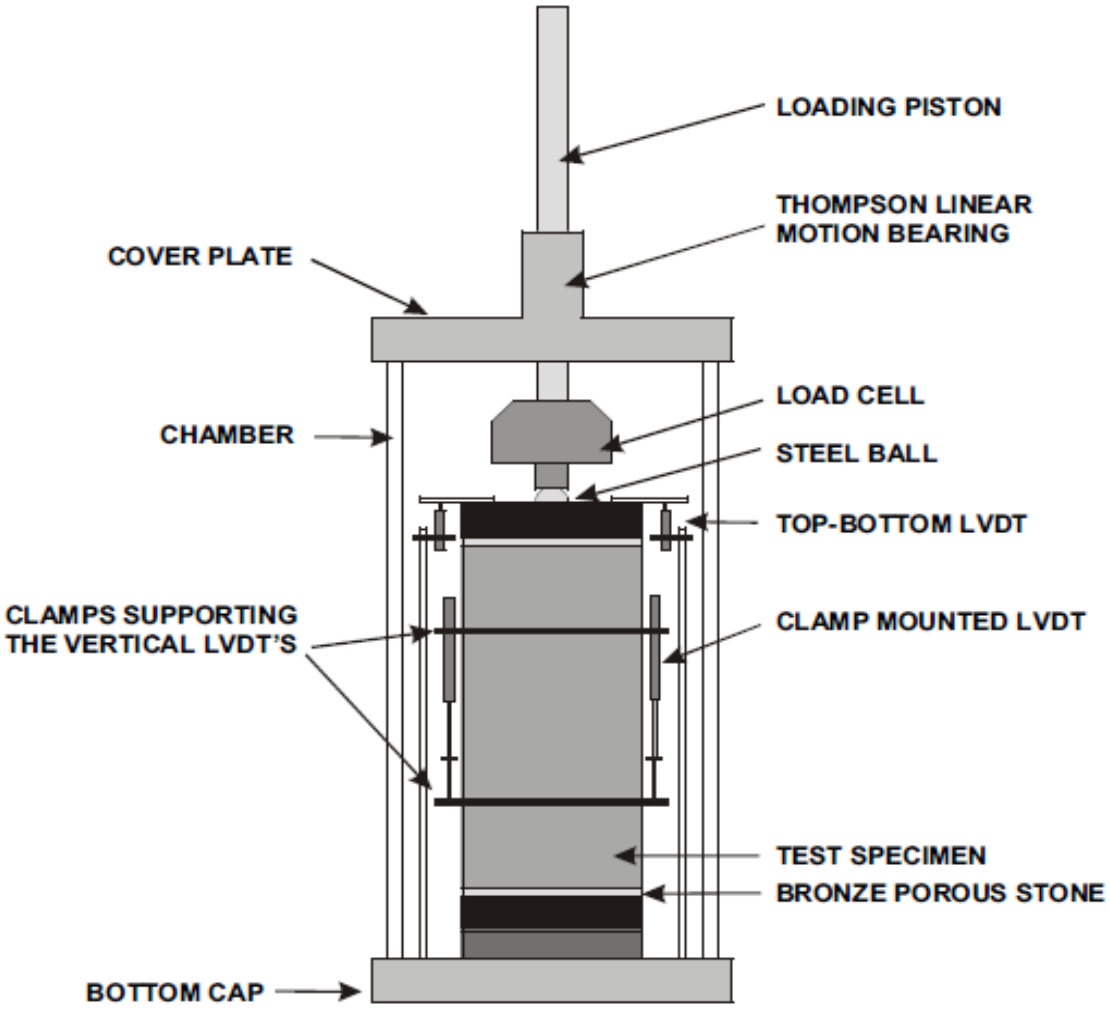

Figure 3.17 Diagrammatic View of Setup for Resilient Modulus Test (NCHRP 1-28A)

A MTS Systems Model 244.12 servo-hydraulic machine was used for loading the specimens. Loading sequences, confining pressure, and data acquisition were controlled by a PC equipped with LABVIEW software. The laboratory test setup is shown in Figure 3.20.

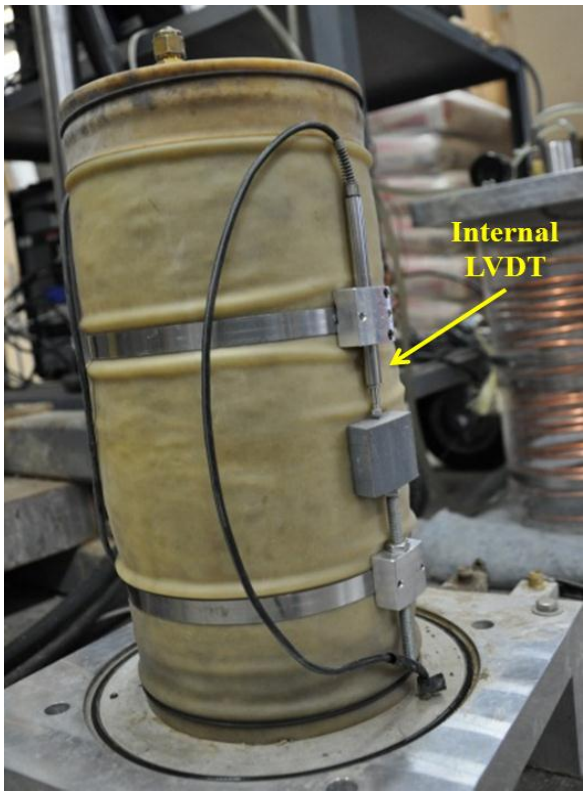

Figure 3.18 Position of Internal LVDTs for Measuring Deflection of Cylindrical Specimens

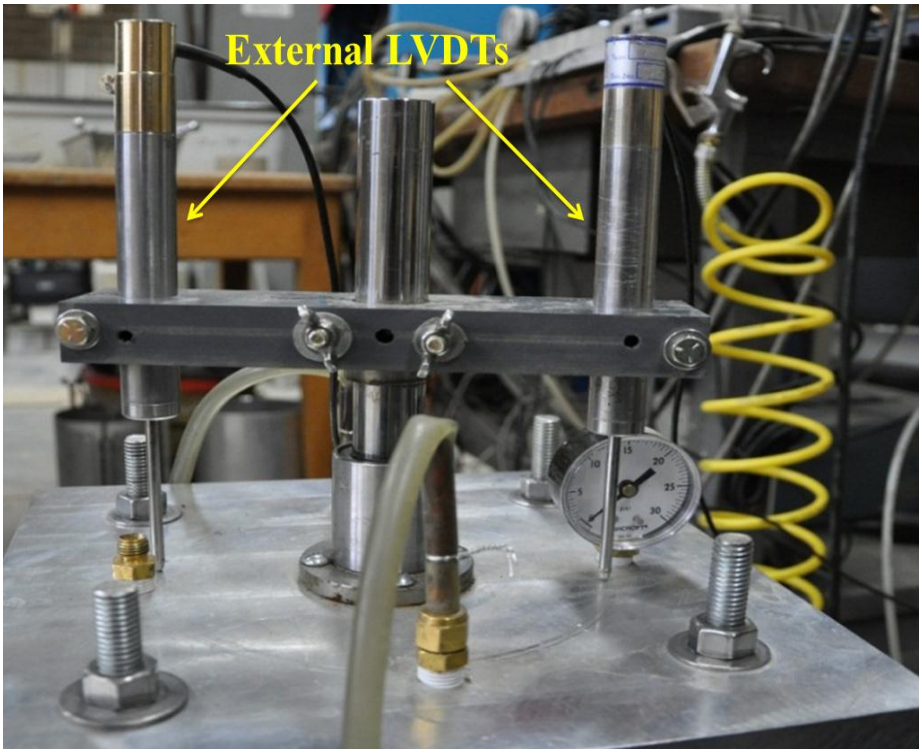

Figure 3.19 Position of Enternal LVDTs for Measuring Deflection of Cylindrical Specimens

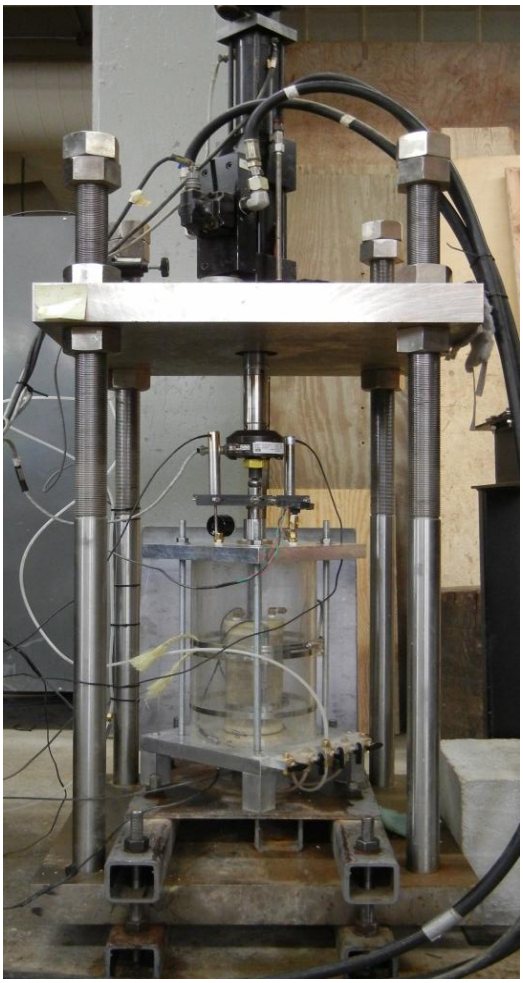

Figure 3.20 Laboratory setup for resilient modulus test

Resilient modulus (M_r) is defined as the ratio of the cyclic deviator stress to the resilient (recoverable) strain:

$$M_r = \left({}^{\sigma_d}/_{\varepsilon_r} \right) \tag{3.3}$$

where ε_r is recoverable elastic strain and σ_d is applied deviator stress

Specimens were prepared and tested at 28, 56, 90, 120, 150 and 180 d. The same specimens were used to record the SRM for different curing days. Table 3.4 shows the loading sequence used to determine the SRM at 28 d of curing.

Only the second sequence was applied to the specimen for testing at 56, 90, 120, 150 and 180 d. The first sequence was for pre-conditioning purpose and was not taken for

calculation of SRM. The SRM was calculated from the second sequence, which was given for 100 cycles. The M_r from the last 5 cycles of the second sequence were averaged to obtain the SRM.

3.3.6 Ultrasonic Pulse Velocity

An ultrasonic velocity test system "PUNDIT (Portable Ultrasonic Nondestructive Digital Indicating Tester)-Plus" manufactured by CNSFARNELL was used to measure the propagation speed of a pulse of ultrasonic longitudinal stress waves (Figure 3.21). The device consists of a transducer and a receiver, which is connected to an electronic timing device for measuring the time interval between the initiation of a pulse generated at the transmitting transducer and its arrival at the receiver. The travel time through the specimen can be read from the PUNDIT-Plus digital display screen.

Figure 3.21 Ultrasonic pulse velocity test equipment (PUNDIT-PLUS)

The PUNDIT-plus Ultrasonic Velocity Test System used in this study operated at a frequency of 54 kHz. ASTM C597, "Standard Test Method for Pulse Velocity through Concrete," was followed in this study.

The beam and cylindrical specimens were tested by the direct transmission of the pulse of ultrasonic longitudinal stress waves. The transducer and the receiver were contacted to the ends of the specimen, as seen in Figure 3.22. A water-based jelly (K-Y by Target) was used as the coupling agent to ensure full contact of the transducers and the surfaces. Travel time and the exact length of the specimens along the direction of testing were recorded for the calculation of the p-wave velocity (V_p). The schematic of the test system is shown in Figure 3.23.

(a) Testing on beam specimen using PUNDIT-PLUS

(b) Testing on cylindrical specimen using PUNDIT-PLUS

Figure 3.22 Testing using PUNDIT-PLUS

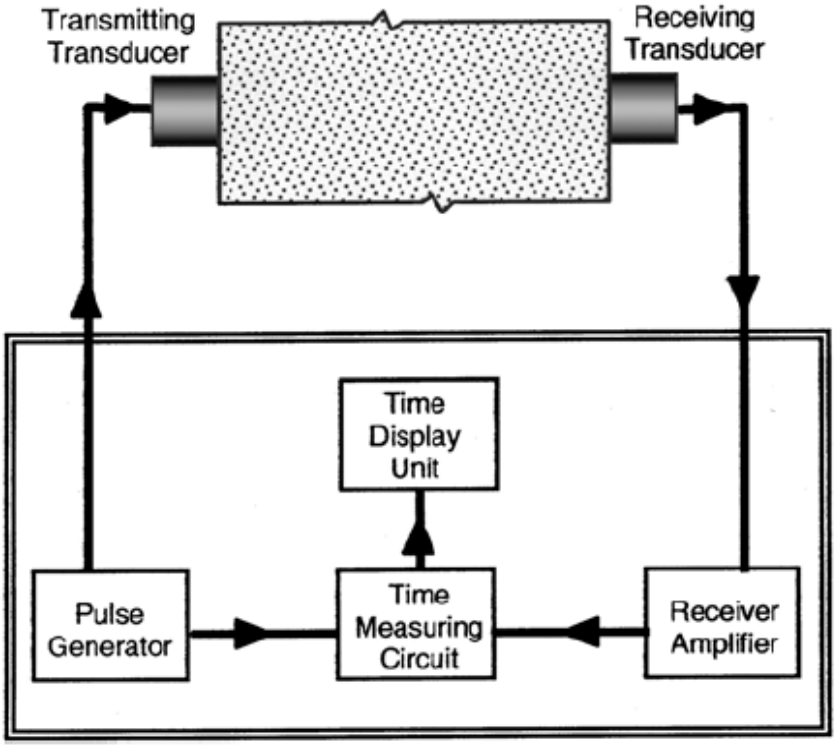

Figure 3.23 Schematic of Pulse Velocity Apparatus (ASTM C597)

P-wave velocity was calculated using Equation 3.4:

$$V_p = \frac{L}{t_2 - t_1} \tag{3.4}$$

where L is length of the specimen (m), and t_2, t_1 is travel times of the p-waves (s).

From the p-wave velocity obtained from the ultrasonic pulse velocity test, the low-strain constrained modulus (D) was calculated using Equation 3.5:

$$D = V_p^2 \times \rho \tag{3.5}$$

where ρ is mass density of the specimen (kg/m^3).

CHAPTER 4 - RESULTS AND ANALYSIS

4.1 FLEXURAL STRENGTH TESTING

This chapter presents the results of flexural strength (or modulus of rupture) tests which were conducted on beam specimens. For each mixture three replicate beam specimens were prepared and tested. Figure 4.1 and 4.2 shows the position of cracks that developed after testing and the failure surfaces of the specimens, respectively. Table 4.1 summarizes the average failure load and average flexural strength of the different mixtures (from Table 3.3). The failure load and flexural strength of each replicate specimen for each mixture is provided in Appendix-A.

Table 4.1 Summary of Flexural Strength Test Results

Specimen (Binder %)	Average Failure Load (kN)	Average Flexural Strength (kPa)	Coefficient of Variance (%)
Clay - cement (12%)	2.22	645	7.5
Gravel - cement (3%)	1.89	548	5.4
Sand - cement (6%)	1.69	490	3.7
Silt - cement (8%)	1.92	558	8.2
Clay - lime (6%)	0.64	187	4.4
Gravel – class C fly ash (13%)	1.17	340	7.5
Sand - class C fly ash (13%)	1.22	354	9.4
Silt - class C fly ash (13%)	0.44	127	4.5
Silt – lime - class F fly ash (4/12%)	1.13	329	4.3

The clay-cement and silt-fly ash have the highest and the lowest flexural strength among these nine mixtures, respectively (Table 4.1). For the three class C fly ash

stabilized soils (sand-fly ash, gravel-fly ash and silt-fly ash), the sand-fly ash specimen has the highest flexural strength, while the silt-fly ash specimen has the lowest flexural strength.

The coefficient of variance for each mixture did not exceed 10%, which indicates that the performance of the replicate specimens were good. For comparison, in a study by Midgley and Yeo (2008), flexural strength of Hornfels cement-stabilized material (CSM) siltstone CSM was evaluated with variability 20% and 15%, respectively. The variability of flexural strength in a study by Pranshoo (2010) for a lime-stabilized V-soil was 6%. Huang (2004) recommended a COV of 15% for the concrete modulus of rupture.

(a) Gravel – cement beam specimen

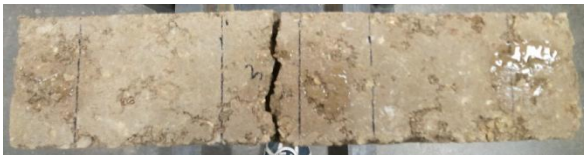

(b) Gravel – class C fly ash beam specimen

(c) Sand – cement beam specimen

(d) Sand – class C fly ash beam specimen

Figure 4.1 Position of Cracks on the Beam Specimens after Flexural Strength Testing (**Size:** 400 mm x 100 mm x 100 mm)

(e) Silt – cement beam specimen

(f) Silt – class C fly ash beam specimen

(g) Clay – cement beam specimen

(h) Clay – lime beam specimen

(i) Silt – lime - class F fly ash beam specimen

Figure 4.1 Position of Cracks on the Beam Specimens after Flexural Strength Testing (**Size:** 400 mm x 100 mm x 100 mm) ***Contd.***

(a) Gravel-cement **(b)** Gravel-fly ash **(c)** Sand-cement

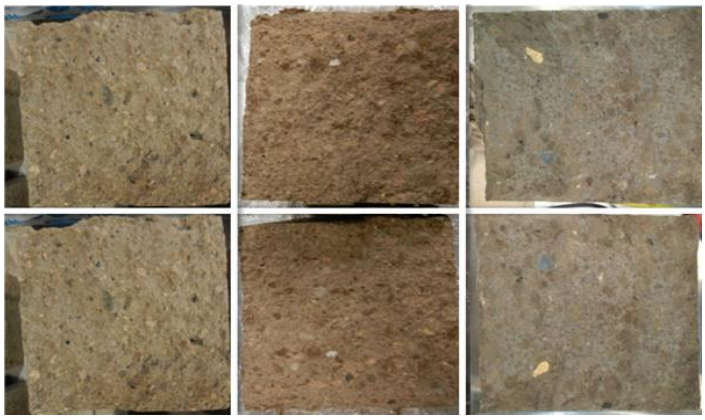

(d) Silt-cement **(e)** Silt-fly ash **(f)** Clay-cement

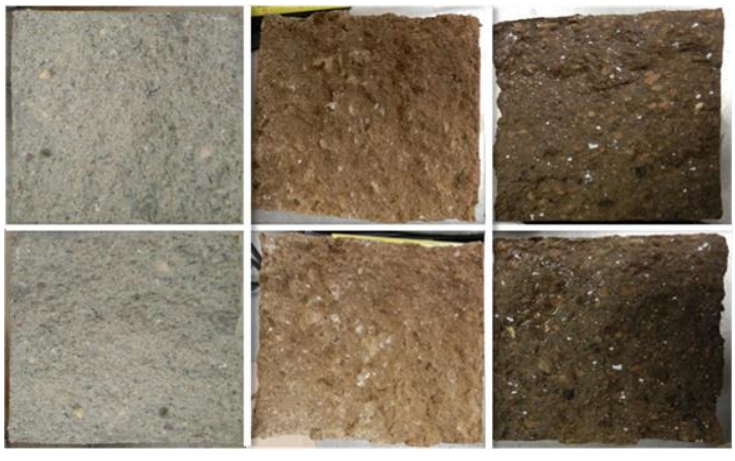

(g) Sand-fly ash **(h)** Clay-lime **(i)** Silt-lime-class F flyash

Figure 4.2 Failure Surfaces of the Beam Specimens after Flexural Strength Tests

4.1.1 Change in Density

The flexural strength (or modulus of rupture) tests were conducted on some of the mixtures (from Table 3.3) with reduced density (than the target density required) to observe the effect of compaction on flexural strength. At least two replicates were prepared for testing. Table 4.2 summarizes the average failure load, average flexural strength, and the percentage of maximum dry density (MDD) of the mixtures. The coefficient of variance for each mix did not exceed 10%, indicating the good performance between the replicate specimens. The failure load and flexural strength of each replicate for the mixtures are provided in Appendix-A.

Table 4.2 Summary of Flexural Strength Test Results (Reduced Density)

Specimen (Binder %)	**Average Failure Load (kN)**	**Average Flexural Strength (kPa)**	**Coefficient of Variance (%)**	**Percentage of MDD (%)**
Clay - cement (12%)	1.07	312	8.0	90
Gravel - cement (3%)	1.60	464	2.2	92
Silt - cement (8%)	1.50	436	9.6	90
Clay - lime (6%)	0.12	36	8.8	84
Silt - class C fly ash (13%)	0.15	44	2.7	90
Silt – lime - class F fly ash (4/12%)	0.64	185	9.7	88

The flexural strength decreases when the specimens are compacted loosely (Tables 4.1 and 4.2). Hence, proper compaction is an important characteristic for pavement design. Figure 4.3 shows the comparison of the specimens with reduced dry density and the specimens compacted with the target dry density. From Figure 4.3, the flexural strength is shown to decrease by 52%, for the clay-cement specimens. For gravel-

cement and silt-cement, the flexural strength decreased by 16% and 22%, respectively. For clay-lime, silt-fly ash, and silt-lime-fly ash flexural strength decreased by 81%, 65% and 44%, respectively. The effect of compaction was most sensitive in the case of clay-lime specimens among the lightly stabilized materials. The clay-lime specimens with reduced density were among the weakest specimens tested for flexural strength. The clay-cement specimens with reduced density showed the maximum decrease in flexural strength among the cement-stabilized materials.

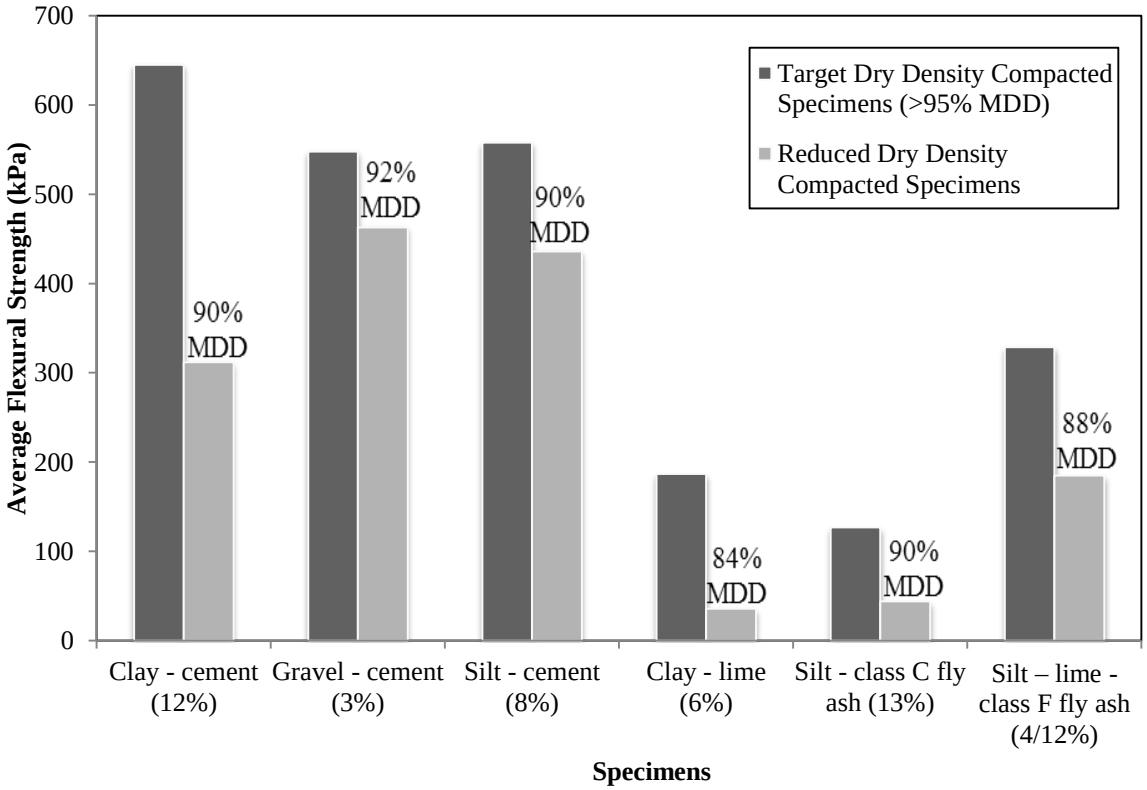

Figure 4.3 Effect of Density/Compaction on CSMs

4.1.2 Change in Binder Content

The flexural strength characteristic with change in binder content was studied. Three mixtures (gravel-cement, sand-cement, and silt-fly ash) were used in this study. Only the binder content for each of these three mixes was increased; the MDUW and OMC were kept the same as in Table 3.3. For gravel-cement specimens, the binder

content was increased from 3% to 5%; for sand-cement specimens, from 6% to 8%; and for silt-fly ash-specimens from 13% to 18%. At least three replicate for each mixture were prepared. Table 4.3 summarizes the average failure load and average flexural strength of the mixtures. The coefficient of variance for each mix did not exceed 8%, indicating the good performance of the replicate specimens. The failure load and flexural strength of each replicate for the mixtures are provided in Appendix-A.

Table 4.3 Summary of Flexural Strength Test Results (Binder Content Change)

Specimen (Binder %)	**Average Failure Load (kN)**	**Average Flexural Strength (kPa)**	**Coefficient of Variance (%)**
Gravel - cement (5%)	3.44	999	6.5
Sand - cement (8%)	3.43	998	6.1
Silt – class C fly ash (18%)	0.55	190	7.2

An increase of 2% in cement increased the flexural strength for gravel-cement specimens, by 82% and, for sand-cement specimens, by 104%. However, an increase of 5% in class C fly ash for silt-fly ash specimens increased the flexural strength by just 50% (Tables 4.1 and 4.3). This indicates that cement is more efficient in increasing the strength of specimens than class C fly ash. Also, the flexural strength for gravel-cement (5%) and sand-cement (8%) are approximately the same (Table 4.3). Figure 4.4 shows the comparison of the specimens with different binder contents.

Zhang and Wei (2011) studied the increase in flexural strength versus percent binder for cement-stabilized soils and reported that the flexural strength increased as the cement content of the specimen increased.

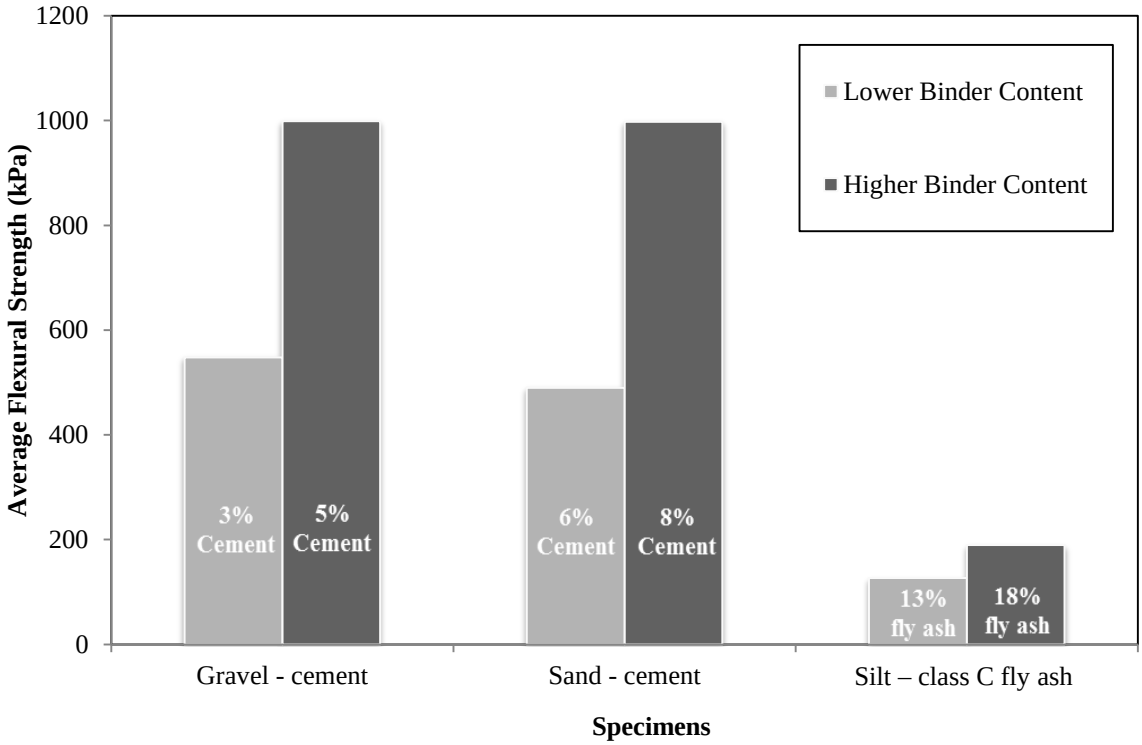

Figure 4.4 Effect of Binder Content on CSMs

4.1.3 Change in Curing Period

The flexural strength characteristic with respect to change in curing period was evaluated. Three mixtures (gravel-cement, sand-cement and clay-cement) were used in this study. These mixtures were cured for 360 d and tested for flexural strength. Sand-cement specimens were also tested at 56 d curing.

Table 4.4 summarizes the average failure load and average flexural strength of the mixtures. At least two replicates were prepared for each mixture. The coefficient of variance for each mix did not exceed 10%, indicating the good performance of the replicate specimens. The failure load and flexural strength of each replicate for the mixtures are provided in Appendix-A. Figure 4.5 shows the comparison of the specimens with different curing times.

Table 4.4 Summary of Flexural Strength Test Results (Effect of Curing)

Specimen (Binder %)	Average Failure Load (kN)	Average Flexural Strength (kPa)	Coefficient of Variance (%)	Days Cured
Clay - cement (12%)	4.95	1,438	6.9	360
Gravel - cement (3%)	4.13	1,202	0.8	360
Sand - cement (6%)	2.99	869	5.2	360
Sand - cement (6%)	2.00	582	9.5	56

In general, after 360 d of curing, there was an increase in flexural strength by 77% for the sand-cement specimens, for gravel-cement specimens cured for 360 d, 119% increase, and for clay-cement specimens cured for 360 d, 123% increase (Tables 4.1 and 4.4).

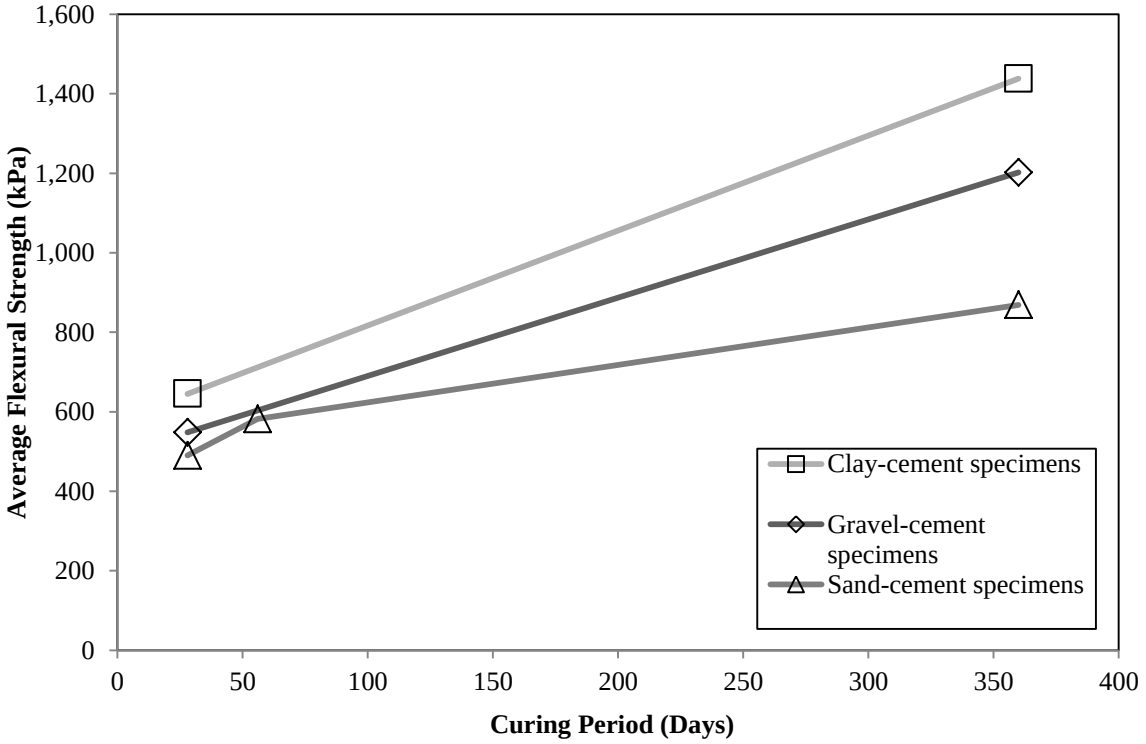

Figure 4.5 Effect of Curing Period on CSMs

Several studies on stabilized soils and crushed rocks (Zhang and Wei, 2011; Midgley and Yeo, 2008; and Siddique and Rajbongshi, 2002) showed that the flexural strength increased with the curing time. Figure 4.6 shows the comparison of the laboratory flexural strength data with data from the literature for cement-stabilized materials.

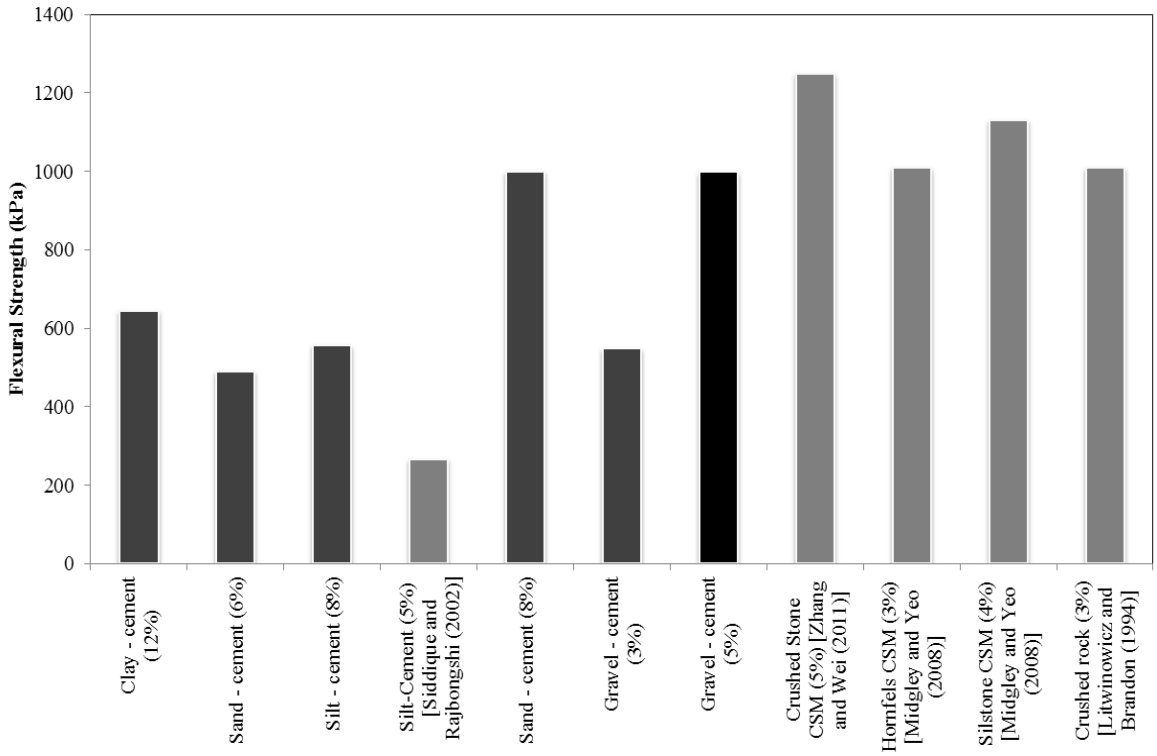

Figure 4.6 Flexural Strength of Cement-Stabilized Specimens

For the cement-stabilized specimens, the flexural strength for crushed stone CSMs is comparable to the gravel-cement in this study, which is found to be lower than the literature strength values (Figure 4.6). One possible reason might be that the aggregate size was larger (30 mm to 2.5 mm) in the study by Zhang and Wei (2011). In the study by Migdley and Yeo (2008), the aggregates size was comparable to the gravel in this study. But, the crushed stone were plastic in nature (gravel aggregate in this study was non-plastic). The silt used in the study by Siddique and Rajbongshi (2002) were similar to the

silt in this study. The flexural strength of gravel-cement (5%) and sand-cement (8%) are close to these crushed stone CSMs. Figure 4.7 shows the comparison of the laboratory flexural strength data with from the literature for fly ash and lime-stabilized materials.

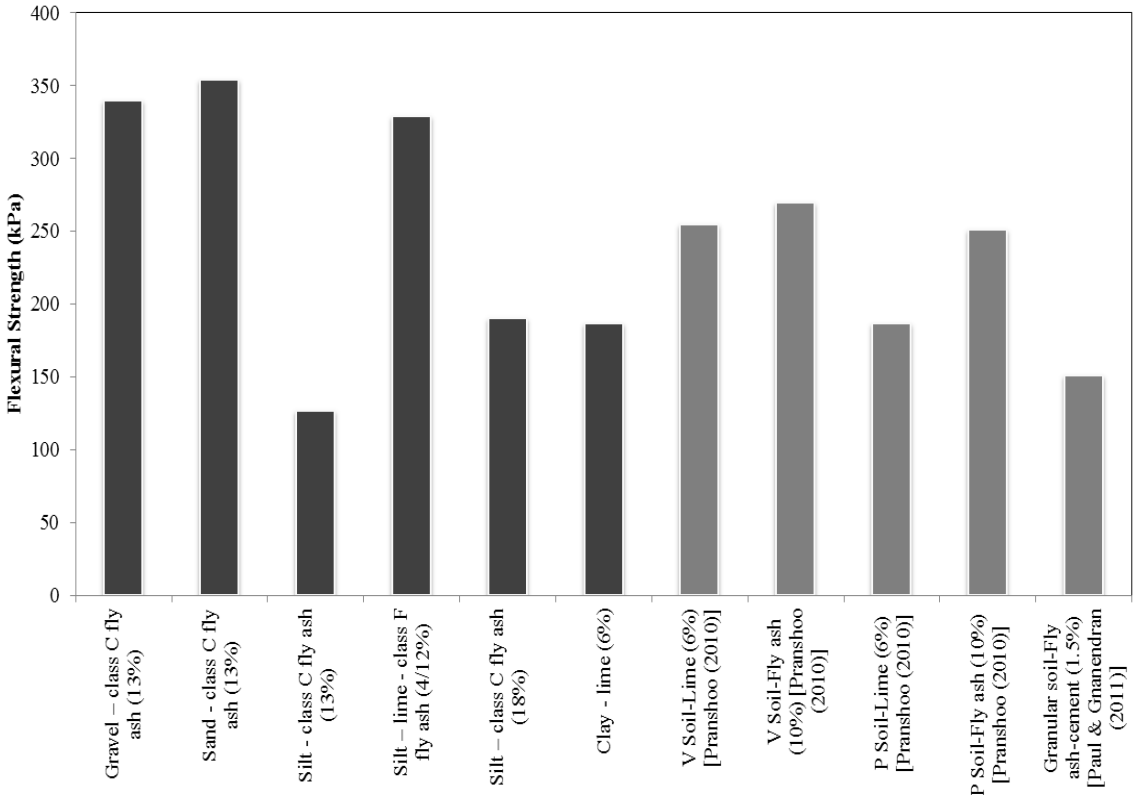

Figure 4.7 Flexural Strength of Fly ash and Lime-Stabilized Specimens

In the study by Pranshoo (2010), the flexural strength test conducted on V-soil (Vernon series) CSM with 6% lime had an average modulus of rupture of 255 kPa. The V-soil was classified as lean clay (CL) with a liquid limit if approximately 37, and PI of approximately 11; which is similar to the clay used in this study, except with lesser PI.

4.2 RELATIONSHIP BETWEEN FLEXURAL STRENGTH AND UNCONFINED COMPRESSIVE STRENGTH

Su (2012) and Casmer (2011) conducted UCS tests on the nine mixtures (from Table 3.3). The results of the UCS tests are shown in Table 4.5. From flexural strength

(this study) and UCS test data, an attempt has been made to find any relationship between the two. Flexural strengths (from Tables 4.1) are plotted against UCS (from Table 4.5), and shown in Figure 4.8.

Table 4.5 UCS Results for CSMs (from Su, 2012, and Casmer, 2011)

Specimens	UCS (MPa)
Clay - cement (12%)	3.68
Gravel - cement (3%)	4.41
Sand - cement (6%)	3.59
Silt - cement (8%)	4.5
Clay - lime (6%)	1.03
Gravel – class C fly ash (13%)	1.99
Sand - class C fly ash (13%)	1.42
Silt - class C fly ash (13%)	0.63
Silt – lime - class F fly ash (4/12%)	1.87

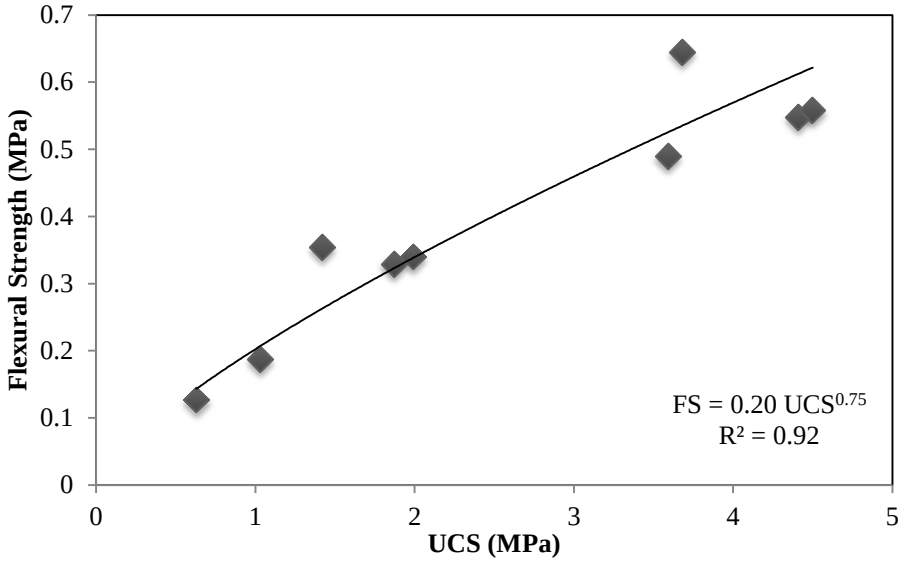

Figure 4.8 Relationship between Flexural Strength and UCS

A relationship exists between flexural strength and UCS (Equation 4.1). As UCS testing is much simpler and well-known than flexural beam testing, this relationship can be used to estimate the flexural strength of CSMs using the UCS test. In general, for the nine mixtures, flexural strength was 17% of the UCS.

$$FS = 0.20\ UCS^{0.75} \qquad \text{(Eq. 4.1)}$$

where *FS* is flexural strength (MPa) and *UCS* is unconfined compressive strength (MPa)

For comparison, flexural tensile strength of cemented materials is about one-third of the UCS for low-strength materials and about one-fifth of the UCS for high-strength materials (TRH 14, 1985). Ronald et al. (1979) gave an almost linear relationship between flexural tensile strength and the UCS. Kersten (1961) compared data on UCS and flexural strength of hardened cement-treated soils and showed a nearly linear relationship at all cement contents and at all ages. The flexural strength was approximately 20 percent of the compressive strength.

4.3 FLEXURAL MODULUS TESTING

Flexural modulus testing was conducted by applying a dynamic load on beam specimens. Three different loading conditions or stress levels were used for each beam specimen - 20%, 30%, and 40% of the average failure load (from the monotonic/flexural strength test). The tests were conducted on three replicates and the average was taken for each stress level. Each replicate specimen was tested at the three different stress levels. The tests were conducted from lower stress levels to higher stress levels, i.e., from 20% to 40%. The variability of the three replicates for each specimen did not exceed 30%, indicating the good performance of the replicate specimens. Table 4.6 shows the summary of the flexural modulus tests conducted (from Table 3.3) at 20%, 30%, and 40% stress levels. The flexural modulus of each replicate is shown in Appendix B.

From Table 4.6, testing at the 20% stress level resulted in lower values of flexural modulus compared to those tested at 30% and 40% stress levels, which yielded comparable results. The results indicate that determination of flexural modulus should be

done at a stress level of 30% to obtain consistent results while minimizing any potential damage that could occur at the 40% stress level. A pavement analysis by Washington State University also showed that 30% stress level was appropriate for determining the flexural modulus. The 20% stress level is not recommended for flexural modulus testing because the load level is too low.

Table 4.6 Summary of Flexural Modulus Test Results

Specimen (Binder %)	**Average Flexural Modulus (20%) (MPa)**	**Average Flexural Modulus (30%) (MPa)**	**Average Flexural Modulus (40%) (MPa)**
Clay - cement (12%)	626	999	1,100
Gravel - cement (3%)	667	929	1,036
Sand - cement (6%)	541	973	1,152
Silt - cement (8%)	573	904	1,114
Gravel – class C fly ash (13%)	621	821	860
Sand - class C fly ash (13%)	537	720	740
Silt - class C fly ash (13%)	360	454	466
Silt – lime - class F fly ash (4/12%)	600	857	940
Clay – lime (6%)	562	601	707

Note: *Average value shown of three replicates*

Among the nine mixtures, the highest and the lowest flexural modulus for the 30% stress level was observed for the clay-cement and the silt-fly ash specimens, respectively. The silt-fly ash specimens were the weakest mixture. Two of the specimens failed while conducting the flexural modulus tests; one failed while applying 20% stress level, while the other failed at 30% stress level. As the silt-fly ash (13% binder) did not perform well, the binder content was increased to 18% and the flexural tests were conducted on the same and found to perform better (discussed in Chapter 4.2.1). For the

fly ash-stabilized soils, the gravel-fly ash had the highest flexural modulus, even though the strength of gravel-fly ash specimens was lower than the sand-fly ash specimens.

Figures 4.9 to 4.11 show the change in flexural modulus during the test for each replicate for each stress level for clay-cement specimens. Figures 4.12 to 4.14 show the change in total, plastic, and elastic displacement during testing for the clay-cement specimens. From these figures, the flexural modulus is shown to degrade and the displacement increases as the test goes on. The change in modulus and displacement (total, elastic, and plastic) during the test for each replicate for the remaining eight mixtures are shown in Appendix B.

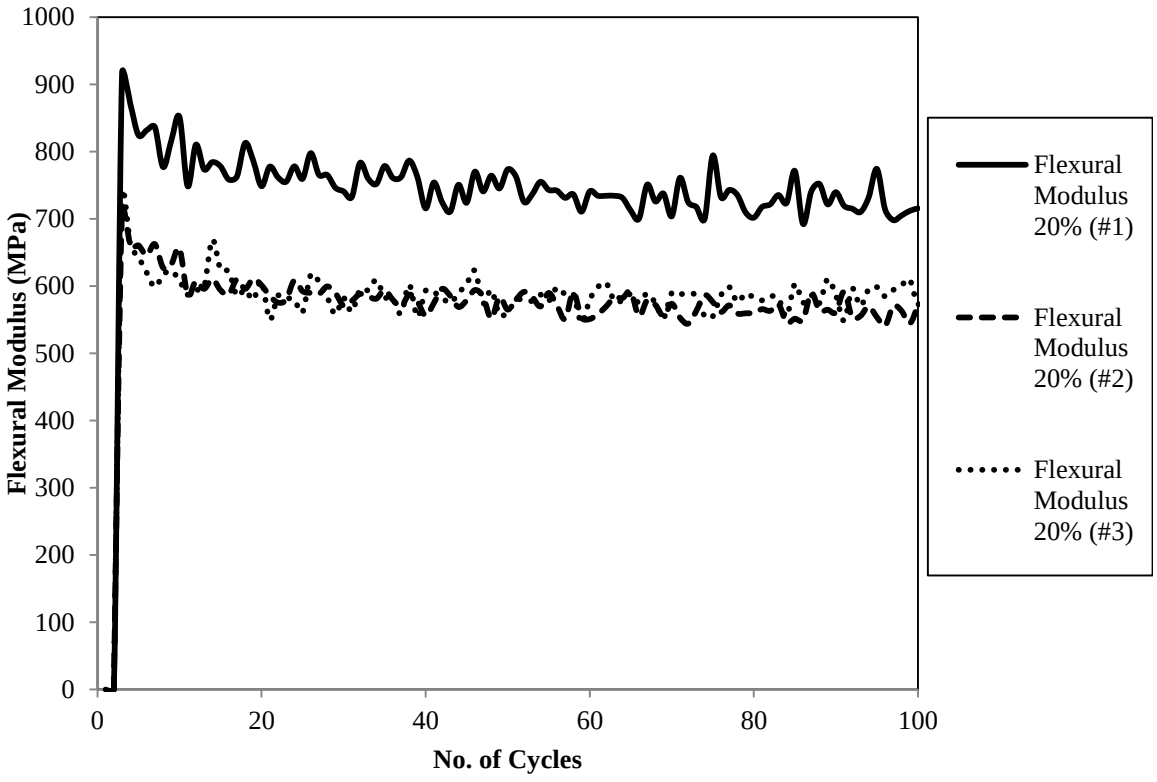

Figure 4.9 Flexural Modulus Variation at 20% Stress Level for 3 Clay-Cement Replicates

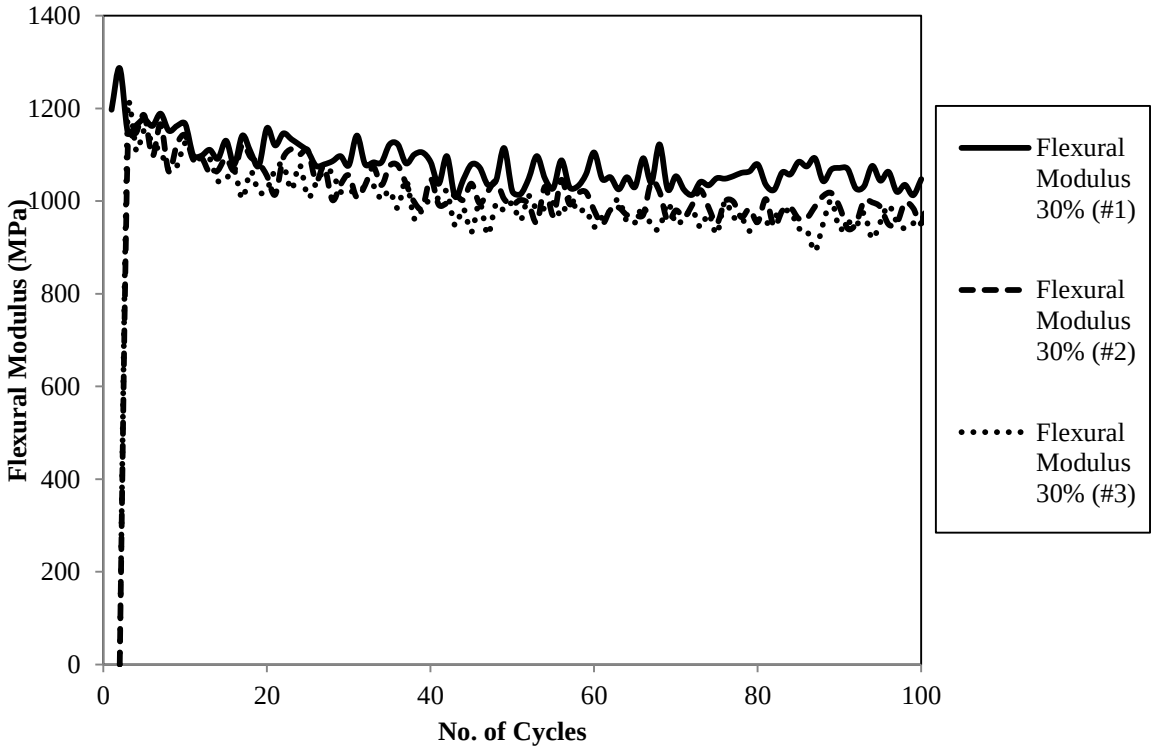

Figure 4.10 Flexural Modulus Variation at 30% Stress Level for 3 Clay-Cement Replicates

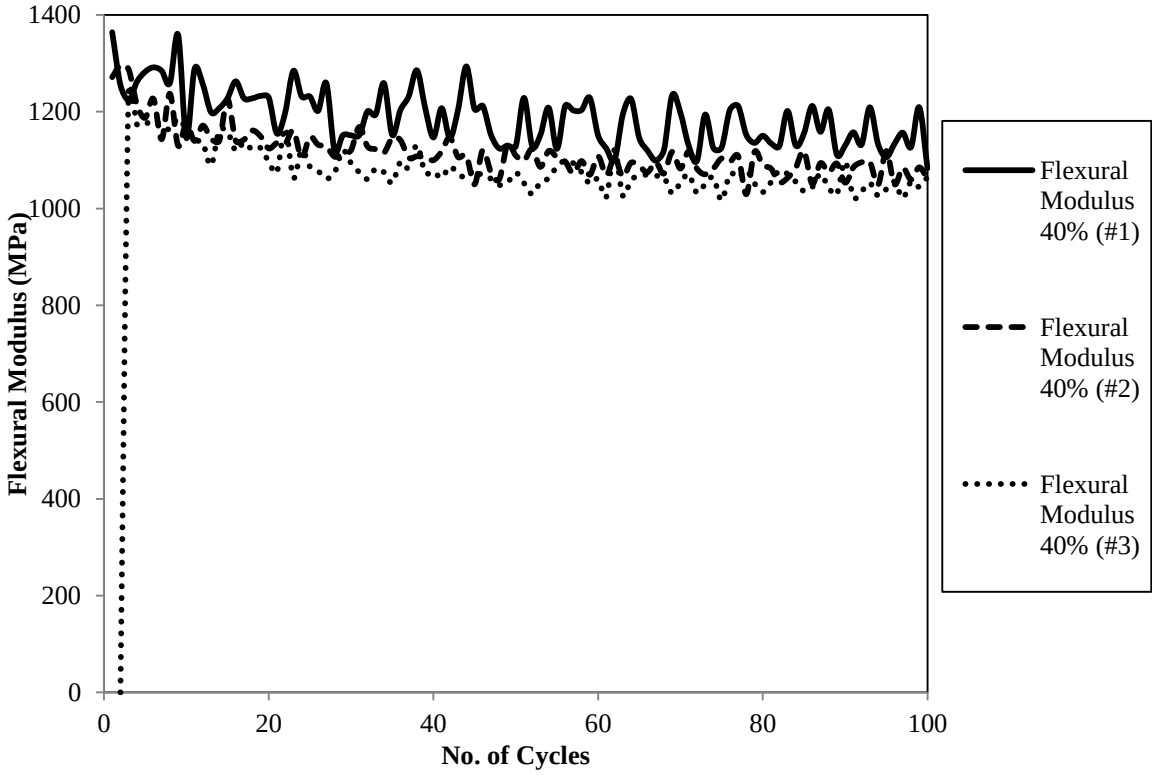

Figure 4.11 Flexural Modulus Variation at 40% Stress Level for 3 Clay-Cement Replicates

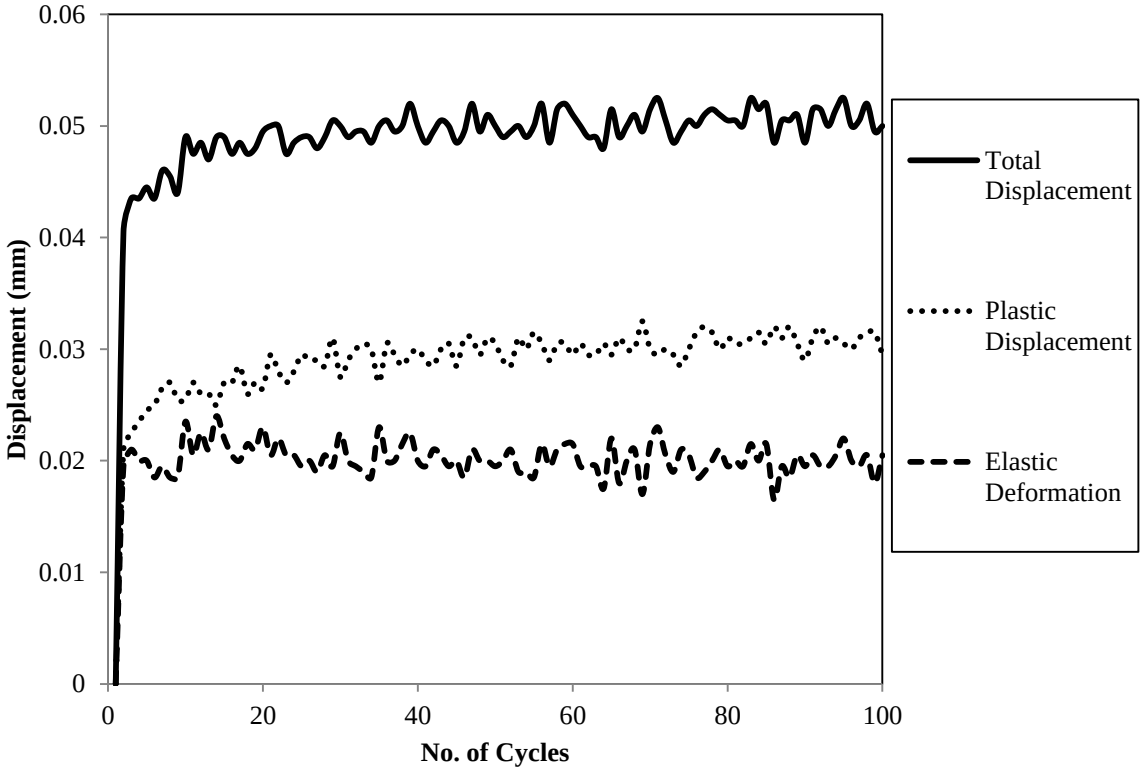

Figure 4.12 Displacement Variation for Flexural Modulus Test at 20% Stress Level for Clay-Cement Specimen

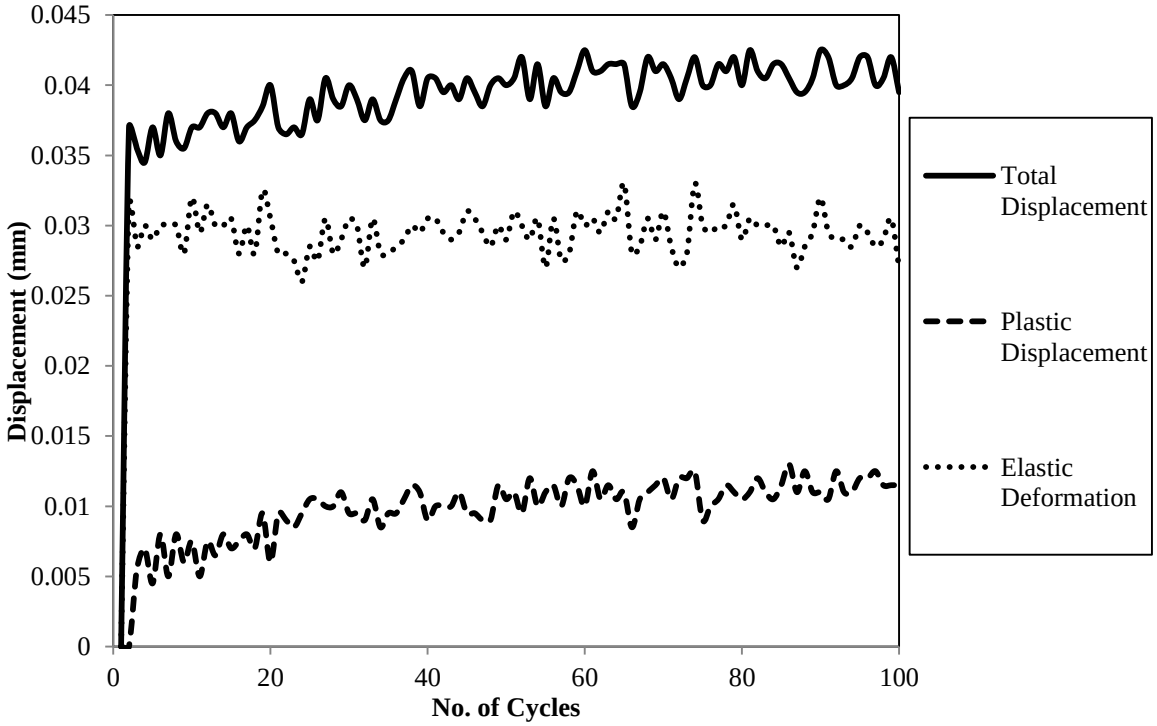

Figure 4.13 Displacement Variation for Flexural Modulus Test at 30% Stress Level for Clay-Cement Specimen

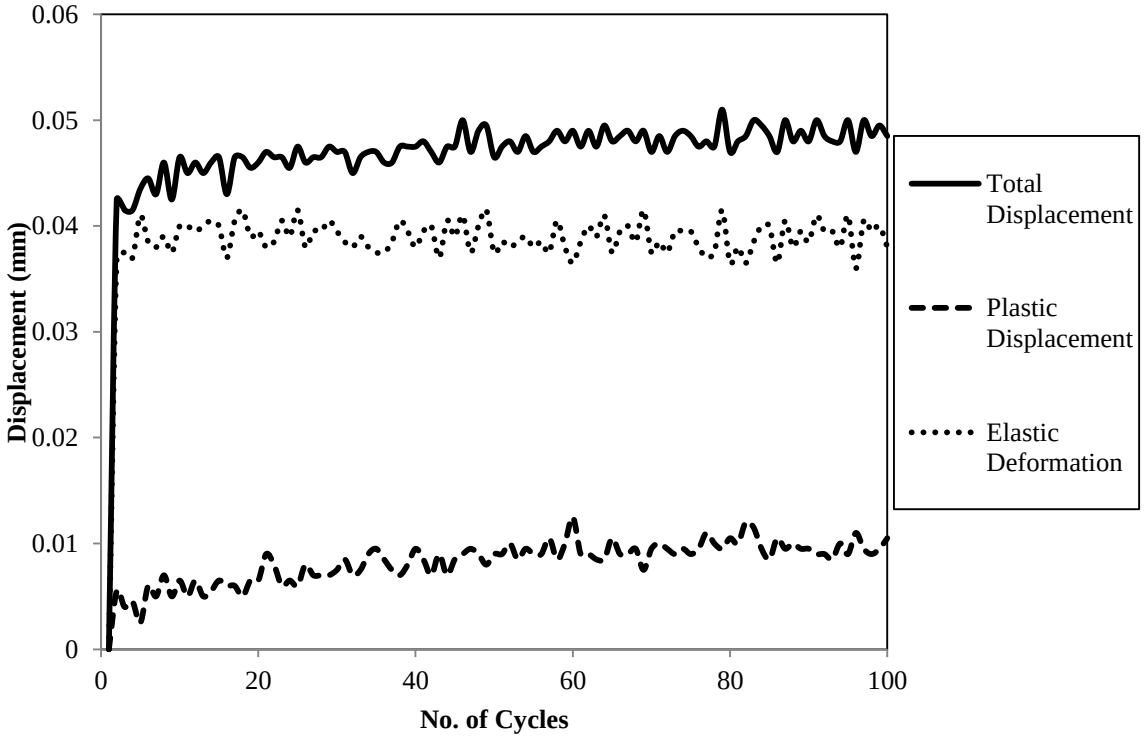

Figure 4.14 Displacement Variation for Flexural Modulus Test at 40% Stress Level for Clay-Cement Specimen

4.3.1 Change in Binder Content

The effect of binder content on flexural modulus was studied on three mixtures (gravel-cement, sand-cement, and silt-fly ash). Only the binder content for these three mixes was increased; the MDUW and OMC were kept the same as in Table 3.3. For gravel-cement specimens, the binder content was increased from 3% to 5%; for sand-cement specimens, from 6% to 8%; and for silt-fly ash specimens, from 13% to 18%.

Three loading conditions/stress levels (20%, 30%, and 40% of the average failure load from monotonic/flexural strength testing) were used for each beam specimen. The tests were conducted on three replicates, and the average was taken for each stress level. Each replicate was used to conduct testing at three stress levels. The tests were conducted from lower stress levels to higher stress levels; i.e., form 20% to 40%. The coefficient of variation of these three replicates for each mixture did not exceed 17%, indicating the

good performance of the replicate specimens. Table 4.7 shows the summary of the flexural modulus tests conducted on the specimens at 20%, 30%, and 40% stress levels with higher binder content. The flexural modulus of each replicate is shown in Appendix B. The change in modulus and displacement (total, elastic, and plastic) during the test for each replicate for the nine mixtures are also shown in Appendix B.

Table 4.7 Summary of Flexural Modulus Test Results (Change of Binder Content)

Specimen (Binder %)	**Average Flexural Modulus (20%) (MPa)**	**Average Flexural Modulus (30%) (MPa)**	**Average Flexural Modulus (40%) (MPa)**
Gravel - cement (5%)	1,004	1,335	1,512
Sand - cement (8%)	872	1,379	1,510
Silt – class C fly ash (18%)	519	587	616

Figure 4.15 shows the effect of binder change on flexural modulus for the three stress levels. The flexural modulus increases with increase in binder content for all stress levels. For the gravel-cement specimens, the flexural modulus increased by 44% (for the 30% stress level). For the sand-cement specimens, flexural modulus increased by 42% (for the 30% stress level); and for silt-fly ash specimens, by 29% (for the 30% stress level). This indicates that cement is better in increasing the flexural modulus. Zhang and Wei (2011), and Siddique and Rajbongshi (2002) studied the increase in flexural modulus versus percent binder for cement-stabilized soils and reported that the flexural modulus increased as the cement content of the specimen increased.

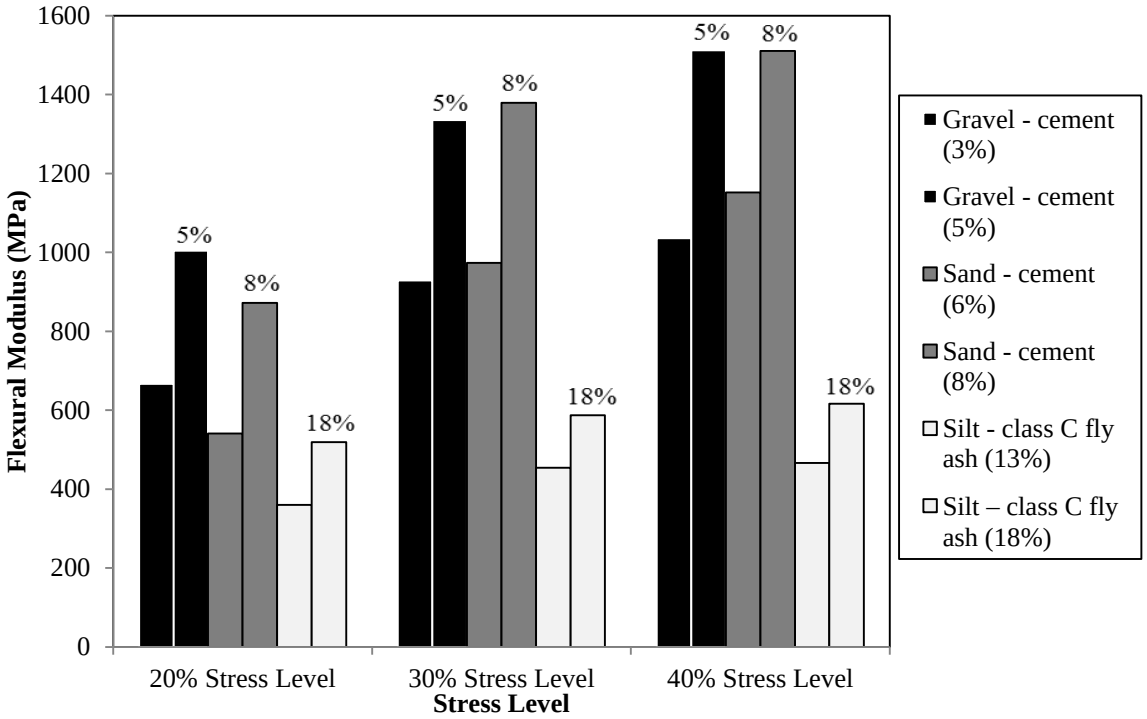

Figure 4.15 Effect of Binder Content and Material Type on Flexural Modulus

4.4 RELATIONSHIP BETWEEN FLEXURAL STRENGTH AND FLEXURAL MODULUS

From the flexural strength and flexural modulus test data of the beam specimens, an attempt has been made to find any relationship between the two. Flexural strengths (from Tables 4.1 and 4.3) are plotted against flexural moduli (from Tables 4.6 and 4.7), and the average values for each stress level are shown in Figure 4.16. A linear co-relationship exists between the flexural strength and flexural modulus. Table 4.8 summarizes those relationships.

Table 4.8 Relationship between Flexural Strength and Flexural Modulus

Stress Level for Flexural Modulus (%)	Relationship	R^2
20	*FS* = 1.55 (*FM*) - 487.02	0.80
30	*FS* = 1.01 (*FM*) - 412.64	0.95
40	*FS* = 0.86 (*FM*) - 359.39	0.93

FS = Flexural strength (in kPa); FM = Flexural modulus (in MPa)

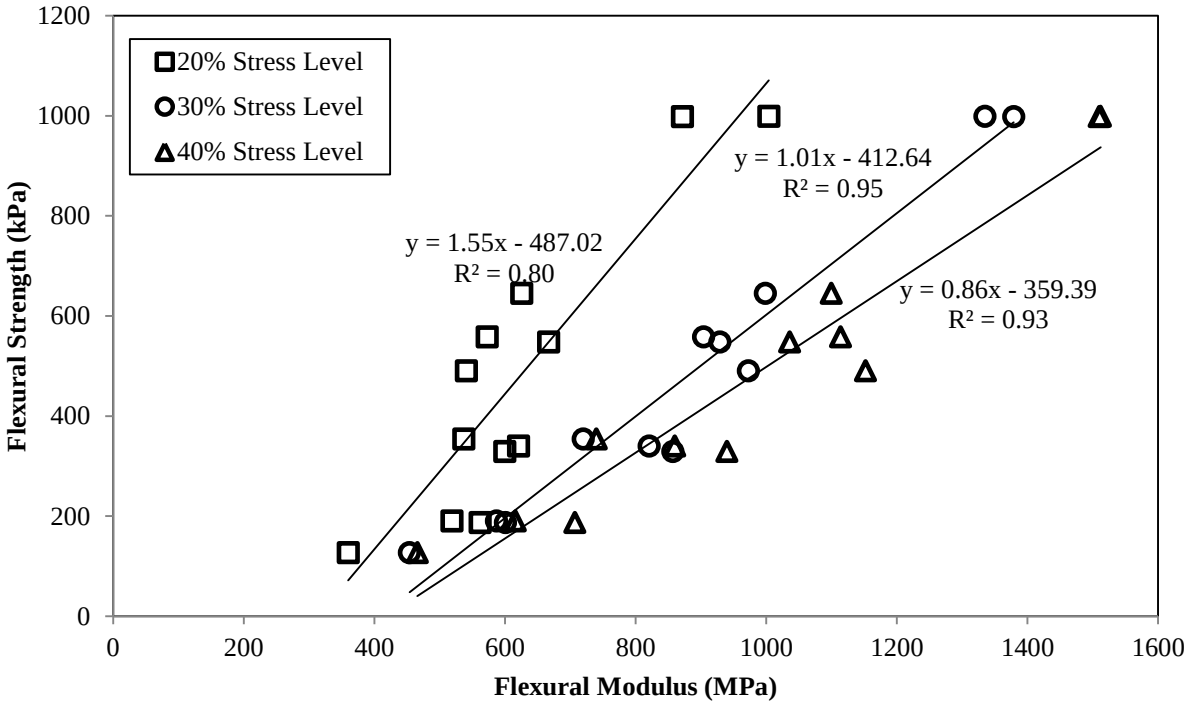

Figure 4.16 Relationship between Flexural Strength and Flexural Modulus

Though the relationships between the flexural strength and flexural modulus is not much of a practical use, but these relationships can be used to get a rough estimate of the flexural modulus after the flexural strength test.

4.5 FATIGUE CRACK TESTING

Fatigue testing was conducted on the nine mixtures (from Table 3.3). The specimens were subjected to dynamic loading of 2 Hz to rupture. At least six beam specimens for each mixture were fatigue tested. Different loading conditions/stress levels (from 40% to 95%) were used. Some beam specimens did not fail even after 100,000 to 200,000 cycles; hence, the number of cycles to failure (fatigue life) had to be estimated for some the unbroken beam specimens. The estimation was based on the initial modulus of the specimen during the fatigue test. Some of the specimen's fatigue life could not be estimated due to technical or LVDT error which resulted error in the strain data. Also,

fatigue life could not be estimated when fatigue life was more than the number of cycles tested in the laboratory data.

Midgley and Yeo (2008) defined the initial modulus as the mean modulus for the first 50 cycles of the fatigue test, while the initial strain was defined as the mean strain during the first 50 cycles of the fatigue test. The laboratory testing conducted by Midgley and Yeo (2008) indicated that the number of cycles of load in which half the initial modulus was reached provided a suitable definition for the fatigue life of laboratory samples. The results showed that, shortly after the cycles to half the initial modulus was reached, the flexural beam samples typically ruptured. The same approach was adopted in this study.

Nine beam specimens were tested for sand-cement (6% binder) beam specimens (Table 4.9). The modulus degradation curves and the displacement variation for the sand-cement specimens are shown in Appendix C. From the sand-cement specimen fatigue curves (graphs presented in Appendix-C), not all specimen ruptured shortly after the cycles to half the initial modulus was reached. The specimens typically ruptured when the initial modulus reached the range of 53% to 70%.

Figure 4.17 shows the typical modulus degradation curve during the fatigue test for specimen FT-4 at 85% stress level. Figure 4.18 shows the variation of displacement (total, plastic and elastic) during the fatigue test for specimen FT-4 at 85% stress level.

Table 4.9 Summary of the Fatigue Strength Test Results on Sand-Cement Specimens (Binder Content: 6%)

SN	SL (%)	IFM (MPa)	FFM (MPa)	PFME (%)	IS (με)	N
FT-1	95	1,382	589	43	504	928
FT-2	95	580	523	90	918	723
FT-3	85	974	800	82	531	23616
FT-4	85	982	664	68	475	30,260
FT-5	85	1,128	722	64	389	22,273
FT-6	80	885	608	69	474	55,202
FT-7*	75	1,056	682	65	372	59,562**
FT-8*	75	256#	166#	65	157	>100,000
FT-9*	65	1,462	899	62	238	>150,000

*SN = Specimen Number; SL = Stress Level; IFM = Initial Flexural Modulus; FFM = Final Flexural Modulus (i.e. Flexural Modulus at the end of Fatigue Test); PFME =Percent of Flexural Modulus at the End of Test; IS = Initial Strain; N = Number of Cycles at the End of Test (i.e. Fatigue Life); * Did not fail; **Predicted value; #Low modulus might be due to LVDT readings*

Note: *Range of Failure: 53% to 70% of IFM (Average: 62%)*

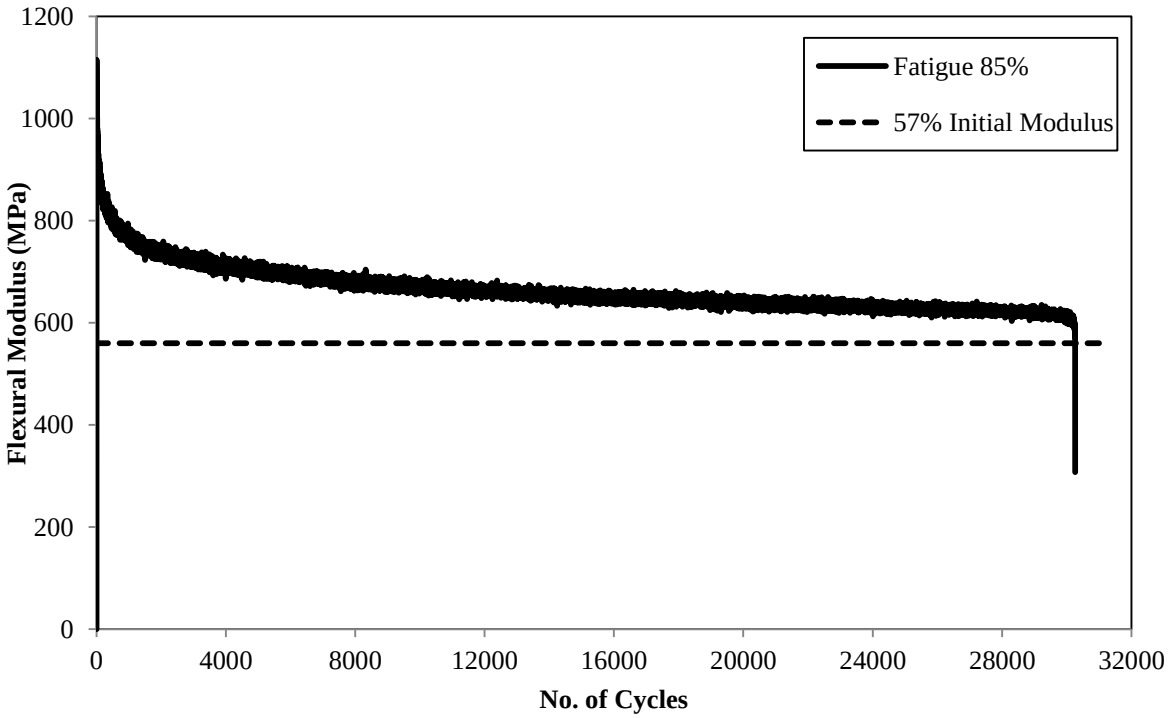

Figure 4.17 Typical Degradation of Flexural Modulus in a Fatigue Test at 85% Stress Level [Sand-Cement (6%) Specimens (FT-4)]

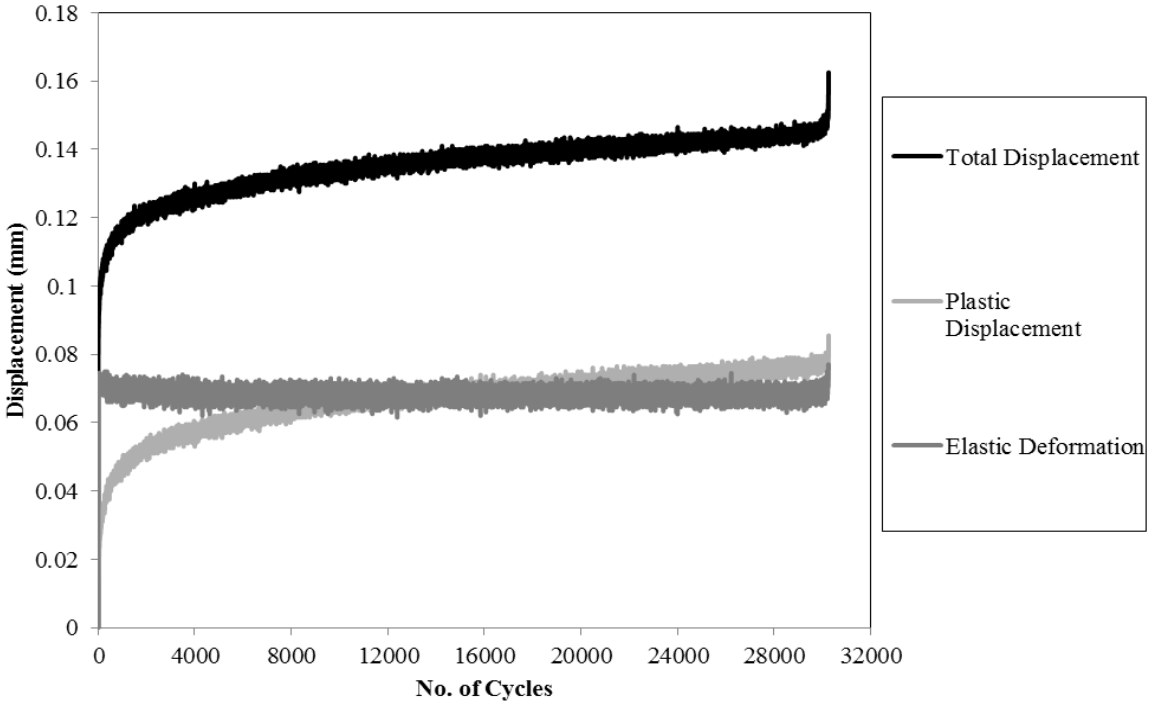

Figure 4.18 Displacement Variation v/s No. of Cycles in a Fatigue Test at 85% Stress Level [Sand-Cement (6%) Specimens (FT-4)]

Three of the sand-cement specimens (FT-7, FT-8 and FT-9) did not fail after 100,000 cycles. However, six of the specimens failed shortly after the initial modulus was reached (53%-70%); thus, the average of the two percentages, (61%) was used to predict the fatigue life for specimens FT-7. From Figure 4.19, 61% of initial modulus was reached at 59,562 cycles. Hence, the fatigue life for FT-7 was taken as 59,562 cycles.

Table 4.10 shows the summary of the tests on the nine mixtures. Detailed results and graphs are presented in Appendix C. In general, the fatigue life was in the range of 1 to 75,537 cycles in this study. Also, the modulus kept degrading as the test continued, whereas the displacement increased. The fatigue life of the specimens, defined by Midgley and Yeo (2008) as cycles to half the initial modulus was not observed in all the mixtures. In general, the fatigue life ranged from 44% to 64% of initial modulus (average = 54%). Tables 4.10, 4.11 and 4.12 show the average initial modulus for all the specimens. For testing purpose, a specimen can complete approximately 57, 600 cycles in

8 hours. Though it is recommended that the specimen be tested till it fails, but, if under circumstances where the specimen cannot fail within a day or some specific period of time, the initial modulus of the specimens can be used to estimate the fatigue life of the unbroken specimens.

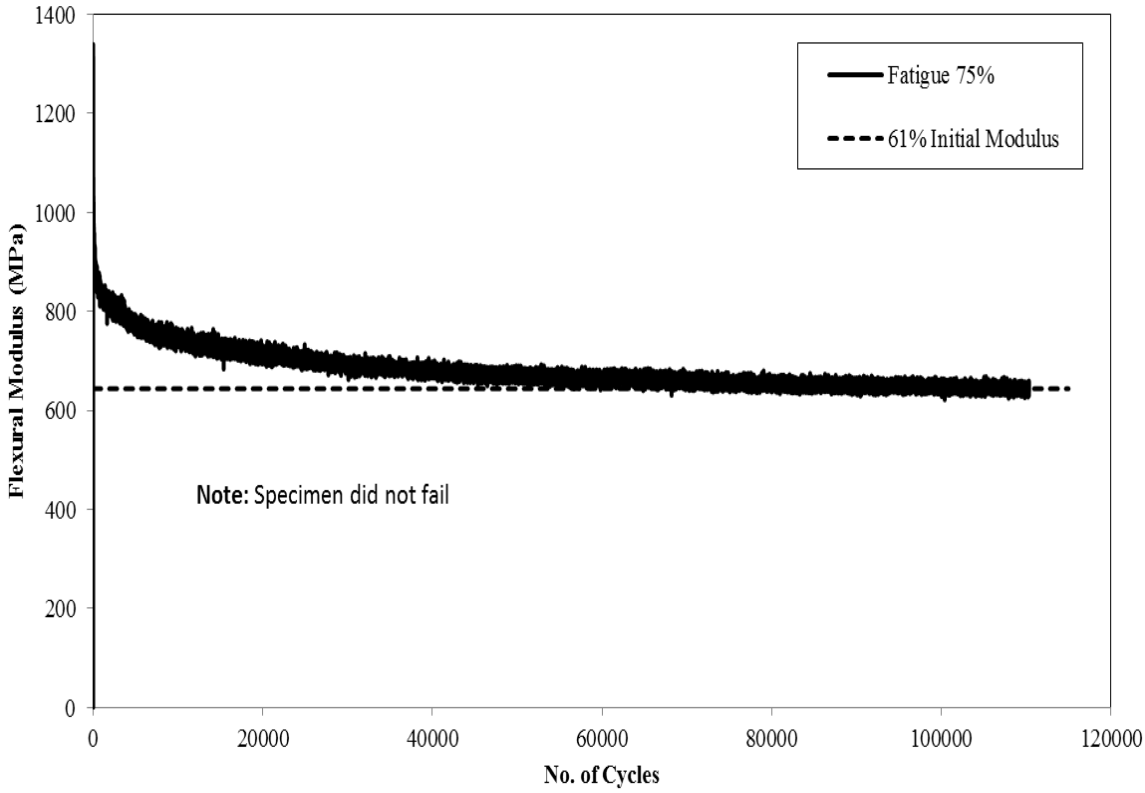

Figure 4.19 Typical Degradation of Flexural Modulus in a Fatigue Test at 75% Stress Level [Sand-Cement (6%) Specimens (FT-7)]

Several studies (e.g., Midgley and Yeo, 2008) have been done on the fatigue crack testing of CSMs and have found a wide range in the fatigue life of the specimens depending on the stress level. Litwinowicz and Brandon (1994) studied fatigue cracking of cement-treated crushed stone specimens. The fatigue life for the crushed stone CSMs was in the range of 357 (for 70% stress level) to 602,000 cycles (for 27% stress level). Li and Dong (2011) studied the fatigue cracking of cement-stabilized recycled base mixtures. Li and Dong (2011) conducted fatigue cracking tests between the stress levels

73% and 83%. The fatigue life showed a range of 378 to 89,411 cycles. In another study by Arnold (2009), the fatigue life of road aggregate CSMs was evaluated as 330 at 70% stress level and 110,000 cycles at 60% stress level. Yu et al. (2011), conducted fatigue cracking tests on lime fly-ash treated aggregate and found fatigue life to be in the range of 7,507 to 15,650. The stress level ranges from 60% to 80%.

4.5.1 Change in Density

Table 4.10 presents the summary of the fatigue cracking test results on two specimens with reduced dry density (compacted lightly) (gravel-cement with 3% binder and silt- cement with 8% binder). Detailed results and graphs are presented in Appendix C.1. The specimens compacted with reduced dry density showed a lesser fatigue life than the specimens compacted with target dry density (Tables 4.10 and 4.11). In comparison, Bhattacharya and Pandey (1986) studied the fatigue behavior of lime-laterite soil mixtures and found lightly compacted specimens to perform pooper in fatigue life.

Table 4.10 Summary of the Fatigue Strength Test Results on the Beam Specimens

Specimen (Binder %)	Range of								No. of Beams		x
	Stress Level Applied for Testing (%)		Fatigue Life after Testing		Initial Modulus (MPa)		Initial Strain (με)		Tested	Did not fail	
	Low	High	Low	High	Low	High	Low	High			
Clay – Cement (12%)	60	85	146	38,161	675	1,096	470	613	6	1	64
Gravel – Cement (3%)	50	85	2	46,329	554	1,216	367	652	7	0	50
Sand – Cement (6%)	65	95	723	59,562	580	1,462	238	918	9	3	62
Silt – Cement (8%)	65	90	1,996	75,537	746	1,302	363	733	7	0	60
Sand – Fly ash (13%)	60	75	9	64,657	741	965	280	383	6	1	44
Gravel – Fly ash (13%)	40	85	2	2,246	448	768	328	347	10	1	*
Silt – Fly ash (13%)	45	75	1	20,000	515	-	147	-	4	1	*
Silt – Lime – Fly ash (4/12%)	60	85	515	32,199	545	1,185	191	537	7	3	62
Clay – Lime (6%)	65	90	14	29,933	401	667	261	479	6	2	50

** Specimens did not perform well in fatigue; x = Average percent of initial modulus (i.e. fatigue life of specimen)*

Table 4.11 Summary of the Fatigue Strength Test Results on the Beam Specimens (Reduced Density, 90% MDD)

Specimen (Binder %)	Range of								No. of Beams		x
	Stress Level Applied for Testing (%)		Fatigue Life after Testing		Initial Modulus (MPa)		Initial Strain (με)		Tested	Did not fail	
	Low	High	Low	High	Low	High	Low	High			
Gravel – Cement (3%)	65	85	8	167	506	1,179	429	941	6	0	50
Silt – Cement (8%)	65	90	141	68,093	525	1,115	345	595	6	2	60

x = Average percent of initial modulus (i.e. fatigue life of specimen)

4.5.2 Change in Binder Content

This section presents the fatigue cracking test results on three specimens with higher binder content than described in Chapter 4.4 to see the effect of binder content on the fatigue of the specimens. The mixes chosen were: gravel-cement with 5% binder, sand-cement with 8% binder, and silt-fly ash with 18% binder. Table 4.12 shows the summary of the tests on the three mixtures. Detailed results and graphs are presented in Appendix C.2.

Table 4.12 Summary of the Fatigue Strength Test Results on the Beam Specimens (Higher Binder Content)

Specimen (Binder %)	**Range of**								**No. of Beams**		**x**
	SR (%)		**FL**		**IM (MPa)**		**IS (με)**		**T**	**DF**	
	L	**H**	**L**	**H**	**L**	**H**	**L**	**H**			
Gravel – Cement (5%)	50	75	24	11,836	1,187	1,893	285	1,465	7	2	50
Sand – Cement (8%)	65	85	142	78,321	1,243	1,983	235	736	6	1	50
Silt – Fly ash (18%)	40	80	2	2,783	619	730	136	186	6	2	50

SR = Stress Level Applied for Testing; FL = Fatigue Life after Testing; IM = Initial Modulus; IS = Initial Strain; L = Low; H = High; T = Tested; DF = Did not fail x = Average percent of initial modulus (i.e. fatigue life of specimen)

The sand-cement specimens with higher binder content did not perform well as compared to the sand-cement specimens with lower binder content. The fatigue life of sand-cement (6% binder) had a greater fatigue life when compared to the fatigue life of sand-cement (8% binder) at the same stress level. For the gravel-cement specimens, there was not much improvement in the fatigue cracking with increase in binder content, but the silt-fly ash specimens performed better with increased binder. Further analysis on the fatigue behavior modeling of all the specimens is shown in Chapter 5.

CHAPTER 5 - FATIGUE PERFORMANCE MODEL

5.1 FATIGUE PERFORMANCE MODEL

Fatigue is one of the major distresses of CSL in a pavement. A fatigue model of CSL is required to predict the fatigue performance of CSL in the field and to determine if the design is sufficient. The overall objective of this study is to develop methods to identify fatigue behavior of cementitiously stabilized layers (CSL). To this extent, validating and developing fatigue performance models is required.

In the past, many researchers have studied fatigue behavior of concrete, asphalt, and cement-stabilized materials; and have developed fatigue cracking models, which are discussed in Chapter 2.2.3. In this chapter, laboratory fatigue data is used to develop a model that represents all CSM mixtures. For validation purposes, the laboratory data was fit to fatigue models from literature.

5.2 STRESS-BASED FATIGUE MODEL

5.2.1 Development of Stress-Based Model

A stress-based fatigue model is developed using the two parameters – stress ratio (*SR*) and fatigue life (*N*). Figure 5.1 shows the general relationship of the model for the beam specimens that were tested for fatigue cracking. The general relationship is:

$$SR = (-a)\ln(N) + b \tag{5.1}$$

where N is flexural fatigue life and a and b are regression parameters. The SR is:

$$SR = \sigma/MR \tag{5.2}$$

where σ is flexural tensile stress (kPa) and MR is flexural tensile strength (kPa)

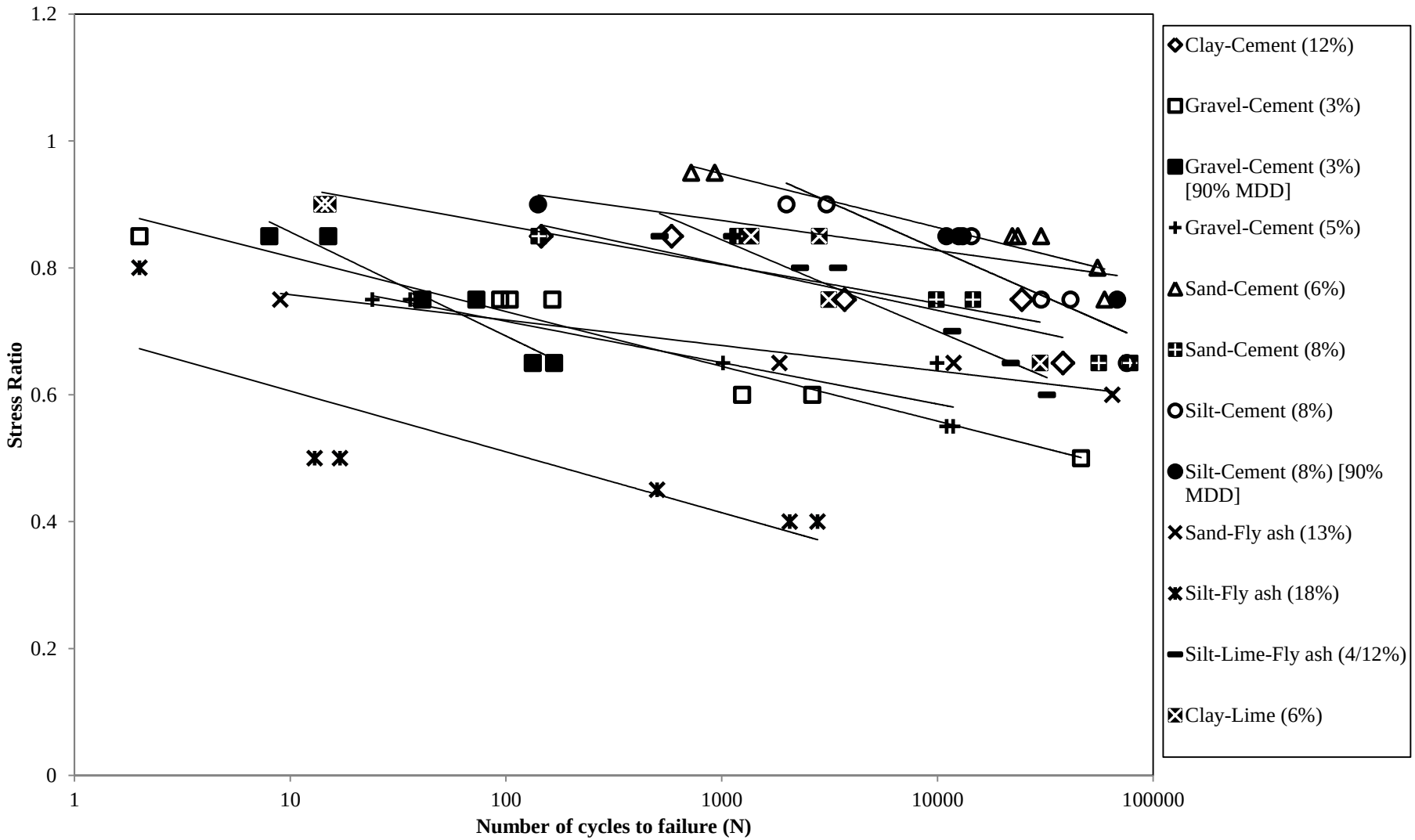

Figure 5.1 Fatigue Modeling of CSLs

The individual plots for each mixture are shown in Appendix D. Equation 5.1 is a good fit for estimating the fatigue life. The R^2 values for the different specimens range between 0.70 and 0.95. Table 5.1 shows the regression parameters and R^2 for each mixture shown in Figure 5.1. The regression parameter "*a*" has a range of 0.02 to 0.07; whereas the parameter "*b*" has a range of 0.70 to 1.43.

Table 5.1 Regression Parameters for Each Mixture

Specimen (Binder Content %)	**Regression parameters**		**R^2**
	a	**b**	
Clay-cement (12%)	0.03	1.03	0.82
Gravel-cement (3%)	0.04	0.90	0.95
Sand-cement (6%)	0.04	1.20	0.88
Silt-cement (8%)	0.06	1.43	0.87
Sand-fly ash (13%)	0.02	0.80	0.95
Silt-lime-fly ash (4/12%)	0.06	1.28	0.94
Clay-Lime (6%)	0.03	0.99	0.72
Gravel-cement (3%) [90% MDD]	0.07	1.02	0.93
Silt-cement (8%) [90% MDD]	0.02	1.02	0.74
Gravel-cement (5%)	0.03	0.85	0.89
Sand-cement (8%)	0.03	1.06	0.89
Silt-fly ash (18%)	0.04	0.70	0.70

Figure 5.2 shows the comparison of various fatigue models for concrete which were evaluated by Smith and Roesler (2003). Figure 5.3 shows the S-N curves for the cement-stabilized recycled aggregate (SRA) and other traditional CSMs which were

evaluated by Sobhan and Das (2007). The fatigue models show a general trend of decreasing stress ratio with increasing logarithmic load cycles to failure.

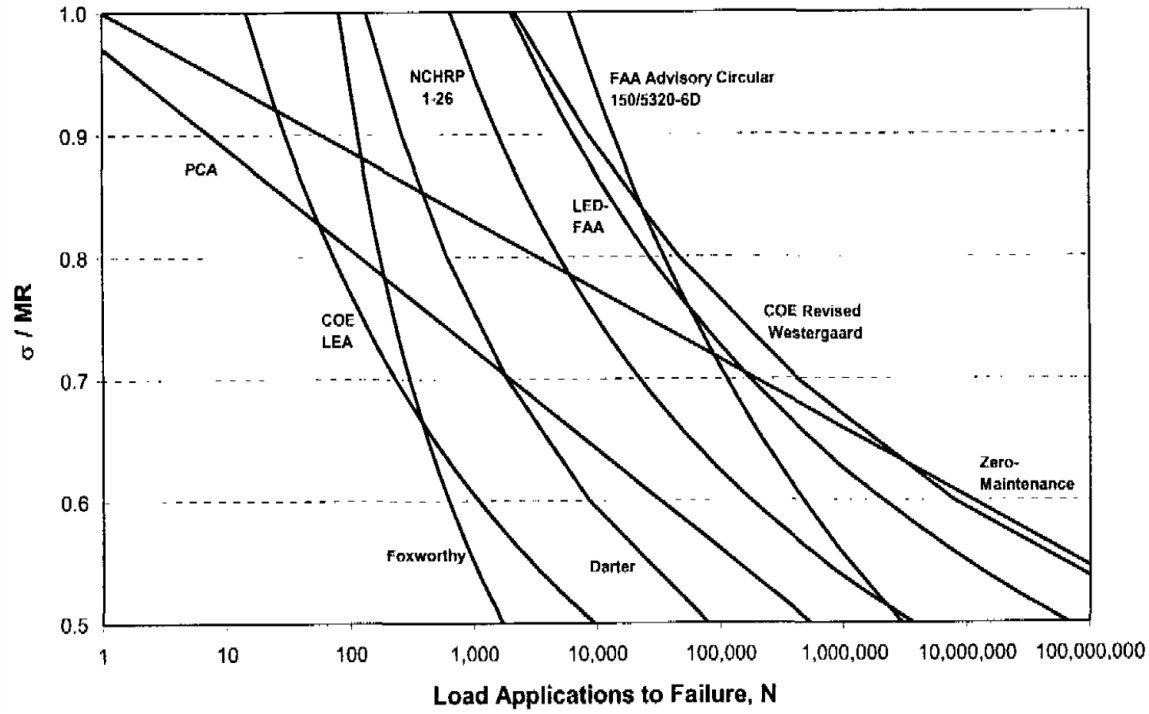

Figure 5.2 Comparison of Concrete Fatigue Models Evaluated by Smith and Roesler (2003)

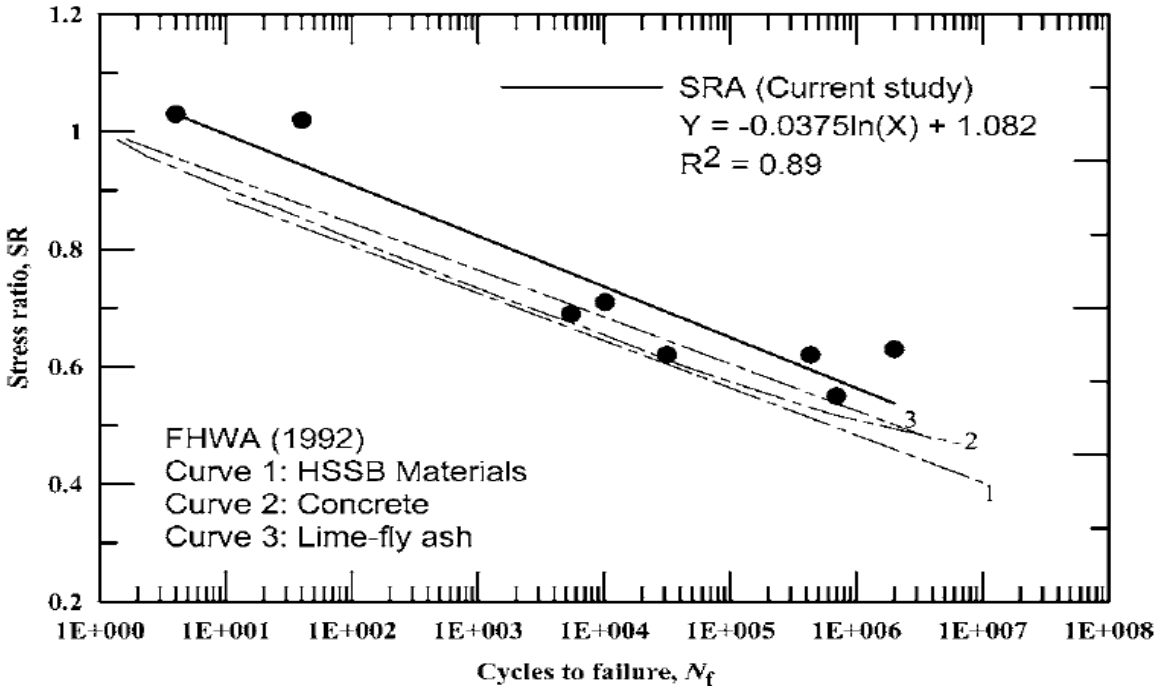

Figure 5.3 Stress Ratio vs. Number of Cycles to Failure for Cement-Stabilized Recycled Aggregate (SRA) and other Traditional Cementitious Materials Evaluated by Sobhan and Das (2007)

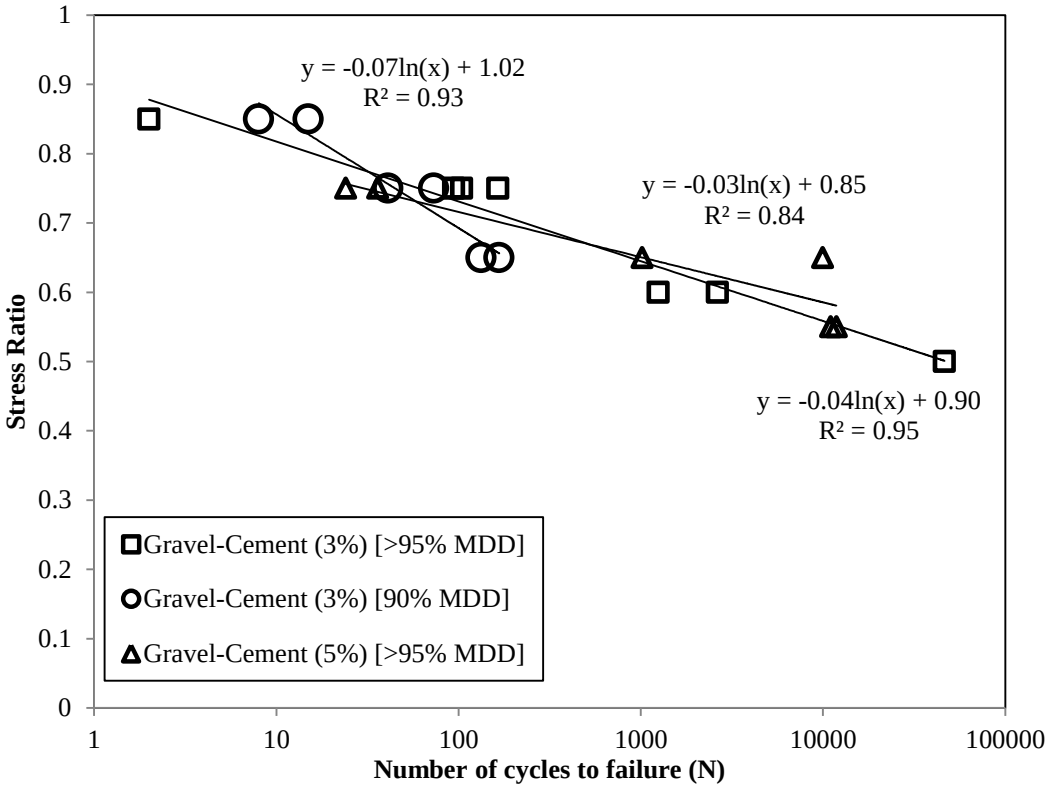

Figure 5.4 Comparison of Fatigue Curves for Gravel-Cement Specimens

Figure 5.4 compares three sets of gravel-cement tests with varying binder content and compaction/density. Fatigue curve for gravel-cement (3% binder) and gravel-cement (5% binder) specimens have nearly the same trend (Figure 5.4). Although the data set is very small, it may be argued that the fatigue life of lower binder content is more than the fatigue life of higher binder content specimens at lower stress levels. Also, for the gravel-cement (3% binder, 90% MDD) specimens, the slope of fatigue curve is steeper than the rest. This implies that specimens at lower density as well do not perform as compared to the specimens compacted to the target density.

Figure 5.5 compares sand-cement specimens with varying binder content. Sand-cement with higher cement content have lower *SR*s at similar *N*, which implies that there is a lower number of cycles to failure at the same *SR* compared to the sand-cement with lower cement content. One explanation may be that specimens with higher cement

content might have more shrinkage cracks, and thus may be more brittle. According to Wu (2011), the higher the percentage of cement, the greater is the susceptibility to shrinkage cracking.

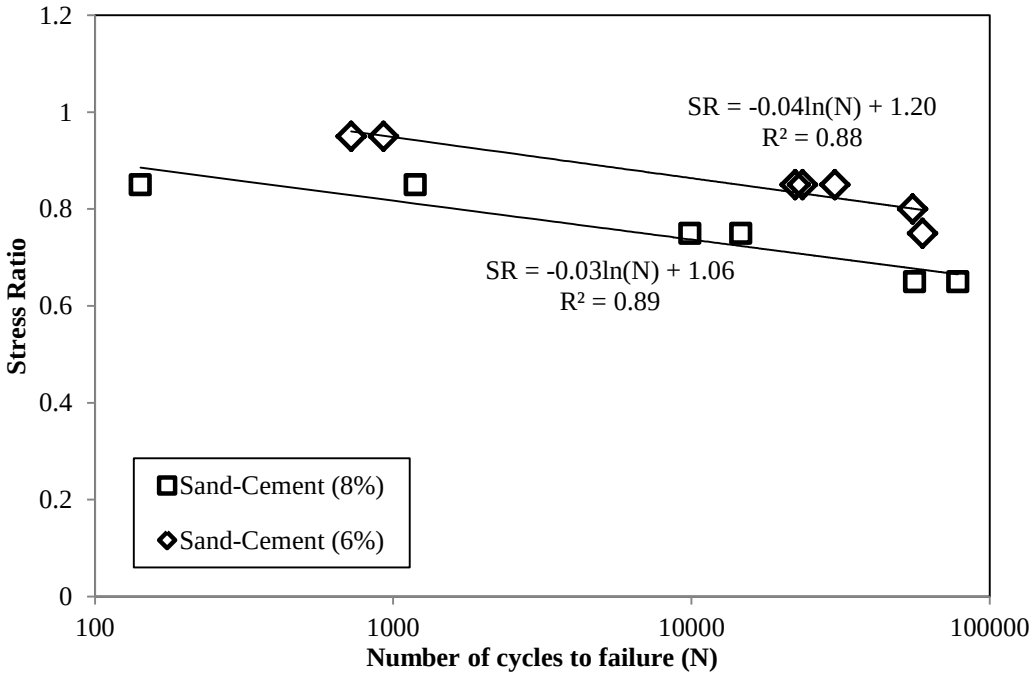

Figure 5.5 Comparison of Fatigue Curves for Sand-Cement Specimens

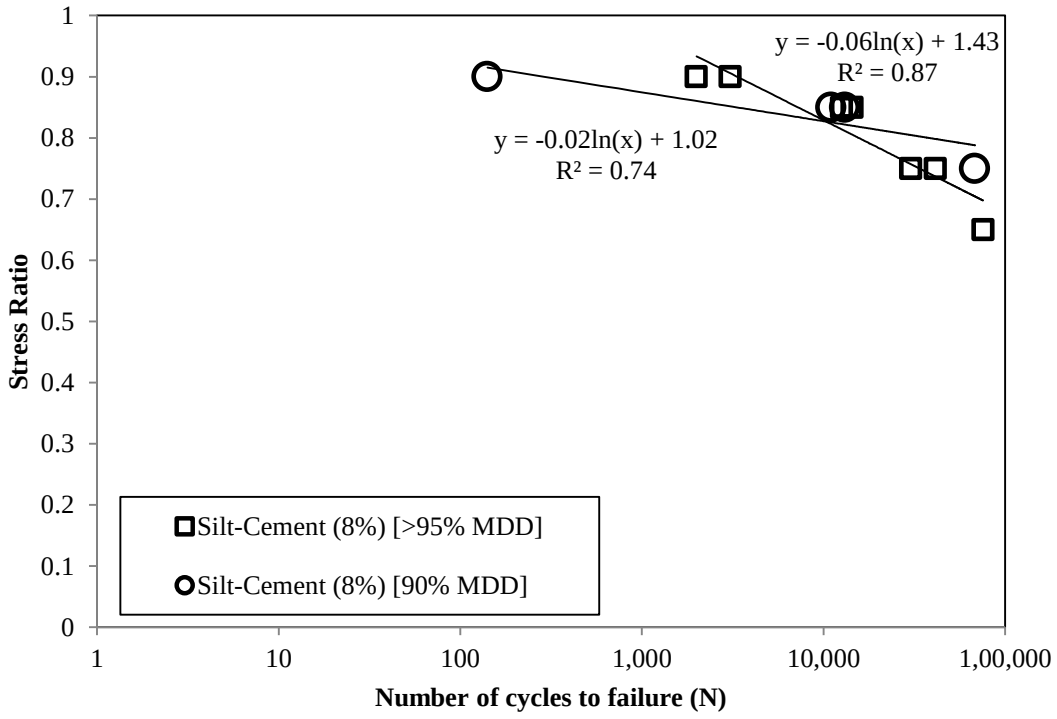

Figure 5.6 Comparison of Fatigue Curves for Silt-Cement Specimens

Figure 5.6 compares silt-cement specimens with respect to compaction effort and the fit lines cross each other; thus, the fatigue life is higher for the specimens stabilized to the target dry density at higher stress levels. However, the fatigue life for the specimens stabilized with reduced density is higher than the specimens stabilized with target dry density at lower stress levels.

Bhattacharya and Pandey (1986) studied the fatigue behavior of lime-laterite soil mixtures with respect to three densities/compaction efforts (light, medium, and heavy), and developed S-N curves similar to this study. The heavily compacted specimens compacted had a better fatigue life. The S-N fatigue curves developed by Bhattacharya and Pandey (1986) showed minimal change. The regression parameter "*b*" was greater than the parameter "*a*" in the S-N curve equation, as in the study conducted by Bhattacharya and Pandey (1986), and Sobhan and Das (2007).

5.2.2 Validation of Experimental Results

The concrete fatigue models described in Table 2.1 are used to check the fit to the laboratory data of this study. Table 5.2 shows the R^2 between the fatigue life from the laboratory data and that from the models. Separate graphs for each mixture showing the relation between laboratory fatigue life and fatigue life calculated from these models are given in Appendix-D.1. The Foxworthy fatigue model is not a good fit to the laboratory data from this study as the R^2 for these models are too low (range between -2.22 to 0.68), except for the silt-fly ash (18%) data (R^2 = 0.79). The other models show varying degrees of suitability in representing the experimental data (range between 0.72 to 1.00).

The FHWA Zero-Maintenance and NCHRP Project 1-26 fatigue models estimated quite a higher fatigue life at lower stress levels (below 60% stress level) (Plots in Appendix-D). The MEPDG fatigue model (Equation 2.3) was also used to validate the

laboratory data. Table 5.3 shows the R^2 between the fatigue life from the laboratory data and the fatigue life calculated from the MEPDG model, including the regression parameters k_1 and k_2. The MEPDG fatigue model is a good fit for our fatigue laboratory data as the R2 for this model or the different mixtures is in the range of 0.74 to 1.00. The regression parameter "k_1" has a range of 0.63 to 1.92; whereas the parameter "k_2" has a range of 0.05 to 0.26. Separate graphs for each mixture showing the relation between laboratory fatigue life and fatigue life calculated from the MEPDG fatigue model are shown in Appendix-D.2.

Roesler et al. (2005) conducted large-scale concrete slab tests in the laboratory to evaluate the effect of multiple wheel gears on the fatigue resistance of concrete slabs. Roesler et al. (2005) found the large-scale slab strengths to be considerably higher than beam strengths which were tested at the same age of curing. The concrete slab flexural strength in the Roesler et al. (2005) study was on an average 2.8 times the strength of simply-supported beams. For slab fatigue testing, Roesler (1998) used the flexural strength of the slab configuration in the stress ratio instead of the beam flexural strength, and found the slab fatigue data resembled the beam fatigue curve of Darter (1977) (i.e. FHWA Zero-Maintenance Fatigue Model). By normalizing the new fatigue data relative to the concrete flexural strength of the test configuration used in the study by Roesler et al. (2005), the fatigue data was found to show a similar behaviour to the Darter (1977) beam fatigue curve and previous slab tests by Roesler (1998).

Table 5.2 Validation of Laboratory Fatigue Data Using Concrete Fatigue Models

Specimens (Binder Content, %)	**R^2 (Laboratory Fatigue Life v/s Model Calculated Fatigue Life)**				
	Darter Fatigue Model	**Foxworthy Fatigue Model**	**NCHRP Project 1-26 Fatigue Model**	**PCA Fatigue Model**	**FHWA Zero-Maintenance Fatigue Model**
	Darter (1990)	**Foxworthy (1985)**	**Thompson and Barenberg (1992)**	**Packard (1973)**	**Darter (1977)**
Clay-cement (12%)	0.72	-0.38	0.74	0.68	0.64
Gravel-cement (3%)	0.99	0.58	1.00	1.00	1.00
Sand-cement (6%)	0.74	-0.99	0.78	0.53	0.42
Silt-cement (8%)	0.89	0.58	0.80	0.67	0.62
Sand-fly ash (13%)	0.51	-2.22	0.81	0.92	0.98
Silt-lime-fly ash (4/12%)	0.93	0.68	0.85	0.77	0.67
Clay-Lime (6%)	0.94	-0.16	0.99	0.99	0.98
Gravel-cement (3%) [90% MDD]	0.93	0.52	0.89	0.82	0.79
Silt-cement (8%) [90% MDD]	0.58	-3.51	0.91	0.96	0.94
Gravel-cement (5%)	0.81	0.58	0.76	0.76	0.68
Sand-cement (8%)	0.82	-0.22	0.88	0.87	0.86
Silt-fly ash (18%)	0.96	0.79	0.95	0.96	0.96

Table 5.3 Validation of Laboratory Fatigue Data Using MEPDG Fatigue Model

Specimens (Binder Content %)	k_1	k_2	R^2
Clay-cement (12%)	1.55	0.20	0.74
Gravel-cement (3%)	0.83	0.07	1.00
Sand-cement (6%)	1.89	0.24	0.82
Silt-cement (8%)	1.92	0.26	0.95
Sand-fly ash (13%)	0.85	0.05	0.98
Silt-lime-fly ash (4/12%)	1.56	0.21	0.98
Clay-Lime (6%)	1.16	0.11	0.99
Gravel-cement (3%) [90% MDD]	1.12	0.22	0.94
Silt-cement (8%) [90% MDD]	1.35	0.12	0.99
Gravel-cement (5%)	1.29	0.18	0.85
Sand-cement (8%)	1.29	0.13	0.95
Silt-fly ash (18%)	0.63	0.07	0.96

5.3 STRAIN-BASED FATIGUE MODEL

5.3.1 Development of Strain-Based Model

Fatigue of a pavement is a form of structural failure. Bottom tension fatigue of CSL occurs as a result of tensile strain at the bottom of the CSL due to repeated traffic loads. The microcracks are initiated at the bottom of the CSL and propagate upwards. The fatigue damage of CSL causes a reduction of CSL modulus and increases the tensile strain at the bottom of the HMA layer and compressive strain at the top of the subgrade (Wen et al., 2009). Otte (1978) developed the strain ratio-based fatigue model which is adopted by the South Africa design guide. Yeo (2008) evaluated the AustROAD's fatigue

model based on laboratory testing and the Accelerated Loading Facility (ALF) pavement performance. It was found that the load-strain exponent in the initial strain-based fatigue model is different between different CSMs. Carteret et al. (2009) studied the strain-based fatigue model, including the South African strain ratio-based fatigue model and AustROAD's initial strain-based fatigue model. Traditional cement-bound materials like concrete and cement stabilized sand have a strain at break of 150 to 200 μm/m and about 125 μm/m, respectively (PowerCem Technologies, 2008).

An attempt to develop a strain-based model using the initial strain (which is calculated from the fatigue test data) is made. The model is a good fit ($R^2 = 0.79$) for only the sand-fly ash mixture. The general equation for the sand-fly ash mixture is:

$$\varepsilon_i = (-m) \ln(N) + n \tag{5.2}$$

where N is flexural fatigue life, m and n are regression parameters, and ε_i is initial strain (με)

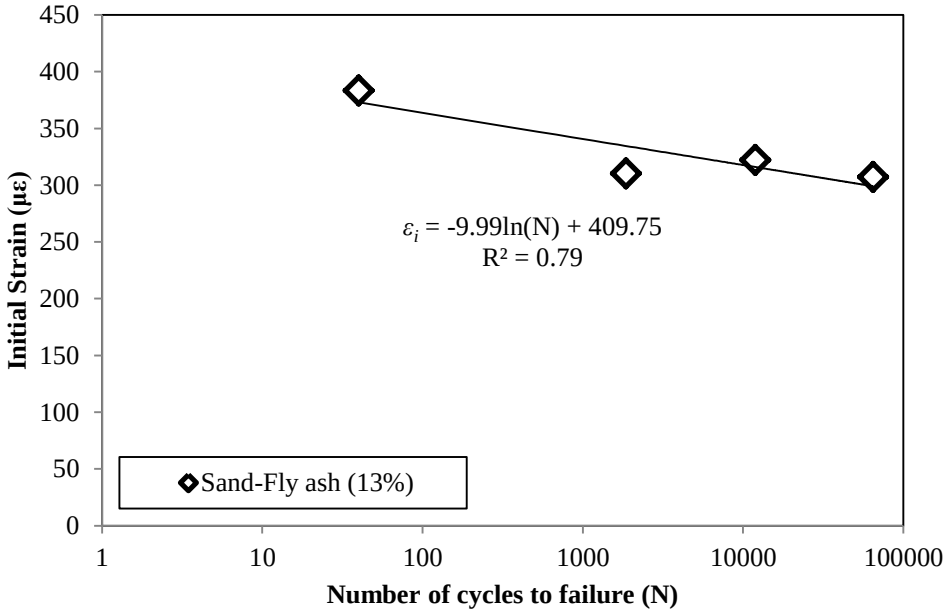

Figure 5.7 Strain Based Fatigue Model for Sand-Fly ash Specimens

Figure 5.7 shows the relationship for the sand-fly ash specimens for the strain-based model. This model was not a good fit (R^2 values ranged from 0.00 to 0.53) for all

other materials (Table 5.4). One possible reason for the model not being a good fit might be due to the limited data. Also, the strain for specimens at different levels was quite wide spread.

5.3.2 Validation of Experimental Results

Several researchers have used the strain and modulus data to develop strain-based fatigue models. Such models are already discussed in Chapter 2.2.3. Our laboratory data are used to fit into the asphalt fatigue models (Table 2.2) and the cement fatigue models (Table 2.3). The strain-based models are not a good fit (R^2 values ranged from -1014.00 to 0.70) to our laboratory data (Table 5.4). Some of the asphalt based models (Dijk and Visser (1977), and Verstraeten et al. (1977 and 1982)) estimated the fatigue life nearly equal to zero using our laboratory data. The asphalt based model (Asphalt Institute, 1982) was a good fit for silt-lime-fly ash mixture ($R^2 = 0.75$), but the predicted fatigue life from this was very high ($> 10^{12}$ cycles).

For the other asphalt-based fatigue models, only the Bonnaure et al. (1980) and Finn et al. (1977) models (Table 5.4) were a good fit to the laboratory data for silt-cement (8%) and silt-lime-fly ash (4/12%) specimens of this study. For silt-cement (3%) specimens, the k1 and k2 values are 1E+20 and 7.12, respectively; and for silt-lime-fly ash (4/12%), the values of k1 and k2 are 2.35E+9 and 3.47, respectively. The relationship between laboratory fatigue life and fatigue life calculated from the models are shown in Appendix D.3. The cement-stabilized fatigue model (Jameson et al., 1992) was a good fit for only the gravel-cement specimens (3%). The relationship between the laboratory fatigue life and the fatigue life calculated from the model is shown in Appendix D.3.

One possible reason that the data from this study was not a good fit for the asphalt based fatigue models was that the variability of the fatigue life for asphalt mixtures is quite high (Pais et al., 2002).

Table 5.4 Validation of Laboratory Fatigue Data Using Strain-Based Fatigue Models

Specimen (Binder %)	Strain-Based Models (R^2)					
	Model from this Study (Eq. 5.2)	**Pell (1987) and Thompson (1987)**	**Bonnaure et al. (1980) and Finn et al. (1977)**	**El-Basyouny and Witzcak (2005)**	**Jameson et al. (1992)**	**Asphalt Institute (1982)**
Clay-cement (12%)	0.00	-1.31	-0.53	-2.70	-0.65	-3.72
Gravel-cement (3%)	0.01	-3.71	-0.93	-18.09	0.70	-0.96
Sand-cement (6%)	0.53	-1014.00	-0.30	-2.36	0.51	-0.05
Silt-cement (8%)	0.00	0.50	0.60	0.49	0.12	0.18
Sand-fly ash (13%)	0.79	21.10	-7.20	-21.1	-0.95	-6.96
Silt-lime-fly ash (4/12%)	0.17	0.29	0.75	0.29	0.39	0.75
Clay-lime (6%)	0.16	-2.21	-2.21	-2.21	0.57	-0.42
Gravel-cement (3%, 90% MDD)	0.00	-0.04	-0.40	-4.29	-0.29	0.28
Silt-cement (8%, 90% MDD)	0.00	-17.91	-17.91	-17.91	-2.11	-4.09
Gravel-cement (5%)	0.13	-0.68	-0.68	-2.76	0.05	0.49
Sand-cement (8%)	0.24	-0.08	-0.08	-1.89	-0.08	-1.61
Silt-fly ash (18%)	0.07	-0.90	-0.90	-88.82	-0.07	-0.46

CHAPTER 6 - RESULTS OF ULTRASONIC PULSE VELOCITY TESTS

6.1 ULTRASONIC PULSE VELOCITY TESTS

The use of seismic modulus tests to monitor the curing or maturity of CSM in a non-destructive way is garnering interest from researchers (Pucci, 2010; Yesiller et al., 2001). Since the ultrasonic pulse velocity test is a non-destructive testing method, the measurement of variation of P-wave velocity (V_p) with curing time for CSMs is possible. Chapter 7 presents the measurement of P-wave velocity and constrained modulus with curing time.

In this study, cement-stabilized soils were cured in a moist room (100% relative humidity at 21°C for 28 days) and fly ash and lime-stabilized soils were cured for 7 days in an oven set at 40 °C. The P-wave velocity measurements were taken after curing. These specimens were then used for flexural strength, flexural modulus, and fatigue cracking testing. PUNDIT-Plus equipment was used to record the time required for the ultrasonic P-wave to travel through the beam specimen, which was then used to calculate the P-wave velocity of the specimen and the constrained modulus (see Chapter 3.3.6). As the ultrasonic pulse velocity test is a non-destructive type of testing, these tests were conducted before the specimens were tested for the flexural strength, flexural modulus and fatigue cracking. ASTM C597 was followed in this study. The constrained modulus and P-wave velocity for the CSM are presented in Appendix E. The results include all

specimens that were tested for the flexural strength; including those specimens with varying density, curing time, and binder content.

Figure 6.1 shows the comparison of the constrained modulus for the specimens with reduced dry density as compared to those specimens compacted with target dry density. The average of all specimens for a specific mixture is provided in Figure 6.1a. The comparison for the P-wave velocity for the specimens with reduced dry density as compared to those specimens compacted with target dry density is shown in Figure 6.1b. With the decrease in density of the specimens, constrained modulus and P-wave velocity decreases (as is the case for flexural strength, see Chapter 4.1.1).

Figure 6.2a and 6.3a show the comparison of constrained modulus for specimens with different binder contents and curing time, respectively. All specimens for a mixture are plotted. The comparison for the P-wave velocity of the specimens is shown in Figure 6.2b and 6.3b. With the increase in binder content and curing time of the specimens, the constrained modulus and P-wave velocity increases (as is the case for flexural strength, see Chapter 4.1.2 and 4.1.3).

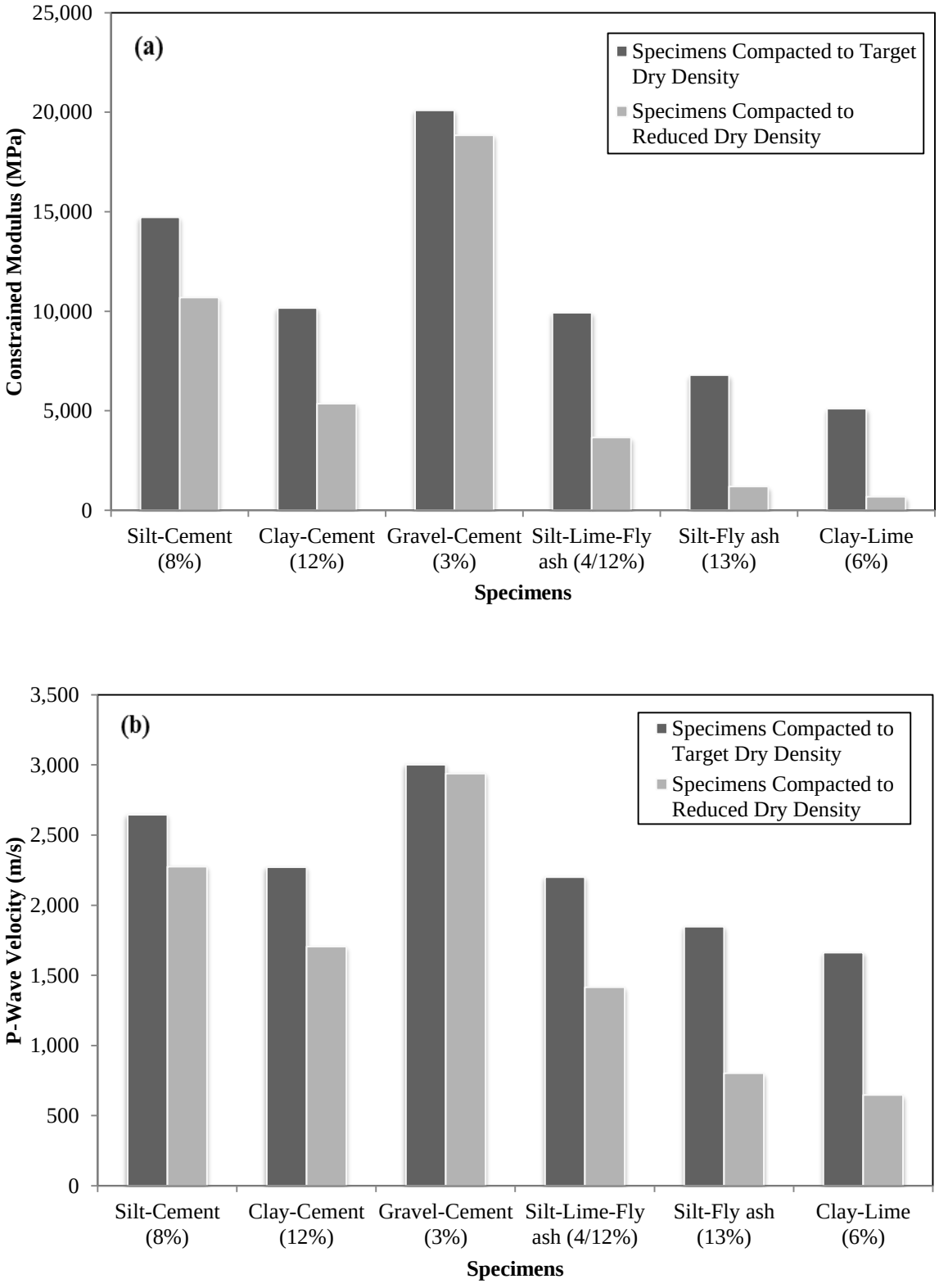

Figure 6.1 Effect of Density/Compaction on CSMs

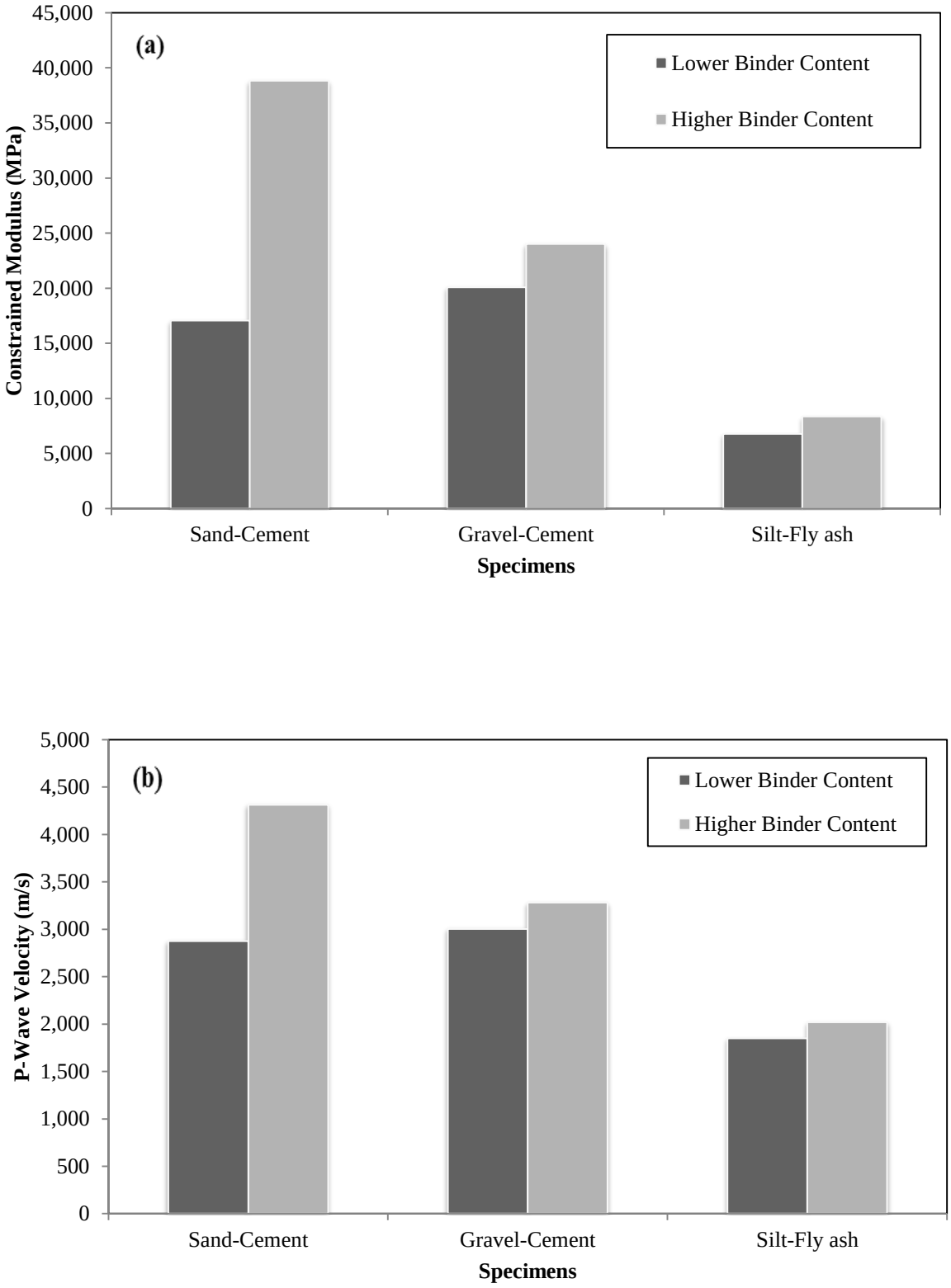

Figure 6.2 Effect of Binder Content on CSMs

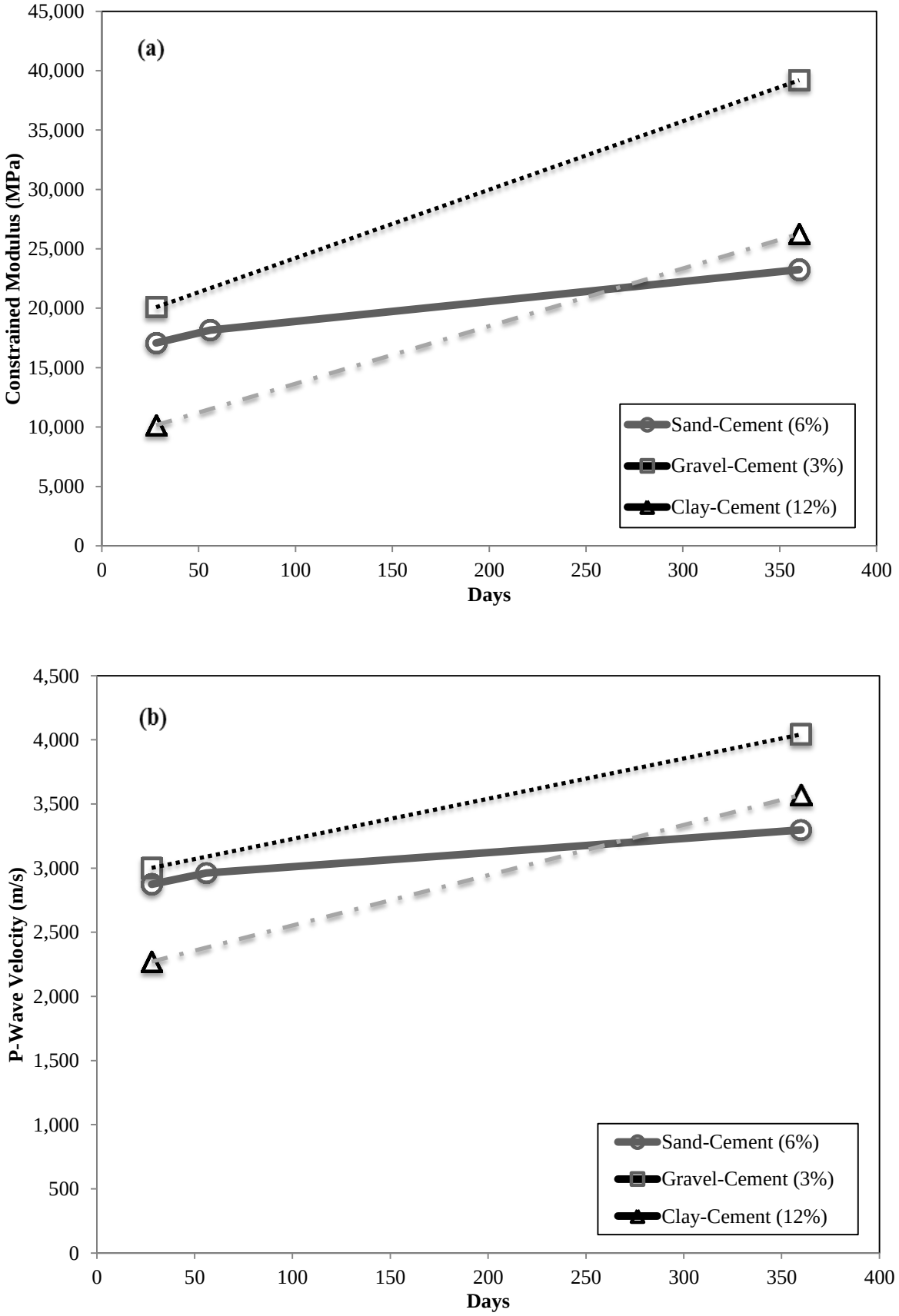

Figure 6.3 Effect of Curing Period on CSMs

6.2 RELATIONSHIP BETWEEN CONSTRAINED MODULUS OR P-WAVE VELOCITY AND FLEXURAL STRENGTH

The ultrasonic pulse velocity technique is a popular non-destructive technique to assess the properties of concrete. The relationship between constrained modulus and flexural strength of the CSMs tested was presented in Figure 6.1. For each mixture, two or more replicate tests were conducted for comparison of constrained modulus and flexural strength. The flexural strength of CSMs increased with increasing constrained modulus; thus, Eq. 6.1 may provide a reasonable method to estimate the flexural strength of CSMs from constrained modulus:

$$FS = 0.08\ (CM)^{0.91} \qquad [R^2 = 0.89] \tag{6.1}$$

where *FS* is flexural strength (kPa) and *CM* is constrained modulus (MPa)

Similarly, Eq. 6.2 may be appropriate to estimate the flexural strength of CSMs from P-wave velocity:

$$FS = 9E\text{-}05\ (V_p)^{1.97} \qquad [R^2 = 0.90] \tag{6.2}$$

where *FS* is flexural strength (kPa) and V_p is P-wave velocity (m/s)

Figures 6.4 and 6.5 show the relationship between constrained modulus and flexural strength and P-wave velocity and flexural strength, respectively, for all stabilized soil. The individual figures for each coarse- and fine-grained soil are shown in Appendix E.

The relationship between constrained modulus (or P-wave velocity) and flexural modulus with respect to soil type (i.e., sand, gravel, silt, and clay) and binder (i.e., cement, class C fly ash, class F fly ash, and lime) are shown in Appendix E. Table 6.1 summarizes the relationships developed between constrained modulus and flexural

strength from the ultrasonic wave testing on the CSMs. The best fit curve was chosen to develop the equations.

Table 6. 1 Summary for Relationship between Constrained Modulus and Flexural Strength

Relationship	**R^2**	**Relationship for Soil Type**
$FS = 0.08\ CM^{0.91}$	0.89	All Stabilized Soils
$FS = 1E\text{-}06\ CM^{2} + 0.03\ CM + 31.99$	0.92	Fine-grained CSMs
$FS = 0.13\ CM^{0.86}$	0.85	Coarse-grained CSMs
$FS = 2E\text{-}06\ CM^{2} + 0.006\ CM + 61.66$	0.88	Silt stabilized with binders
$FS = 0.06\ CM - 20.99$	0.98	Clay stabilized with binders
$FS = 0.31\ CM^{0.77}$	0.90	Sand stabilized with binders
$FS = 0.04\ CM^{0.98}$	0.83	Gravel stabilized with binders
$FS = 0.92\ CM^{0.67}$	0.64	Cement-stabilized soils
$FS = 33.57\ e^{0.0002CM}$	0.91	Class C fly ash-stabilized soils
$FS = 0.21\ CM^{0.80}$	0.96	Lime/class F fly ash-stabilized soils

FS = Flexural strength (in kPa); CM = Constrained modulus (in MPa)

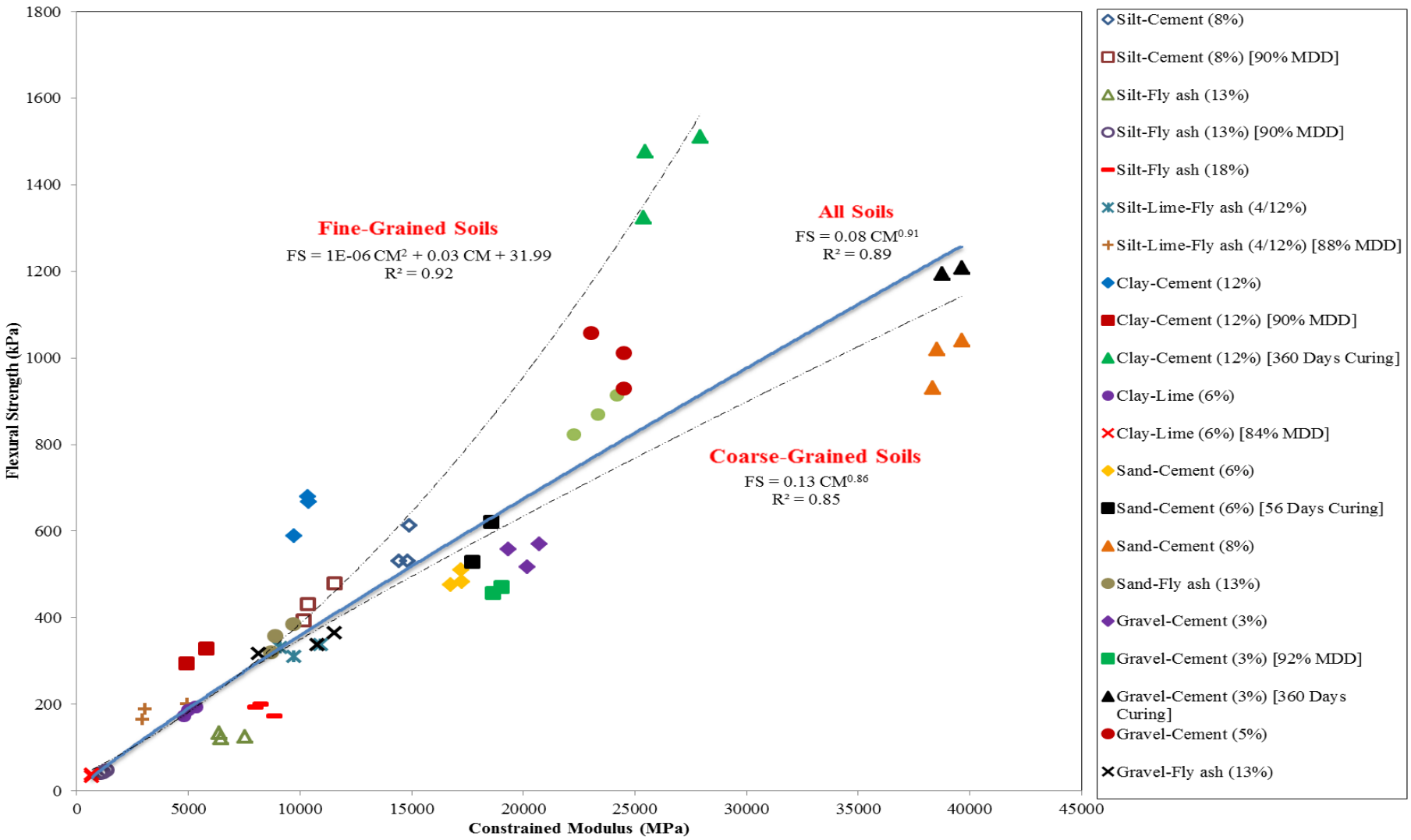

Figure 6.4 Relationship between Constrained Modulus and Flexural Strength for CSMs

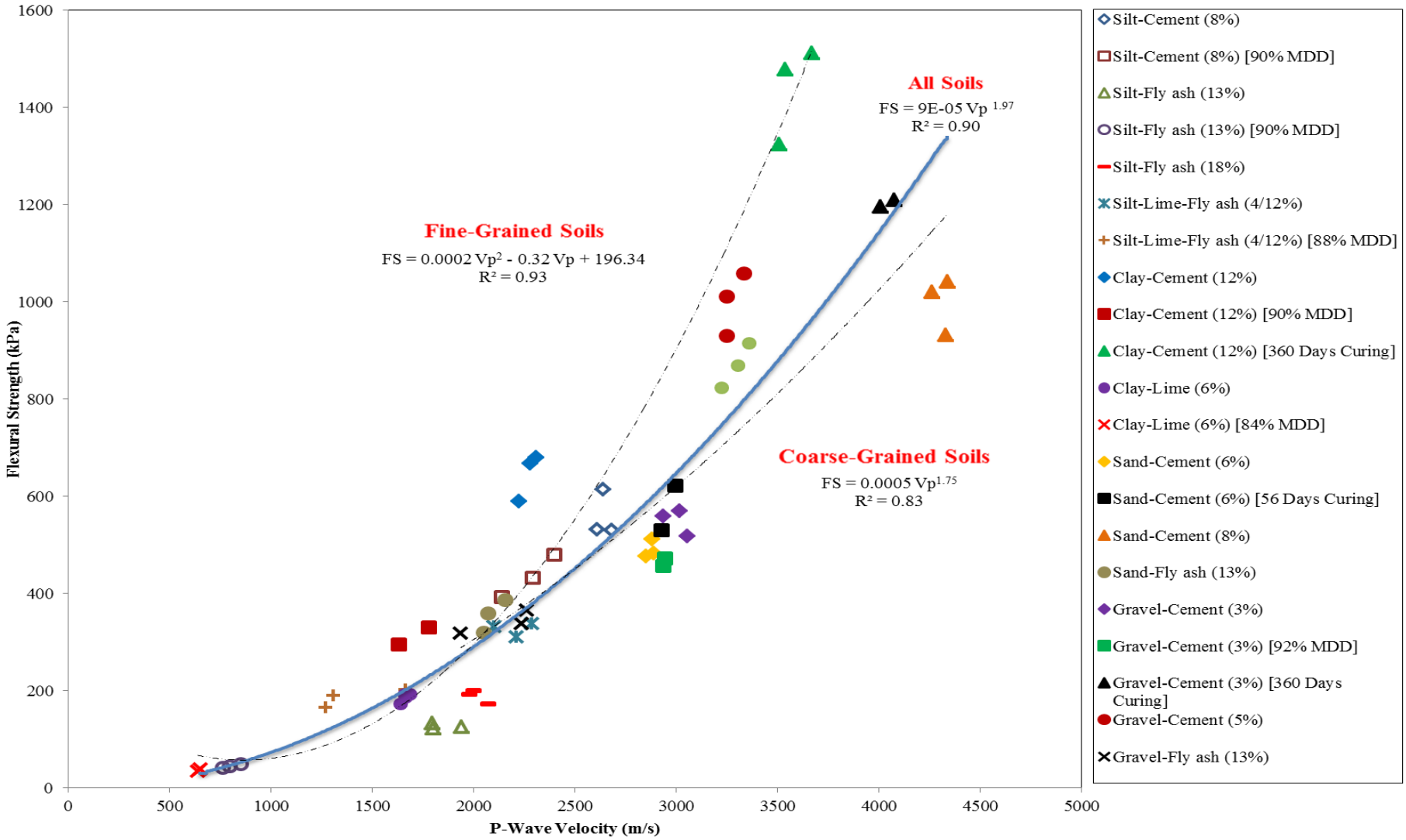

Figure 6.5 Relationship between P-wave Velocity and Flexural Strength for CSMs

Table 6.2 shows the summary of all the relationships developed between P-wave velocity and flexural strength from the ultrasonic wave testing on the CSMs. The best fit curve was chosen to develop the equations.

Table 6.2 Summary for Relationship between P-wave Velocity and Flexural Strength

Relationship	**R^2**	**Relationship for Soil Type**
FS = 9E-05 $V_p^{1.97}$	0.90	All Stabilized Soils
FS = 0.0002 V_p^2 - 0.32 V_p + 196.34	0.93	Fine-grained CSMs
FS = 0.0005 $V_p^{1.75}$	0.83	Coarse-grained CSMs
FS = 18.50 $e^{0.0013\,Vp}$	0.85	Silt stabilized with binders
FS = 2E-05 $V_p^{2.23}$	0.97	Clay stabilized with binders
FS = 0.003 $V_p^{1.54}$	0.89	Sand stabilized with binders
FS = 70.12 $e^{0.0007Vp}$	0.85	Gravel stabilized with binders
FS = 0.005 $V_p^{1.48}$	0.66	Cement-stabilized soils
FS = 13.39 $e^{0.0014Vp}$	0.87	Class C fly ash-stabilized soils
FS = 0.0005 $V_p^{1.75}$	0.96	Lime/class F fly ash-stabilized soils

FS = Flexural strength (in kPa); V_p = P-Wave Velocity (in m/s)

The constrained modulus was calculated using the dry density for each specimen. The R^2 for constrained modulus and flexural strength (Table 6.1) and for P-wave velocity and flexural strength (Table 6.2) is essentially the same (difference of 0.01 and 0.02) and slightly higher for the class C fly ash-stabilized specimens (0.04). Because the change in density does not significantly change the fit, P-wave velocity is proposed to compute

flexural strength. For comparison, Yesiller et al. (2001) studied the use of ultrasonic pulse velocity testing method on stabilized soils and found the strength to increase to increase over time. Yesiller et al. (2001) found good co-relation between velocity and strength for fly ash-stabilized soil. Su (2012) studied the characteristics of ultrasonic wave on cementitiously stabilized materials and found the P-wave velocity or/and constrained modulus of the CSMs increased with curing time. Toohey and Mooney (2011) found the growth in seismic modulus for lime-stabilized soil exhibited a power law relationship with curing time.

6.3 RELATIONSHIP BETWEEN CONSTRAINED MODULUS AND FLEXURAL MODULUS

This section describes the relationship between constrained modulus and flexural modulus of the CSMs tested. The ultrasonic wave testing of the specimen was conducted before testing for flexural modulus for each mixture. The constrained modulus for each beam specimen was thus the same, but the flexural modulus at 20%, 30%, and 40% stress level was different. For each mixture, three replicates were tested. Figures 6.6, 6.7, and 6.8 show the relationships for 20%, 30%, and 40% stress level, respectively.

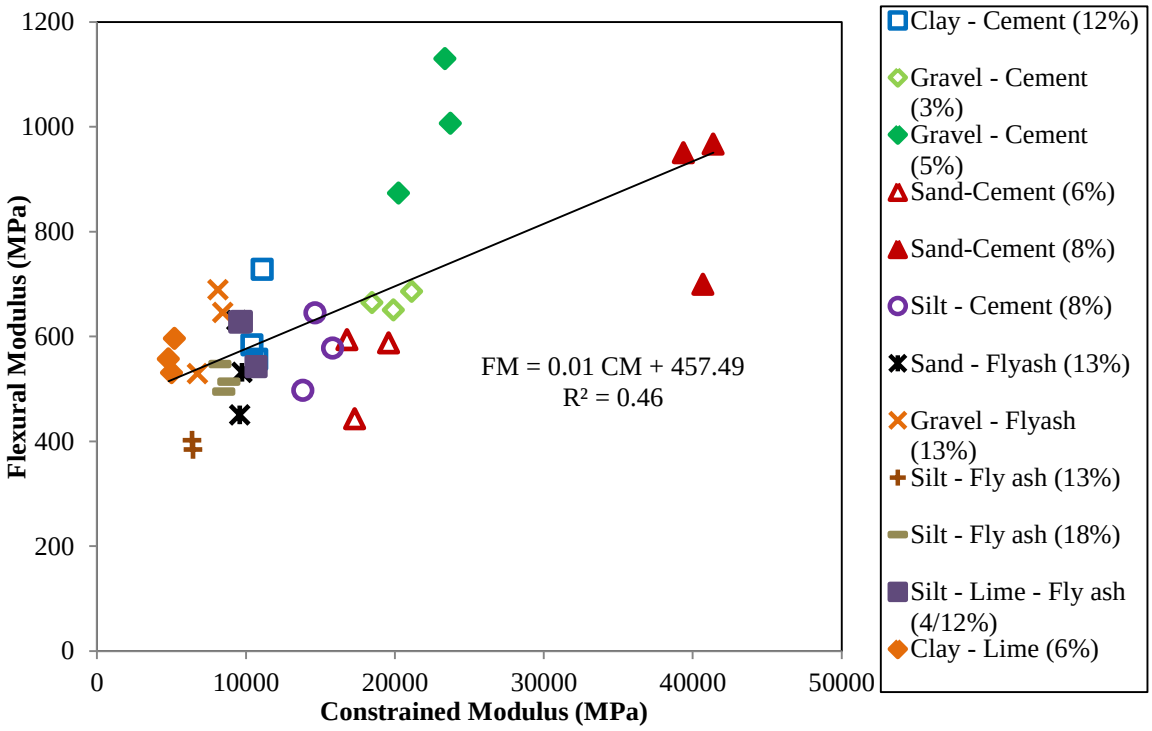

Figure 6.6 Relationship between Constrained Modulus and Flexural Modulus (20% Stress Level) for CSMs

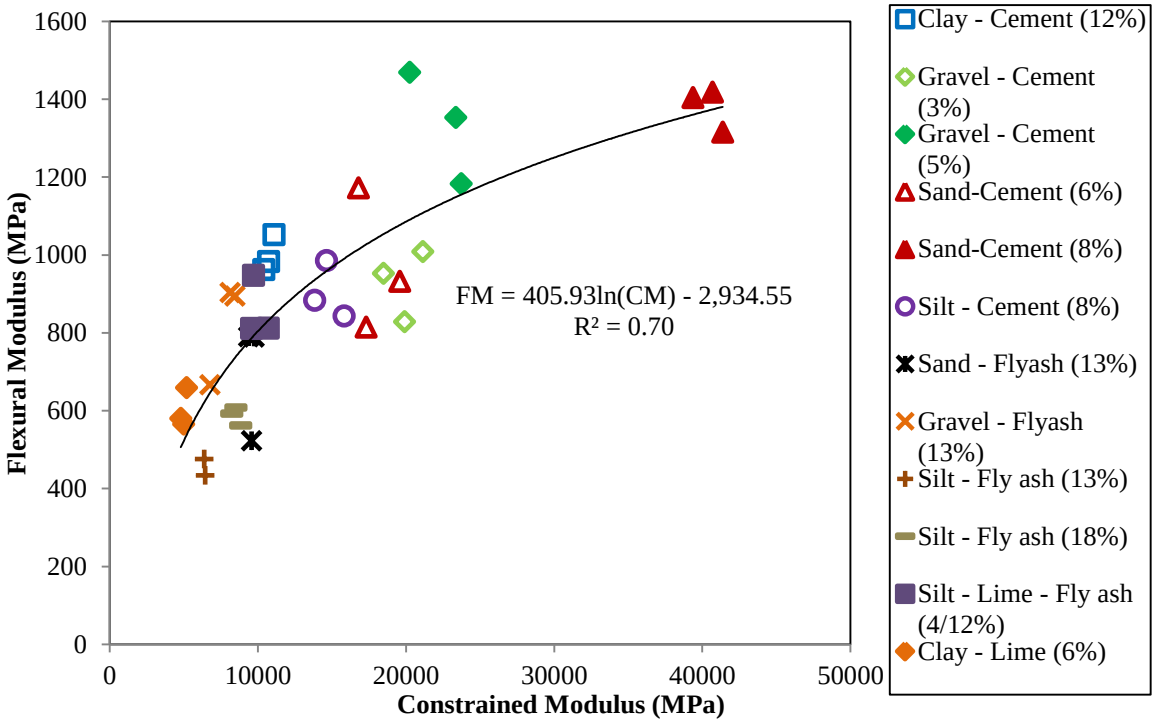

Figure 6.7 Relationship between Constrained Modulus and Flexural Modulus (30% Stress Level) for CSMs

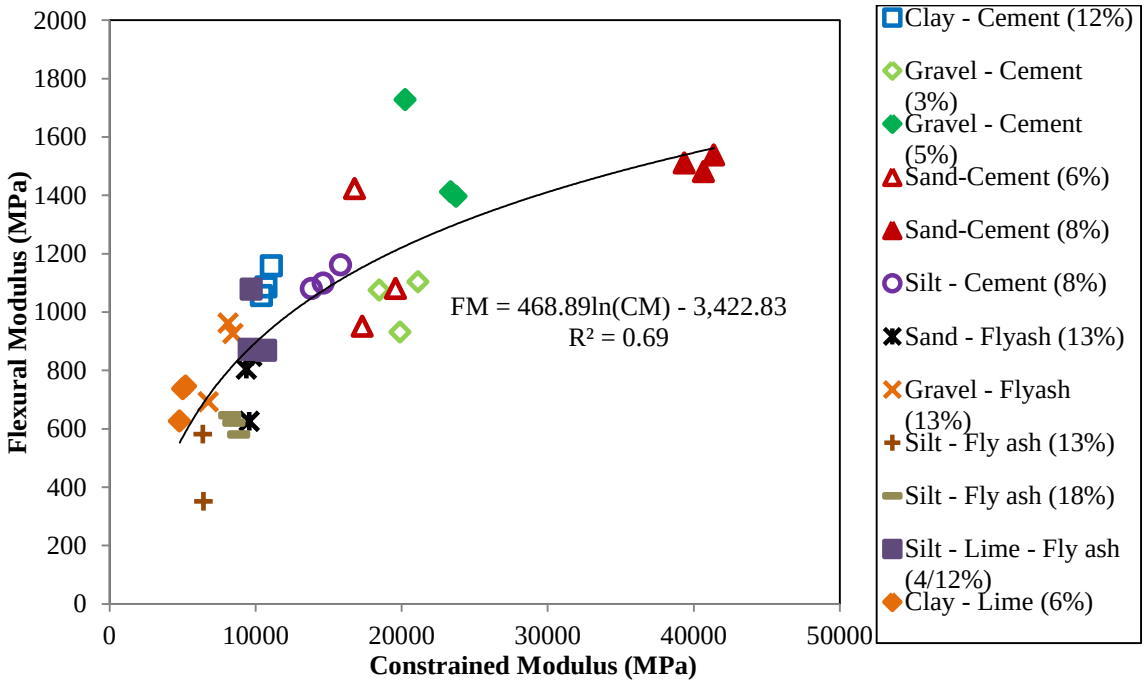

Figure 6.8 Relationship between Constrained Modulus and Flexural Modulus (40% Stress Level) for CSMs

There is a better co-relation for between the constrained modulus and flexural modulus for 30% and 40% stress level (R^2 = 0.70 and 0.69, respectively). The R^2 values for 20% stress levels are quite low (0.46). Table 6.3 summarizes those relationships, which can be used to estimate the flexural modulus of CSMs by using the ultrasonic pulse velocity test. For comparison, in the study by Yesiller et al. (2001), the P-wave velocity increased with increasing modulus of the mixture. P-wave velocity was directly correlated to the stiffness of the stabilized mixtures.

Table 6.3 Summary for Relationship between Constrained Modulus and Flexural Modulus

Stress Level for Flexural Modulus (%)	Relationship	R^2
20	$FM = 0.01\ CM + 457.49$	0.46
30	$FM = 405.93 \ln(CM) - 2{,}934.55$	0.70
40	$FM = 468.89 \ln(CM) - 3{,}422.83$	0.69

CM = Constrained Modulus (in MPa); FM = Flexural modulus (in MPa)

CHAPTER 7 - MODULUS GROWTH TESTS

7.1 MODULUS GROWTH TESTS

This chapter presents results from flexural and constrained moduli testing of gravel-cement, sand-cement, silt-cement, clay-cement and sand-fly ash beam specimens with respect to cure time. In addition, the resilient and constrained moduli testing of the silt-fly ash, silt-lime-fly ash, gravel-fly ash and clay-lime cylindrical specimens are presented with respect to time.

7.2 FLEXURAL MODULUS GROWTH TESTS

The flexural modulus tests were conducted on gravel-cement (3%), sand-cement (6%), silt-cement (8%), clay-cement (12%), and sand-fly ash (13%) beam specimens with the binder contents given in parentheses. Flexural modulus tests were carried out at 30% of the flexural strength (from monotonic tests). Ultrasonic wave testing was used to measure the constrained modulus of the beam specimens. The flexural modulus test procedure was previously detailed in Chapter 3.3.3. The beam specimens were tested for flexural modulus after curing at 28, 56, 90, 120, 150, and 180 days. The silt-cement specimens were tested up to 150 days. Constrained modulus was also determined at 3 and 7 days of curing period. The same specimens were used to conduct the tests over time as these tests are considered non-destructive. Three replicate specimens were tested for each mixture. Table 7.1 and Figure 7.1 show the flexural modulus and constrained modulus of the sand-fly ash specimens for each specimen at different curing period, respectively. As

shown in Table 7.1, the flexural modulus increases over time for Specimen No. 1 and Specimen No. 3, but there is a decrease in flexural modulus at 150 days curing period for Specimen No. 2. This may be due to some damage in the specimens, which are physically handled at each curing period. A similar trend is observed in Figure 7.1, where the constrained modulus increases over time, but decreases for Specimen No. 2 after 120 days of curing.

Table 7.1 Summary of Flexural Modulus Growth over Time (Sand-Fly ash Specimens)

Days Cured	Flexural Modulus (MPa)				COV (%)
	Specimen # 1	Specimen # 2	Specimen # 3	Average	
28	785	736	666	729	8
56	1007	806	838	884	12
90	1032	989	1209	1077	11
120	1258	1370	1235	1288	6
150	1354	373	1324	1017	55
180	1879	407	2026	1437	62

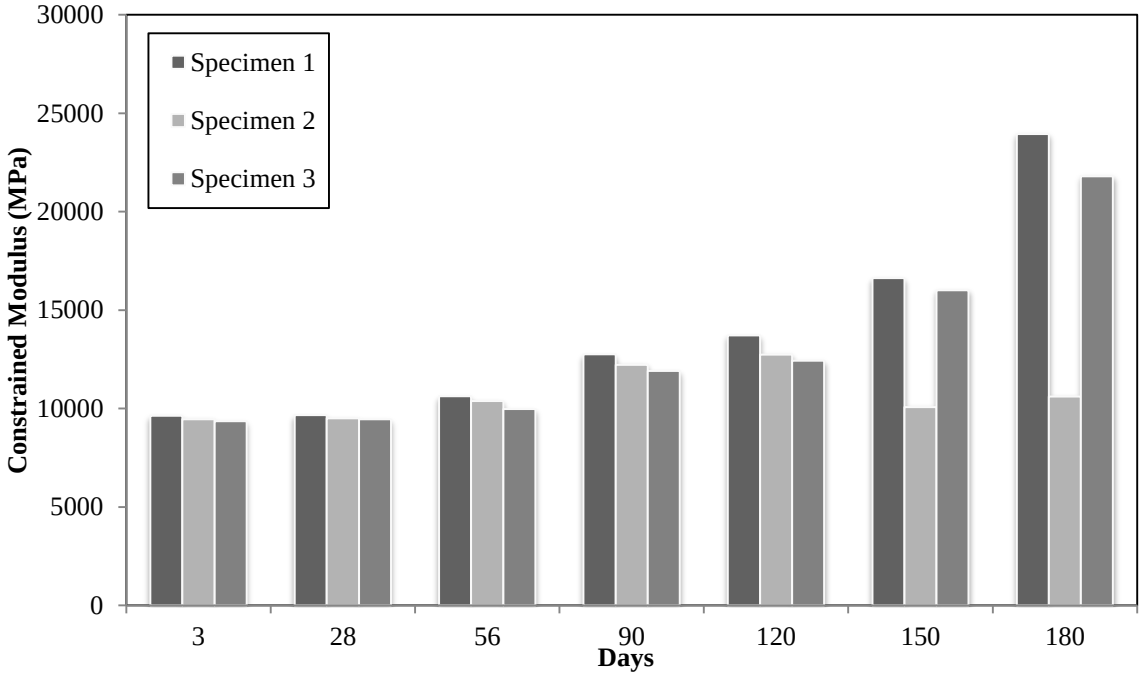

Figure 7.1 Summary of Constrained Modulus Growth over time (Sand-Fly ash Specimens)

Flexural modulus test results for the other specimens are shown in Appendix F.1, and the constrained modulus test results are shown in Appendix F.2. There is a general growth in flexural modulus in at least one specimen for each mixture. Similar trends can be seen in the constrained modulus testing of the same specimens. In general, the gravel-cement specimens had a flexural modulus growth of 82%, sand-cement specimens about 104%, sand-fly ash specimens about 203%, clay-cement specimens about 126% and silt-cement specimens about 120%. The sand-fly ash specimens showed the most rise in flexural modulus over time. For comparison, Su (2012) studied the characteristics of ultrasonic wave on cementitiously stabilized materials and found the P-wave velocity or/and constrained modulus of the CSMs increased with curing time.

7.3 RESILIENT MODULUS GROWTH TESTS

The resilient modulus tests were performed on silt-fly ash (13%), silt-lime-fly ash (4/12%), gravel-fly ash (13%) and clay-lime (6%) cylindrical specimens with the binder content given in the parentheses. Ultrasonic wave testing was used to measure the constrained modulus of the specimens. The resilient modulus test procedure followed is explained in Chapter 3.3.5. The cylindrical specimens were tested for resilient modulus after curing for 28, 56, 90, 120, 150 and 180 days. The clay-lime specimens were tested up to 150 days. Constrained modulus was also determined at 3 and 7 days curing period. The same specimens were used to conduct the tests over time as these tests are considered non-destructive. Three replicate specimens were tested for each mixture.

Figure 7.2 and 7.3 shows the internal and external resilient modulus, respectively for the silt-fly ash specimen at different curing periods. The internal and external resilient moduli were determined based on the LVDT installed internally on the specimen and externally.

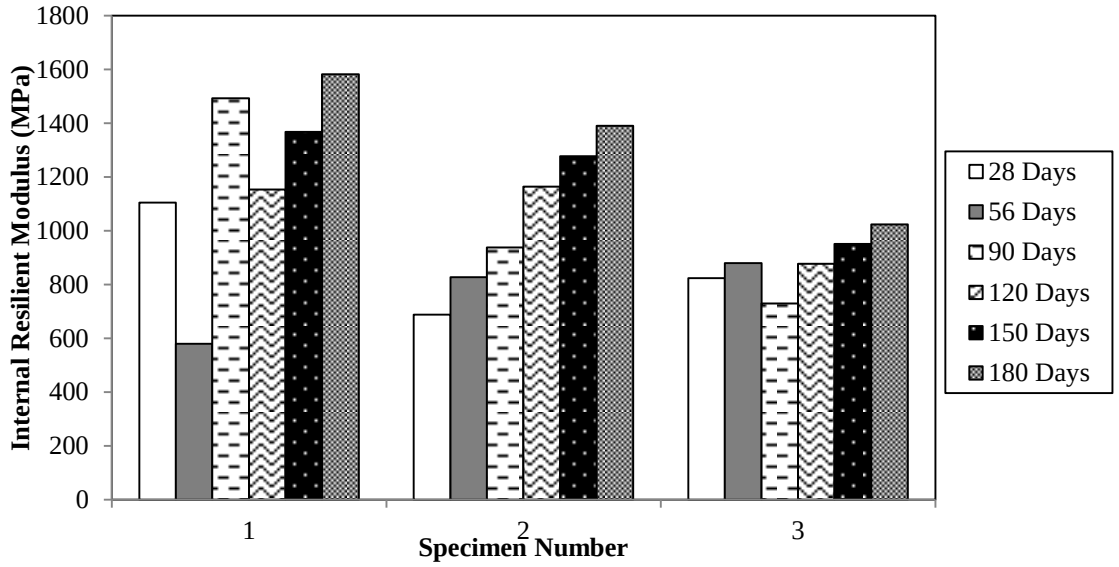

Figure 7.2 Summary of Internal Resilient Modulus Growth over time (Silt-Fly ash Specimens)

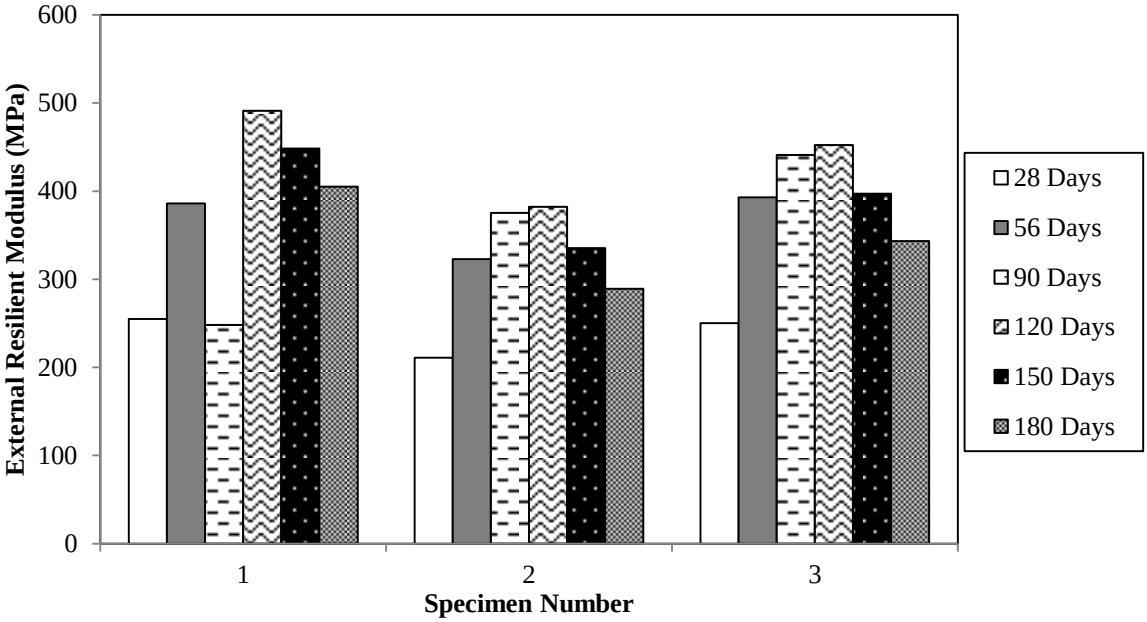

Figure 7.3 Summary of External Resilient Modulus Growth over time (Silt-Fly ash Specimens)

Figure 7.4 shows the constrained modulus for the silt-fly ash specimens at different curing periods.

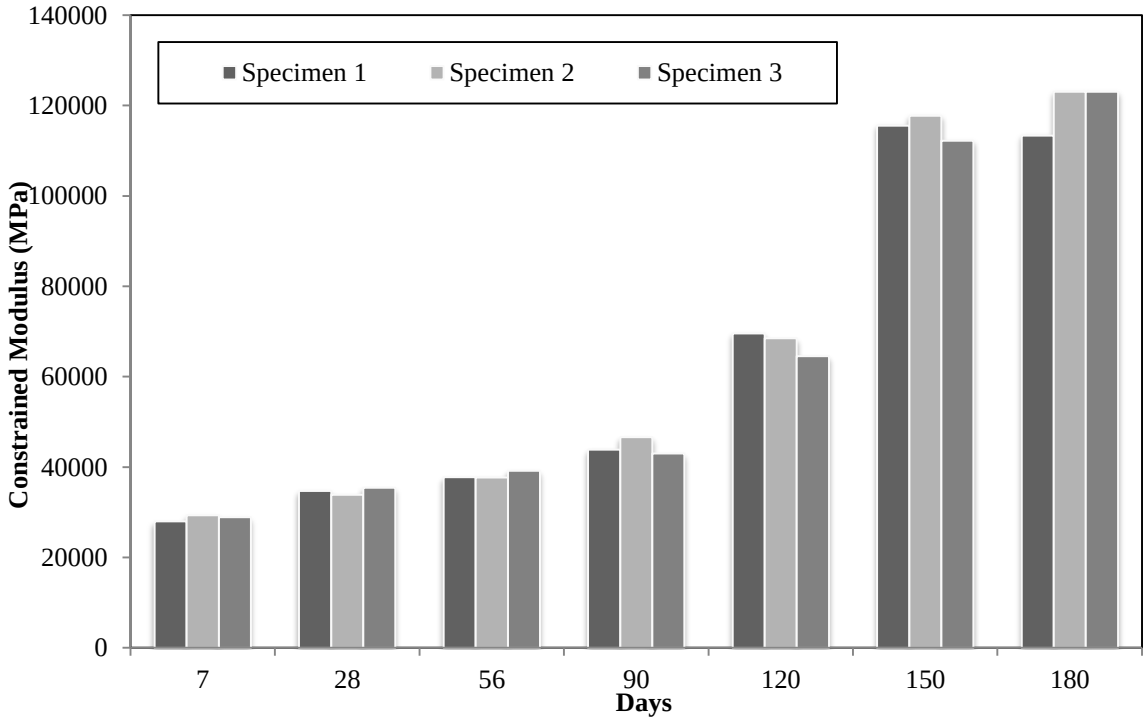

Figure 7.4 Summary of Constrained Modulus Growth over time (Silt-Fly ash Specimens)

The results of constrained modulus and resilient modulus for the other specimens are shown in Appendix F.2 and F.3, respectively. From these results, the resilient modulus does not increase with time for these specimens in all cases. This might be due to the testing of the same specimen at different curing periods, which may have damaged the specimen. For comparison, Pericleous and Metcalf (1996) studied the dependence of resilient modulus of cement-stabilized phosphogypsum on material parameters and found resilient modulus to increase with curing period. Achampong et al. (1997) studied the effect of curing period on resilient modulus of lime- and cement-stabilized cohesive soils, and found the resilient modulus to increase with curing period.

CHAPTER 8 - CONCLUSIONS

The objective of this research was to recommend laboratory procedures to measure performance related characteristics of pavement layers stabilized with cement, lime, and fly ash and to provide validated distress models to be incorporated into MEPDG. To reach this objective, nine CSMs, including gravel, sand, silt, and clay stabilized with cement, lime, and fly ash, were selected for laboratory fatigue and modulus growth tests. Third-point flexural beam test was found suitable to characterize the fatigue behavior of all cementitiously stabilized materials. Ultrasonic pulse velocity measurements were also conducted to assess non-destructively the flexural strength and flexural modulus of base and subgrade soil stabilized with cement, fly ash, and lime and to track modulus growth with time.

8.1 FLEXURAL STRENGTH

The current flexural strength test is applicable for the whole range of CSMs – both heavily- and lightly-stabilized soils. Flexural strength tests showed clay-cement and silt-fly ash to have the highest (645 kPa) and the lowest flexural strength (127 kPa) among these nine mixtures, respectively. For the three class C fly ash stabilized soils (sand-fly ash, gravel-fly ash and silt-fly ash), the sand-fly ash specimen had the highest flexural strength (354 kPa), while the silt-fly ash specimen had the lowest flexural strength (127 kPa). The range of flexural strength for the nine mixtures was between 127 kPa – 645 kPa. The flexural strength was found to decrease when the specimens were under-compacted, and increase when the binder content and curing period was increased.

8.2 FLEXURAL MODULUS

The results indicate that determination of flexural modulus should be done at a stress level of 30% to obtain consistent results. Flexural modulus testing of the mixtures showed clay-cement and silt-fly ash to have the highest (999 MPa) and the lowest flexural modulus (454 MPa) at the 30% stress level, respectively. The silt-fly ash specimens were the weakest mixture. Two of the specimens failed while conducting the flexural modulus tests. For the fly ash-stabilized soils, the gravel-fly ash had the highest flexural modulus (821 MPa). The flexural modulus was found to increase with binder content for all stress levels. A linear relationship was developed between the flexural strength and flexural modulus (R^2 = 0.95). Also, a relationship between the unconfined compressive strength and flexural strength was found (R^2 = 0.92).

8.3 FATIGUE CRACKING

From the fatigue cracking testing of the CSMs, the fatigue life was found to be in the range of 1 to 75,537 cycles. The modulus of the specimens kept degrading as the fatigue cracking test continued and the displacement (or deflection) of the specimens increased. The under-compacted specimens showed a lesser fatigue life than the specimens compacted to the target dry density. The sand-cement specimens with higher binder content did not perform well as compared to the sand-cement specimens with lower binder content. The fatigue life of sand-cement (6% binder) was greater compared to the fatigue life of sand-cement (8% binder) at the same stress level. For the gravel-cement specimens, there was not much improvement in the fatigue cracking with increase

in binder content, but the silt-fly ash specimens performed better with increased binder. Based on results, 40% is recommended as lower stress ratio, as some materials have lower fatigue life and 90% is recommended as upper stress ratio.

Sometimes, fatigue cracking tests takes a long time (>8 hrs.) before failure. For practical purposes, the tests should be completed in 8 hrs. i.e., in a working day. This time based on frequency of loading corresponds to approximately 57,600 cycles of loading. When all of the tests are considered (see Appendix C), fatigue failure corresponds to 44% to 64% reduction of the initial modulus (average: 54%). The initial modulus of the specimens can be used to estimate the fatigue life of the unbroken specimens at the end of day-long testing. Midgley and Yeo (2008) recommended a 50% reduction in initial modulus as the fatigue life of cement-stabilized siltstone and cement-stabilized hornfels soils. According to the test results, it is also recommended that a 50% of initial modulus reduction to be used to define the number of cycles to fatigue failure for the specimens which do not fail within 8 hrs. This level of reduction is consistent with Midgley and Yeo (2008) and conservatively approximates the average reduction observed in the tests covering a wider range of materials and binders presented herein. The only exception is sand-Class C fly ash specimens that failed at 44% reduction of their initial modulus.

8.4 FATIGUE PERFORMANCE MODEL

A stress-based fatigue model was developed using two parameters – stress ratio (SR) and fatigue life (N) that resulted in a good fit for estimating the fatigue life. The R^2 values for the different specimens ranged between 0.70 and 0.95. The fatigue data from

this study fitted to the MEPDG fatigue model, and also to most of the concrete fatigue models with varying levels of success. An attempt to develop a strain-based model using the initial strain (which is calculated from the fatigue test data) was also made. The model was a good fit (R^2 = 0.79) for only the sand-fly ash mixture. The strain-based fatigue data was not found to be a suitable fit in this study.

8.5 ULTRASONIC WAVE VELOCITY OF CEMENTITIOUSLY STABILIZED MATERIALS

Results from the ultrasonic pulse velocity tests showed that with decrease in density of the specimens, constrained modulus and P-wave velocity decreases, whereas, with increase in binder content and curing time of the specimens, the constrained modulus and P-wave velocity increases. A relationship was found between the flexural strength and P-wave velocity (R^2 = 0.90) and also between flexural modulus and P-wave velocity (R^2 = 0.70 at 30% stress level).

8.6 MODULUS GROWTH TESTS

Modulus growth tests were conducted using flexural and resilient moduli testing of the specimens. Flexural modulus was found to increase with time. Resilient modulus did not follow the same trend probably due to the selected method that proved to be destructive. This might be due to the testing of the same specimen at different curing periods, which may have damaged the specimens. The ultrasonic pulse velocity tests showed a clear trend of increasing stiffness (constrained modulus) with time for all mixtures.

REFERENCES

AASHTO (2004). "Distribution of the Recommended Mechanistic-Empirical Pavement Design Guide (NCHRP Project 1-37A)",Memo to Interested Reviewers.

AASHTO (2006). "Mechanistic-empirical design of new and rehabilitated pavement structures (NCHRP 1-37)",. Transportation Research Board USA. http://www.trb.org/mepdg/guide.htm last accessed 09/11/2006.

Achampong, F. (1996). "Evaluation of resilient modulus for lime and cement-stabilized synthetic cohesive soils", *PhD Dissertation*, Wayne State University, Michigan.

Adhikari, S. & You, Z. (2010). "Fatigue Evaluation of Asphalt Pavement Using Beam Fatigue Apparatus", *Electronic Journal for Engineering Technology: Technology Interface Journal*, 10(3).

American Coal Ash Association (2008). "Soil Stabilization and Pavement Recycling with Self-Cementing Coal Fly Ash".

ARA (2004). "Guide for Mechanistic-Empirical Design of New and Rehabilitated Pavement Structures," NCHRP Project 1-37A, prepared for National Cooperative Highway Research Program, Washington D.C.

Arnold, G. (2009). "Reducing the risk of pavement failure and utilisation of local materials in New Zealand through Repeated Load Triaxial and Beam Fatigue Tests". *AAPA Thirteenth International Flexible Pavements Conference*, Gold Coast, Queensland, Australia, October 11-13, 2009.

Arora S. and Aydilek A. H., (2005). “Class F Fly-Ash-Amended Soils as Highway Base Material”, *Journal of Materials in Civil Engineering*, Vol. 17, No. 6, November 2005, pp. 640-649.

Achampong, F., Usmen, M., and Kagawa, T. (1997). “Evaluation of Resilient Modulus for Lime- and Cement-Stabilized Synthetic Cohesive Soils”, *Transportation Research Record* 1589, pp70-75

Austroads (2004). “Pavement design”, a guide to the structural design of road pavements. Austroads, Sydney.

Batioja, D.D. (2011). "Evaluation of Cement Stabilization of a Road Base Material in Conjunction with Full-Depth Reclamation in Huaquillas, Ecuador", *MS Thesis*, Brigham Young University, UT.

Bhattacharya, P. G. and Pandey, B. B. (1986). “Flexural Fatigue Strength of Lime-Laterite Soil Mixtures,” *Transportation Research Record*: Journal of the Transportation Research Board, Vol. 1089, pp. 86 – 92.

Bonnaure, F., A. Gravois, and J. Udron, (1980). “A New Method for Predicting The Fatigue Life of Bituminous Mixes,” *Association of Asphalt Paving Technologists*, Vol. 49 Proc., Louisville, KY, Feb 1980.

Carteret R. D., Chen H., Comport L., Firth D., and Howard A., (2009). “Cost-effective Structural Treatments for Rural Highways--Cemented Materials,” Interim Report, Austroads Project No: TT1359, June 2009.

Casmer, J. D., (2011). “Fatigue Cracking Of Cementitiously Stabilized Pavement Layers Through Large-Scale Model Experiments,” *MS Thesis*, University of Wisconsin-Madison, Madison, WI.

Chai, G. W. K., Oh, E. Y. N., and Balasubramaniam, A. S. (2005). "In-Situ Stabilization of Road Base Using Cement - A Case Study in Malaysia", *Proceedings of the fifteenth International Offshore and Polar Engineering Conference*, Seol, Korea. Pp 400

Consoli, N. C., da Silva Lopes Jr., L., and Heineck, K. S. (2009). "Key Parameters for the Strength Control of Lime Stabilized Soils," *Journal of Materials in Civil Engineering*, ASCE, 210-216.

Darter, M.I. (1977). "Design of Zero-Maintenance Plain Jointed Concrete Pavement", Volume I - Development of Design Procedure. FHWA-RD-77-111. Federal Highway Administration, Washington, DC.

Darter, M.I. (1990). "Concrete Slab vs Beam Fatigue Models." *Proceedings of Second International Workshop on the Theoretical Design of Concrete Pavements*. Siguenza, Spain.

Department of the Army, the Navy, and the Air Force (1994). "Soil Stabilization for Pavements," Army TM 5-822-14/Air Force AFJMAN 32-1019, October 1994.

Edil, T., Acosta, H., and Benson, C. H., (2006). "Stabilizing Soft Fine-Grained Soils with Fly Ash," *Journal of Materials in Civil Engineering*, 18(2), 283-294.

El-Basyouny, and Witczak, M., (2005). "Development of the Fatigue Cracking Models for the 2002 Design Guide," *Presented at the 84th Annual Meeting of the Transportation Research Board*, Jan 2005.

Finn, F., C. L. Saraf, K. Kulkarni, K. Nair, W. Smith, and A. Abdullah, (1977). "Development of Pavement Structural Subsystems," Final Report, Project 1-10B, Feb 1977.

Federal Highway Administration, (2003). "Ch. 4 Fly Ash in Stabilized Base Course," Fly Ash Facts for Highway Engineers, Web Site, http:www.fhwa.dot.gov/pavement/recycling/fach04.cfm.

Foxworthy, P.T. (1985). "Concepts for the Development of a Nondestructive Testing and Evaluation System for Rigid Airfiels Pavements". *Ph.D. Dissertation*. University of Illinois, Urbana, IL.

Freeme CR, Maree, JH and Viljoen AW (1982). "Mechanistic design of asphalt pavements and verification using the Heavy Vehicle Simulator". *Proceedings of 5th Int. Conf. Structural Design of Asphalt Pavements*, Ann Arbor, Vol. 1, pp. 156-73.

Gnanendran, C. T., and Piratheepan, J. (2008). "Characterisation of a Lightly Stabilised Granular Material by Indirect Diametrical Tensile Testing," *International Journal of Pavement Engineering*, Vol. 9, No. 6, pp. 445 – 456.

Huang, Y. (2004). "Pavement Analysis and Design", 2nd Ed., Prentice-Hall, Inc., Upper Saddle River, New Jersey.

Hou, X., Zhang, P., and Zhang, M. (2011). "Study on Fracture Toughness of Cement Treated Aggregate", *Advanced Materials Research* Vol. 280 (2011) pp 76-79.

Jameson GW, Sharp KG, Yeo R. (1992). "Cement-treated crushed rock pavement fatigue under accelerated loading: the Mulgrave (Victoria) ALF trial", 1989/1991. Australian Road Research Board Report ARR 229. ARRB, Vermont South.

Judycki, J., (1997). "Comparison of fatigue criteria for flexible and semi-rigid pavements", *Proceedings, 8th International Conference on Asphalt Pavements*, Seattle, Vol.2, p135

Kersten, M. S. (1961). “Soil Stabilization with Portland Cement”. Washington, D. C., National Academy of Sciences National Research Council.

Kim, D., Kweon, G., and Lee, K. (2001). "Alternative method of determining resilient modulus of subgrade soils using a static triaxial test", *Can. Geotech. Journal*, Vol. 38

Laguros, J. G. (1965). “Lime-Stabilized Soil Properties and the Beam Action Hypothesis,” *Highway Research Record*, Vol. 92, pp. 12 – 20.

Lee, J. C., Edil, T.B., Benson, C.H., and Tinjum, J.M. (2010). “Use of BE2ST in-Highways for Green Highway Construction Rating in Wisconsin.” *Proceeding of The 1st T&DI Green Streets & Highway Conference*, Denver, Colorado.

Li, X., and Dong, M. (2011). "Experimental Research on Pavement Performance of Cement-Stabilized Base Recycled Mixture", *Applied Mechanics and Materials* Vols. 94-96 (2011) pp 31-37

Little, D. N. and Nair, S. (2009). “Recommended Practice for Stabilization of Subgrade Soils and Base Materials,” NCHRP Web-Only Document 144, Contractor‟s Final Task Report for NCHRP Project 20-07, Transportation Research Board, National Research Council, Washington, DC.

Litwinowicz, A. and Brandon, A.N. (1994). “Dynamic Flexural Testing for Prediction of Cement-Treated Pavement Life”. *17th ARRB Conference*, Gold Coast, Queensland, August 15-19, 1994, 17(2), 229–247.

Mitchell, J.K. (1970). “Theoretical Approach to Soil-Cement Pavement Thickness Design”, Panel Discussion, Highway Research Board Annual Meeting, January 1970.

Midgley, L. and Yeo, R. (2008). “The Development and Evaluation of Protocols for the Laboratory Characterisation of Cemented Materials,” Austroads Technical Report AP-T101/08, Austroads Inc.

Miner, M.A. (1945). “Cumulative Damage in Fatigue,” Trans. ASME, 67, A159-A164.

Molenaar, A. A. A., and Pu, B. (2008). “Prediction of Fatigue Cracking in Cement Treated Base Courses,” *Proceedings of 6th RILEM International Conference on Cracking in Pavements*, Chicago, IL, pp. 191 – 199.

NAASRA (1987). “Pavement design”, a guide to the structural design of road pavements. Austroads, Sydney.

National Lime Association (2006). “Technical Brief: Mixture Design and Testing Procedures for Lime Stabilized Soil.” Web Site, http://www.lime.org.

Nussbaum, P. J. and Childs, L. D. (1975). “Repetitive Load Tests of Concrete Slabs on Cement-Treated Subbases,” Research and Development Bulletin RD025.01P, Portland Cement Association, Skokie, IL.

Osinubi, K.J., and Nwaiwu, C.M.O. (2006). "Compaction Delay Effects on Properties of Lime-Treated Soil", *Journal of Materials in Civil Engineering*, Vol. 18, No. 2, April 1, 2006.

Otte, E. (1978). “A Structural Design Procedure for Cement-Treated Layers In Pavements,” *PhD Dissertation*, Faculty of Engineering, University of Pretoria.

Packard, R.G. 1973. Design of Concrete Airport Pavement. Engineering Bulletin EB050.03P. Portland Cement Association, Skokie, IL.

Paige-Green, P. and Netterberg, F. (2004). "Cement Stabilization of Road Pavement Materials: Laboratory Testing Programme Phase 1," Confidential Contract Report CR-2003/42 prepared for Cement and Concrete Institute.

Pais, J., Pereira, P., and Picado-Santos, L., (2002). "Variability of Laboratory Fatigue Life of Asphalt Mixes Using Four Point Ebnding Test Results", IJP 2002 Vol 1 Number 2.

Paul, D.K., and Gnanendran, C.T. (2011). "Effect of loading rate on the properties of lightly stabilized granular materials by using flexural beam testing", *Proceedings of Pan-Am CGS Geotechnical Conference*.

Pell, P. S., (1987). "Pavement Materials", Sixth International Conference on The Structural Design of Asphalt Pavements, Vol. 2 Proc., Ann Arbor, MI, Jul 1987.

Pericleous, M.I., and Metcalf, J.B. (1996). "Resilient Modulus of Cement-Stabilized Phosphogypsum", *Journal of materials in Civil Engineering*, 8, pp7-10

Phanikumar, B. R., and Sharma, R. S., (2007), "Volume change behavior of fly ash-stabilized clays," *Journal of Materials in Civil Engineering*., 19(1), 67–74.

Portland Cement Association, (1992). Soil-Cement Laboratory Handbook.

Portland Cement Association, (2011). Web Site, http://www.cement.org

PowerCem Technologies (2008). RoadCem Laboratory guide

Pretorius, P.C., (1970), "Design considerations for pavements containing soil-cement bases", *Ph.D. Dissertation*, University of California, Berkeley, California.

Pucci, M. J. (2010). “Development of a Multi-Measurement Confined Free-Free Resonant Column Device and Initial Studies.” *MS Thesis*, University of Texas, Austin,TX.

Raad, L.(1982). "A Mechanistic Model for Strength and Fatigue of Cement-Treated Soils", *Geotechnical Testing Journal*, Vol. 4, No. 3, Pp. 104-110

ReliaSoft Corporation (2007). Accelerated Life Testing Reference, Tucson, AZ: ReliaSoft Publishing.

Roesler, J.R., Littleton, P.C., Hiller, J.E., and Long, G.E. (2004), “Effect of Stress State on Concrete Slab Fatigue Resistance”, Final Report, Federal Aviation Administration, Atlantic City, NJ, October 2004.

Roesler, J.R., Hiller, J.E., and Littleton, P.C. (2005). "Large-Scale Airfield Concrete Slab Fatigue Tests", *International Journal of Concrete Pavements*, ISCP, Vol. 1, No. 1, Dec. 2005, pp. 66-87.

Sariosseiri, F., and Muhunthan, B. (2008). "Effect of cement treatment on geotechnical properties of some Washington State soils", *Eng Geol* 104(1-2):7

Shirazi, H. (1999). "Field and Laboratory Evaluation of the Use of Lime Fly Ash to Replace Soil Cement as a Base Course", *Transportation Research Record* 1652, pp 270-275

Siqqidue A. and Rajbongshi B., (2005). “An Analytical Study on Design and Analysis of Stabilised Rural Roads,” *Proceedings of the Eastern Asia Society for Transportation Studies*, Vol. 5, 2005, pp. 813 – 828.

Smith, K. D. and Roesler, J. R., (2003). “Review of Fatigue Models for Concrete Airfield Pavement Design”, *ASCE Airfield Pavement Specialty Conference*, Las Vegas, NV, Sept. 21-24, American Society of Civil Engineering.

Sobhan, K. and Das, B. M. (2007). “Durability of Soil-Cements against Fatigue Fracture,” *Journal of Materials in Civil Engineering*, ASCE, pp. 26-32.

Sobhan K. and Krizek R. J., “Resilient Properties and Fatigue Damage in Stabilized Recycled Aggregate Base Course Material,” *Transportation Research Record*, No. 1611, 1998, pp. 28-37.

Sobhan, K., and Mashnad, M., (2003). “Fatigue Behavior of a Pavement Foundation with Recycled Aggregate and Waste HDPE Strips,” *ASCE Journal of Geotechnical and Geoenvironmental Engineering*, Vol. 129, No. 7, pp. 630 – 638.

Solanki, P. (2010). "Characterization of Cementitiously Stabilized Subgrades for Mechanistic-Empirical Pavement Design". *Ph.D. Dissertation*, University of Oklahoma, Norman

Su, Z. (2012). “Durability Performance of Cementitiously Stabilized Layers” *MS Thesis*, University of Wisconsin-Madison, Madison, WI.

Tastan E. O., Edil T. B., Benson C. H. and Aydilek, A. H., (2011),"Stabilization of Organic Soils with Fly Ash," *Journal of Geotechnical and Geoenvironmental Engineering*, 137(9): 819-833.

The Asphalt Institute, (1982). “Research and Development of The Asphalt Institute’s Thickness Design Manual (MS-1) Ninth Edition,” Research Report No. 82-2, Aug 1982.

Thompson, M. R., (1987). "ILLI-PAVE Based Full-Depth Asphalt Concrete Pavement Design Procedure*," Sixth International Conference on The Structural Design of Asphalt Pavements*, Vol. 1 Proc., Ann Arbor, MI, Jul 1987.

Thompson, M.R., and Barenberg, E.J. (1992). "Calibrated Mechanistic Structureal Analysis Procedure for Pavements - Phase 2". Final Report, NCHRP Project 1-26. Transportation Research Board, Washington, DC.

Tian, P., Zaman, M. M., and Laguros, J.G. (1998). "Gradation and Moisture Effects on Resilient Moduli of Aggregate Bases". *In Transportation Research Record: Journal of the Transportation Research Board*, No.1619, Transportation Research Board of the Natonal Accademies, Washington, D.C., 75-84.

Toohey, N.M., and Mooney, M.A. (2011). "Seismic modulus growth of lime-stabilised soil during curing", *Ge´otechnique* 62, No. 2, 161–170.

TRH 14. (1985). "Cementitious Stabilizers in Road Construction South Africa", TRH 14, Pretoria, South Africa.

Verstraeten, J., J. E. Romain, and V. Veverka, (1977) "The Belgian Road Research Center's Overall Approach Structural Design", *Fourth International Conference on The Structural Design of Asphalt Pavements*, Vol. 1, Proc., Ann Arbor, MI, Aug 1977.

Verstraeten, J., V. Veverka, and L. Francken, (1982) "Rational and Practical Design of Asphalt Pavements to Avoid Cracking and Rutting," *Fifth International Conference on The Structural Design of Asphalt Pavements*, Vol. 1 Proc., Netherlands, Aug 1982.

Wang, Y., Zhang, M., Xu, P., and Jian, W. (2011) "Research on the fatigue damage characters of the cement soil under dynamic load", *Advanced Materials Research* Vols. 160-162 (2011) pp 990-995.

Weibull, W. (1961). "Fatigue Testing and Analysis of Results", Pergamon Press, 1961

Wen, H., Balasingam, M., Edil, T., Tinjum, J., Gokce, A., Wang, J., and Casmer, J. (2010). "Characterization of Cementitiously Stabilized Layers for Use in Pavement Design and Analysis," Project 04-36 Interim Report, prepared for National Cooperative Highway Research Program, Washington D.C.

Wen, H., Balasingam, M., Edil, T., Tinjum, J., Gokce, A., Wang, J., Casmer, J., Su, Z. (2011). "Characterization of Cementitiously Stabilized Layers for Use in Pavement Design and Analysis," Project 04-36 Test Procedure Evaluation Report, prepared for National Cooperative Highway Research Program, Washington D.C.

Williams, R. R. and Nazarian, S. (2007). "Correlation of Resilient and Seismic Modulus Test Results." *Journal of Materials in Civil Engineering*, ASCE, No.12, 1026-1032.

Yeo, R., Vuong, B., Alderson, A. (2002). "Towards National Test Methods for Stiffness and Fatigue Characterisation of Stabilised Materials," Report RC2028-002 for Austroads, ARRB Transport Research.

Yeo Y., "Fatigue Performance of Cemented Materials under Accelerated Loading – Influence of Vertical Loading on the Performance of Unbound and Cemented Materials," Austroads, August 2008.

Yesiller N., Hanson J.L., Rener A.T. and Usmen M.A., (2001), “Ultrasonic testing for evaluation of stabilized mixtures,” *Transport Research Record*, 1757, 32–39

Yu, S., Wei, J., and Ma, S. (2011). "Study on Fatigue Life of Lime Fly-ash Treated Aggregate Based on SHRP Standard", *Advanced Materials Research* Vols. 261-263 (2011) pp 111-114

Zha F., Liu S., Du Y., and Cui K., (2008). “Behavior of Expansive Soils Stabilized with Fly Ash,” *Nat Hazards*, Vol. 47, 2008, pp. 509–523.

Zhang, P., Li, Q., and Wei,H. (2010). "Investigation of Flexural Properties of Cement-Stabilized Macadam Reinforced with Polypropylene Fiber", *Journal of Materials in Civil Engineering*, Vol. 22, No. 12.

Zhang, P., Li, Q.F., and Huang, C.K. (2009), *Journal of Grey System*. Vol. 18, p. 355

Zhang, P. & Wei, X. (2011). "Study on Flexural Strength and Flexural Modulus of Elasticity of Cement." *Advanced Materials Research*, 287-290, 990–993.

APPENDIX – A: FLEXURAL STRENGTH TESTING

This section shows the flexural strength test results for all the replicates for each mixture. Tables A1 to A3 provides the flexural strength test results of each of the specimen for clay-cement specimens, clay-cement specimens cured for 360 days, and clay-cement specimens tested with 90% MDD respectively.

Table A1. Flexural Strength Test Results of Clay-Cement Specimens (Binder: 12%)

Specimen Number	Maximum Load at Failure (kN)	Flexural Strength (kPa)	Average Flexural Strength (kPa)	COV (%)
FS-1	2.34	679.06	645.14	7.5
FS-2	2.29	666.79		
FS-3	2.03	589.43		

Table A2. Flexural Strength Test Results of Clay-Cement Specimens (Binder: 12%, 360 Days Cured)

Specimen Number	Maximum Load at Failure (kN)	Flexural Strength (kPa)	Average Flexural Strength (kPa)	COV (%)
FS-1	5.08	1,477.48	1,437.49	6.9
FS-2	4.56	1,324.28		
FS-3	5.20	1,510.71		

Table A3. Flexural Strength Test Results of Clay-Cement Specimens (Binder: 12%, 90% MDD)

Specimen Number	Maximum Load at Failure (kN)	Flexural Strength (kPa)	Average Flexural Strength (kPa)	COV (%)
FS-1	1.13	329.63	312.06	8.0
FS-2	1.01	294.48		

Tables A4 to A7 provides the flexural strength test results of each of the specimen for gravel-cement, gravel-cement specimens tested with 92% MDD, gravel-cement specimens cured for 360 days, and gravel-cement specimens with 5% cement, respectively.

Table A4. Flexural Strength Test Results of Gravel-Cement Specimens (Binder: 3%)

Specimen Number	Maximum Load at Failure (kN)	Flexural Strength (kPa)	Average Flexural Strength (kPa)	COV (%)
FS-1	1.96	569.37	548.06	5.4
FS-2	1.93	560.54		
FS-3	1.77	514.35		

Table A5. Flexural Strength Test Results of Gravel-Cement Specimens (Binder: 3%, 92% MDD)

Specimen Number	Maximum Load at Failure (kN)	Flexural Strength (kPa)	Average Flexural Strength (kPa)	COV (%)
FS-1	1.62	471.12	463.81	2.2
FS-2	1.57	456.50		

Table A6. Flexural Strength Test Results of Gravel-Cement Specimens (Binder: 3%, 360 Days Cured)

Specimen Number	Maximum Load at Failure (kN)	Flexural Strength (kPa)	Average Flexural Strength (kPa)	COV (%)
FS-1	4.16	1,208.72	1,201.69	0.8
FS-2	4.11	1,194.65		

Table A7. Flexural Strength Test Results of Gravel-Cement Specimens (Binder: 5%)

Specimen Number	Maximum Load at Failure (kN)	Flexural Strength (kPa)	Average Flexural Strength (kPa)	COV (%)
FS-1	3.64	1,057.24	999.26	6.5
FS-2	3.20	929.69		
FS-3	3.48	1,010.77		

Tables A8 to A11 provides the flexural strength test results of each of the specimen for sand-cement, sand-cement specimens cured for 360 days, sand-cement specimens cured for 56 days, and sand-cement specimens with 8% cement, respectively.

Table A8. Flexural Strength Test Results of Sand-Cement Specimens (Binder: 6%)

Specimen Number	Maximum Load at Failure (kN)	Flexural Strength (kPa)	Average Flexural Strength (kPa)	COV (%)
FS-1	1.64	476.70	490.08	3.7
FS-2	1.77	510.83		
FS-3	1.67	482.70		

Table A9. Flexural Strength Test Results of Sand-Cement Specimens (Binder: 6%, 360 Days Cured)

Specimen Number	Maximum Load at Failure (kN)	Flexural Strength (kPa)	Average Flexural Strength (kPa)	COV (%)
FS-1	2.83	823.03	862.47	5.2
FS-2	3.14	913.76		
FS-3	2.99	869.29		

Table A10. Flexural Strength Test Results of Sand-Cement Specimens (Binder: 6%, 56 Days Cured)

Specimen Number	Maximum Load at Failure (kN)	Flexural Strength (kPa)	Average Flexural Strength (kPa)	COV (%)
FS-1	1.87	542.69	581.57	9.5%
FS-2	2.14	620.53		

Table A11. Flexural Strength Test Results of Sand-Cement Specimens (Binder: 8%)

Specimen Number	Maximum Load at Failure (kN)	Flexural Strength (kPa)	Average Flexural Strength (kPa)	COV (%)
FS-1	3.60	1,043.59	997.53	6.1
FS-2	3.20	928.58		
FS-3	3.51	1,020.36		

Tables A12 and A13 provides the flexural strength test results of each of the specimen for silt-cement and silt-cement specimens with 90% MDD, respectively. Table A14 shows the flexural strength test results of each of the specimen for sand-fly ash specimens.

Table A12. Flexural Strength Test Results of Silt-Cement Specimens (Binder: 8%)

Specimen Number	Maximum Load at Failure (kN)	Flexural Strength (kPa)	Average Flexural Strength (kPa)	COV (%)
FS-1	1.84	533.58	558.06	8.2
FS-2	1.83	529.86		
FS-3	2.10	610.87		

Table A13. Flexural Strength Test Results of Silt-Cement Specimens (Binder: 8%, 90% MDD)

Specimen Number	Maximum Load at Failure (kN)	Flexural Strength (kPa)	Average Flexural Strength (kPa)	COV (%)
FS-1	1.65	479.19	432.09	9.6
FS-2	1.36	396.03		
FS-3	1.49	432.09		

Table A14. Flexural Strength Test Results of Sand-Fly ash Specimens (Binder: 13%)

Specimen Number	Maximum Load at Failure (kN)	Flexural Strength (kPa)	Average Flexural Strength (kPa)	COV (%)
FS-1	1.33	385.62	353.56	9.4
FS-2	1.22	355.49		
FS-3	1.10	319.43		

Table A15 shows the flexural strength test results of each of the specimen for gravel-fly ash specimens.

Table A15. Flexural Strength Test Results of Gravel-Fly ash Specimens (Binder: 13%)

Specimen Number	Maximum Load at Failure (kN)	Flexural Strength (kPa)	Average Flexural Strength (kPa)	COV (%)
FS-1	1.17	340.11	339.77	7.5
FS-2	1.08	313.99		
FS-3	1.26	365.15		

Tables A16 to A18 provides the flexural strength test results of each of the specimen for silt-fly ash, silt-fly ash specimens with 90% MDD, and silt-fly ash specimens with 18% class C fly ash, respectively.

Table A16. Flexural Strength Test Results of Silt-Fly ash Specimens (Binder: 13%)

Specimen Number	Maximum Load at Failure (kN)	Flexural Strength (kPa)	Average Flexural Strength (kPa)	COV (%)
FS-1	0.43	124.45	126.65	4.5
FS-2	0.46	133.07		
FS-3	0.42	122.38		

Table A17. Flexural Strength Test Results of Silt-Fly ash Specimens (Binder: 13%, 90% MDD)

Specimen Number	Maximum Load at Failure (kN)	Flexural Strength (kPa)	Average Flexural Strength (kPa)	COV (%)
FS-1	0.15	43.71	43.85	2.7
FS-2	0.14	42.75		
FS-3	0.16	45.09		

Table A18. Flexural Strength Test Results of Silt-Fly ash Specimens (Binder: 18%)

Specimen Number	Maximum Load at Failure (kN)	Flexural Strength (kPa)	Average Flexural Strength (kPa)	COV (%)
FS-1	0.69	202.43	190.36	7.2
FS-2	0.60	175.47		
FS-3	0.66	193.26		

Tables A19 and A20 provides the flexural strength test results of each of the specimen for silt-lime-fly ash (class F) and for silt-lime-fly ash (class F) specimens with 88% MDD, respectively.

Table A19. Flexural Strength Test Results of Silt-Lime-Class F Fly ash Specimens (Binder: 4/12%)

Specimen Number	Maximum Load at Failure (kN)	Flexural Strength (kPa)	Average Flexural Strength (kPa)	COV (%)
FS-1	1.17	339.02	328.54	4.3
FS-2	1.07	312.40		
FS-3	1.15	334.19		

Table A20. Flexural Strength Test Results of Silt-Lime-Class F Fly ash Specimens (Binder: 4/12%, 88% MDD)

Specimen Number	Maximum Load at Failure (kN)	Flexural Strength (kPa)	Average Flexural Strength (kPa)	COV (%)
FS-1	0.69	200.98	185.33	9.7
FS-2	0.57	165.75		
FS-3	0.65	189.26		

Tables A21 and A22 provides the flexural strength test results of each of the specimen for clay-lime and for clay-lime specimens with 84% MDD, respectively.

Table A21. Flexural Strength Test Results of Clay-Lime Specimens (Binder: 6%)

Specimen Number	Maximum Load at Failure (kN)	Flexural Strength (kPa)	Average Flexural Strength (kPa)	Coefficient Of Variation (%)
FS-1	0.66	192.43	186.57	4.4
FS-2	0.63	184.43		
FS-3	0.67	193.67		
FS-4	0.61	175.75		

Table A22. Flexural Strength Test Results of Clay-Lime Specimens (Binder: 6%, 84% MDD)

Specimen Number	Maximum Load at Failure (kN)	Flexural Strength (kPa)	Average Flexural Strength (kPa)	Coefficient Of Variation (%)
FS-1	0.12	33.72	35.92	8.8
FS-2	0.13	38.06		

APPENDIX – B: FLEXURAL MODULUS TESTING

This section shows the flexural modulus test results for all the replicates for the mixtures. Table B1 shows the flexural modulus of each replicate for gravel-cement specimens stabilized with 3% cement.

Table B1. Summary of the Flexural Modulus Test Results for Gravel-Cement Specimens (Binder: 3%)

Specimen Number	Stress level by percentage of flexural strength (%)	Flexural Modulus (MPa)	Average Flexural Modulus (MPa)	COV (%)
FM-1	20	650.66	667.14	3
FM-2		664.59		
FM-3		686.16		
FM-1	30	827.99	929.34	10
FM-2		952.03		
FM-3		1,008.15		
FM-1	40	930.86	1,036.28	9
FM-2		1,074.82		
FM-3		1,103.09		

Figures B1 to B3 shows the change in flexural modulus during the test for each replicate for the three different stress level for gravel-cement (3% binder) specimens.

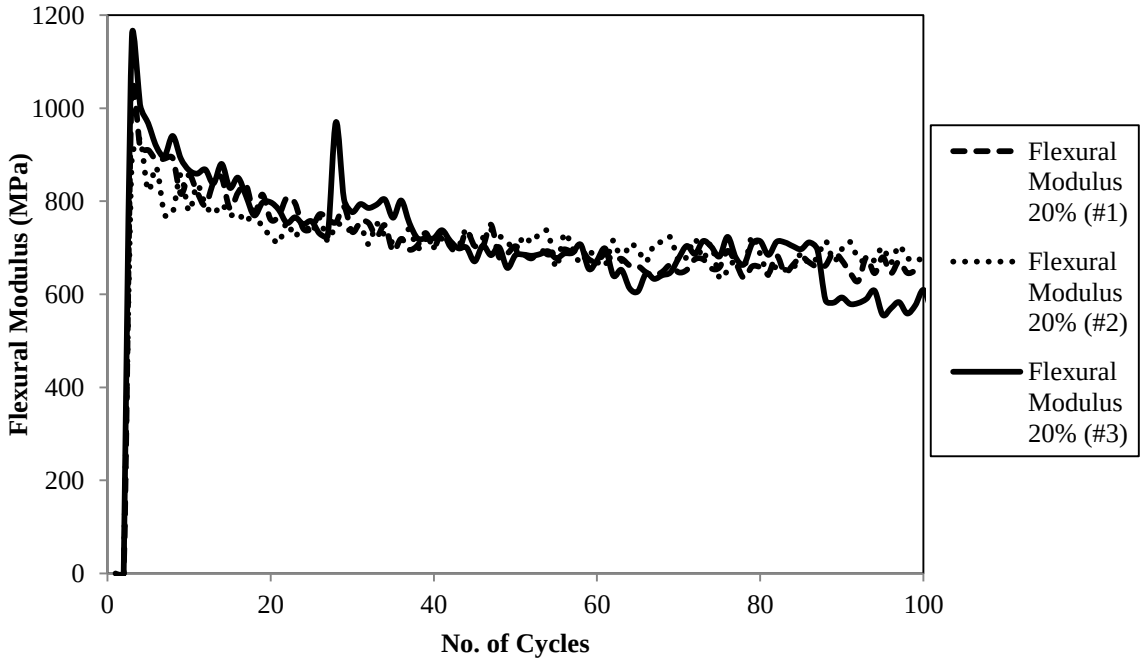

Figure B1. Flexural Modulus Variation at 20% Stress Level for 3 Gravel-Cement Replicates

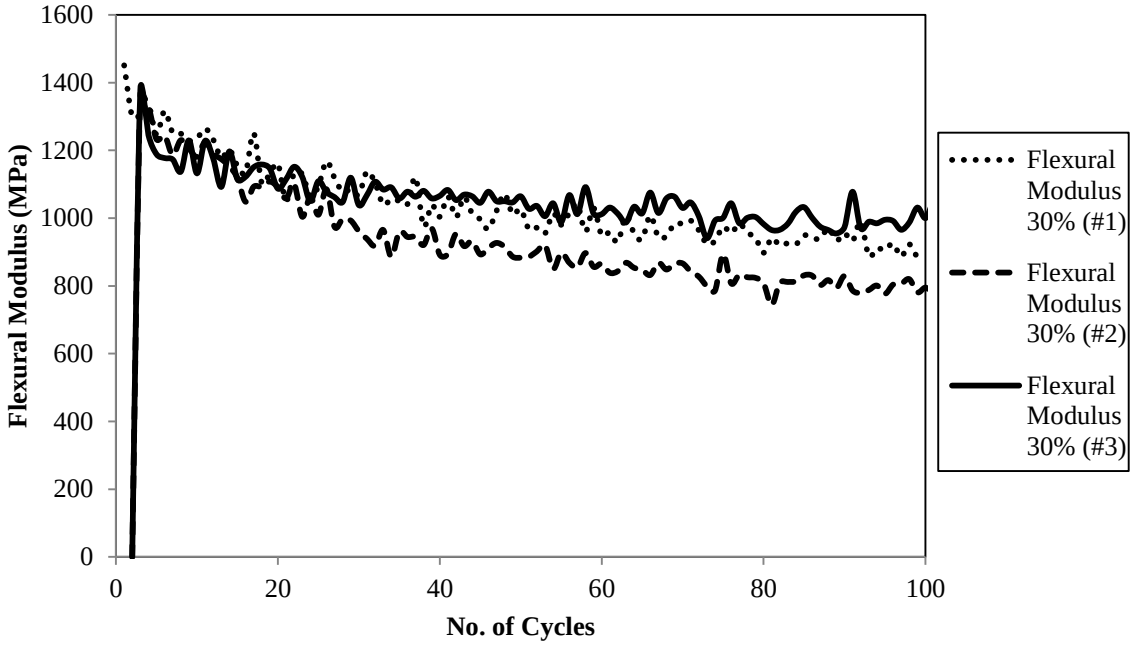

Figure B2. Flexural Modulus Variation at 30% Stress Level for 3 Gravel-Cement Replicates

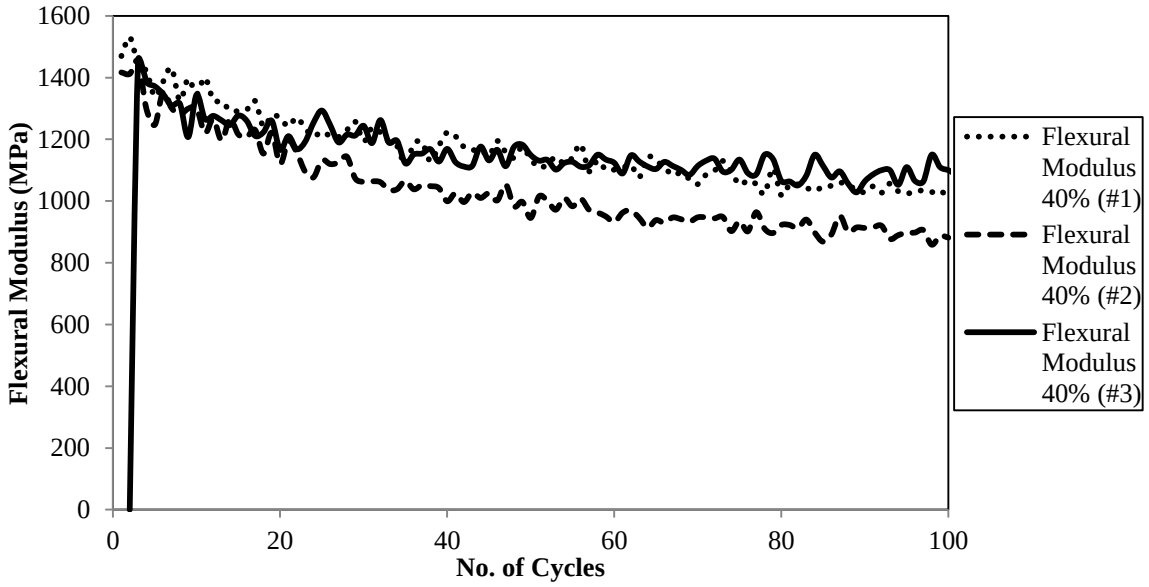

Figure B3. Flexural Modulus Variation at 40% Stress Level for 3 Gravel-Cement Replicates

Figures B4 to B6 shows the change in total, plastic and elastic displacement during the test for the three different stress levels for gravel-cement specimens.

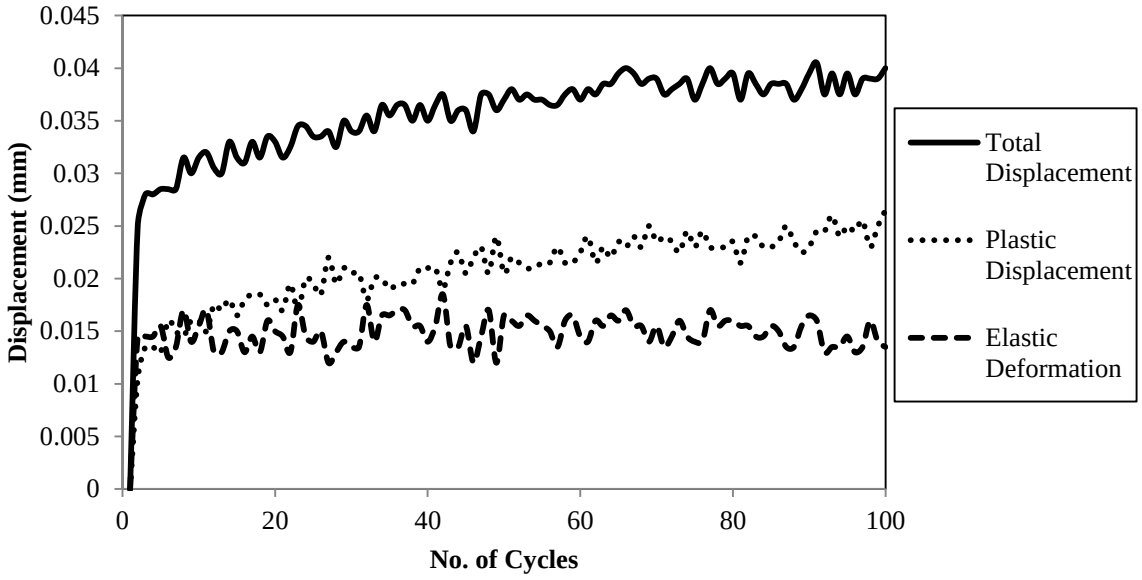

Figure B4. Displacement Variation for Flexural Modulus Test at 20% Stress Level for Gravel-Cement Specimen

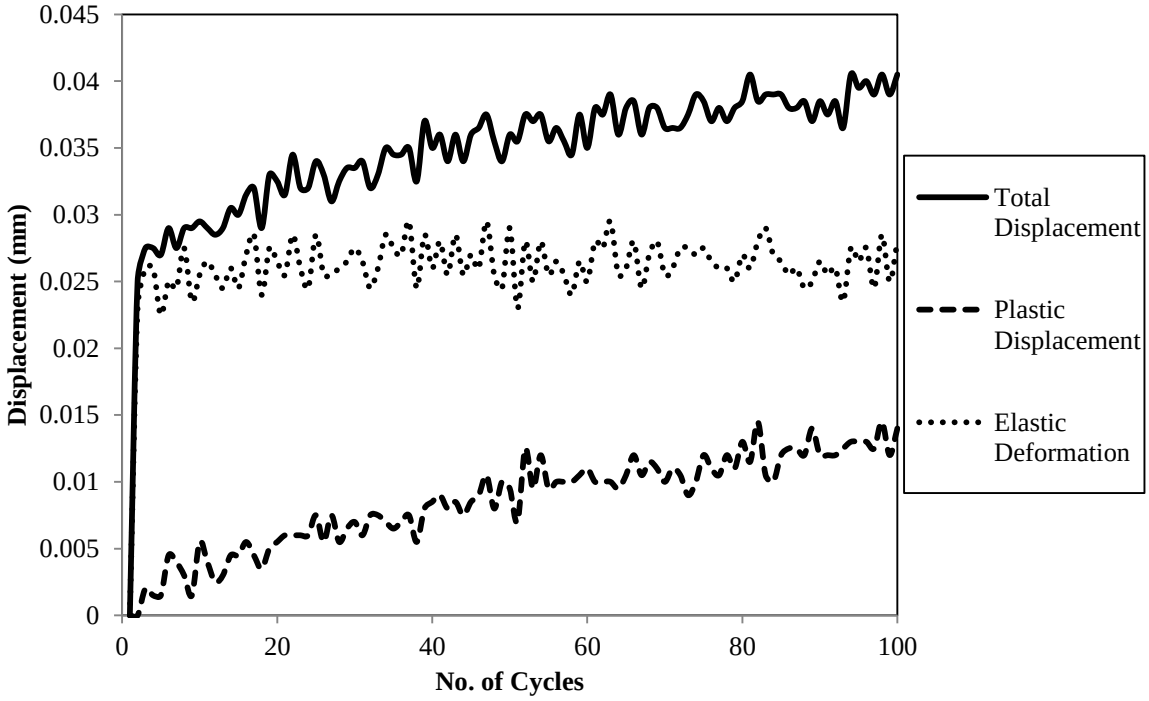

Figure B5. Displacement Variation for Flexural Modulus Test at 30% Stress Level for Gravel-Cement Specimen

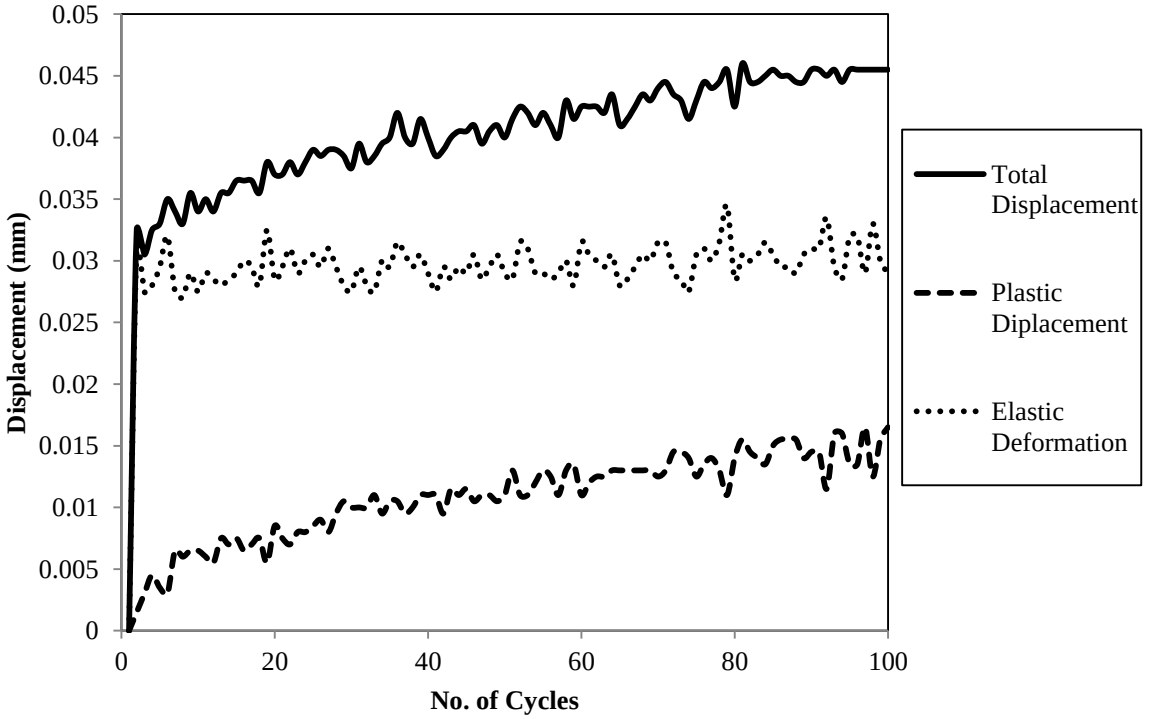

Figure B6. Displacement Variation for Flexural Modulus Test at 40% Stress Level for Gravel-Cement Specimen

Table B2 shows the flexural modulus of each replicate for gravel-cement specimens stabilized with 3% cement.

Table B2. Summary of the Flexural Modulus Test Results for Sand-Cement Specimens (Binder: 6%)

Specimen Number	**Stress level by percentage of flexural strength (%)**	**Flexural Modulus (MPa)**	**Average Flexural Modulus (MPa)**	**COV (%)**
FM-1	20	587.78	541.45	16
FM-2		442.99		
FM-3		593.50		
FM-1	30	931.96	972.71	19
FM-2		814.06		
FM-3		1,172.04		
FM-1	40	1,080.89	1,151.49	21
FM-2		951.20		
FM-3		1,422.32		

Figures B7 to B9 shows the change in flexural modulus during the test for each replicate for the three different stress level for the sand-cement (6% binder) specimens.

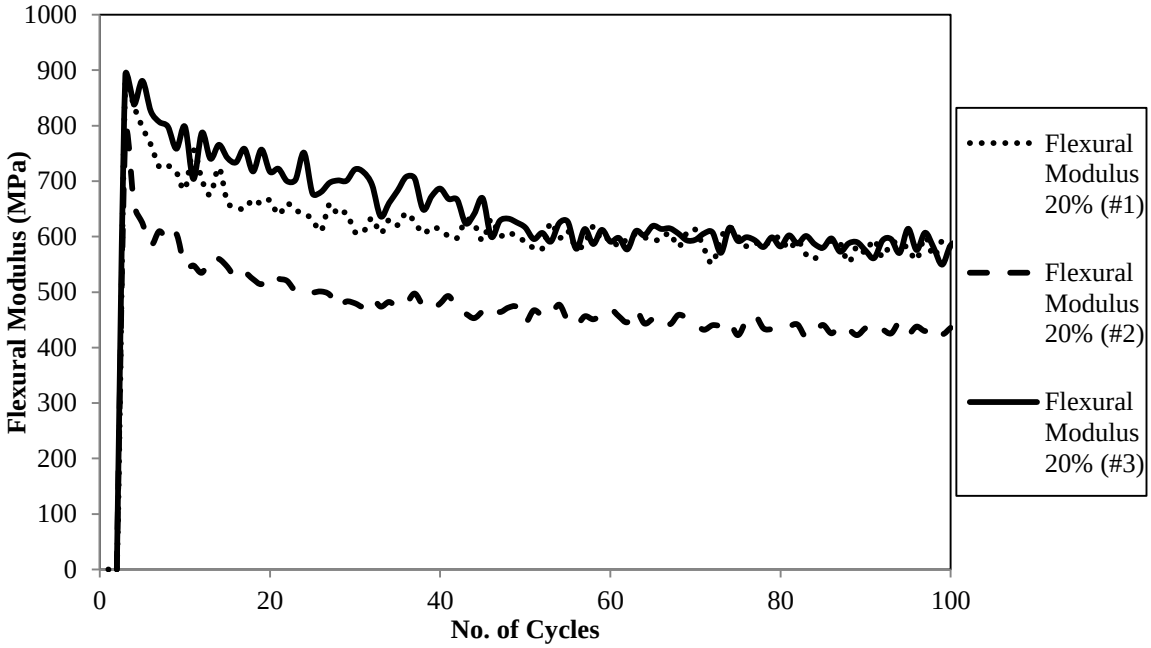

Figure B7. Flexural Modulus Variation at 20% Stress Level for 3 Sand-Cement Replicates

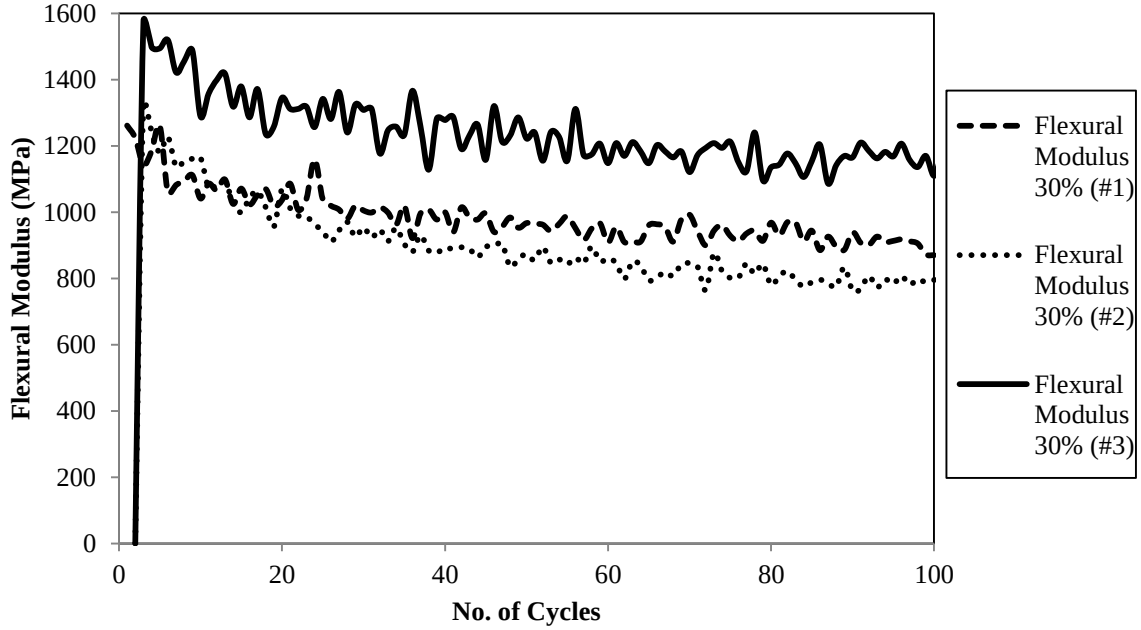

Figure B8. Flexural Modulus Variation at 30% Stress Level for 3 Sand-Cement Replicates

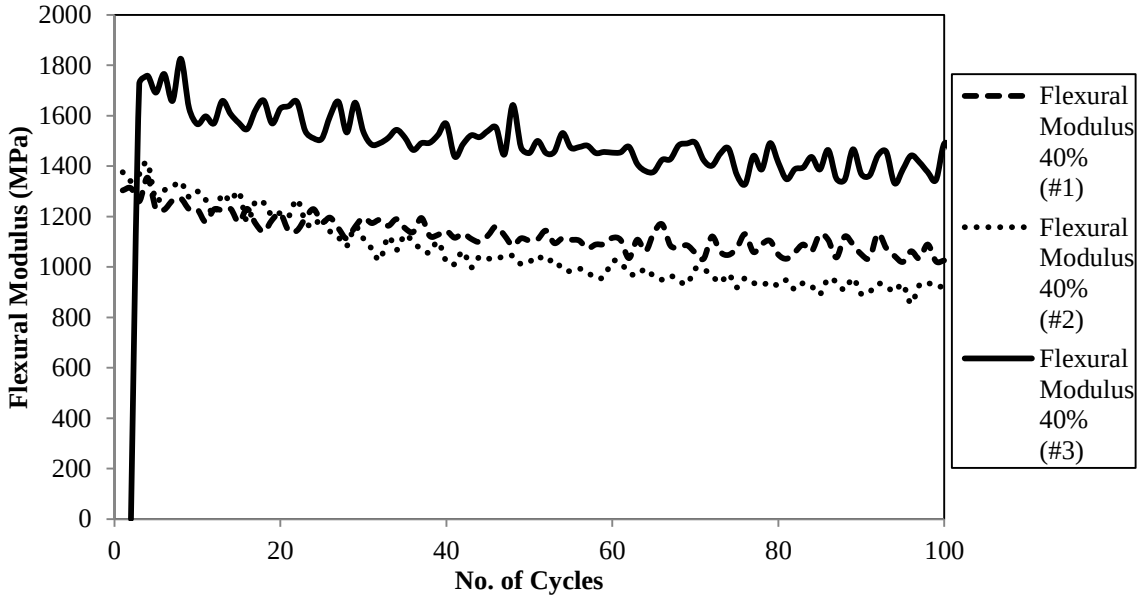

Figure B9. Flexural Modulus Variation at 40% Stress Level for 3 Sand-Cement Replicates

Figures B10 to B12 shows the change in total, plastic and elastic displacement during the test for the three different stress levels for sand-cement specimens.

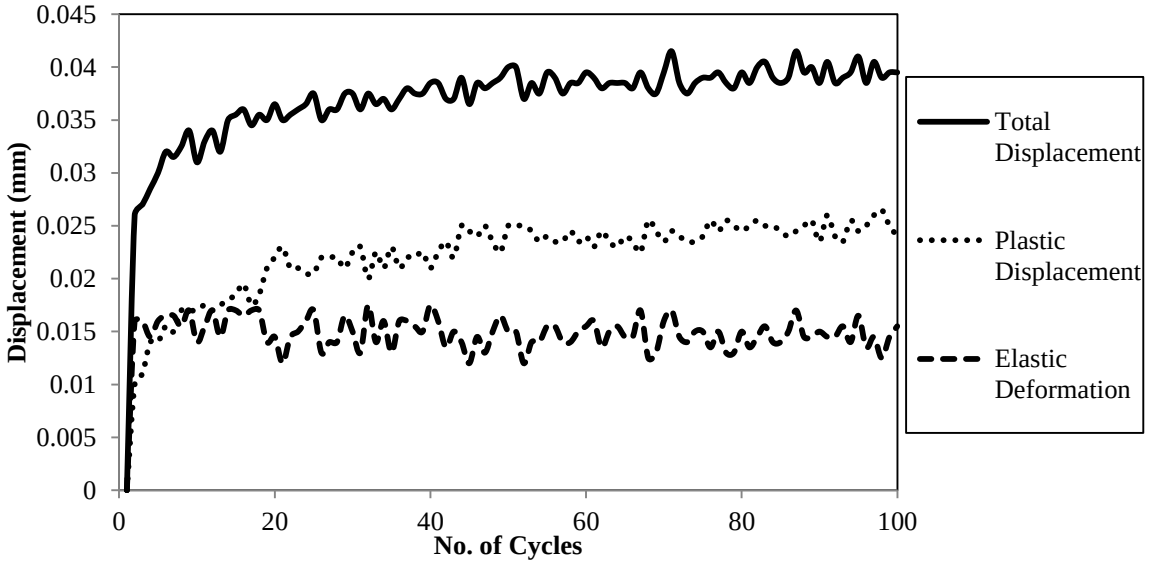

Figure B10. Displacement Variation for Flexural Modulus Test at 20% Stress Level for Sand-Cement Specimen

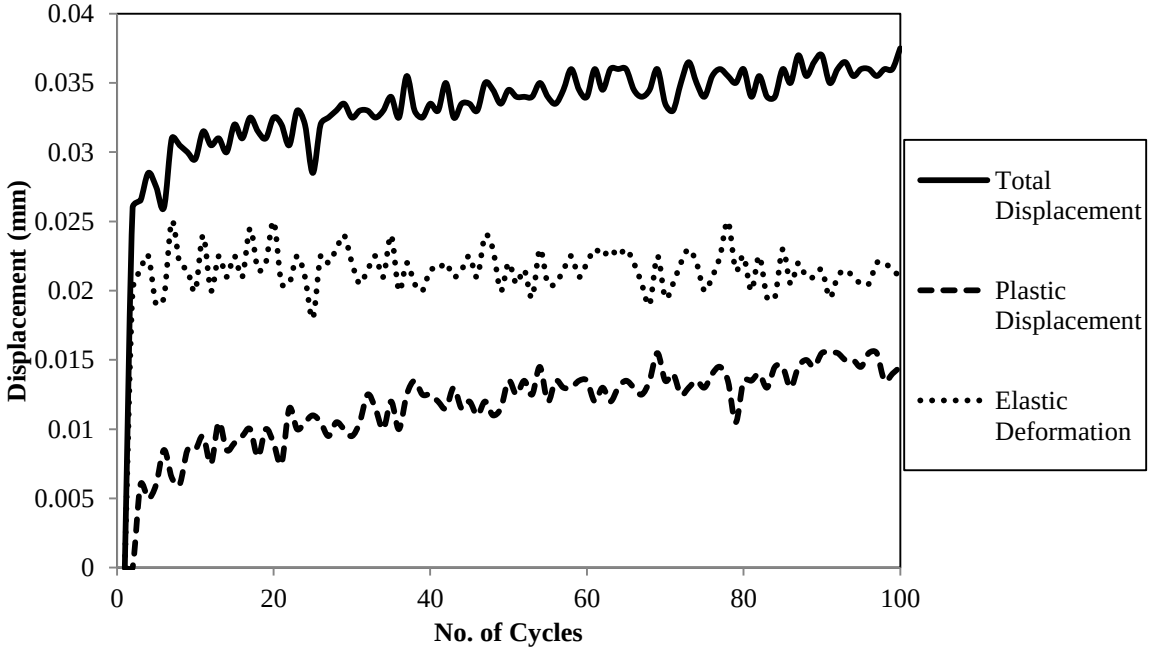

Figure B11. Displacement Variation for Flexural Modulus Test at 30% Stress Level for Sand-Cement Specimen

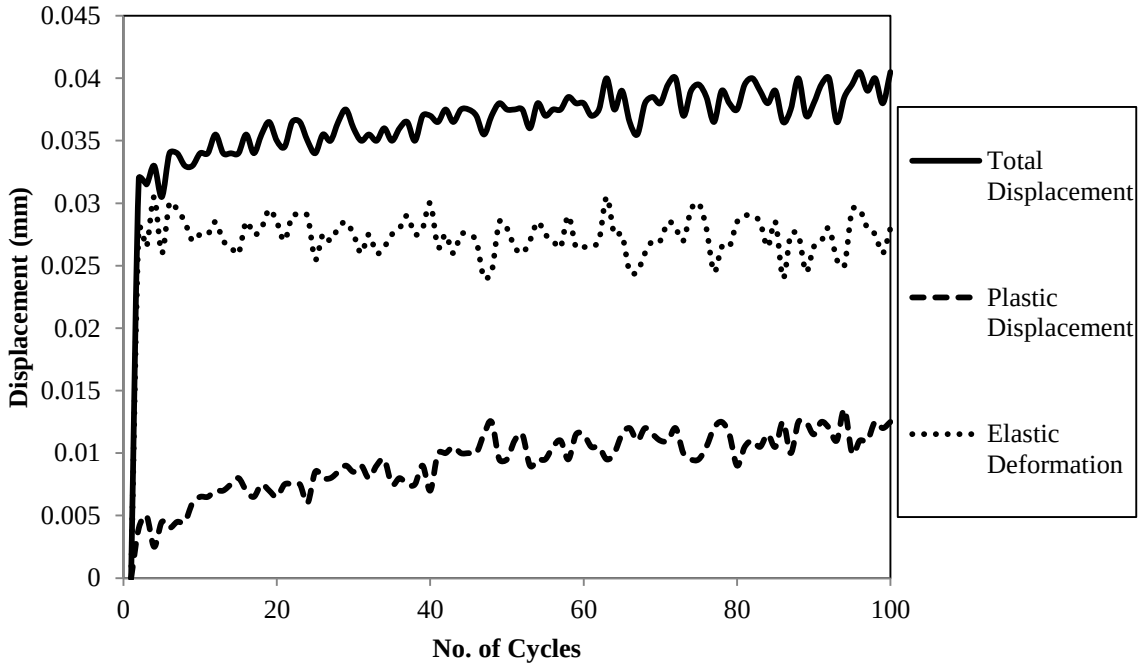

Figure B12. Displacement Variation for Flexural Modulus Test at 40% Stress Level for Sand-Cement Specimen

Table B3 shows the flexural modulus of each replicate for silt-cement specimens stabilized with 8% cement.

Table B3. Summary of the Flexural Modulus Test Results for Silt-Cement Specimens (Binder: 8%)

Specimen Number	Stress level by percentage of flexural strength (%)	Flexural Modulus (MPa)	Average Flexural Modulus (MPa)	COV (%)
FM-1	20	497.59	573.23	13
FM-2		577.71		
FM-3		645.07		
FM-1	30	883.49	903.83	8
FM-2		842.68		
FM-3		985.40		
FM-1	40	1,080.48	1,113.92	4
FM-2		1,161.90		
FM-3		1,099.37		

Figures B13 to B15 shows the change in flexural modulus during the test for each replicate for the three different stress levels for the silt-cement (8% binder) specimens.

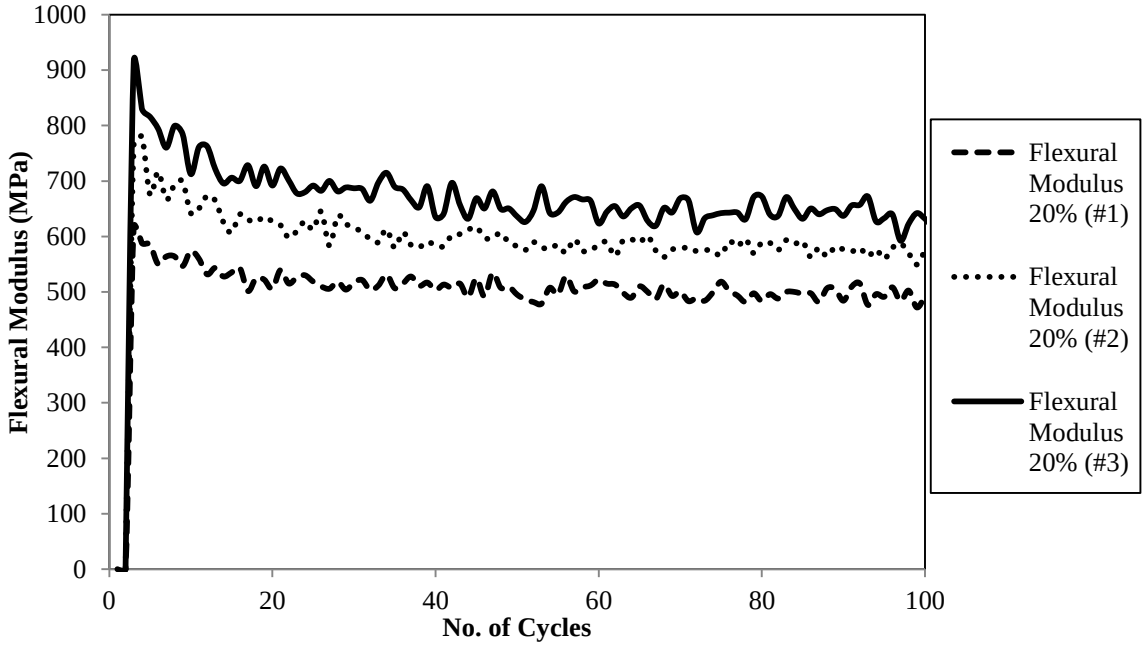

Figure B13. Flexural Modulus Variation at 20% Stress Level for 3 Silt-Cement Replicates

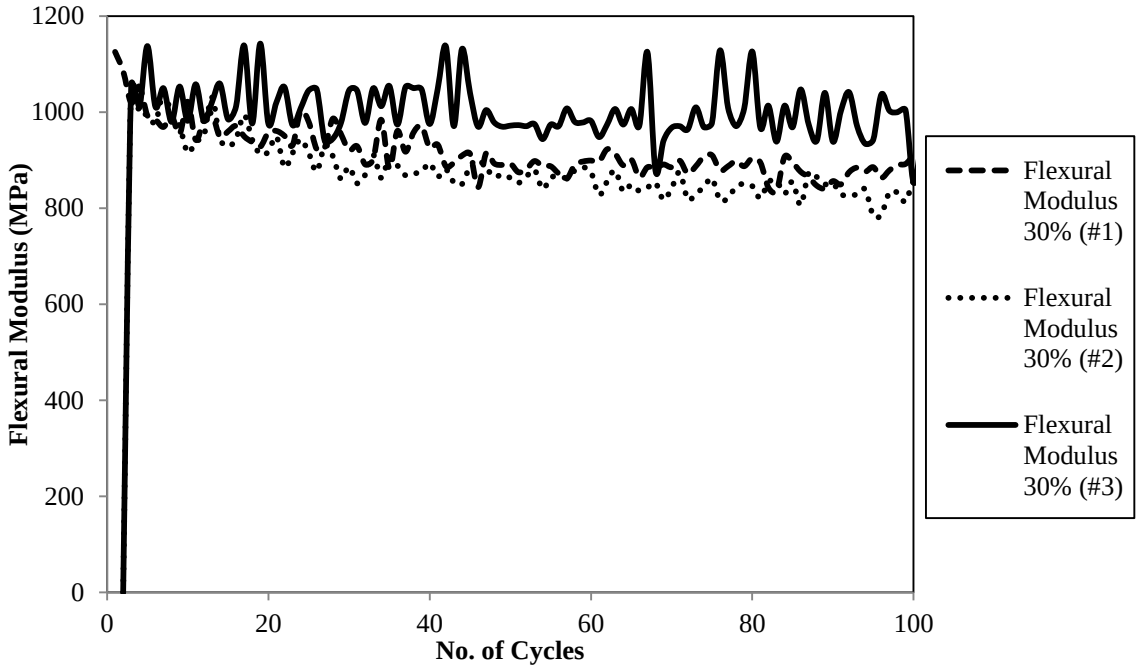

Figure B14. Flexural Modulus Variation at 30% Stress Level for 3 Silt-Cement Replicates

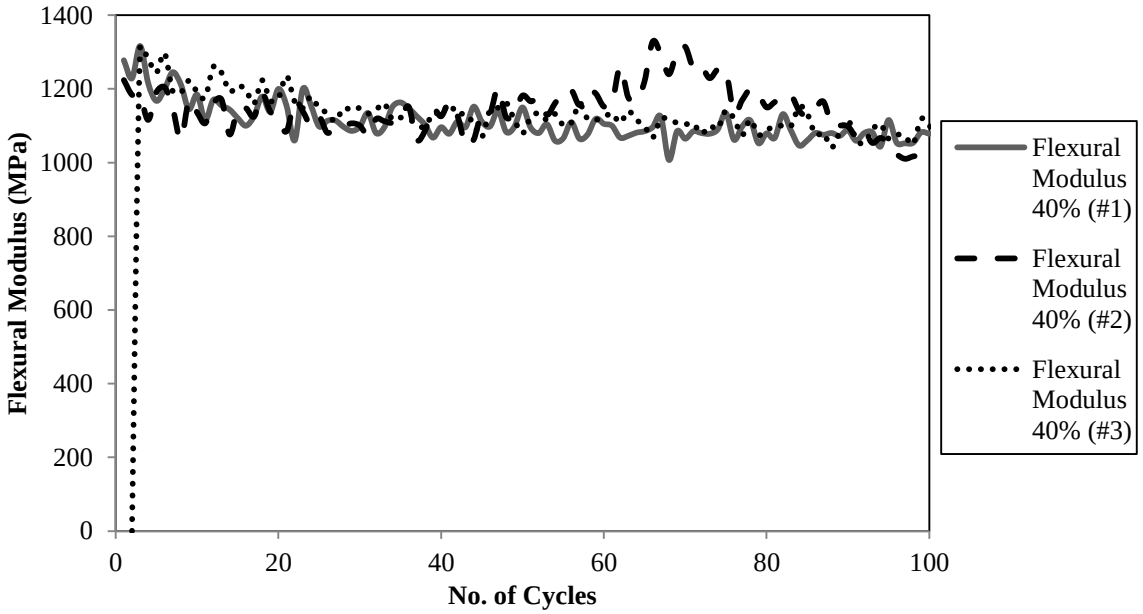

Figure B15. Flexural Modulus Variation at 40% Stress Level for 3 Silt-Cement Replicates

Figures B16 to B18 shows the change in total, plastic and elastic displacement during the test for the three different stress levels for the silt-cement specimens.

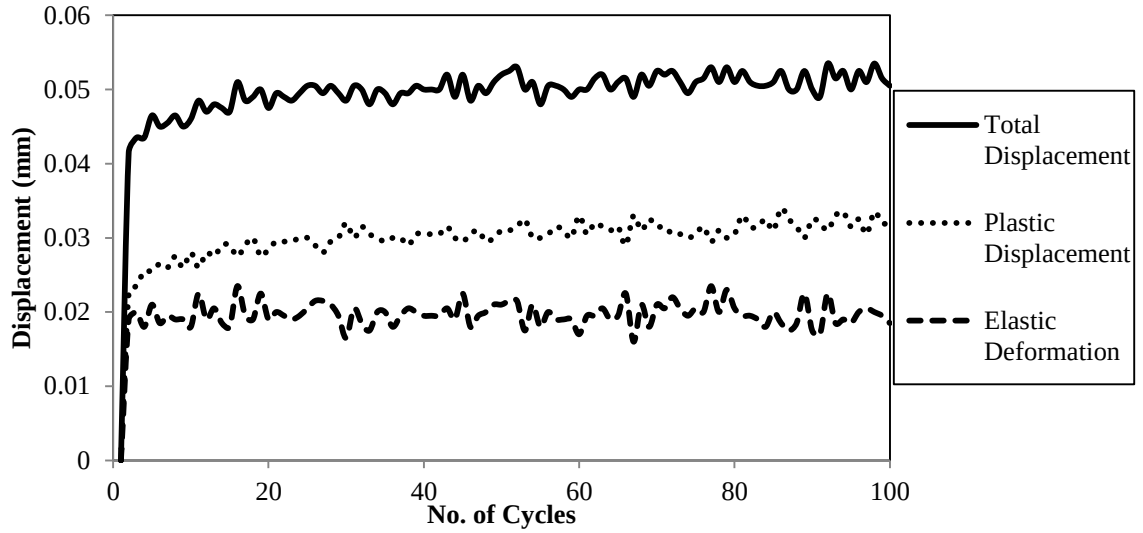

Figure B16. Displacement Variation for Flexural Modulus Test at 20% Stress Level for Silt-Cement Specimen

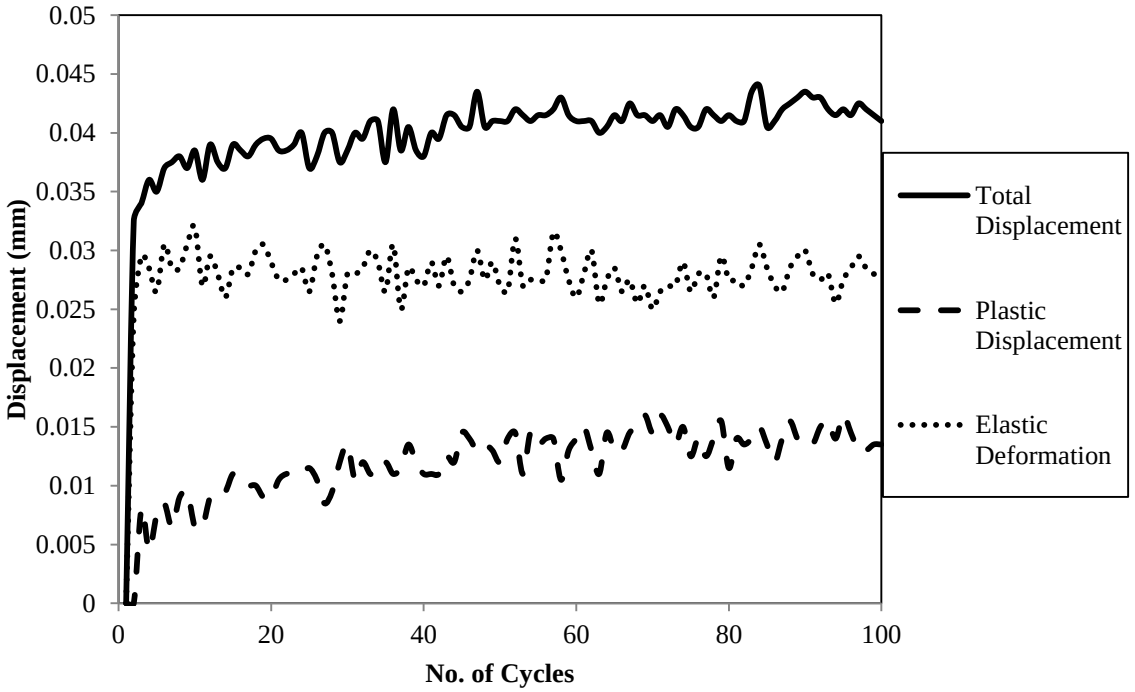

Figure B17. Displacement Variation for Flexural Modulus Test at 30% Stress Level for Silt-Cement Specimen

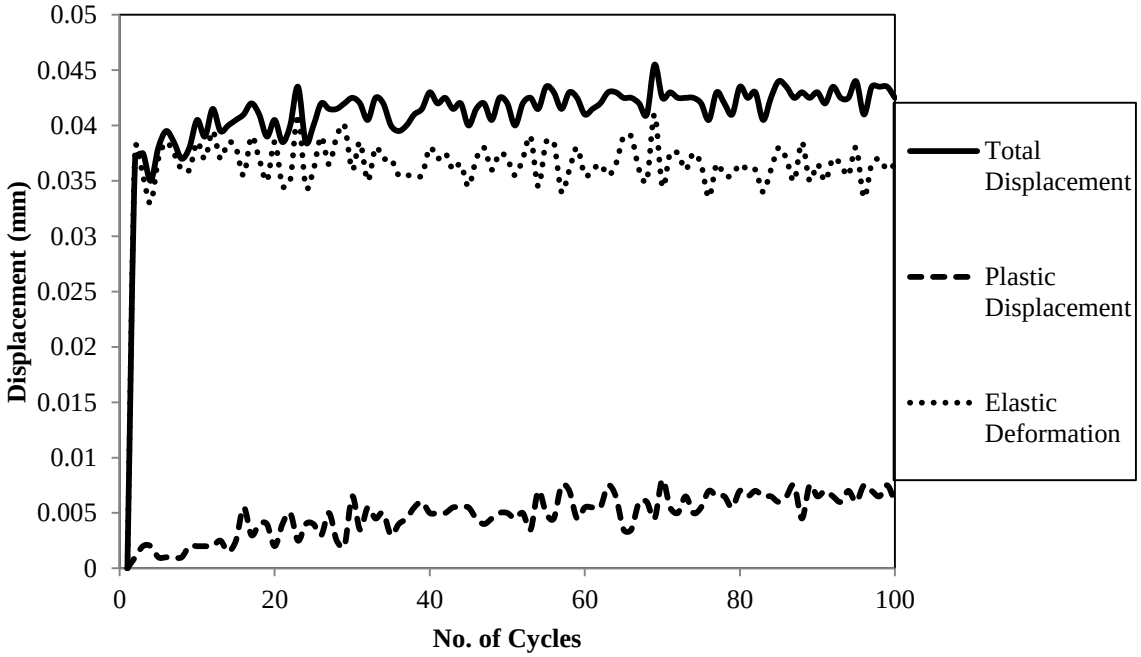

Figure B18. Displacement Variation for Flexural Modulus Test at 40% Stress Level for Silt-Cement Specimen

Table B4 shows the flexural modulus of each replicate for sand-fly ash specimens stabilized with 13% class C fly ash.

Table B4. Summary of the Flexural Modulus Test Results for Sand-Fly ash Specimens (Binder: 13%)

Specimen Number	Stress level by percentage of flexural strength (%)	Flexural Modulus (MPa)	Average Flexural Modulus (MPa)	COV (%)
FM-1	20	450.09	537.31	17
FM-2		531.24		
FM-3		630.66		
FM-1	30	522.76	748.70	22
FM-2		788.83		
FM-3		789.66		
FM-1	40	625.91	759.39	15
FM-2		848.19		
FM-3		803.99		

Figures B19 to B21 shows the change in flexural modulus during the test for each replicate for the three different stress levels for the sand-fly ash (13% binder) specimens.

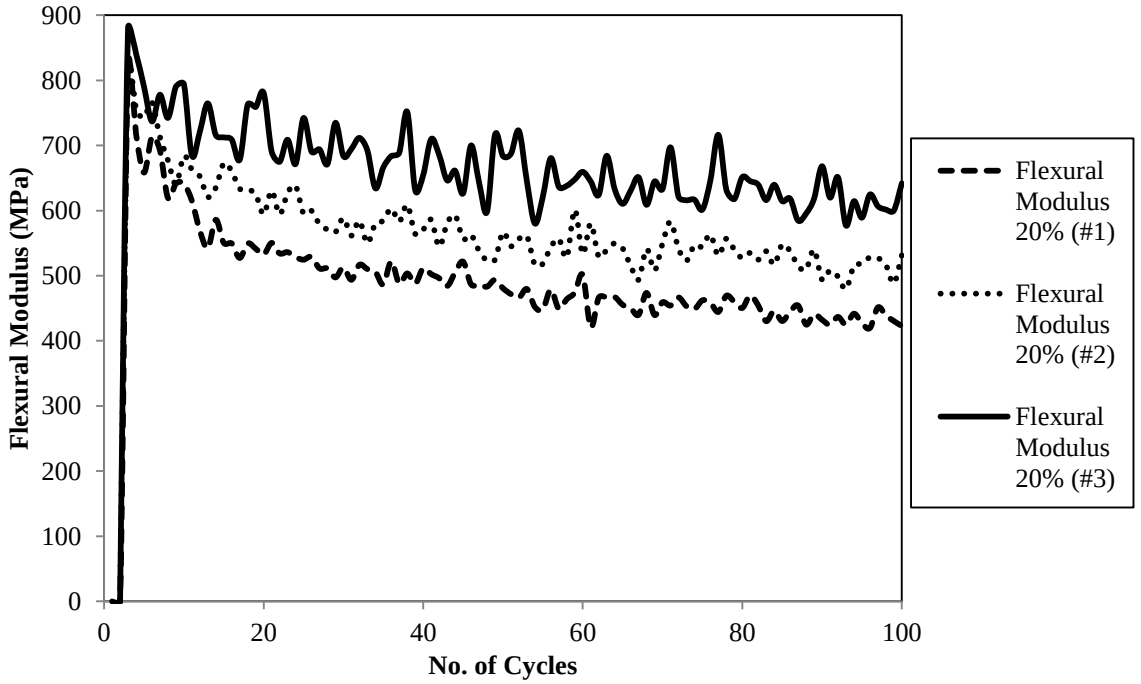

Figure B19. Flexural Modulus Variation at 20% Stress Level for 3 Sand-Fly ash Replicates

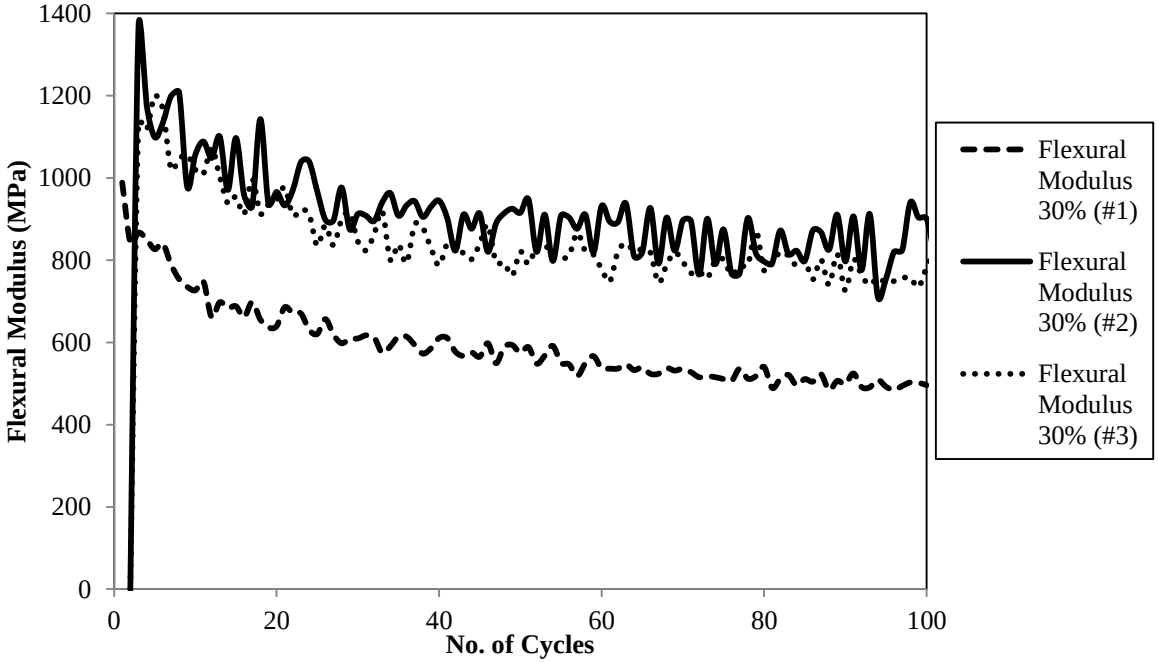

Figure B20. Flexural Modulus Variation at 30% Stress Level for 3 Sand- Fly ash Replicates

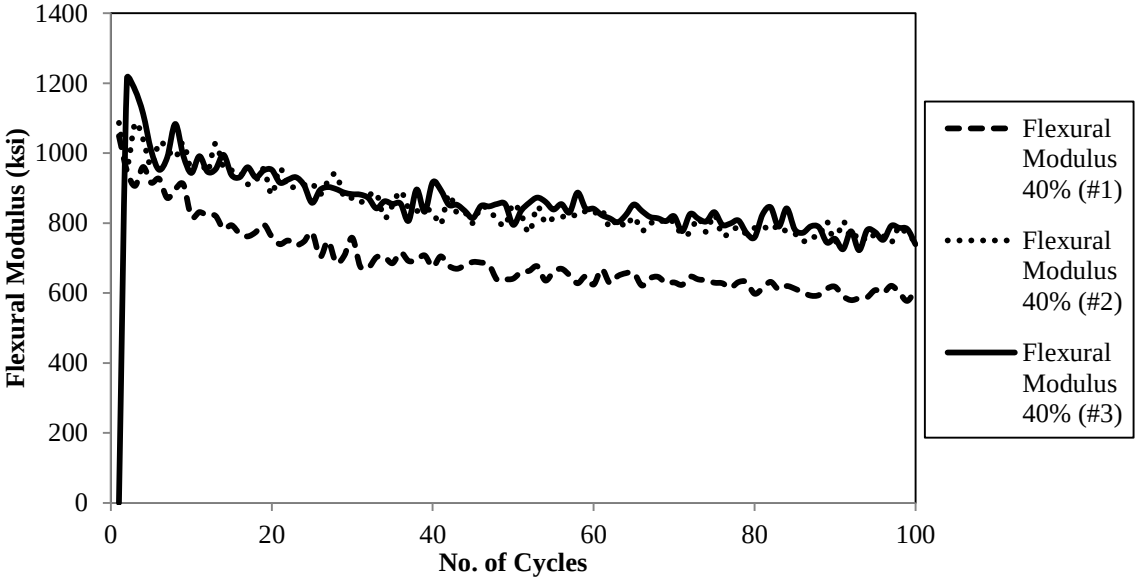

Figure B21. Flexural Modulus Variation at 40% Stress Level for 3 Sand- Fly ash Replicates

Figures B22 to B24 shows the change in total, plastic and elastic displacement during the test for the three different stress levels for sand-fly ash specimens.

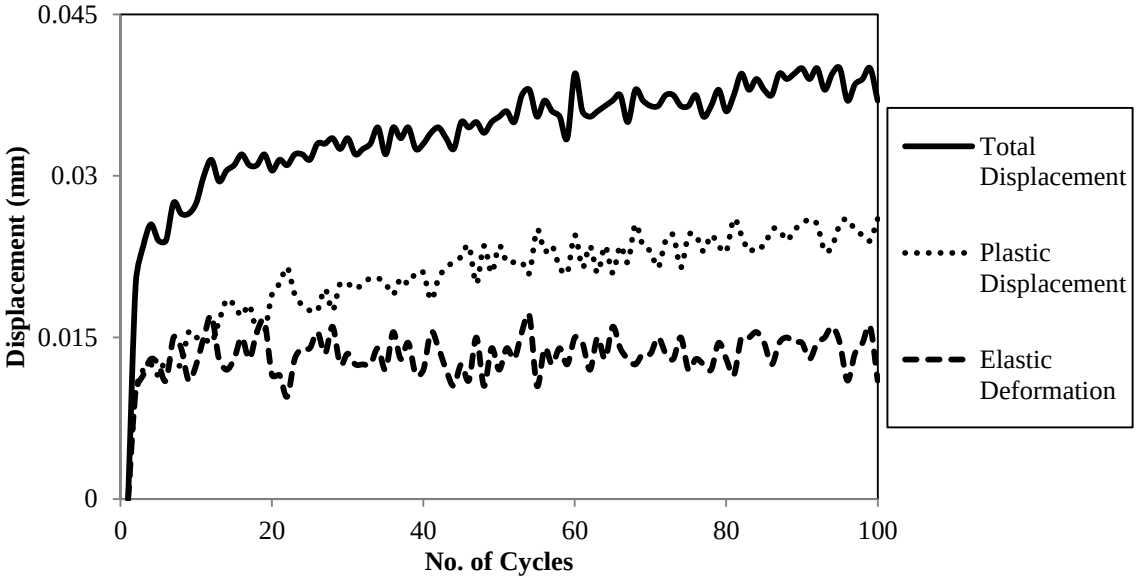

Figure B22. Displacement Variation for Flexural Modulus Test at 20% Stress Level for Sand- Fly ash Specimen

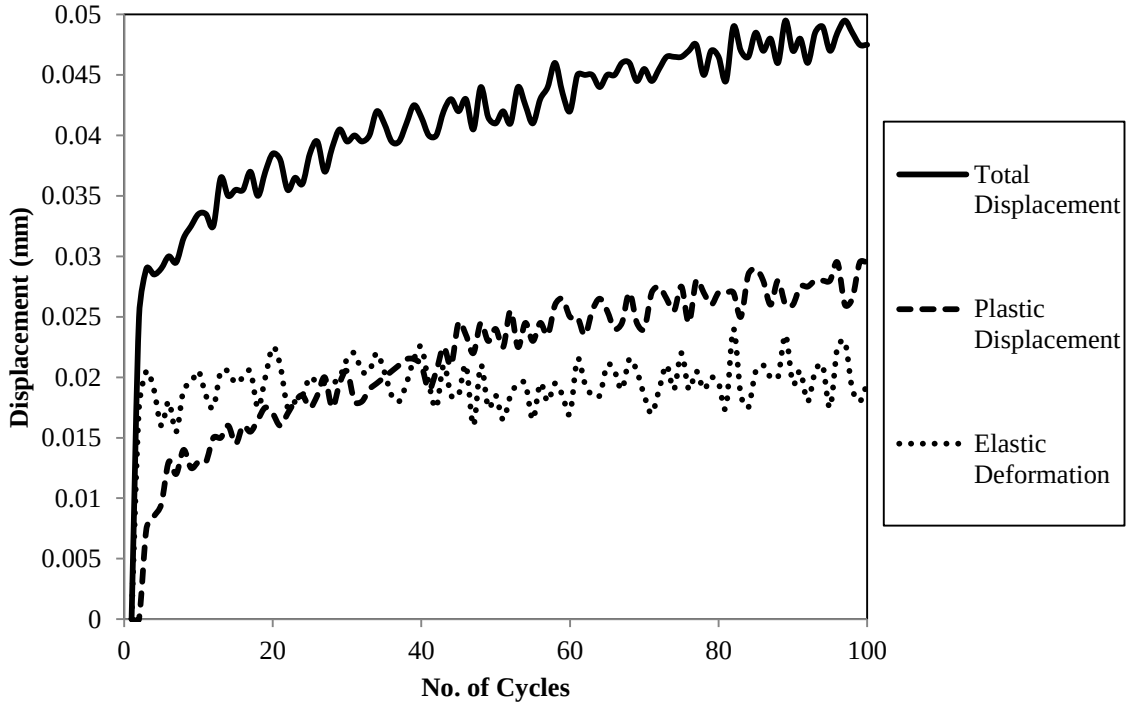

Figure B23. Displacement Variation for Flexural Modulus Test at 30% Stress Level for Sand- Fly ash Specimen

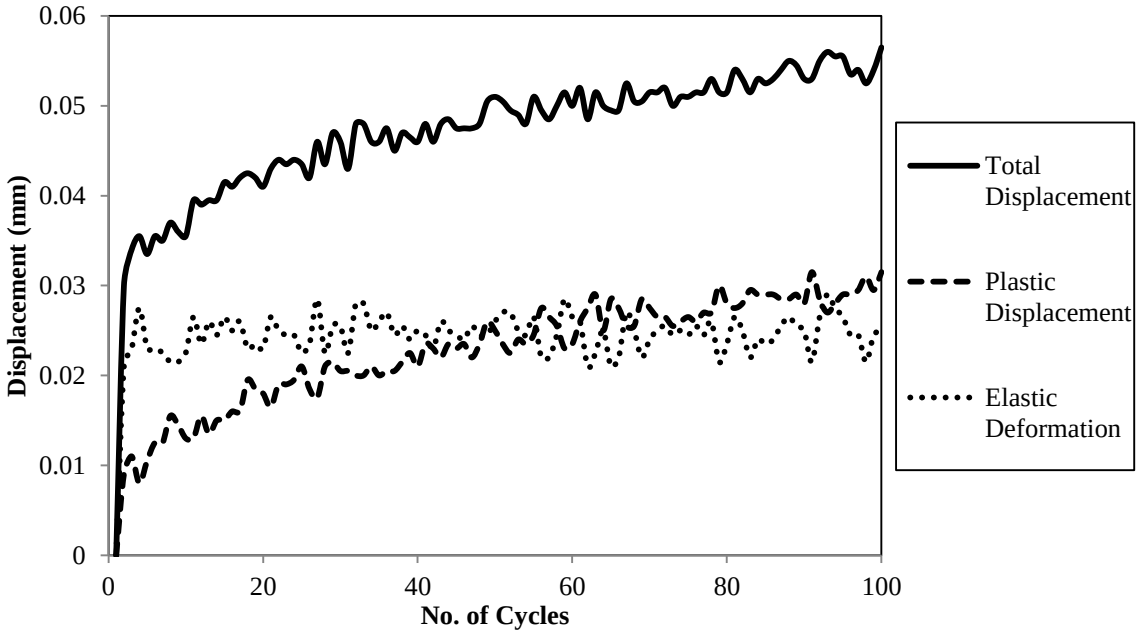

Figure B24. Displacement Variation for Flexural Modulus Test at 40% Stress Level for Sand- Fly ash Specimen

Table B5 shows the flexural modulus of each replicate for gravel-fly ash specimens stabilized with 13% class C fly ash.

Table B5. Summary of the Flexural Modulus Test Results for Gravel-Fly ash Specimens (Binder: 13%)

Specimen Number	**Stress level by percentage of flexural strength (%)**	**Flexural Modulus (MPa)**	**Average Flexural Modulus (MPa)**	**COV (%)**
FM-1	20	645.97	621.36	13
FM-2		528.97		
FM-3		689.06		
FM-1	30	893.70	821.09	16
FM-2		666.17		
FM-3		903.49		
FM-1	40	926.24	860.26	17
FM-2		692.78		
FM-3		961.68		

Figures B25 to B27 shows the change in flexural modulus during the test for each replicate for the three different stress levels for the gravel-fly ash (13% binder) specimens.

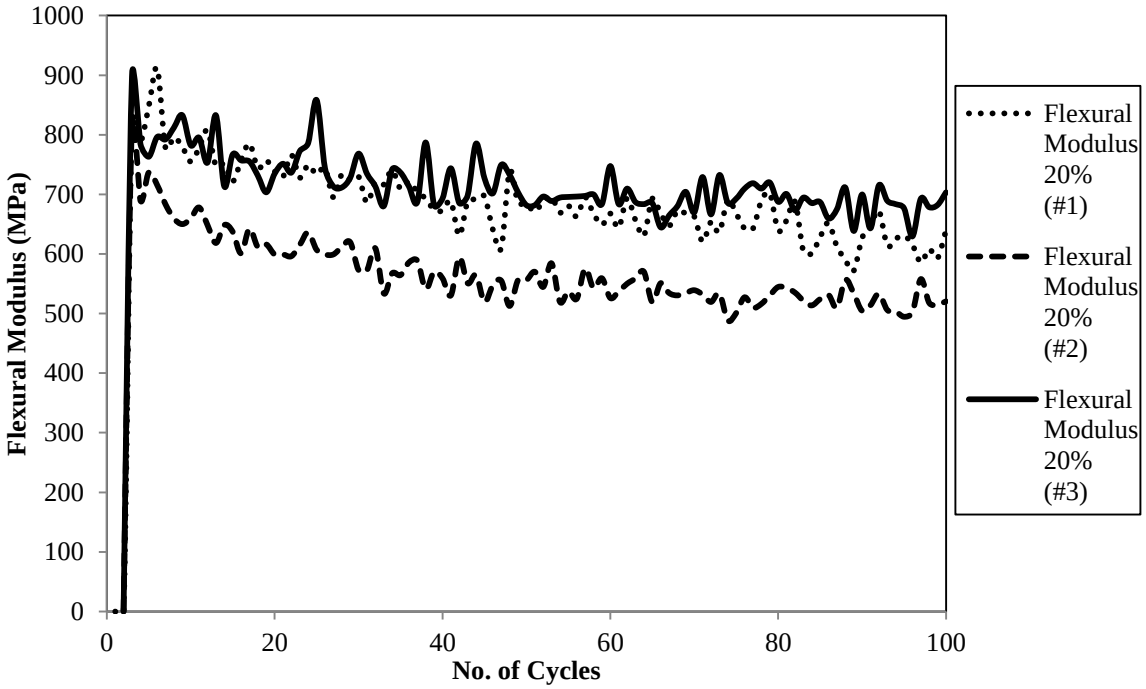

Figure B25. Flexural Modulus Variation at 20% Stress Level for 3 Gravel-Fly ash Replicates

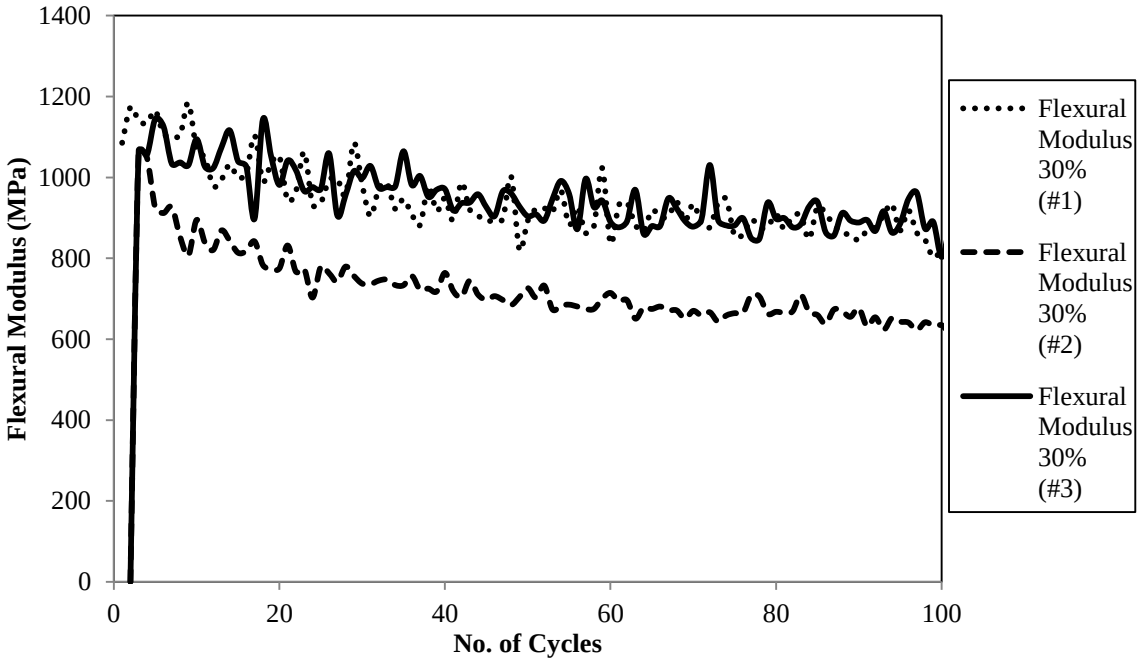

Figure B26. Flexural Modulus Variation at 30% Stress Level for 3 Gravel-Fly ash Replicates

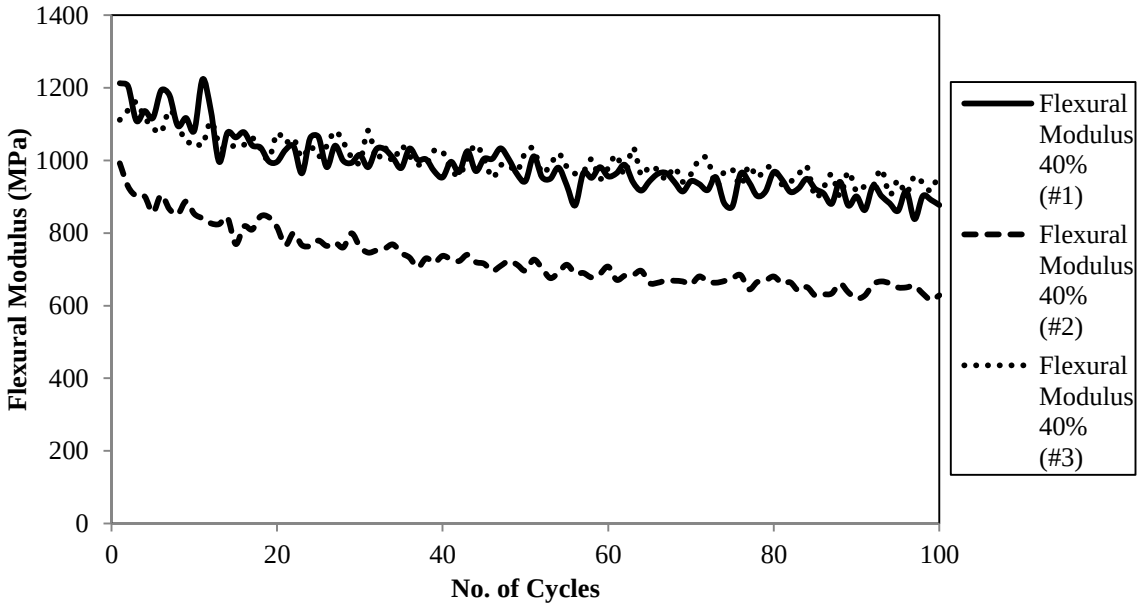

Figure B27. Flexural Modulus Variation at 40% Stress Level for 3 Gravel-Fly ash Replicates

Figures B28 to B30 shows the change in total, plastic and elastic displacement during the test for the three different stress levels for gravel-fly ash specimens.

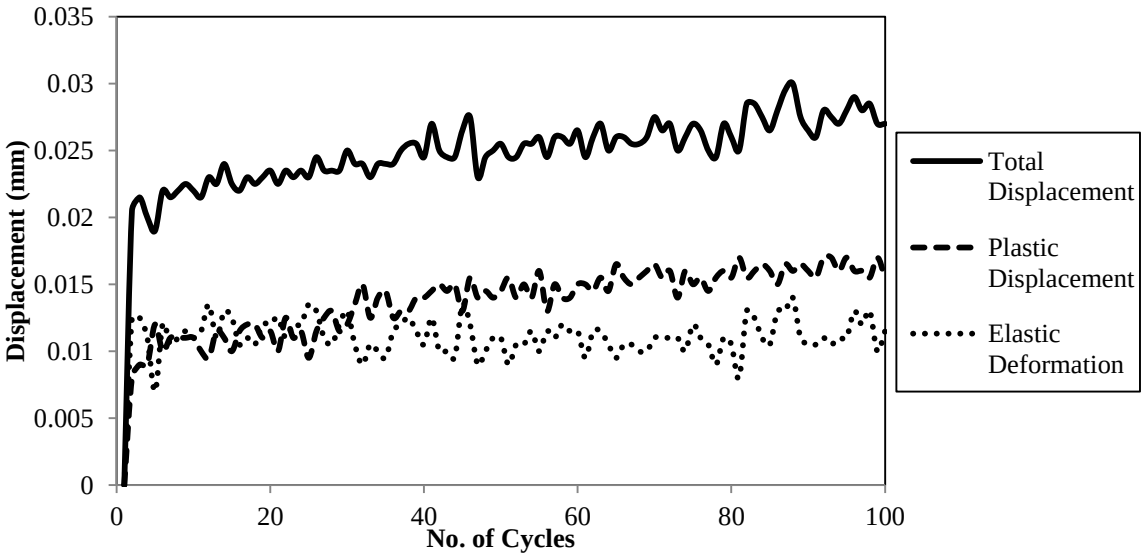

Figure B28. Displacement Variation for Flexural Modulus Test at 20% Stress Level for Gravel-Fly ash Specimen

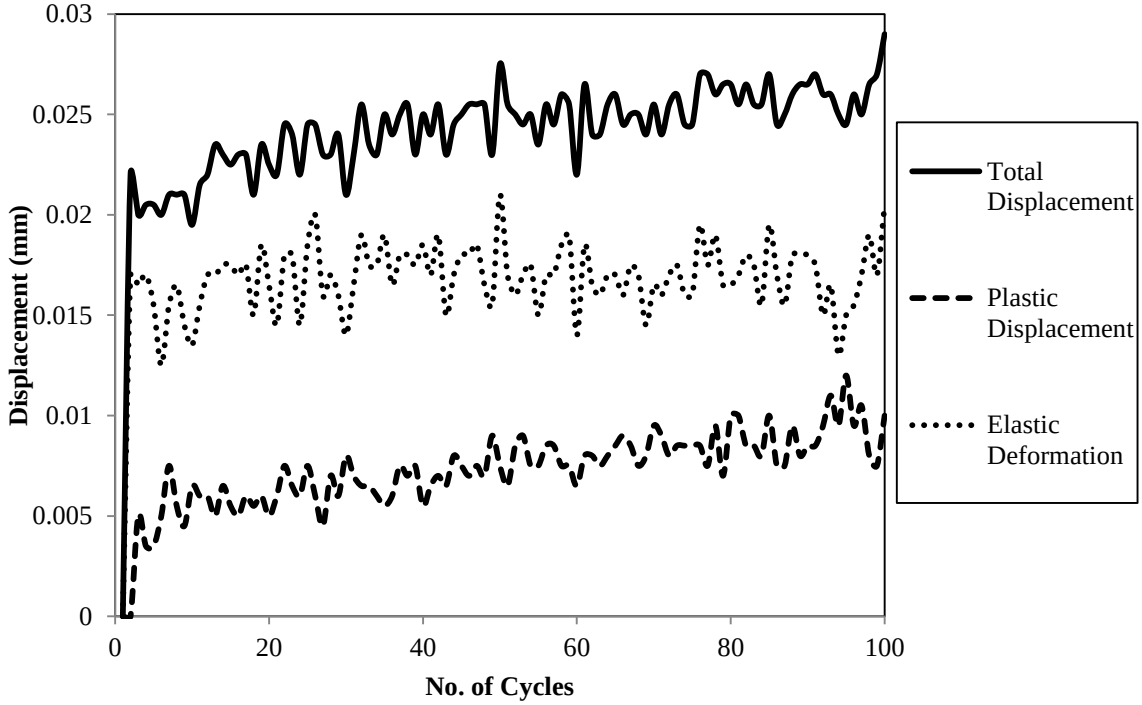

Figure B29. Displacement Variation for Flexural Modulus Test at 30% Stress Level for Gravel- Fly ash Specimen

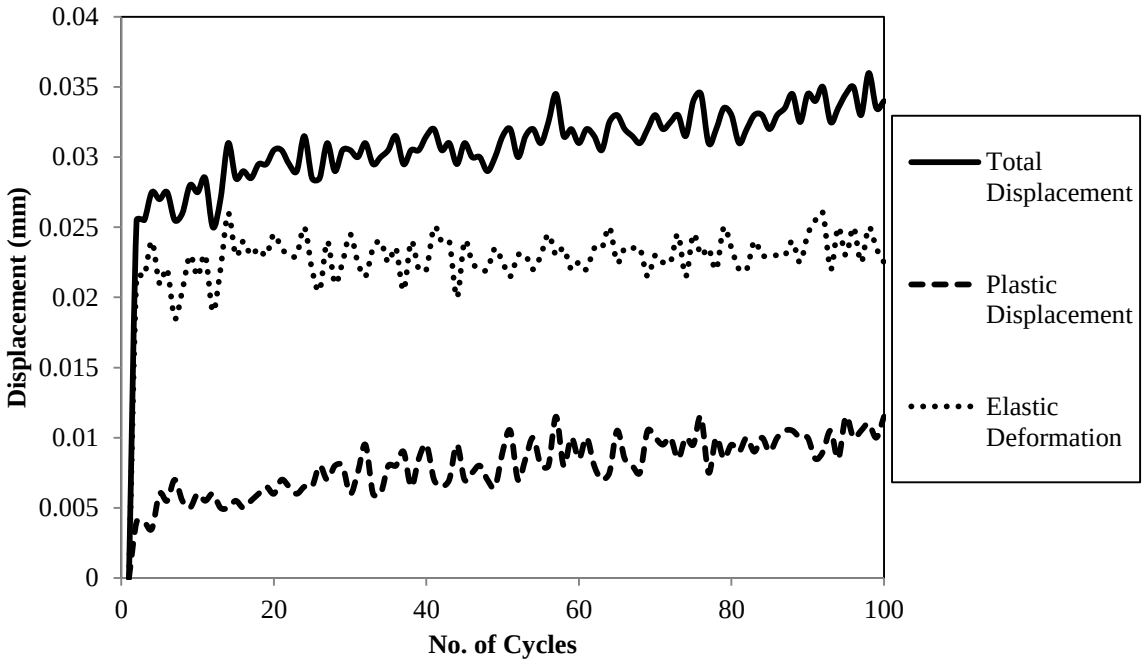

Figure B30. Displacement Variation for Flexural Modulus Test at 40% Stress Level for Gravel- Fly ash Specimen

Table B6 shows the flexural modulus of each replicate for silt-fly ash specimens stabilized with 13% class C fly ash.

Table B6. Summary of the Flexural Modulus Test Results for Silt-Fly ash Specimens (Binder: 13%)

Specimen Number	Stress level by percentage of flexural strength (%)	Flexural Modulus (MPa)	Average Flexural Modulus (MPa)	COV (%)
FM-1	20	401.76	359.49	19
FM-2		384.31		
FM-3		276.62		
FM-1	30	475.32	454.43	7
FM-2		433.54		
FM-1	40	581.92	466.36	35
FM-2		350.81		

*1 specimen failed after 13 cycles at 20 % Stress Level and another specimen failed after 44 cycles at 30 % Stress Level

Figures B31 to B33 shows the change in flexural modulus during the test for each replicate for the three different stress levels for the silt -fly ash (13% binder) specimens.

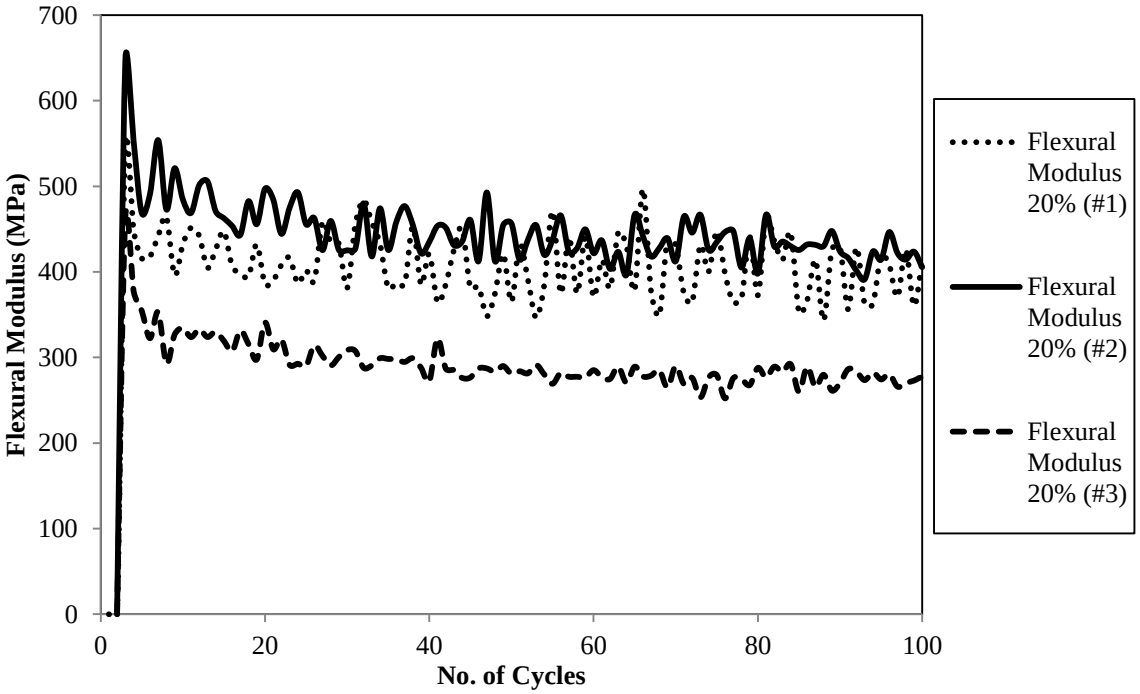

Figure B31. Flexural Modulus Variation at 20% Stress Level for 3 Silt-Fly ash Replicates

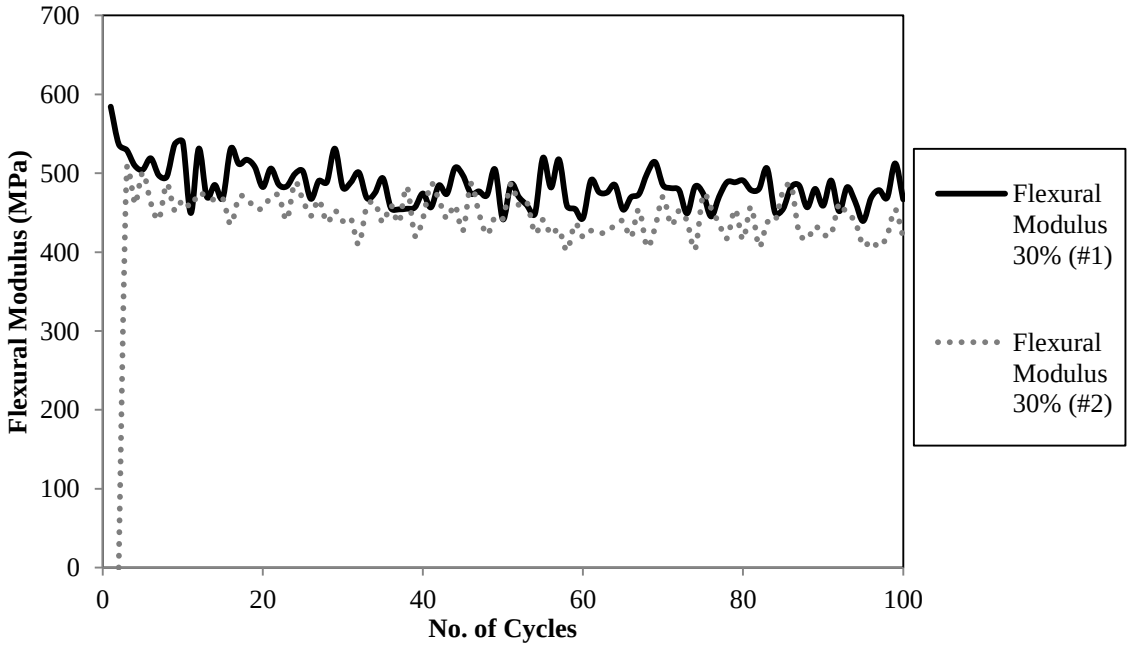

Figure B32. Flexural Modulus Variation at 30% Stress Level for 2 Silt-Fly ash Replicates

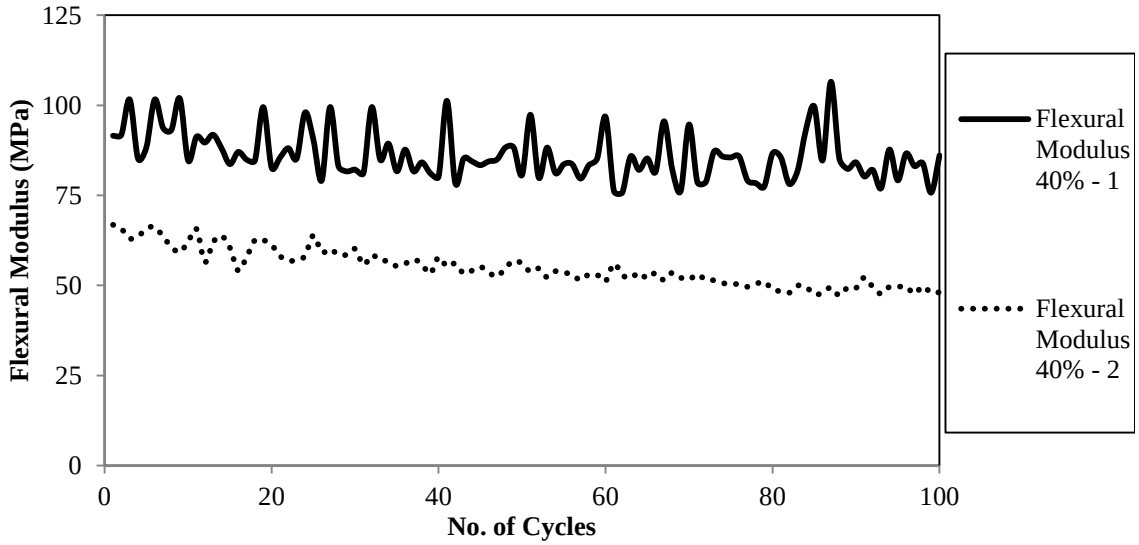

Figure B33. Flexural Modulus Variation at 40% Stress Level for 2 Silt-Fly ash Replicates

Figures B34 to B36 shows the change in total, plastic and elastic displacement during the test for the three different stress levels for silt-fly ash specimens.

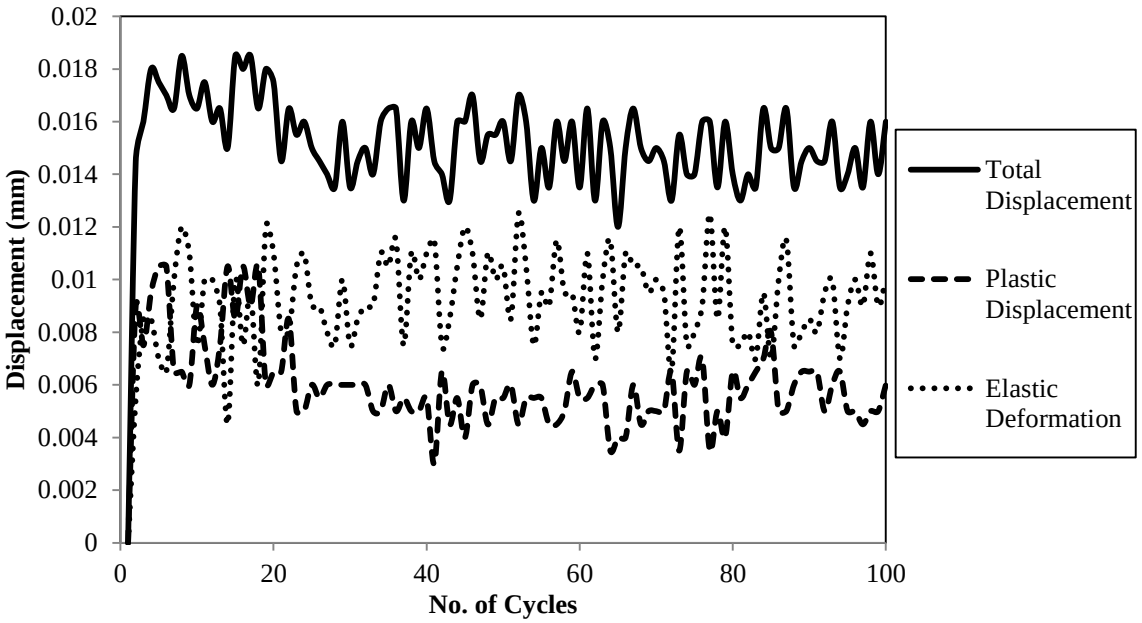

Figure B34. Displacement Variation for Flexural Modulus Test at 20% Stress Level for Silt-Fly ash Specimen

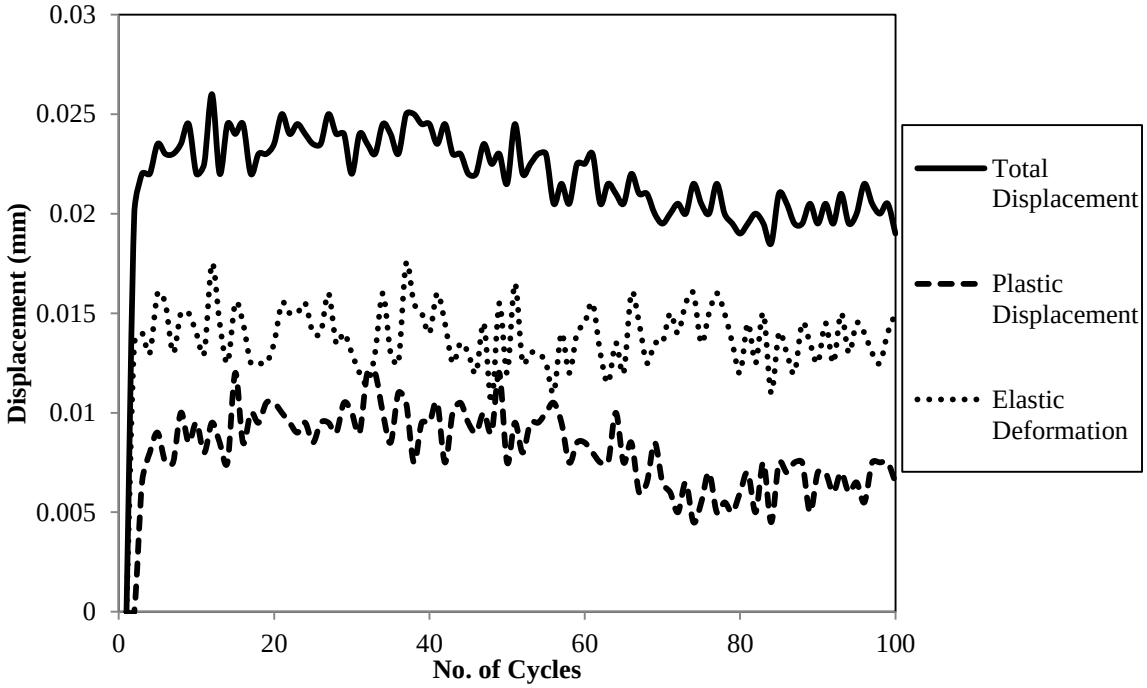

Figure B35. Displacement Variation for Flexural Modulus Test at 30% Stress Level for Silt-Fly ash Specimen

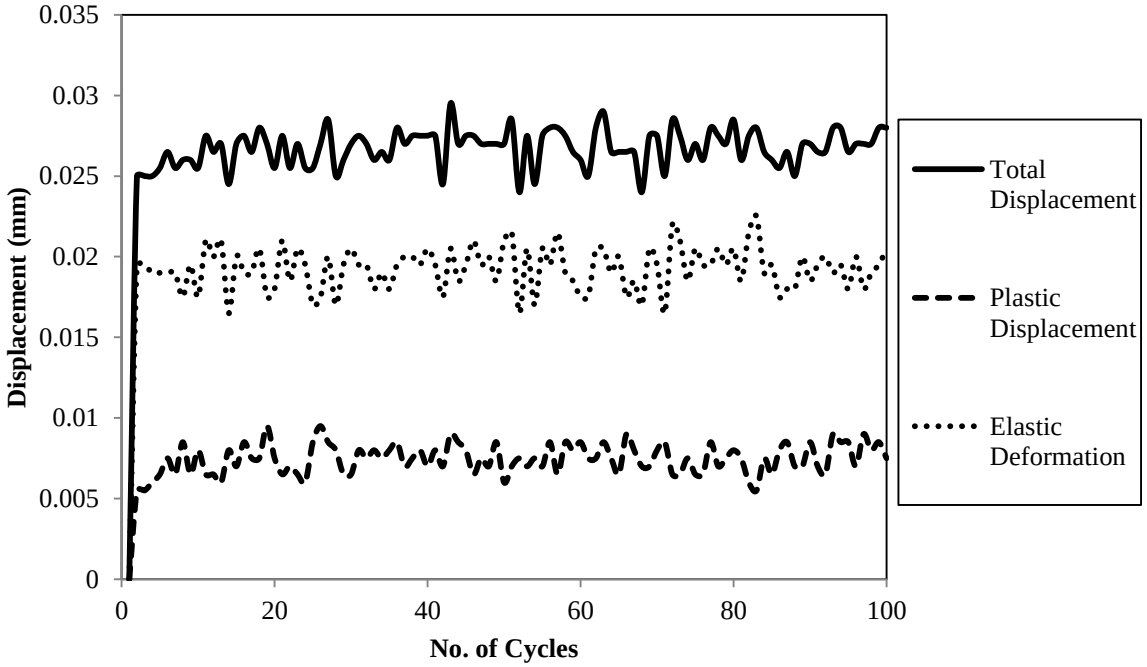

Figure B36. Displacement Variation for Flexural Modulus Test at 40% Stress Level for Silt-Fly ash Specimen

Table B7 shows the flexural modulus of each replicate for silt-lime-fly ash specimens stabilized with 4% lime and 12% class F fly ash.

Table B7. Summary of the Flexural Modulus Test Results for Silt-Lime-Fly ash Specimens (Binder: 4/12%)

Specimen Number	Stress level by percentage of flexural strength (%)	Flexural Modulus (MPa)	Average Flexural Modulus (MPa)	COV (%)
FM-1	20	627.63	588.57	8
FM-2		628.39		
FM-3		542.62		
FM-1	30	810.69	856.67	9
FM-2		947.68		
FM-3		811.58		
FM-1	40	872.32	940.10	13
FM-2		1,078.82		
FM-3		869.15		

Figures B37 to B39 shows the change in flexural modulus during the test for each replicate for the three different stress levels for the silt-lime-fly ash (4/12% binder) specimens.

Figure B37. Flexural Modulus Variation at 20% Stress Level for 3 Silt-Lime-Fly ash Replicates

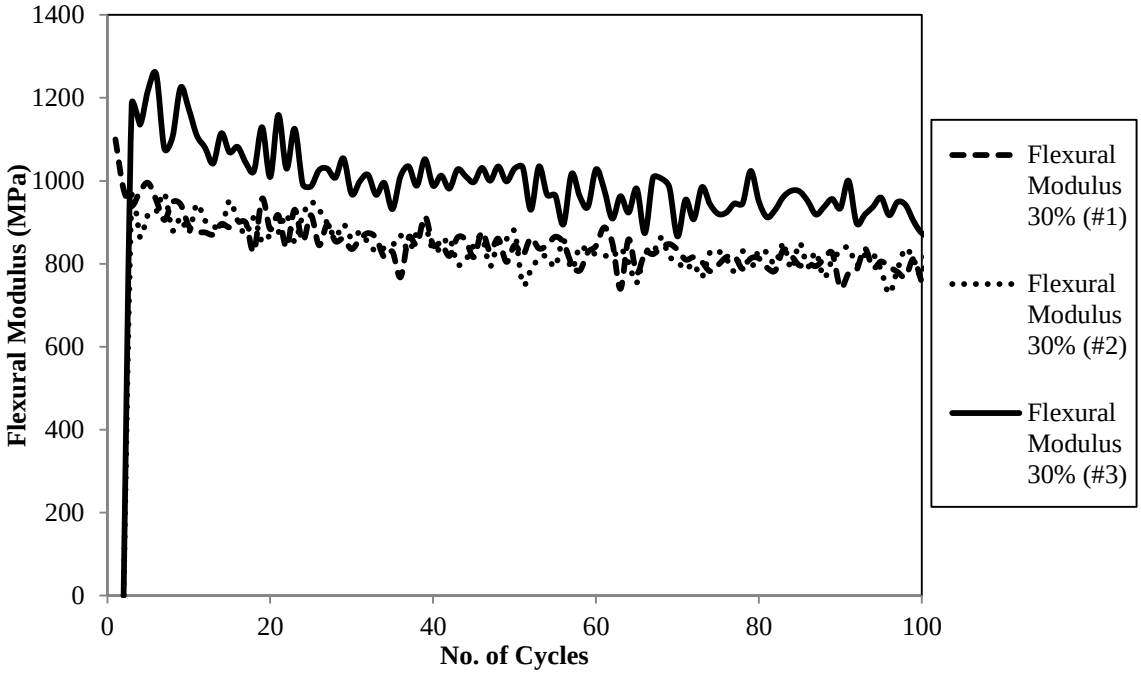

Figure B38. Flexural Modulus Variation at 30% Stress Level for 3 Silt-Lime-Fly ash Replicates

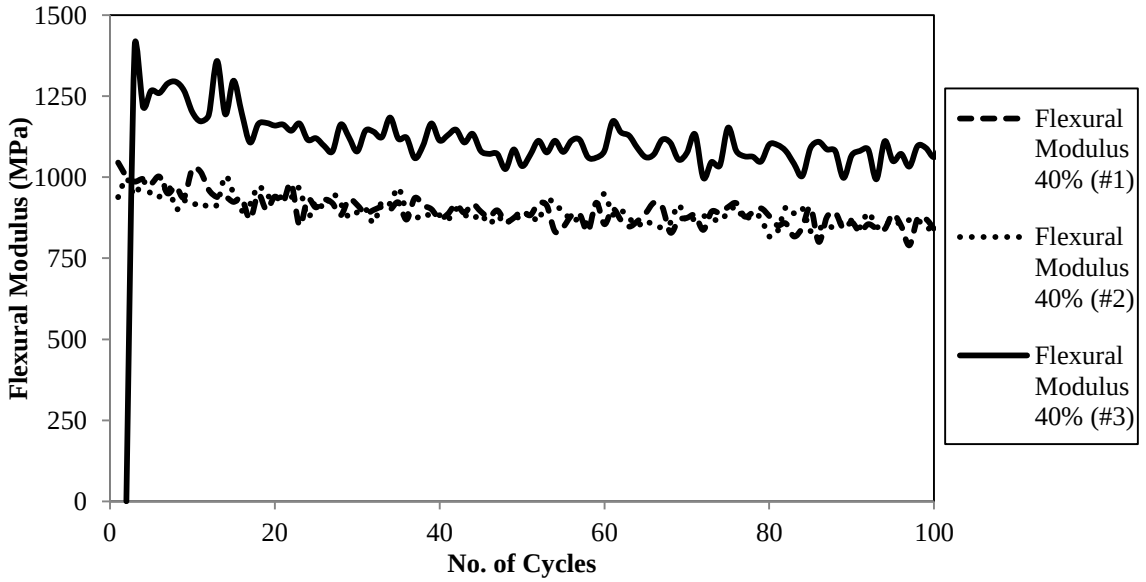

Figure B39. Flexural Modulus Variation at 40% Stress Level for 3 Silt-Lime-Fly ash Replicates

Figures B40 to B42 shows the change in total, plastic and elastic displacement during the test for the three different stress levels for silt-lime-fly ash specimens.

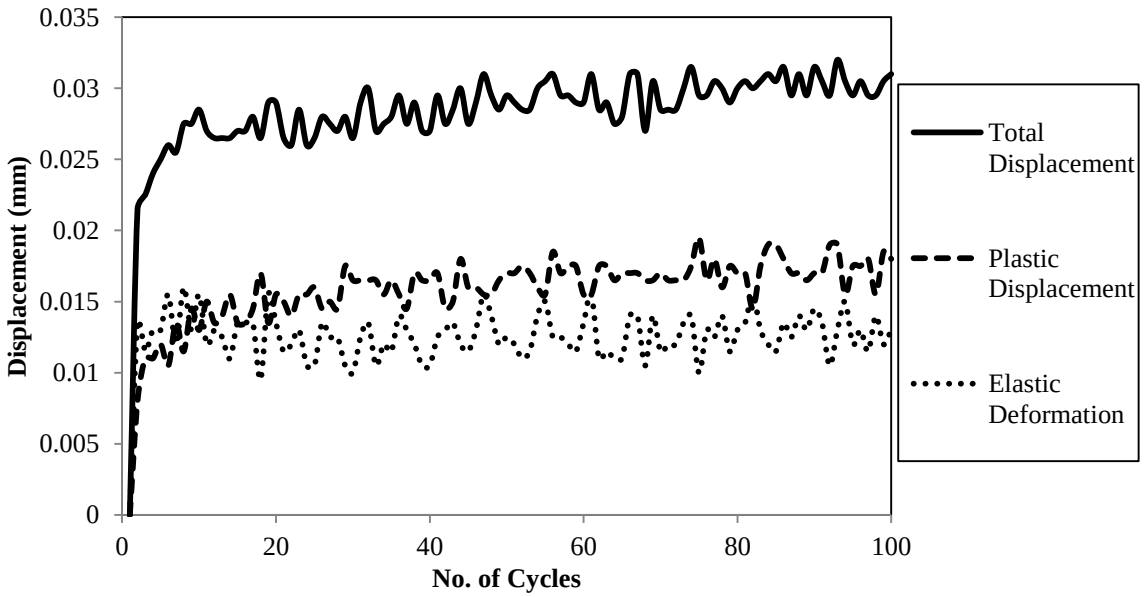

Figure B40. Displacement Variation for Flexural Modulus Test at 20% Stress Level for Silt-Lime-Fly ash Specimen

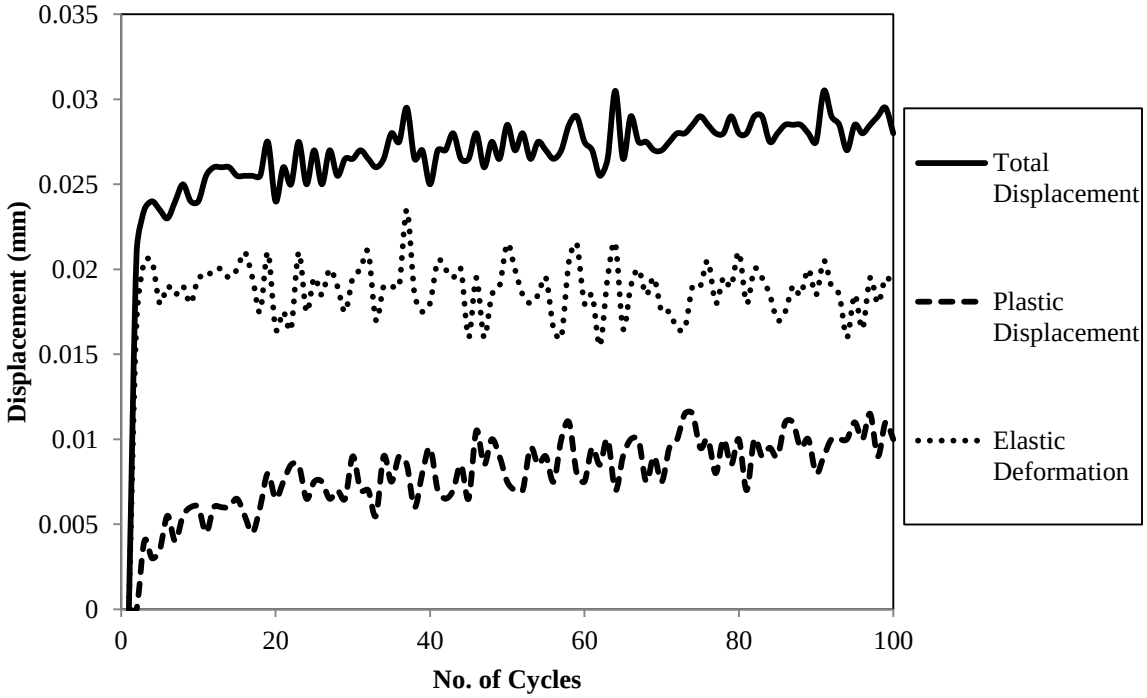

Figure B41. Displacement Variation for Flexural Modulus Test at 30% Stress Level for Silt-Lime-Fly ash Specimen

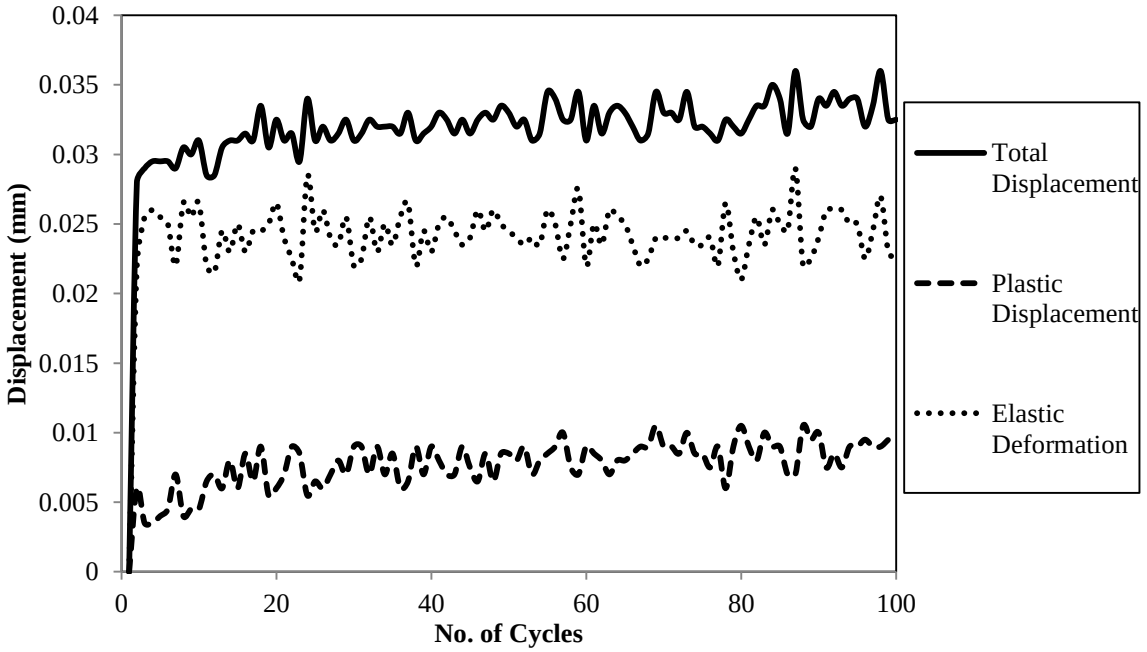

Figure B42. Displacement Variation for Flexural Modulus Test at 40% Stress Level for Silt-Lime-Fly ash Specimen

Table B8 shows the flexural modulus of each replicate for clay-lime specimens stabilized with 6% lime.

Table B8. Summary of the Flexural Modulus Test Results for Clay-Lime Specimens (Binder: 6%)

Specimen Number	**Stress level by percentage of flexural strength (%)**	**Flexural Modulus (MPa)**	**Average Flexural Modulus (MPa)**	**COV (%)**
FM-1	20	530.83	561.51	6
FM-2		557.44		
FM-3		596.26		
FM-1	30	565.44	601.36	8
FM-2		579.85		
FM-3		658.86		
FM-1	40	737.46	706.51	9
FM-2		626.11		
FM-3		745.94		

Figures B43 to B45 shows the change in flexural modulus during the test for each replicate for the three different stress levels for the clay-lime (6% binder) specimens.

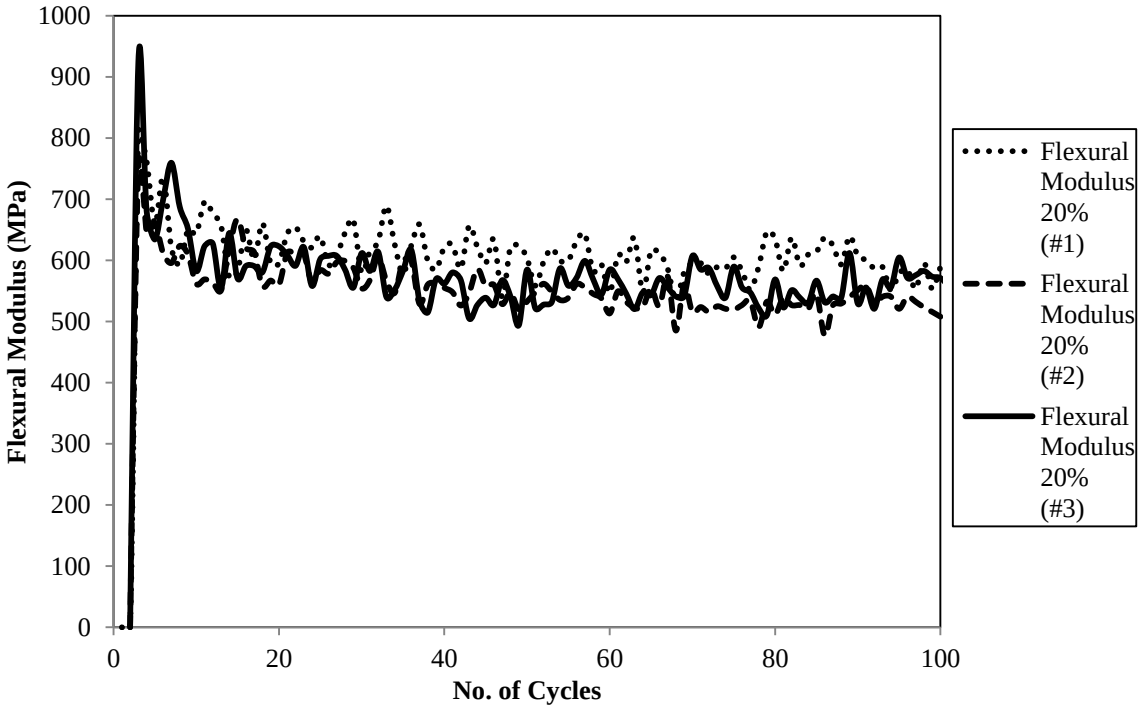

Figure B43. Flexural Modulus Variation at 20% Stress Level for 3 Clay-Lime Replicates

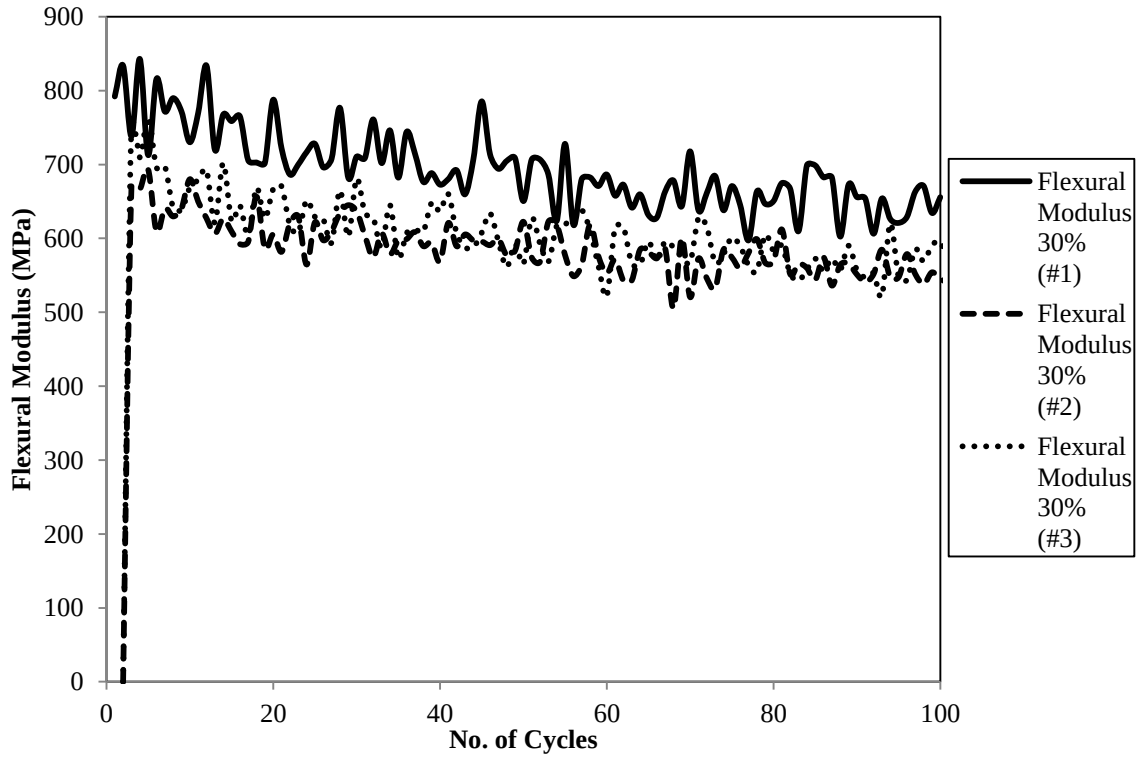

Figure B44. Flexural Modulus Variation at 30% Stress Level for 3 Clay-Lime Replicates

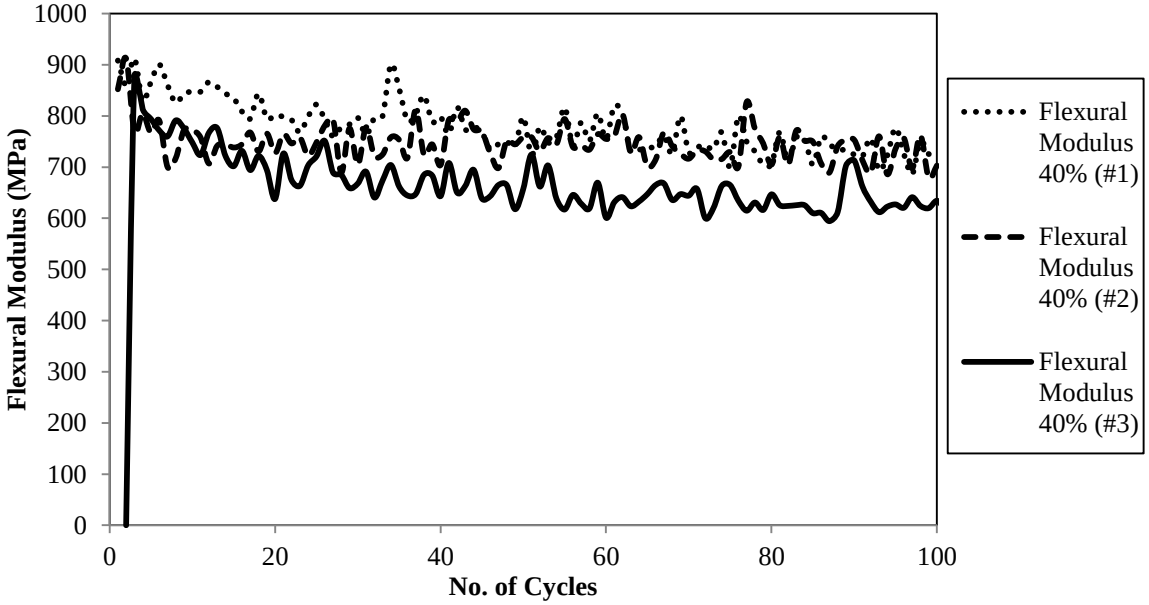

Figure B45. Flexural Modulus Variation at 40% Stress Level for 3 Clay-Lime Replicates

Figures B46 to B48 shows the change in total, plastic and elastic displacement during the test for the three different stress levels for clay-lime specimens.

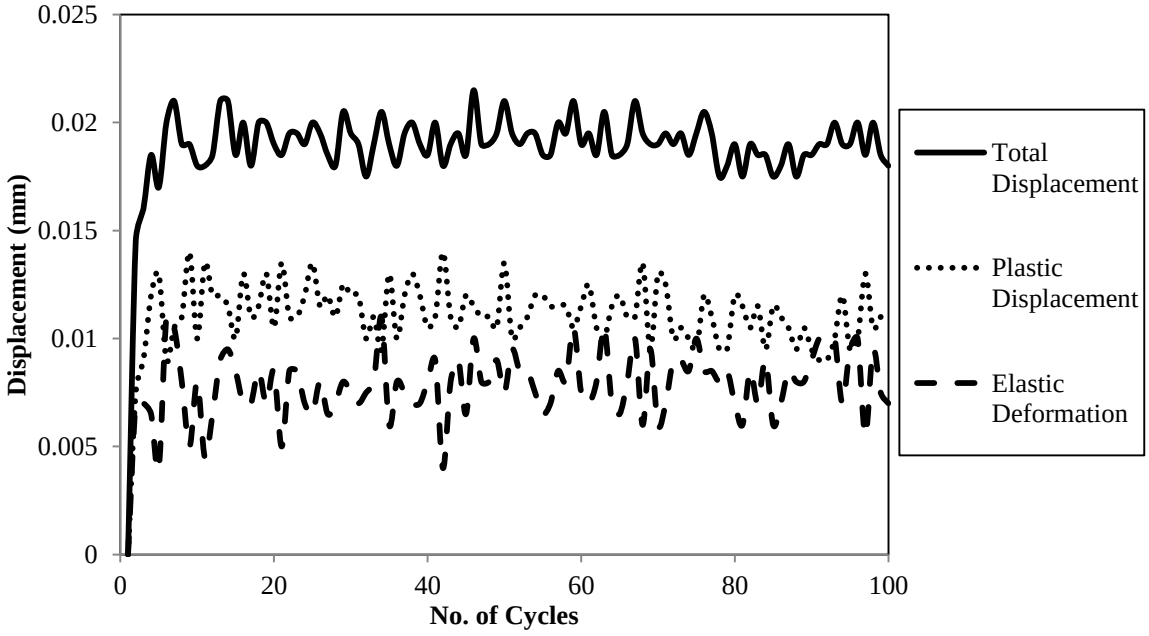

Figure B46. Displacement Variation for Flexural Modulus Test at 20% Stress Level for Clay-Lime Specimen

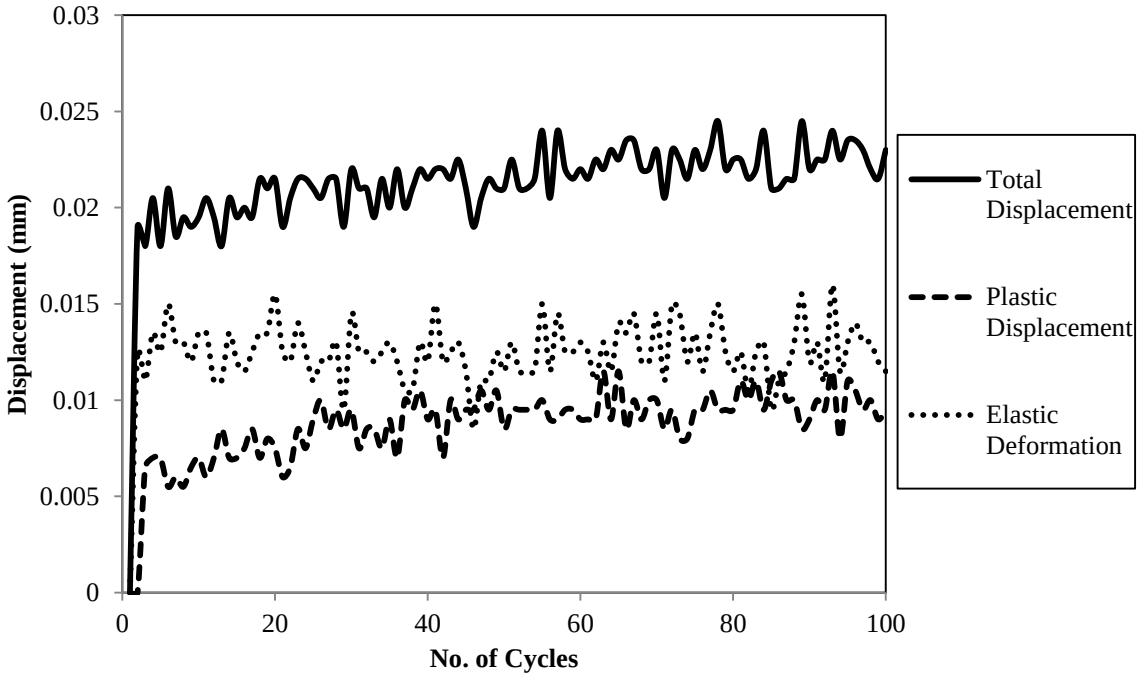

Figure B47. Displacement Variation for Flexural Modulus Test at 30% Stress Level for Clay-Lime Specimen

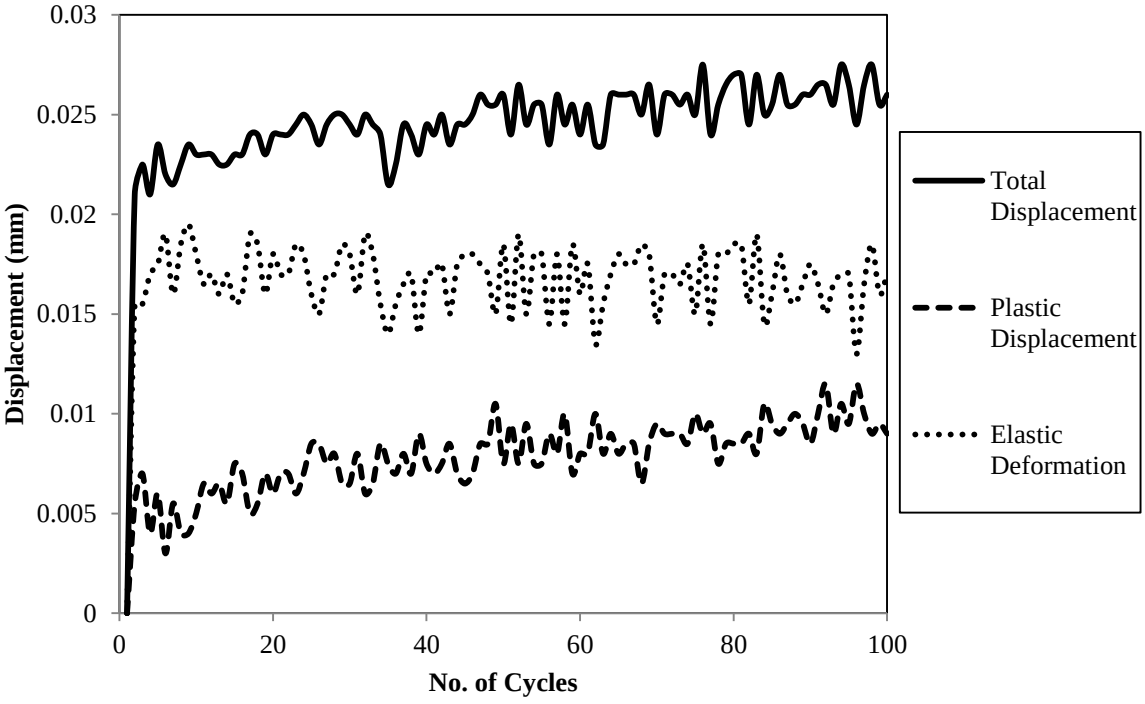

Figure B48. Displacement Variation for Flexural Modulus Test at 40% Stress Level for Clay-Lime Specimen

Table B9 shows the flexural modulus of each replicate for clay-cement specimens stabilized with 12% cement.

Table B9. Summary of the Flexural Modulus Test Results for Clay-Cement Specimens (Binder: 12%)

Specimen Number	**Stress level by percentage of flexural strength (%)**	**Flexural Modulus (MPa)**	**Average Flexural Modulus (MPa)**	**COV (%)**
FM-1	20	728.09	625.70	14
FM-2		556.51		
FM-3		583.87		
FM-1	30	1,052.00	999.19	5
FM-2		983.19		
FM-3		962.44		
FM-1	40	1,158.87	1,100.33	5
FM-2		1,085.92		
FM-3		1,056.14		

B.1. FLEXURAL MODULUS TESTING OF BEAM SPECIMENS WITH HIGHER BINDER CONTENT

Table B10 shows the flexural modulus of each replicate for gravel-cement specimens stabilized with 5% cement.

Table B10. Summary of the Flexural Modulus Test Results for Gravel-Cement Specimens (Binder: 5%)

Specimen Number	Stress level by percentage of flexural strength (%)	Flexural Modulus (MPa)	Average Flexural Modulus (MPa)	COV (%)
FM-1	20	873.64	1,003.46	13
FM-2		1,006.77		
FM-3		1,129.91		
FM-1	30	1,468.58	1,334.69	11
FM-2		1,182.52		
FM-3		1,352.89		
FM-1	40	1,727.89	1,512.16	12
FM-2		1,396.87		
FM-3		1,411.77		

Figures B49 to B51 shows the change in flexural modulus during the test for each replicate for the three different stress levels for the gravel-cement (5% binder) specimens.

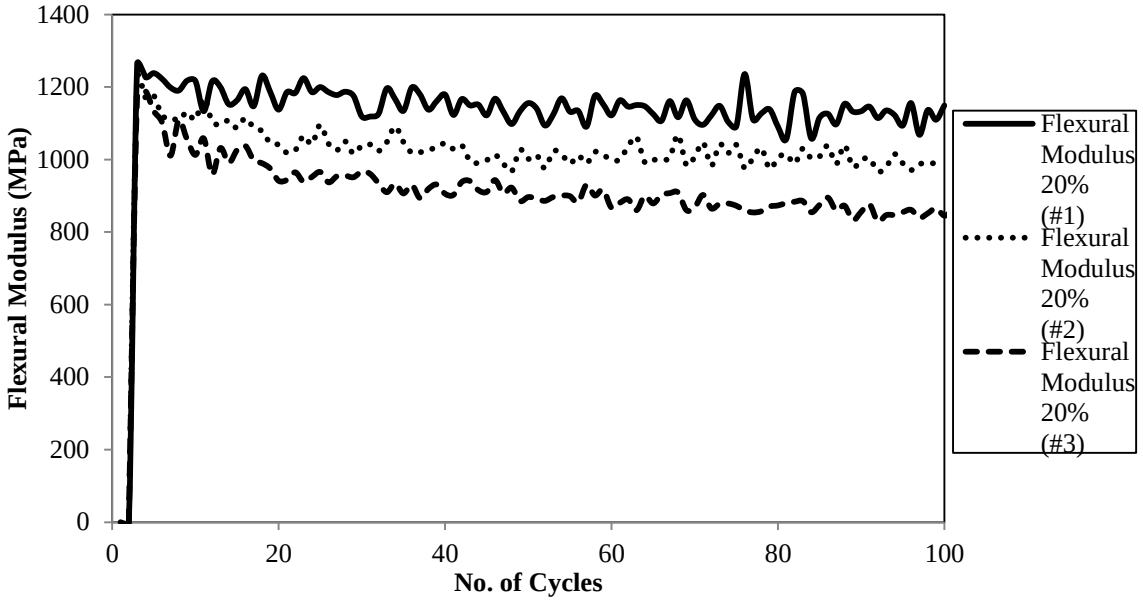

Figure B49. Flexural Modulus Variation at 20% Stress Level for 3 Gravel-Cement Replicates (Binder: 5%)

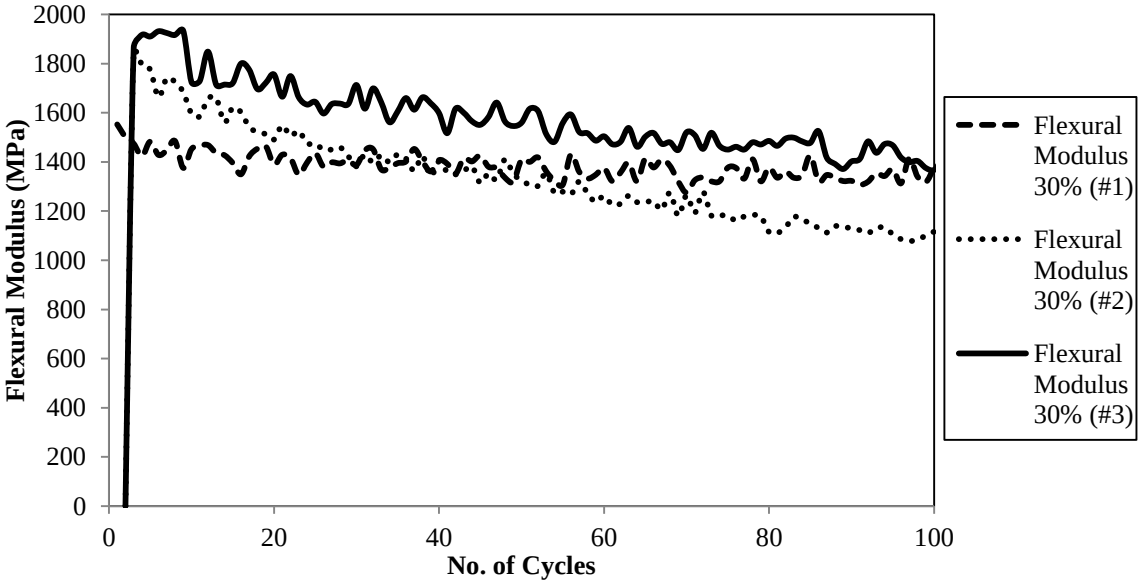

Figure B50. Flexural Modulus Variation at 30% Stress Level for 3 Gravel-Cement Replicates (Binder: 5%)

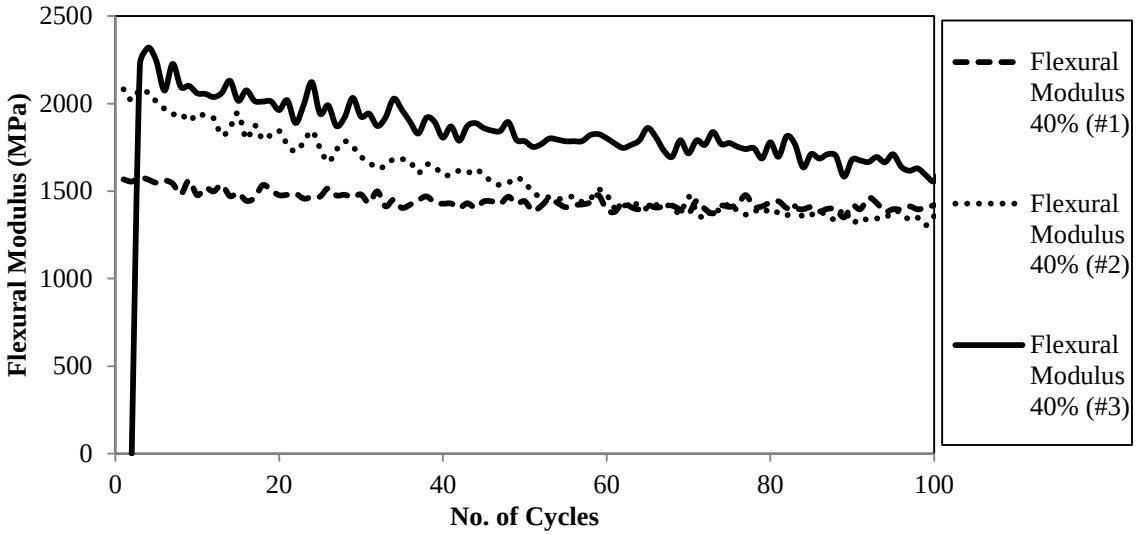

Figure B51. Flexural Modulus Variation at 40% Stress Level for 3 Gravel-Cement Replicates (Binder: 5%)

Figures B52 to B54 shows the change in total, plastic and elastic displacement during the test for the three different stress levels for gravel-cement (with 5% cement) specimens.

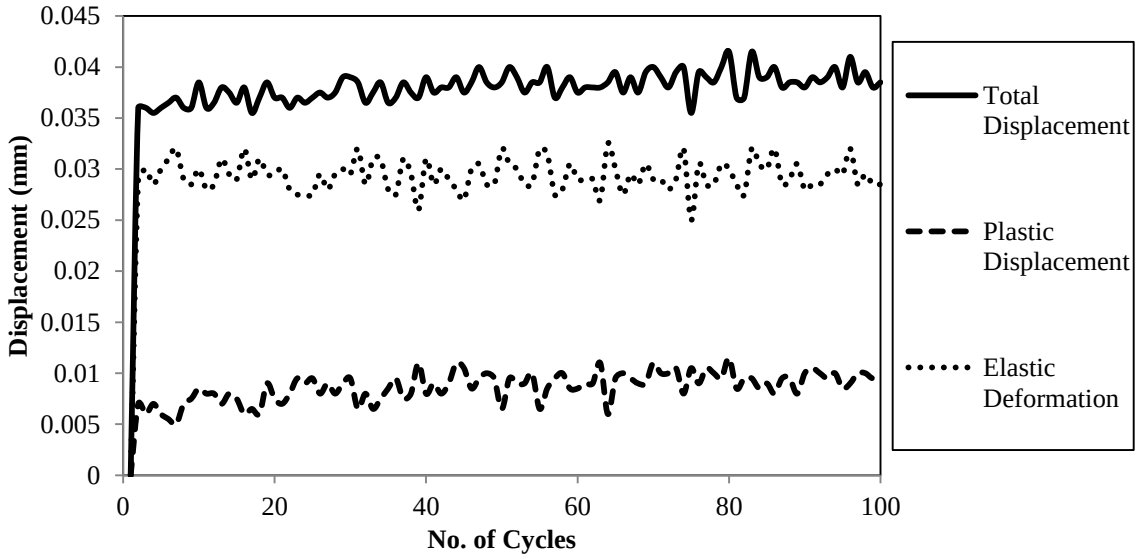

Figure B52. Displacement Variation for Flexural Modulus Test at 20% Stress Level for Gravel-Cement Specimens (Binder: 5%)

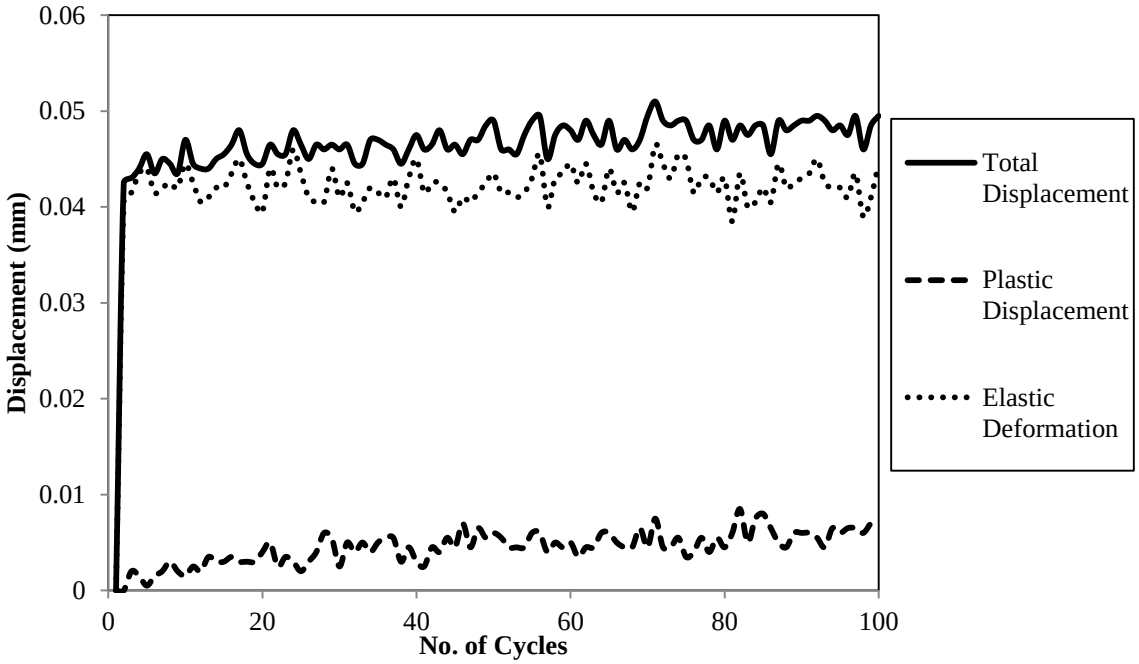

Figure B53. Displacement Variation for Flexural Modulus Test at 30% Stress Level for Gravel-Cement Specimens (Binder: 5%)

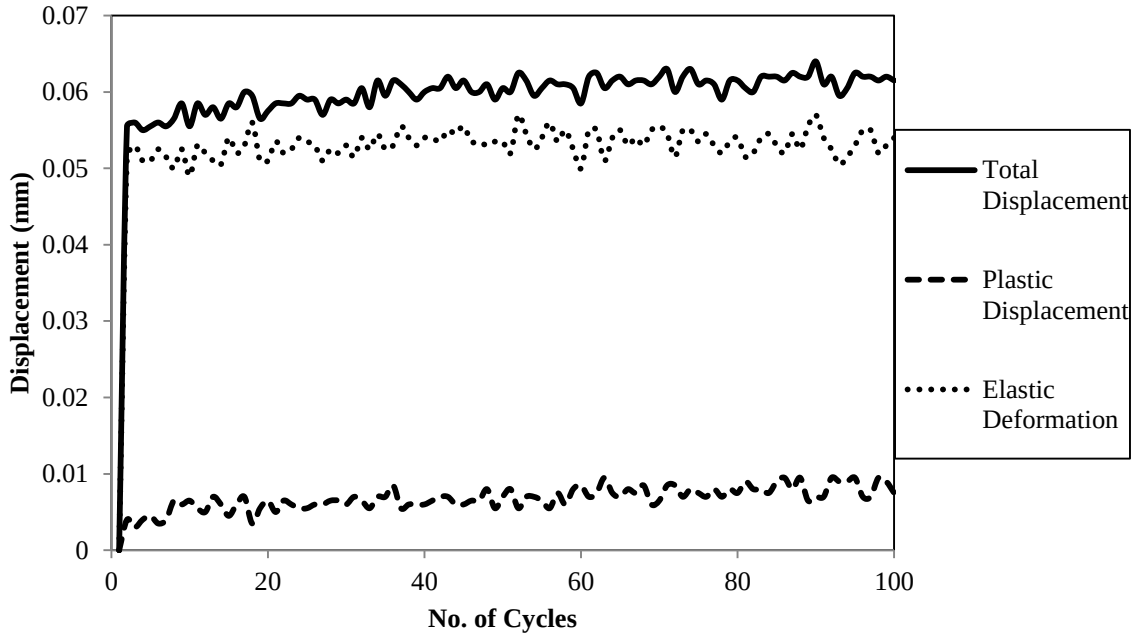

Figure B54. Displacement Variation for Flexural Modulus Test at 40% Stress Level for Gravel-Cement Specimens (Binder: 5%)

Table B11 shows the flexural modulus of each replicate for sand-cement specimens stabilized with 8% cement.

Table B11. Summary of the Flexural Modulus Test Results for Sand-Cement Specimens (Binder: 8%)

Specimen Number	Stress level by percentage of flexural strength (%)	Flexural Modulus (MPa)	Average Flexural Modulus (MPa)	COV (%)
FM-1	20	699.27	872.16	17
FM-2		950.44		
FM-3		967.13		
FM-1	30	1,418.18	1,379.16	4
FM-2		1,404.26		
FM-3		1,314.97		
FM-1	40	1481.27	1509.75	2
FM-2		1510.29		
FM-3		1537.60		

Figures B55 to B57 shows the change in flexural modulus during the test for each replicate for the three different stress levels for the sand-cement (8% binder) specimens.

Figure B55. Flexural Modulus Variation at 20% Stress Level for 3 Sand-Cement Replicates (Binder: 8%)

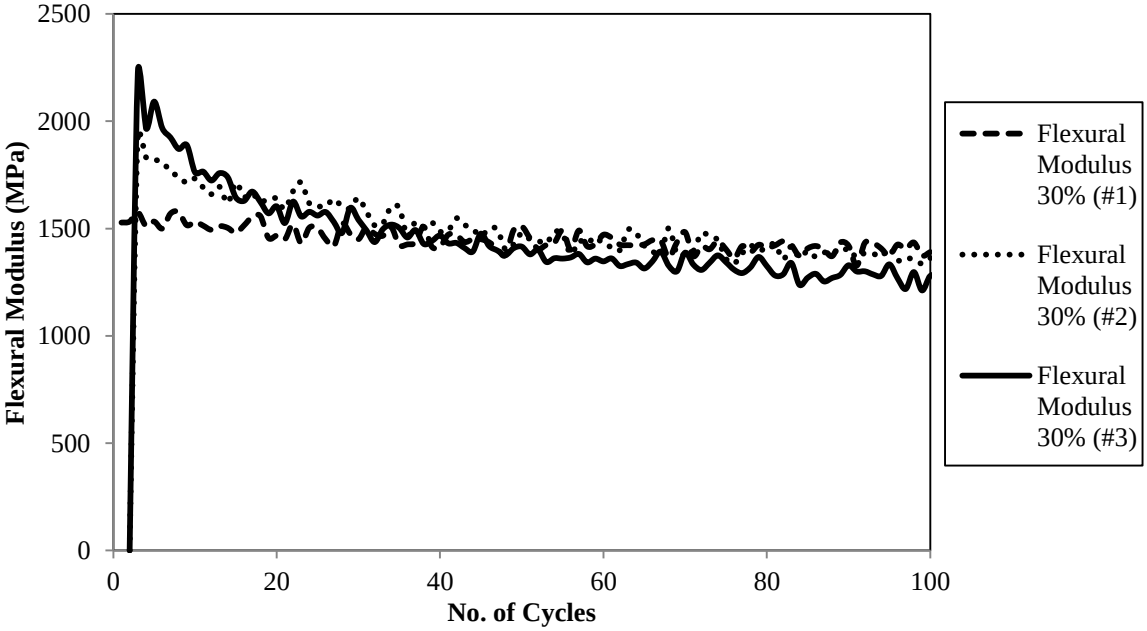

Figure B56. Flexural Modulus Variation at 30% Stress Level for 3 Sand-Cement Replicates (Binder: 8%)

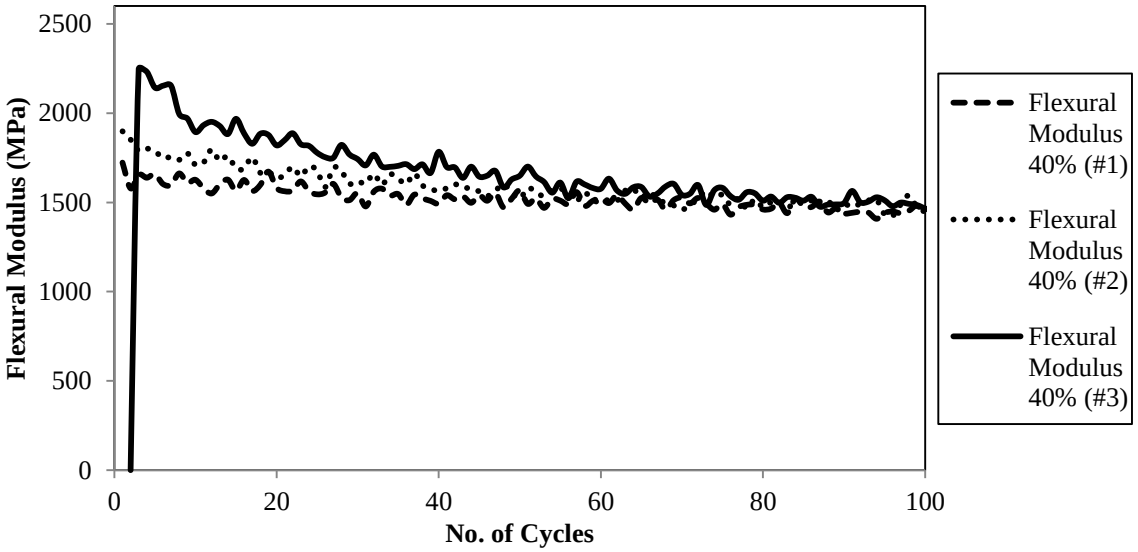

Figure B57. Flexural Modulus Variation at 40% Stress Level for 3 Sand-Cement Replicates (Binder: 8%)

Figures B58 to B60 shows the change in total, plastic and elastic displacement during the test for the three different stress levels for sand-cement (with 8% cement) specimens.

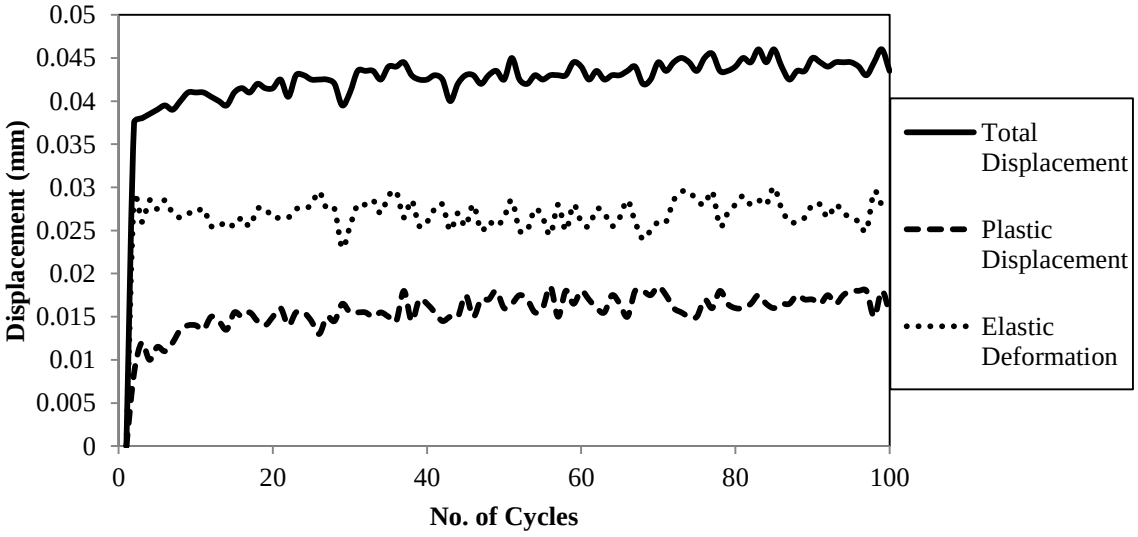

Figure B58. Displacement Variation for Flexural Modulus Test at 20% Stress Level for Sand-Cement Specimens (Binder: 8%)

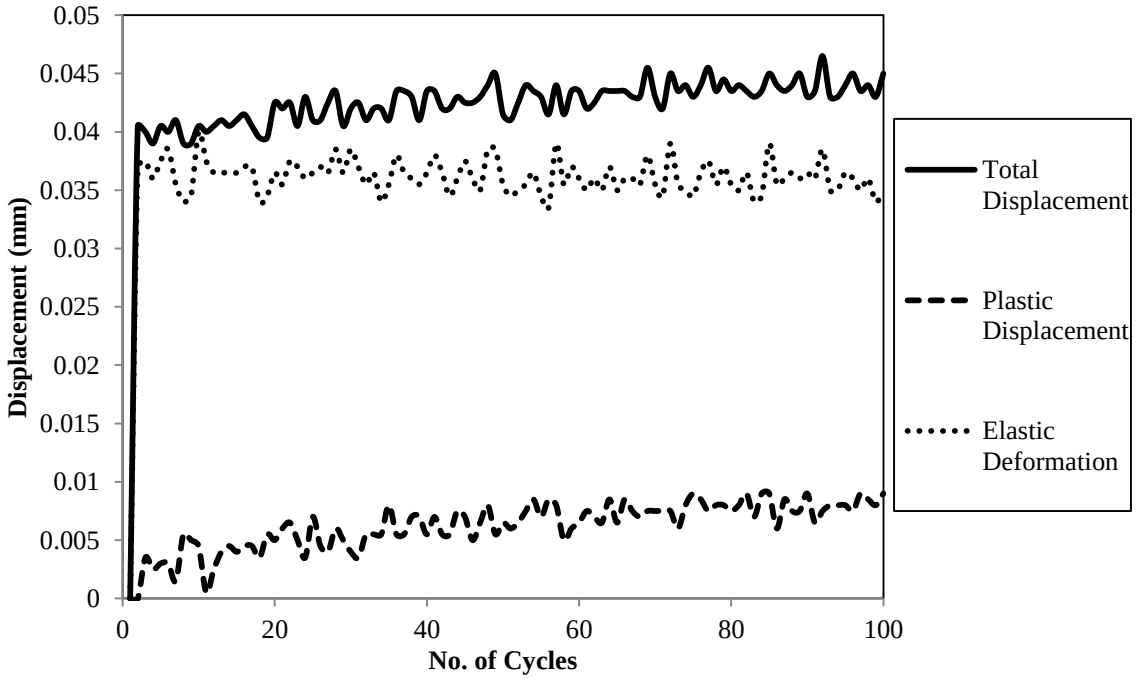

Figure B59. Displacement Variation for Flexural Modulus Test at 30% Stress Level for Sand-Cement Specimens (Binder: 8%)

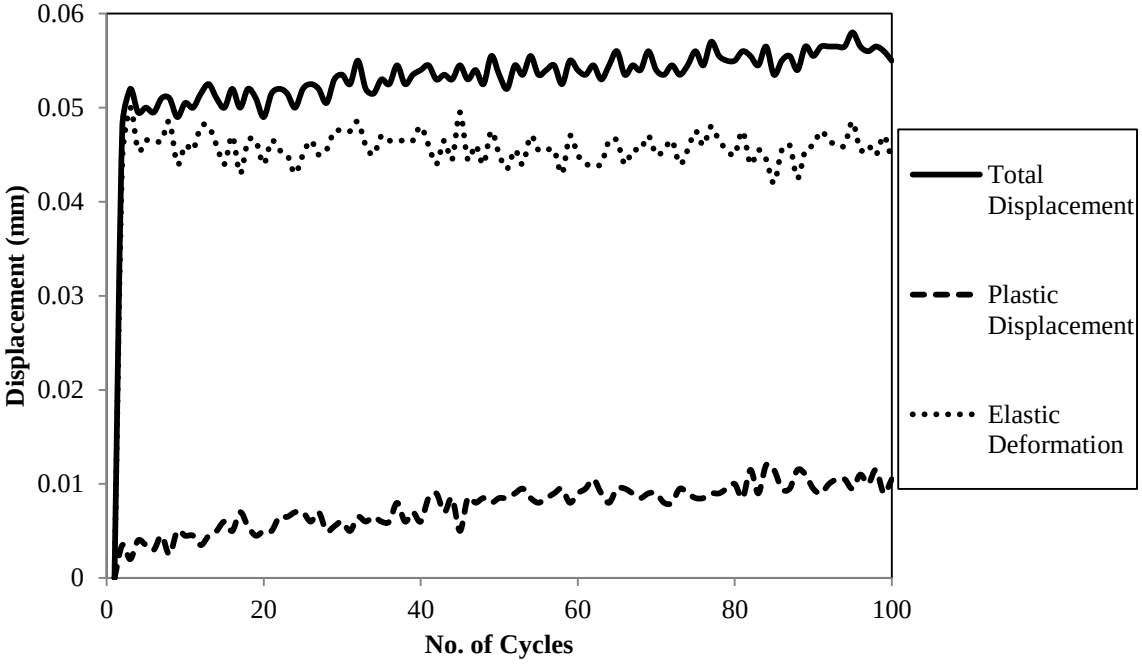

Figure B60. Displacement Variation for Flexural Modulus Test at 40% Stress Level for Sand-Cement Specimens (Binder: 8%)

Table B12 shows the flexural modulus of each replicate for silt-fly ash specimens stabilized with 18% class C fly ash.

Table B12. Summary of the Flexural Modulus Test Results for Silt-Fly ash Specimens (Binder: 18%)

Specimen Number	Stress level by percentage of flexural strength (%)	Flexural Modulus (MPa)	Average Flexural Modulus (MPa)	COV (%)
FM-1	20	547.51	518.62	5
FM-2		494.84		
FM-3		513.52		
FM-1	30	592.05	587.82	4
FM-2		607.84		
FM-3		561.85		
FM-1	40	645.97	615.77	5
FM-2		621.08		
FM-3		580.33		

Figures B61 to B63 shows the change in flexural modulus during the test for each replicate for the three different stress levels for the silt-fly ash (18% binder) specimens.

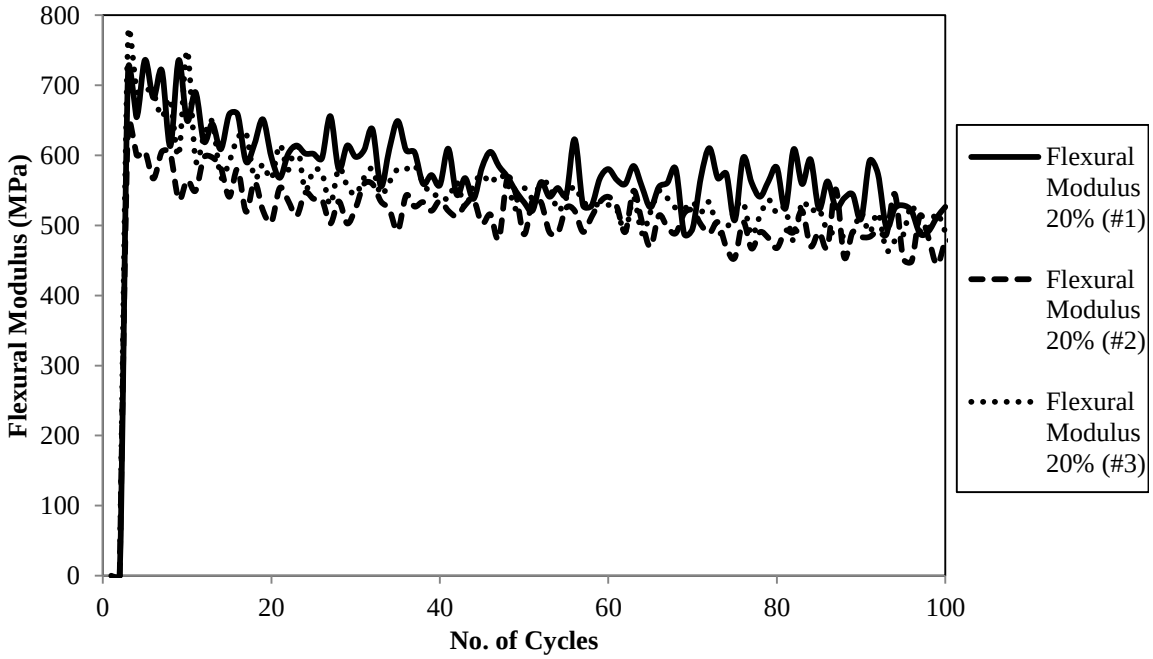

Figure B61. Flexural Modulus Variation at 20% Stress Level for 3 Silt-Fly ash Replicates (Binder: 18%)

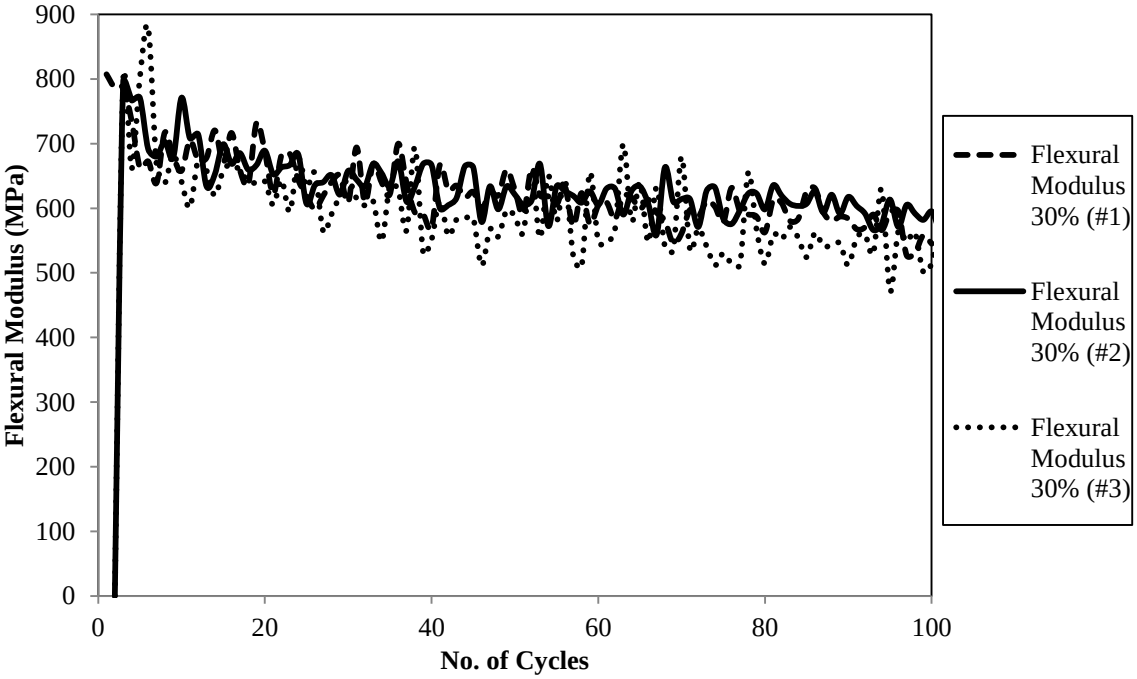

Figure B62. Flexural Modulus Variation at 30% Stress Level for 3 Silt-Fly ash Replicates (Binder: 18%)

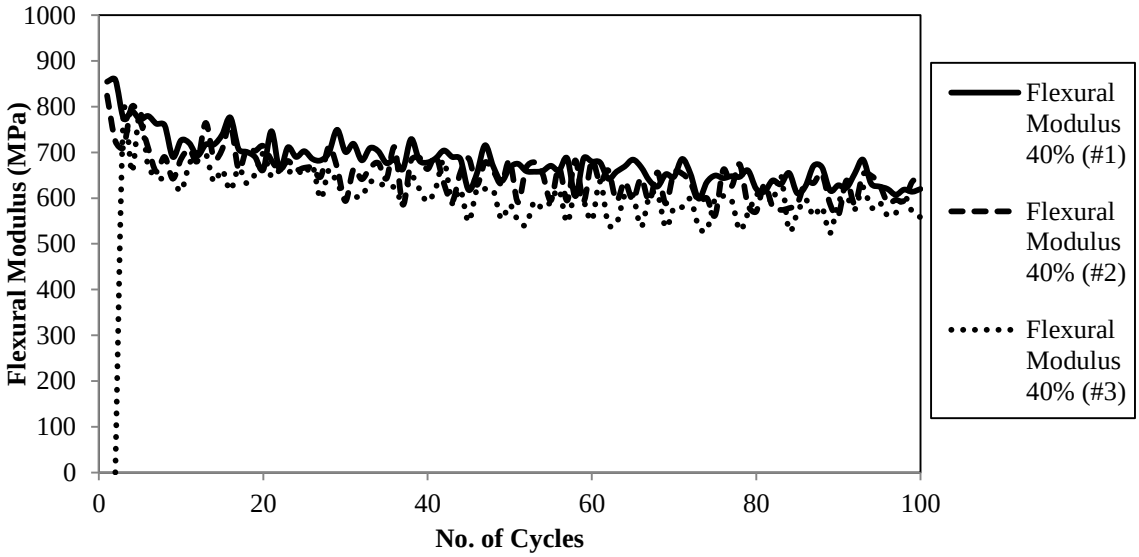

Figure B63. Flexural Modulus Variation at 40% Stress Level for 3 Silt-Fly ash Replicates (Binder: 18%)

Figures B64 to B66 shows the change in total, plastic and elastic displacement during the test for the three different stress levels for silt-fly ash (with 18% class C fly ash) specimens.

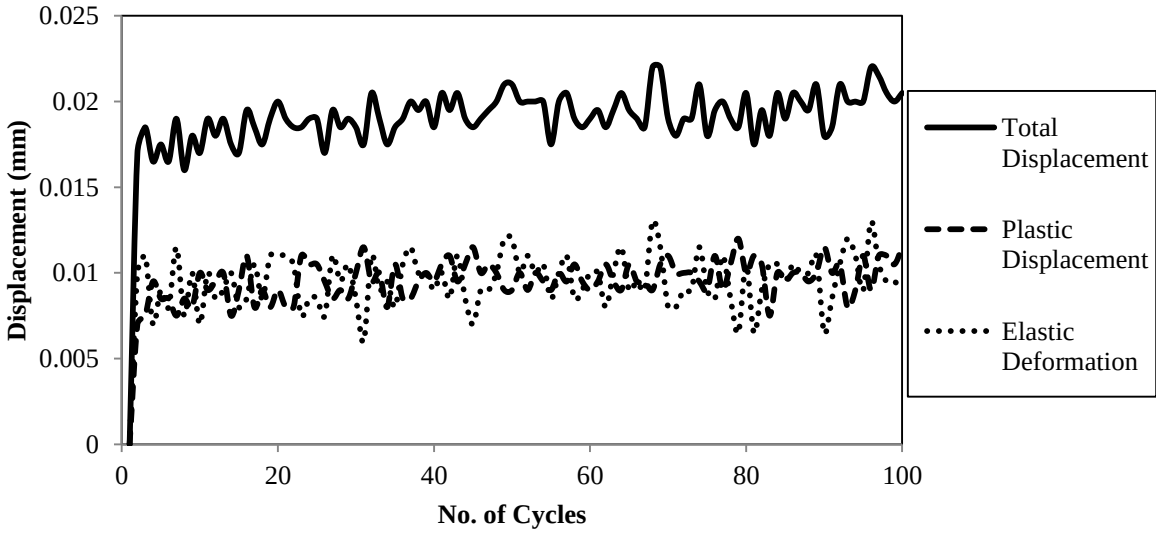

Figure B64. Displacement Variation for Flexural Modulus Test at 20% Stress Level for Silt-Fly ash Specimens (Binder: 18%)

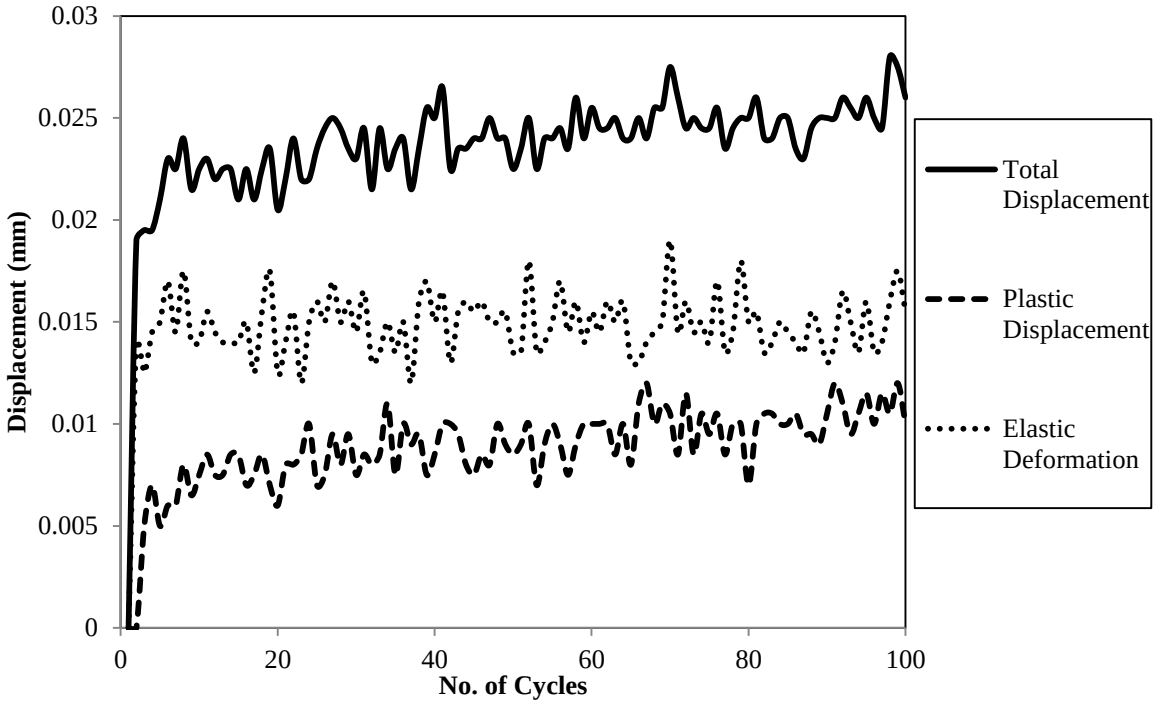

Figure B65. Displacement Variation for Flexural Modulus Test at 30% Stress Level for Silt-Fly ash Specimens (Binder: 18%)

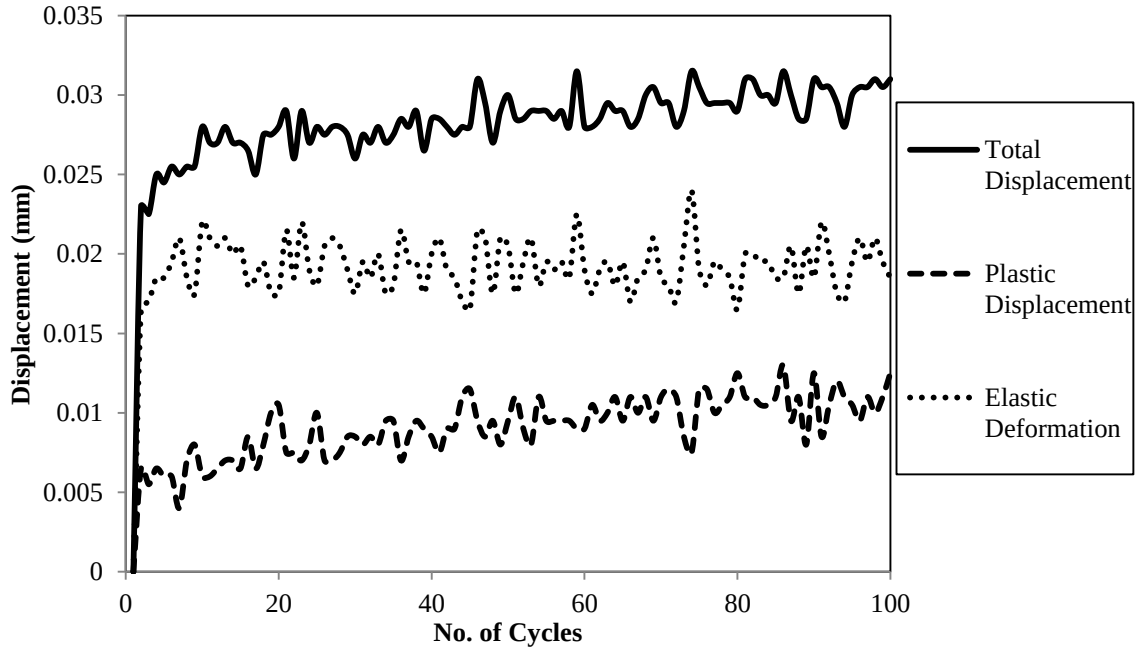

Figure B66. Displacement Variation for Flexural Modulus Test at 40% Stress Level for Silt-Fly ash Specimens (Binder: 18%)

APPENDIX – C: FATIGUE CRACK TESTING

This section shows the fatigue cracking test results for the mixtures. Six beam specimens were tested for the clay-cement beam specimens (12% binder). Table C1 shows the summary of the fatigue test results on the clay-cement beam specimens. Specimen FT-6 did not rupture even after 131,000 cycles of loading.

Table C1. Summary of the Fatigue Strength Test Results on Clay-Cement Specimens (Binder Content: 12%)

SN	SL (%)	IFM (MPa)	FFM (MPa)	PFME (%)	IS (με)	N
FT-1	85	1,062	938	88	545	587
FT-2	85	1,096	1,000	91	522	146
FT-3	75	979	841	86	528	3,715
FT-4	75	675	607	90	613	24,625
FT-5	65	1,076	910	84	470	38,161
FT-6*	60	834	724	87	496	>131,000

*SN = Specimen Number; SL = Stress Level; IFM = Initial Flexural Modulus; FFM = Final Flexural Modulus (i.e. Flexural Modulus at the end of Fatigue Test); PFME =Percent of Flexural Modulus at the End of Test; IS = Initial Strain; N = Number of Cycles at the End of Test (i.e. Fatigue Life); * Did not fail*

Note: *Range of Failure: 50% to 78% of IFM (Average: 64%)*

Figure C1 shows the typical fatigue curve at 85% stress level for the clay-cement specimens (FT-1). From this fatigue curve, the failure occurs shortly after the cycles to half the initial modulus was reached. Figure C2 shows the total, plastic and elastic deformations of the same beam specimen (FT-1) during the fatigue test. The beam specimen ruptures when as the displacement reaches its peak.

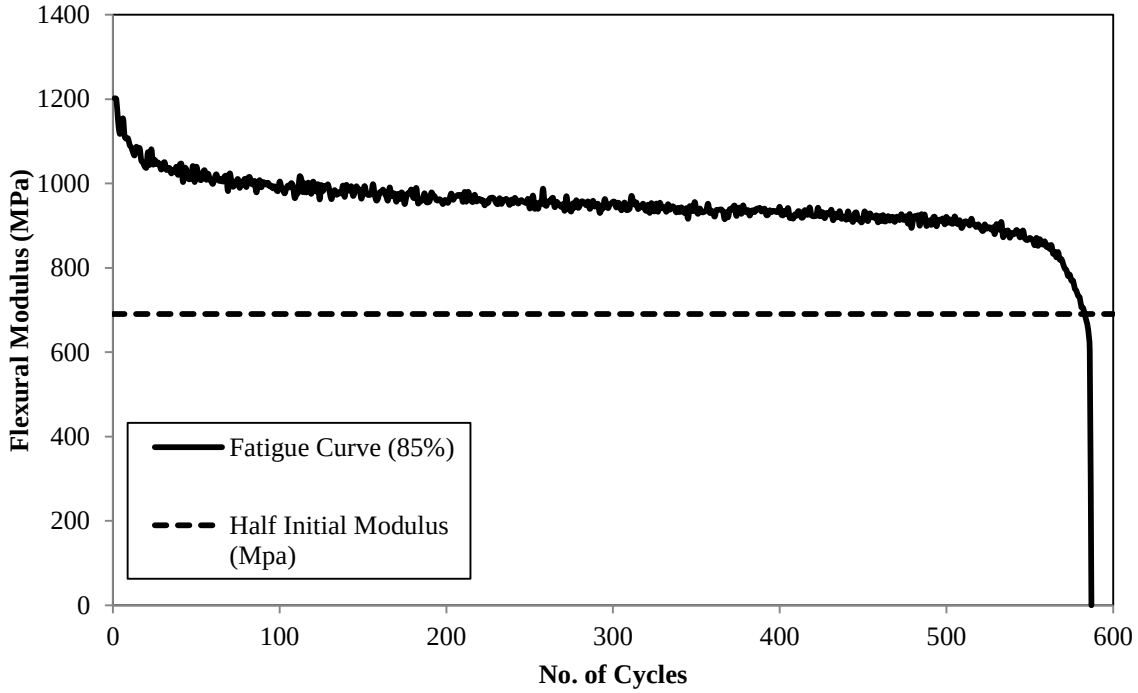

Figure C1. Typical Degradation of Flexural Modulus in a Fatigue Test at 85% Stress Level [Clay-Cement (12%) Specimens (FT-1)]

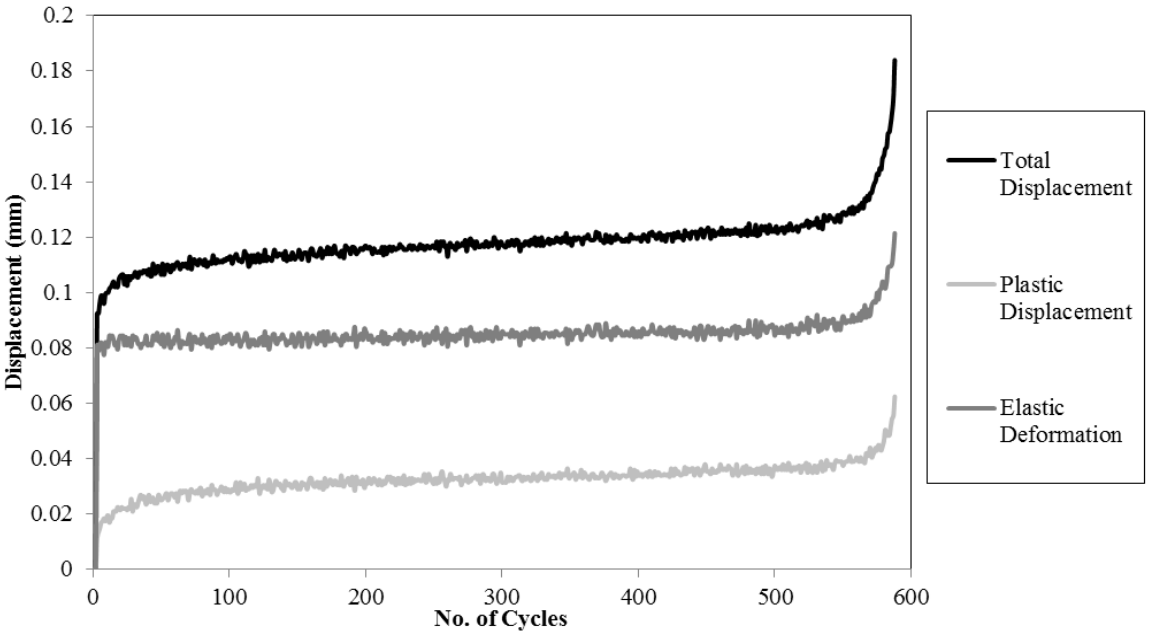

Figure C2. Displacement Variation v/s No. of Cycles in a Fatigue Test at 85% Stress Level [Clay-Cement (12%) Specimens (FT-1)]

From the clay-cement specimen fatigue curves, not all the specimen ruptured shortly after the cycles to half the initial modulus was reached. The specimens ruptured when the initial modulus reached in the range of 50% to 78%. One possible reason might be that the test conducted by Migdley and Yeo (2008) were on stone stabilized with cement and had a higher flexural strength. Figures C3 to C6 shows the flexural modulus degradation curves for specimens FT-2 to FT-5 for clay-cement specimens stabilized with 12% cement.

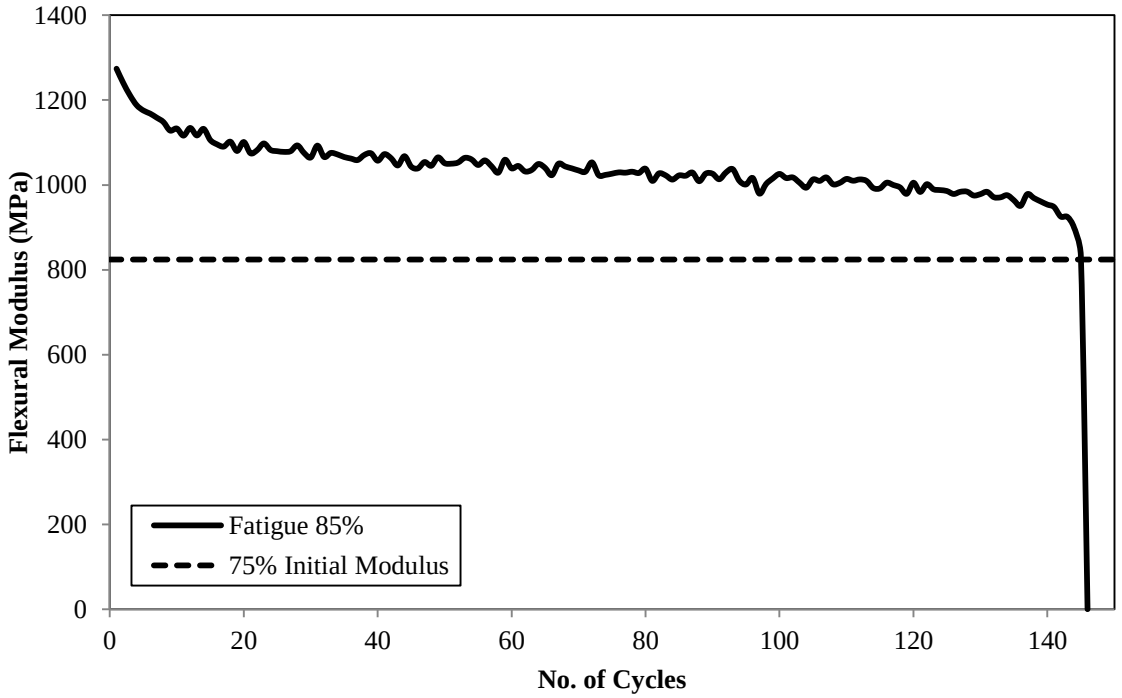

Figure C3. Typical Degradation of Flexural Modulus in a Fatigue Test at 85% Stress Level [Clay-Cement (12%) Specimens (FT-2)]

Figures C7 to C10 shows the displacement (total, plastic and elastic) variation curves for specimens FT-2 to FT-5 for clay-cement specimens stabilized with 12% cement.

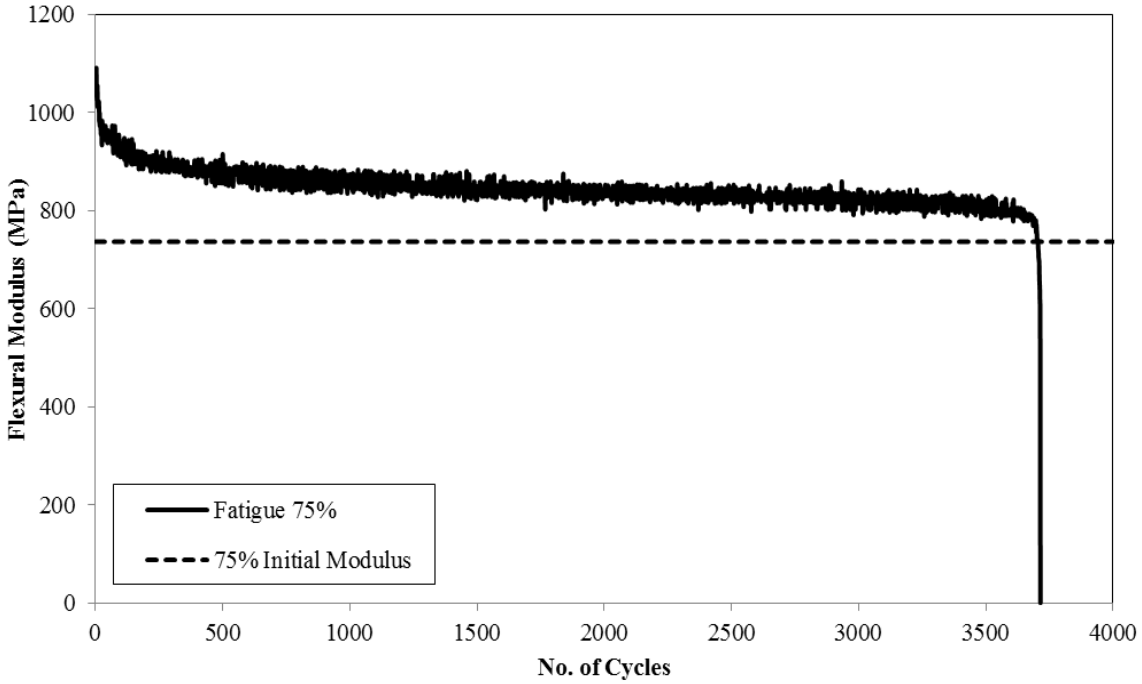

Figure C4. Typical Degradation of Flexural Modulus in a Fatigue Test at 75% Stress Level [Clay-Cement (12%) Specimens (FT-3)]

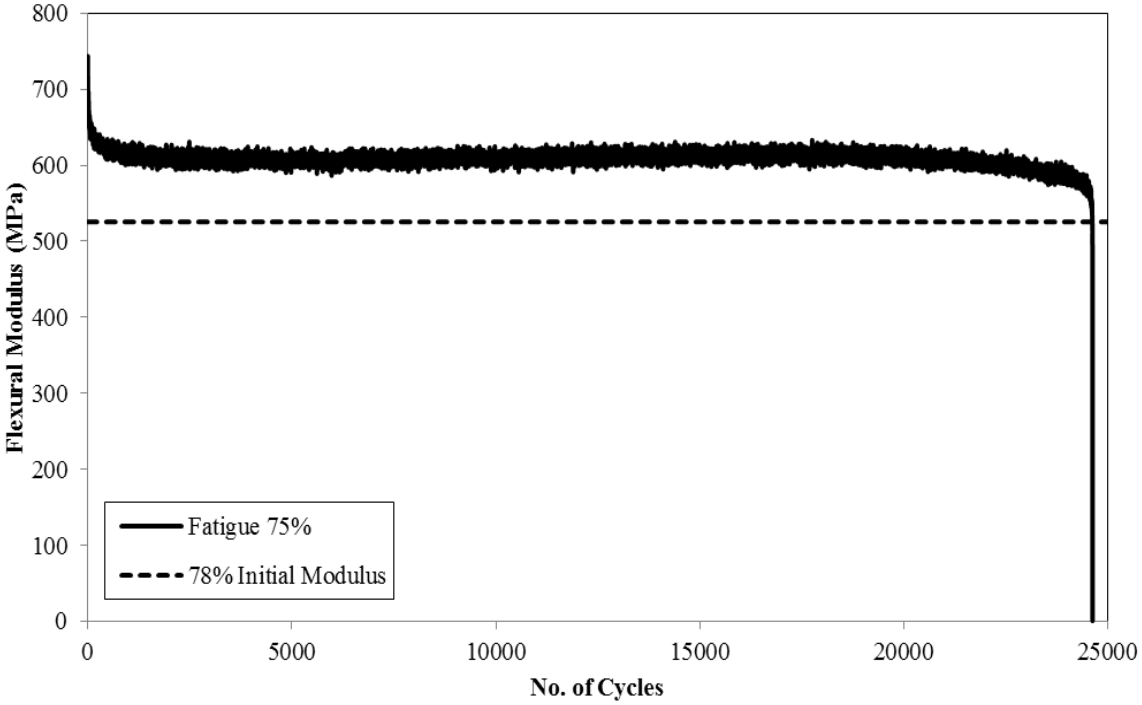

Figure C5. Typical Degradation of Flexural Modulus in a Fatigue Test at 75% Stress Level [Clay-Cement (12%) Specimens (FT-4)]

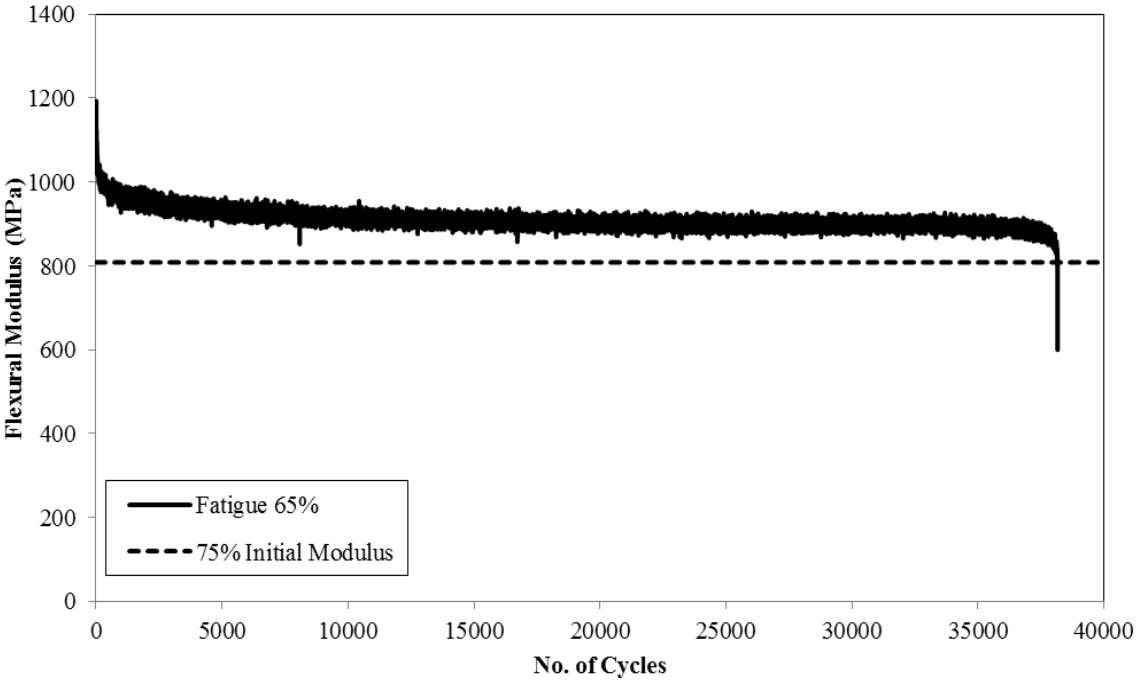

Figure C6. Typical Degradation of Flexural Modulus in a Fatigue Test at 65% Stress Level [Clay-Cement (12%) Specimens (FT-5)]

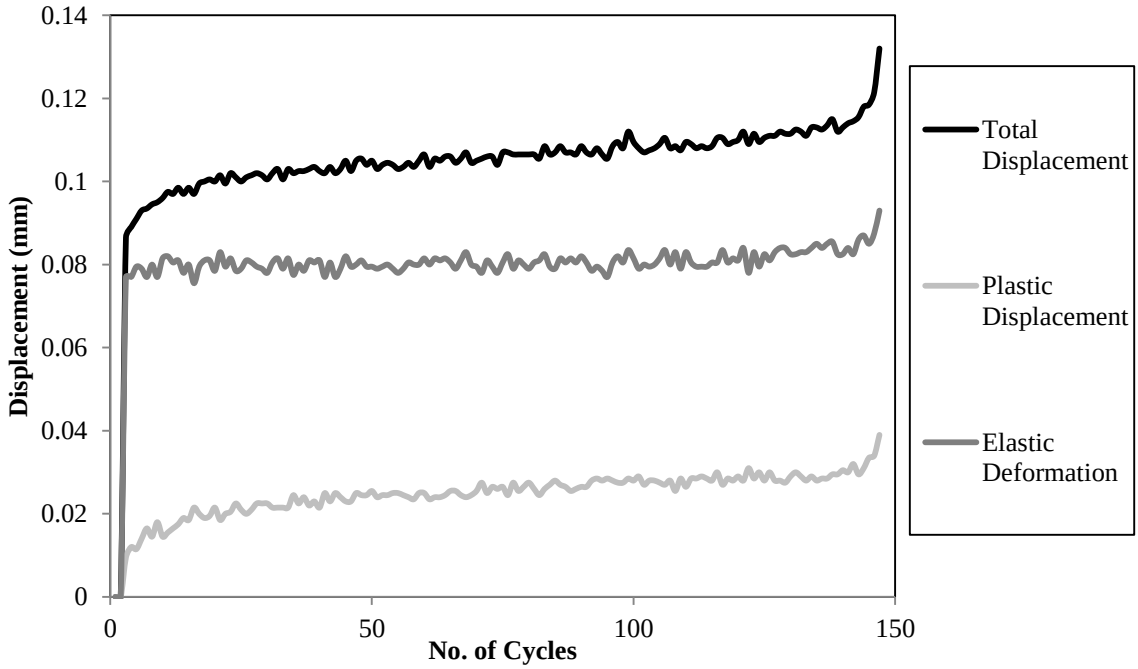

Figure C7. Displacement Variation v/s No. of Cycles in a Fatigue Test at 85% Stress Level [Clay-Cement (12%) Specimens (FT-2)]

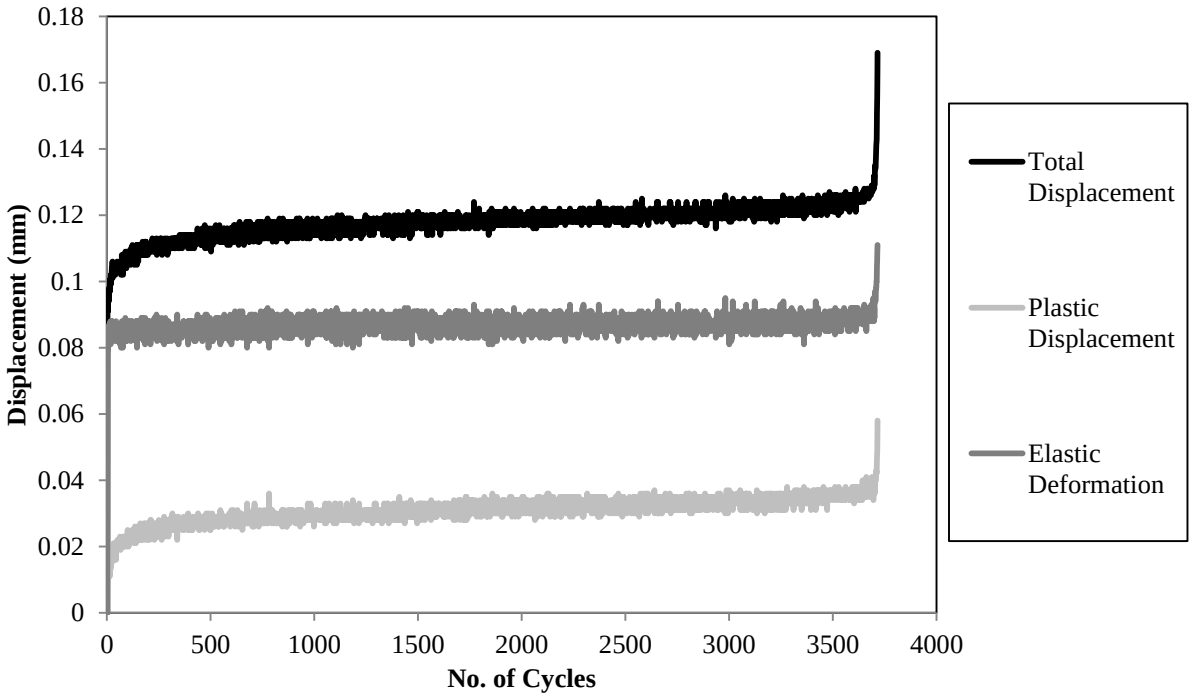

Figure C8. Displacement Variation v/s No. of Cycles in a Fatigue Test at 75% Stress Level [Clay-Cement (12%) Specimens (FT-3)]

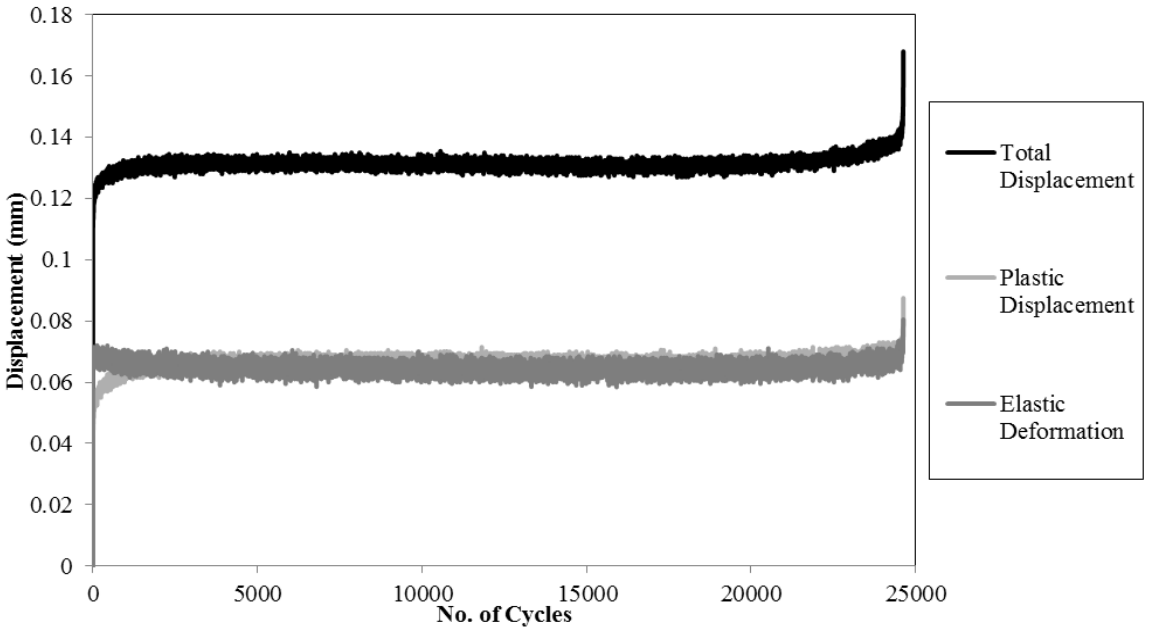

Figure C9. Displacement Variation v/s No. of Cycles in a Fatigue Test at 75% Stress Level [Clay-Cement (12%) Specimens (FT-4)]

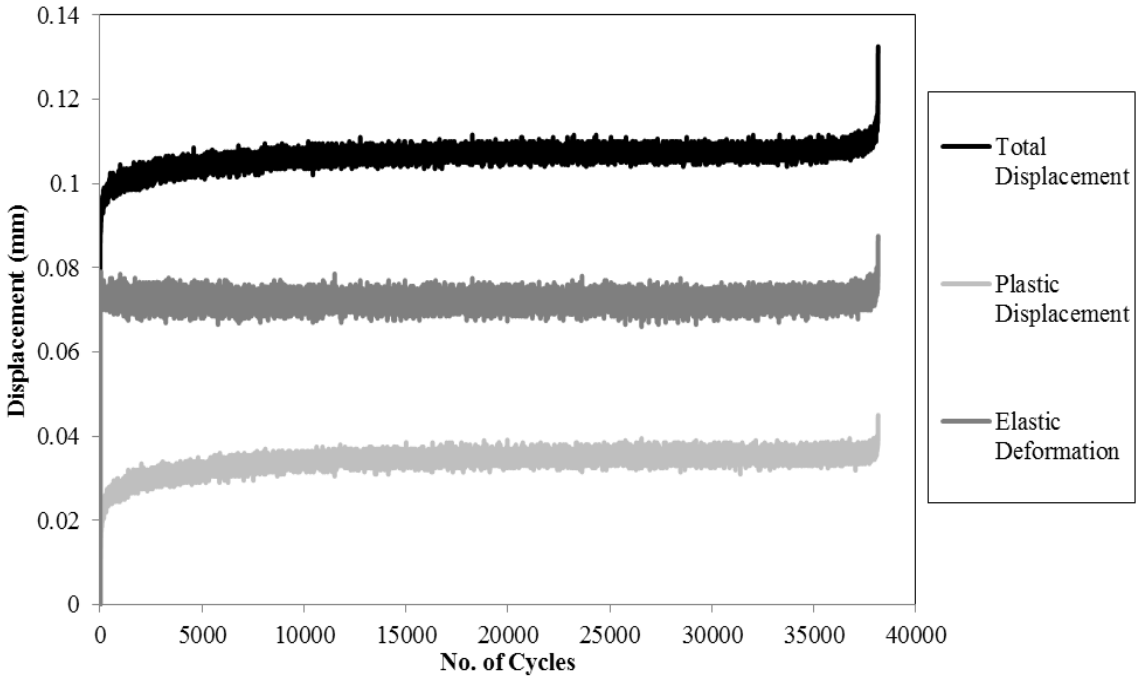

Figure C10. Displacement Variation v/s No. of Cycles in a Fatigue Test at 65% Stress Level [Clay-Cement (12%) Specimens (FT-5)]

Seven beam specimens were tested for the gravel-cement beam specimens (3% binder). Table C2 shows the summary of the fatigue test results on the gravel-cement beam specimens.

Figures C11 to C15 shows the flexural modulus degradation curves for specimens FT-2, 3, 5, 6 and 7 for gravel-cement specimens stabilized with 3% cement. Figures C16 to C19 shows the displacement (total, plastic and elastic) variation curves for specimens FT-, 5, 6 and 7 for gravel-cement specimens stabilized with 3% cement. From the gravel-cement specimen curves, the specimen ruptured shortly after the cycles to half the initial modulus was reached.

Table C2. Summary of the Fatigue Strength Test Results on Gravel-Cement Specimens (Binder Content: 3%)

SN	SL (%)	IFM (MPa)	FFM (MPa)	PFME (%)	IS (με)	N
FT-1	85	-	-	-	-	2
FT-2	75	927	607	65	491	94
FT-3	75	1,216	919	76	367	164
FT-4	75	867	712	82	617	104
FT-5	60	829	600	72	569	2,628
FT-6	60	544	442	81	652	1,244
FT-7	50	700	557	80	427	46,329

SN = Specimen Number; SL = Stress Level; IFM = Initial Flexural Modulus; FFM = Final Flexural Modulus (i.e. Flexural Modulus at the end of Fatigue Test); PFME =Percent of Flexural Modulus at the End of Test; IS = Initial Strain; N = Number of Cycles at the End of Test (i.e. Fatigue Life)

Note: *All specimens failed at 50% of IFM*

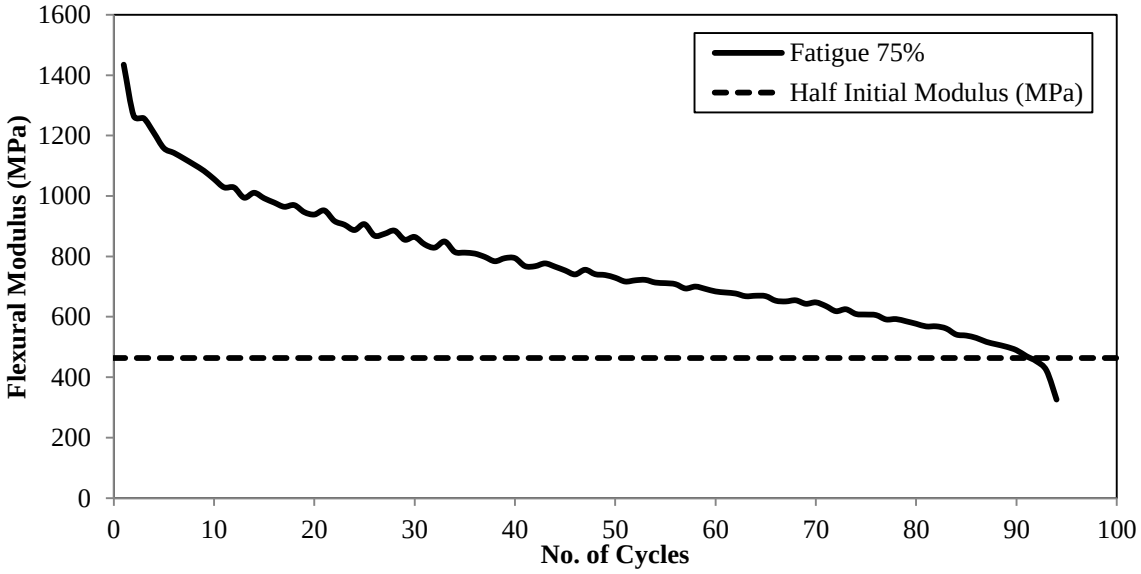

Figure C11. Typical Degradation of Flexural Modulus in a Fatigue Test at 75% Stress Level [Gravel-Cement (3%) Specimens (FT-2)]

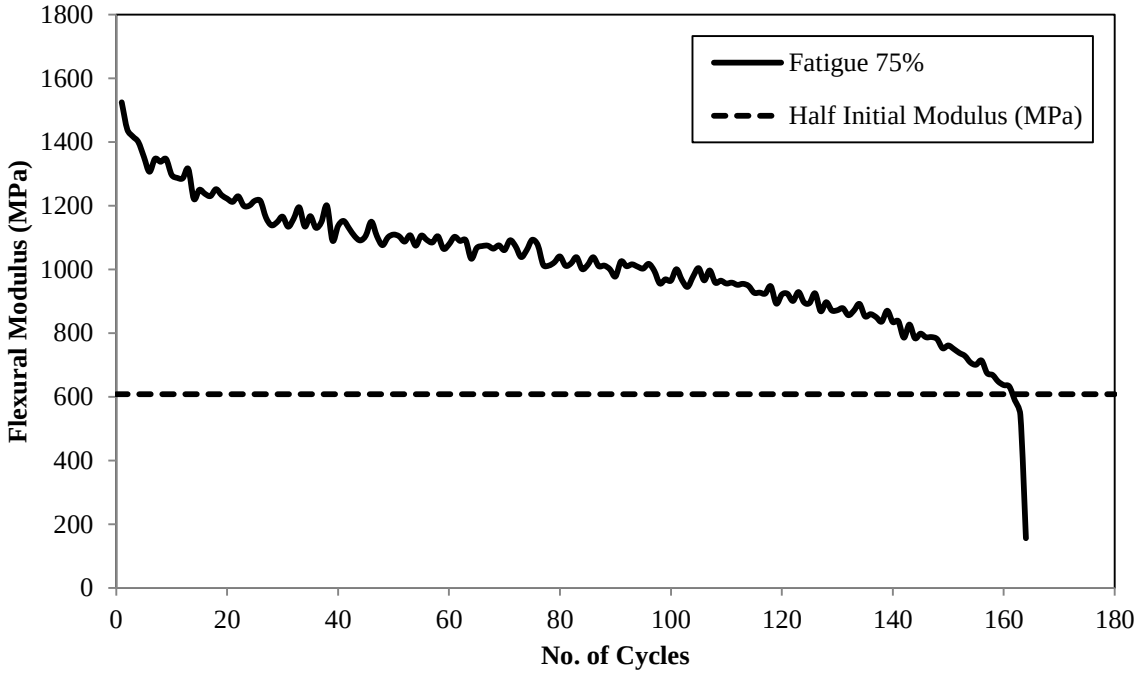

Figure C12. Typical Degradation of Flexural Modulus in a Fatigue Test at 75% Stress Level [Gravel-Cement (3%) Specimens (FT-3)]

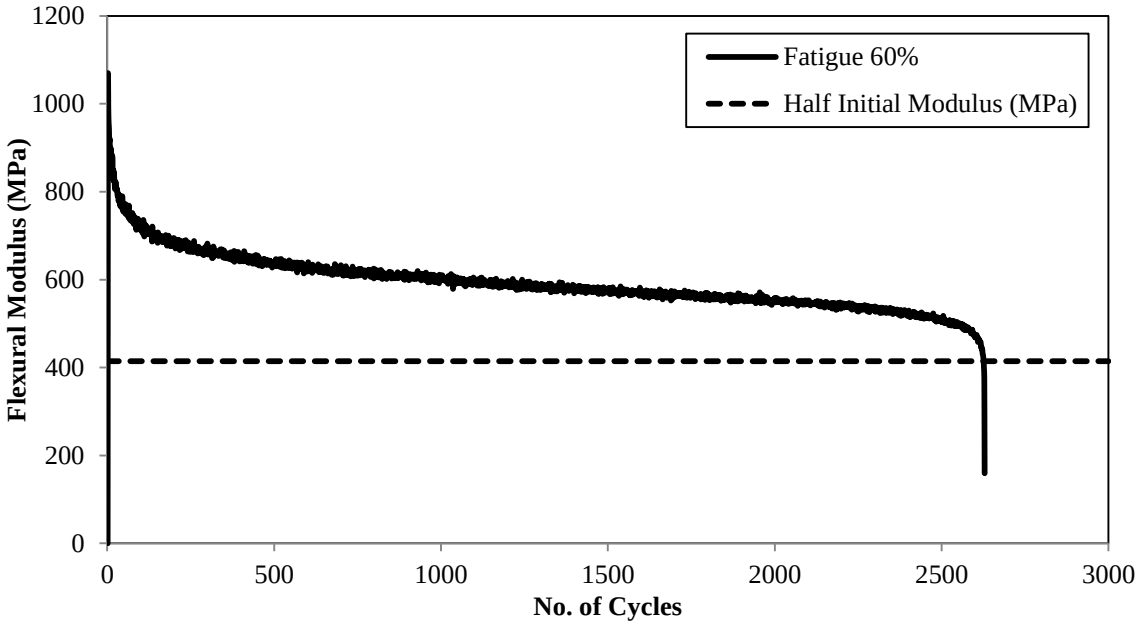

Figure C13. Typical Degradation of Flexural Modulus in a Fatigue Test at 60% Stress Level [Gravel-Cement (3%) Specimens (FT-5)]

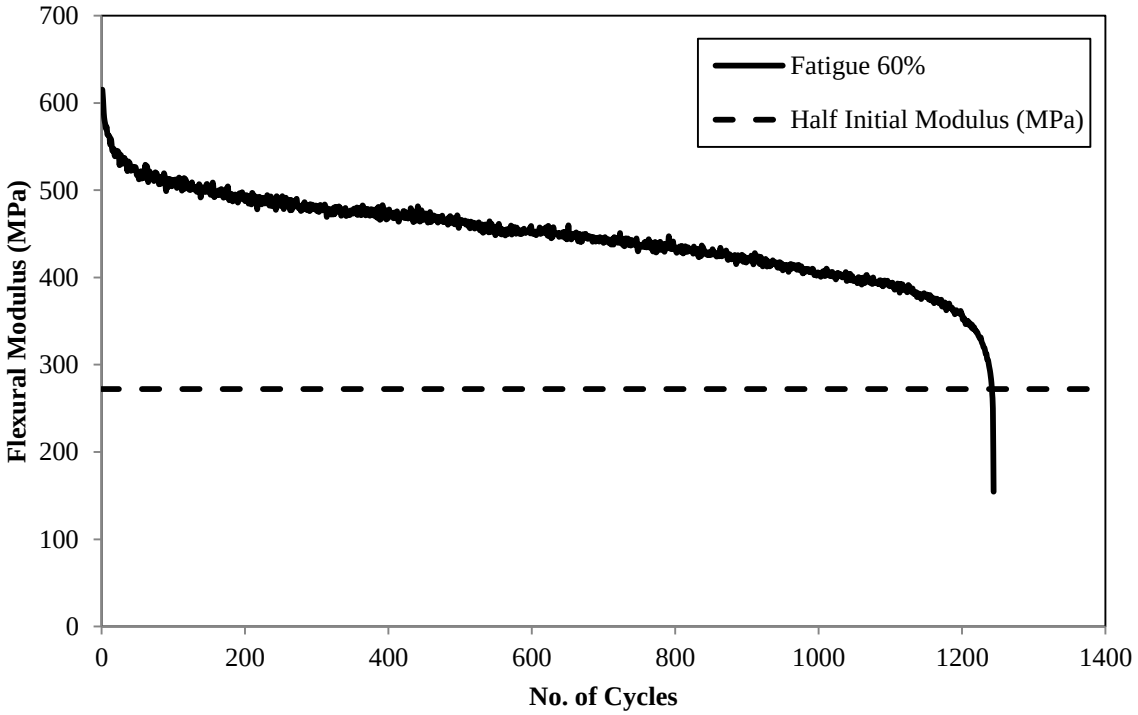

Figure C14. Typical Degradation of Flexural Modulus in a Fatigue Test at 60% Stress Level [Gravel-Cement (3%) Specimens (FT-6)]

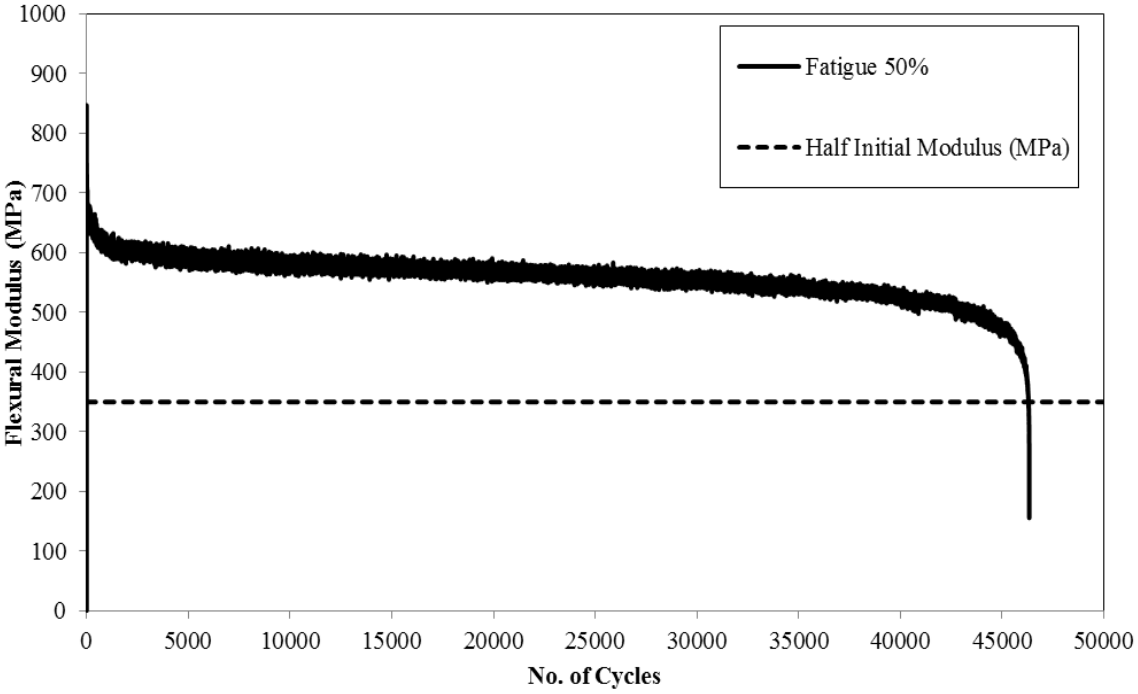

Figure C15. Typical Degradation of Flexural Modulus in a Fatigue Test at 50% Stress Level [Gravel-Cement (3%) Specimens (FT-7)]

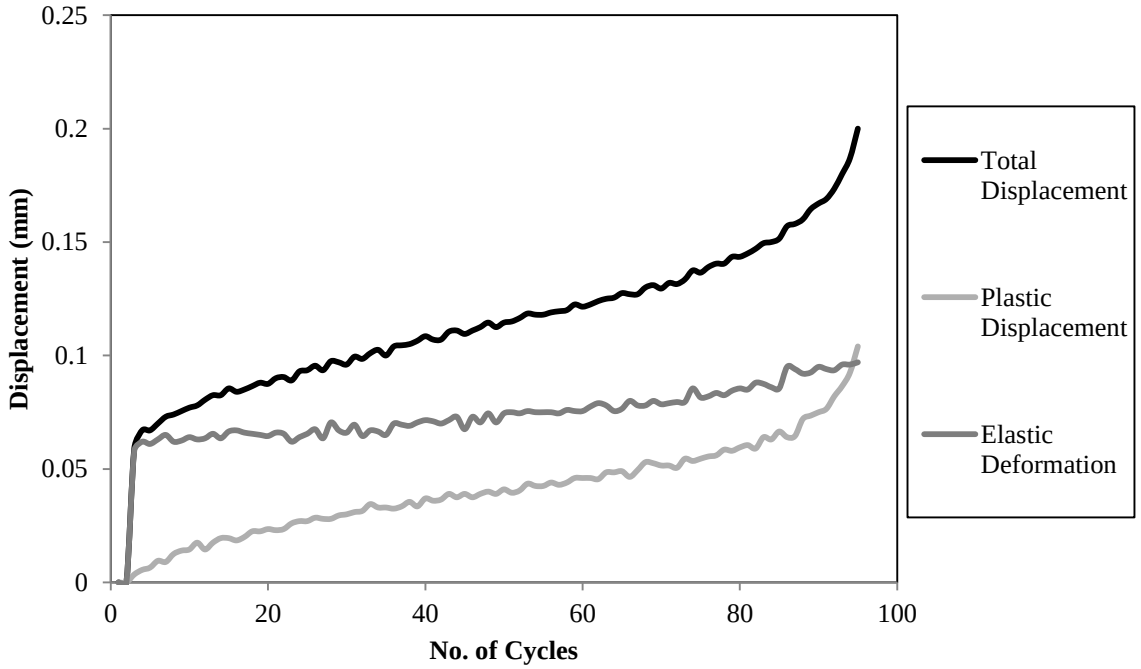

Figure C16. Displacement Variation v/s No. of Cycles in a Fatigue Test at 75% Stress Level [Gravel-Cement (3%) Specimens (FT-2)]

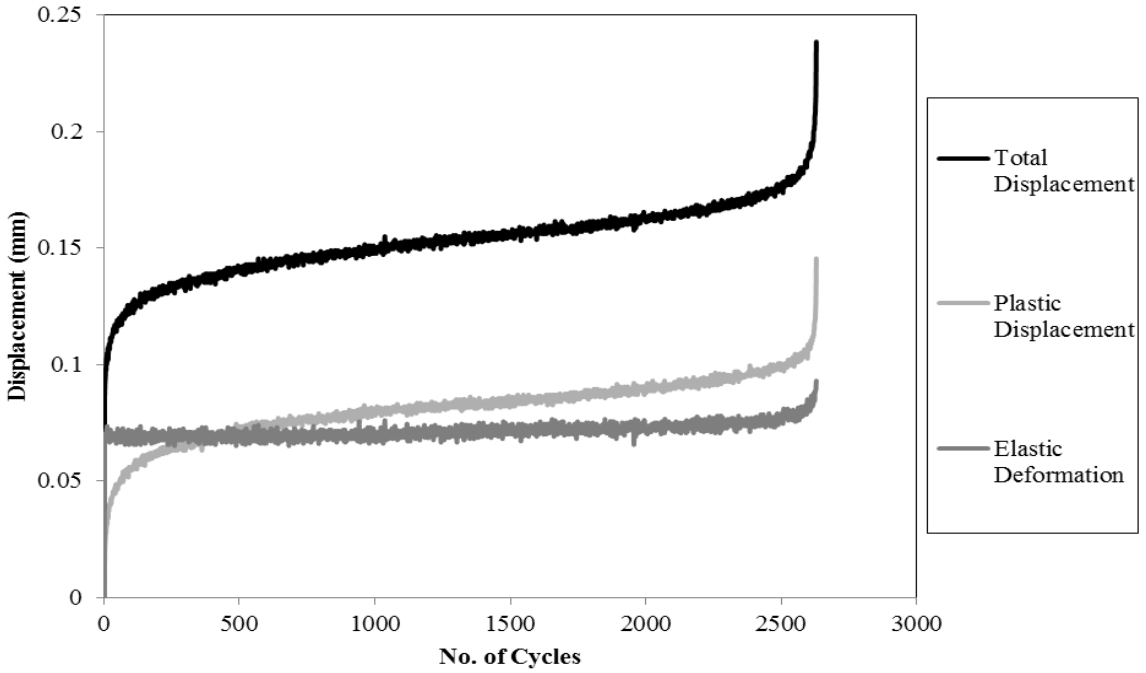

Figure C17. Displacement Variation v/s No. of Cycles in a Fatigue Test at 60% Stress Level [Gravel-Cement (3%) Specimens (FT-5)]

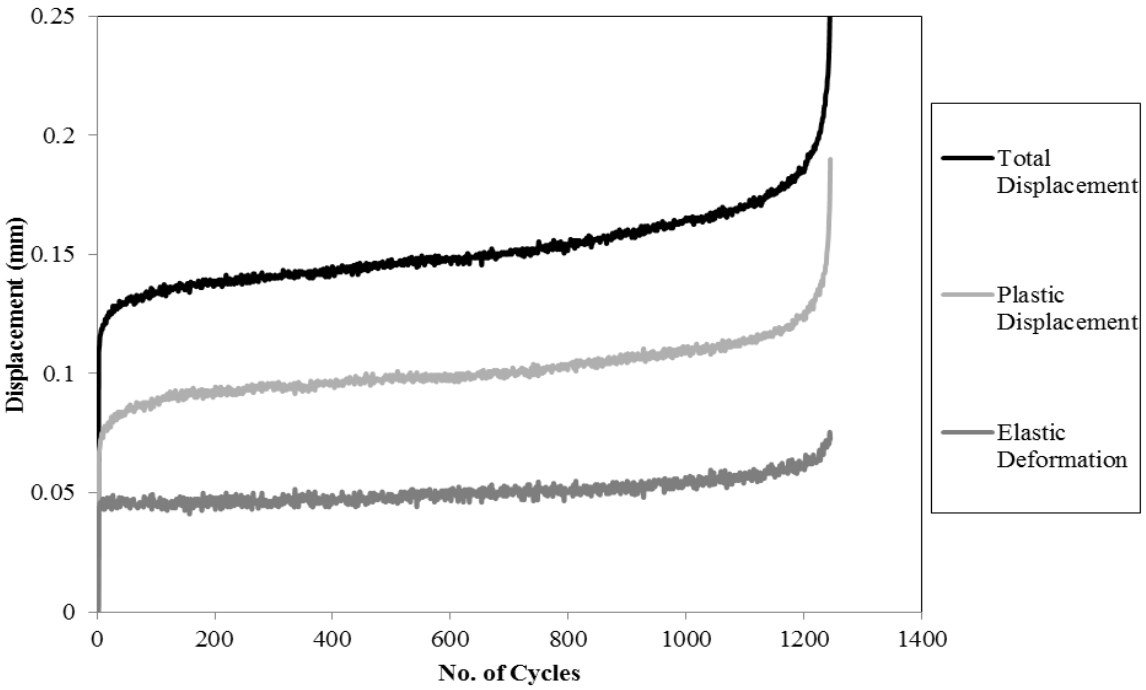

Figure C18. Displacement Variation v/s No. of Cycles in a Fatigue Test at 60% Stress Level [Gravel-Cement (3%) Specimens (FT-6)]

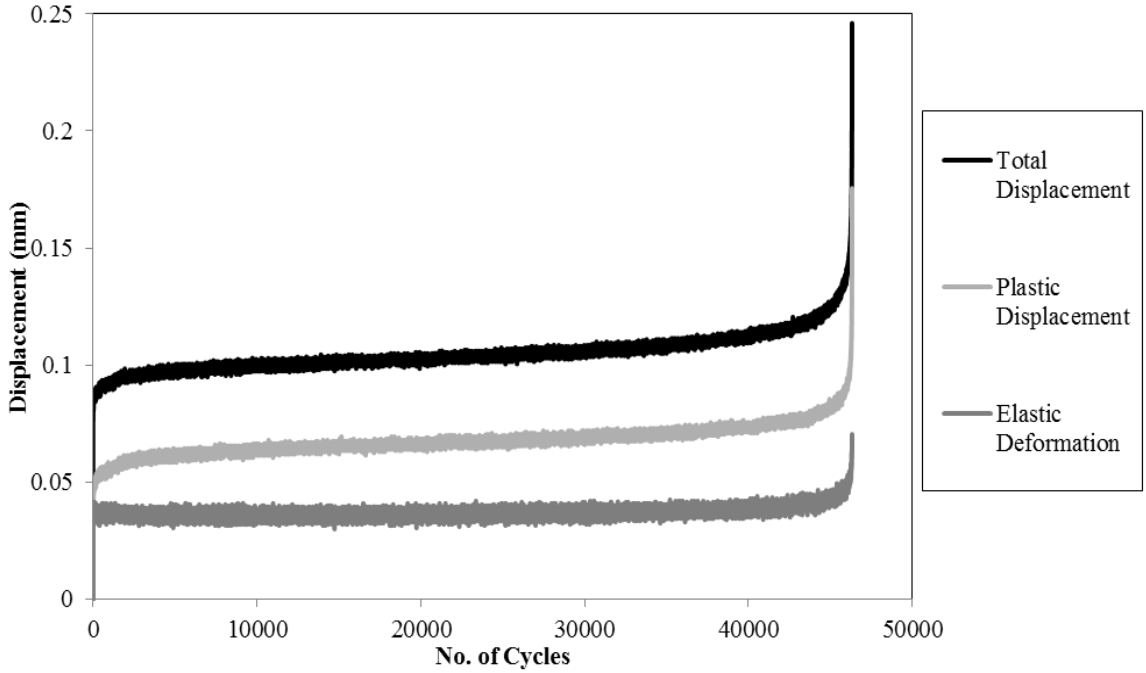

Figure C19. Displacement Variation v/s No. of Cycles in a Fatigue Test at 50% Stress Level [Gravel-Cement (3%) Specimens (FT-7)]

Figures C20 to C23 shows the flexural modulus degradation curves for specimens FT-2 to FT-6 (from Table 4.8) for sand-cement specimens stabilized with 6% cement.

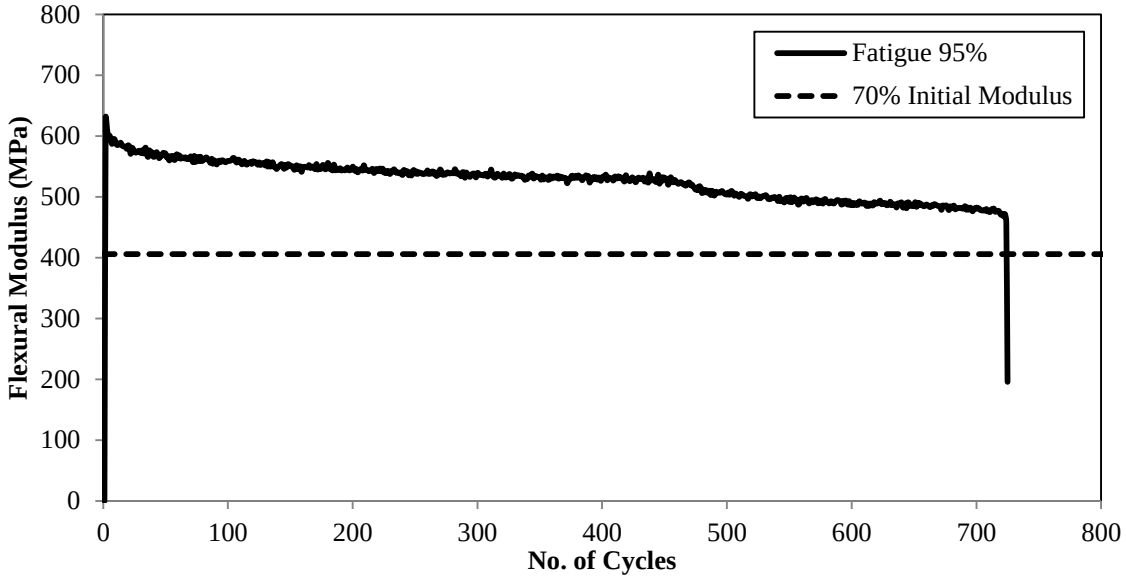

Figure C20. Typical Degradation of Flexural Modulus in a Fatigue Test at 95% Stress Level [Sand-Cement (6%) Specimens (FT-2)]

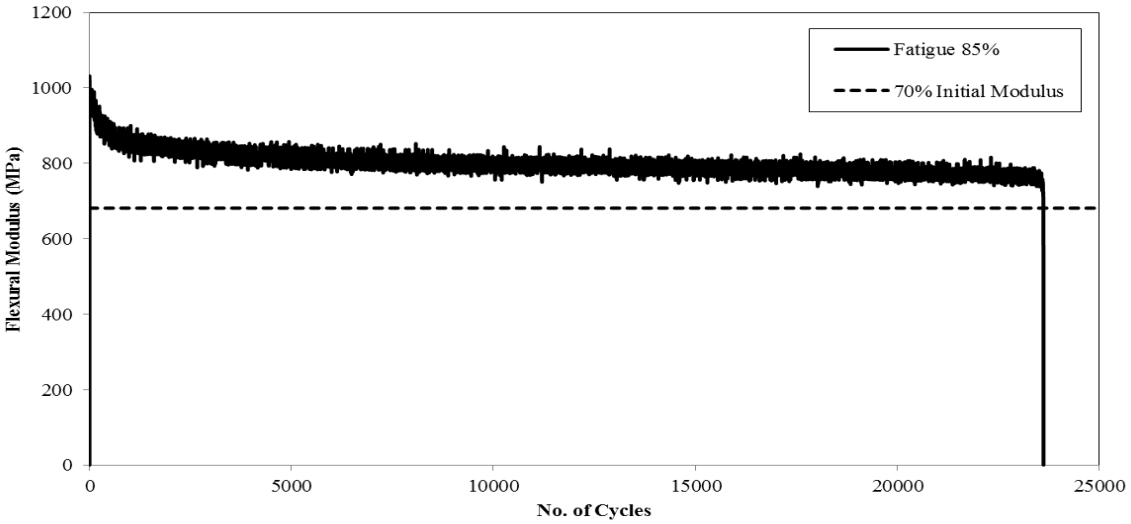

Figure C21. Typical Degradation of Flexural Modulus in a Fatigue Test at 85% Stress Level [Sand-Cement (6%) Specimens (FT-3)]

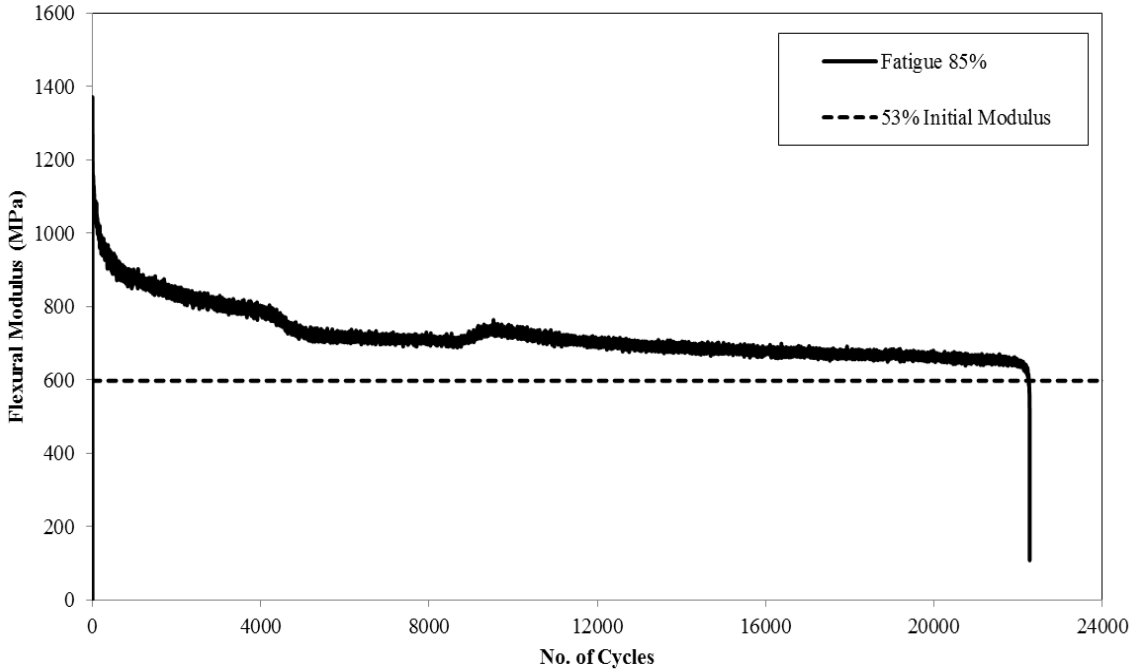

Figure C22. Typical Degradation of Flexural Modulus in a Fatigue Test at 85% Stress Level [Sand-Cement (6%) Specimens (FT-5)]

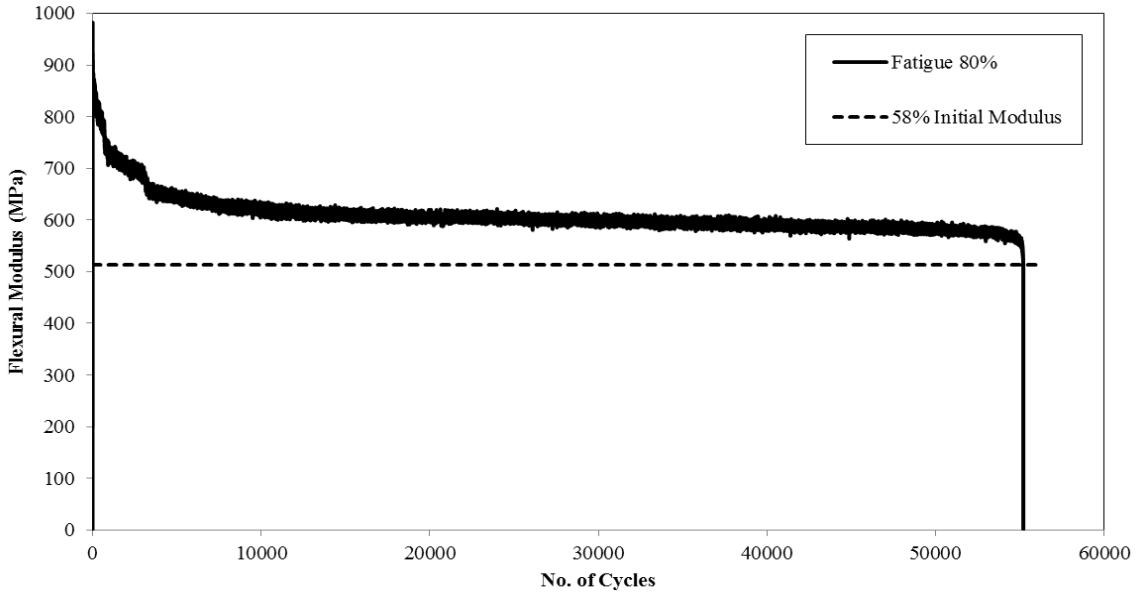

Figure C23. Typical Degradation of Flexural Modulus in a Fatigue Test at 80% Stress Level [Sand-Cement (6%) Specimens (FT-6)]

Figures C24 to C27 shows the displacement (total, plastic and elastic) variation curves for specimens FT-2 to FT-6 (from Table 4.8) for sand-cement specimens stabilized with 6% cement.

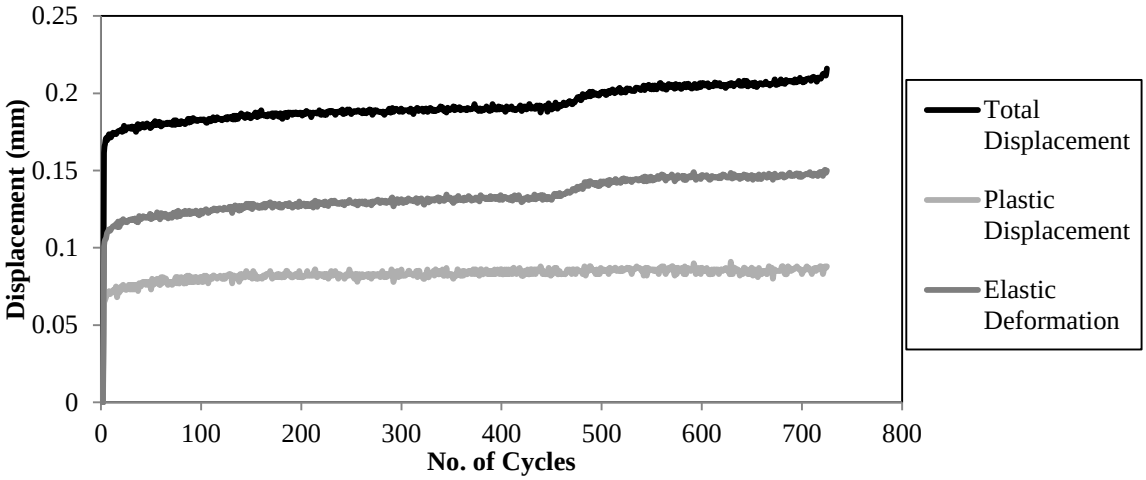

Figure C24. Displacement Variation v/s No. of Cycles in a Fatigue Test at 95% Stress Level [Sand-Cement (6%) Specimens (FT-2)]

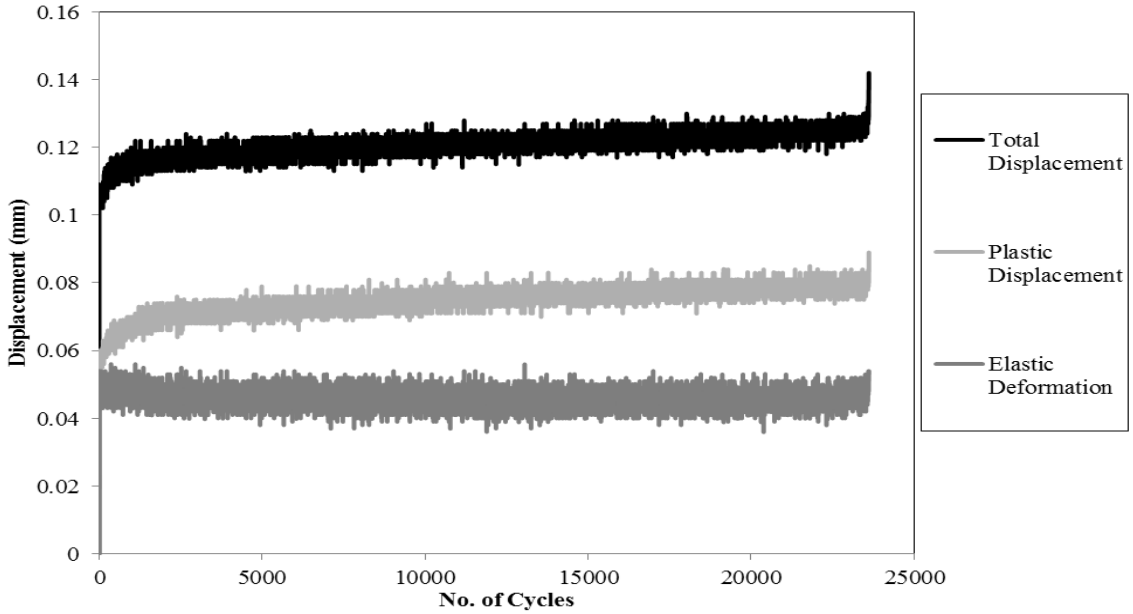

Figure C25. Displacement Variation v/s No. of Cycles in a Fatigue Test at 85% Stress Level [Sand-Cement (6%) Specimens (FT-3)]

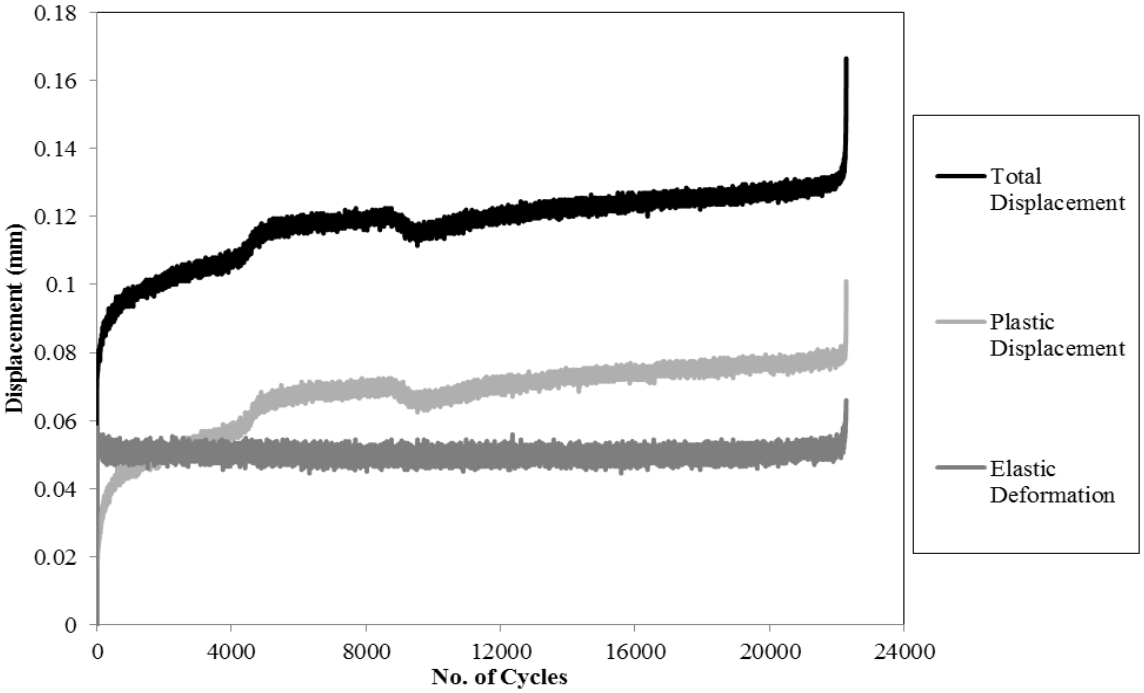

Figure C26. Displacement Variation v/s No. of Cycles in a Fatigue Test at 85% Stress Level [Sand-Cement (6%) Specimens (FT-5)]

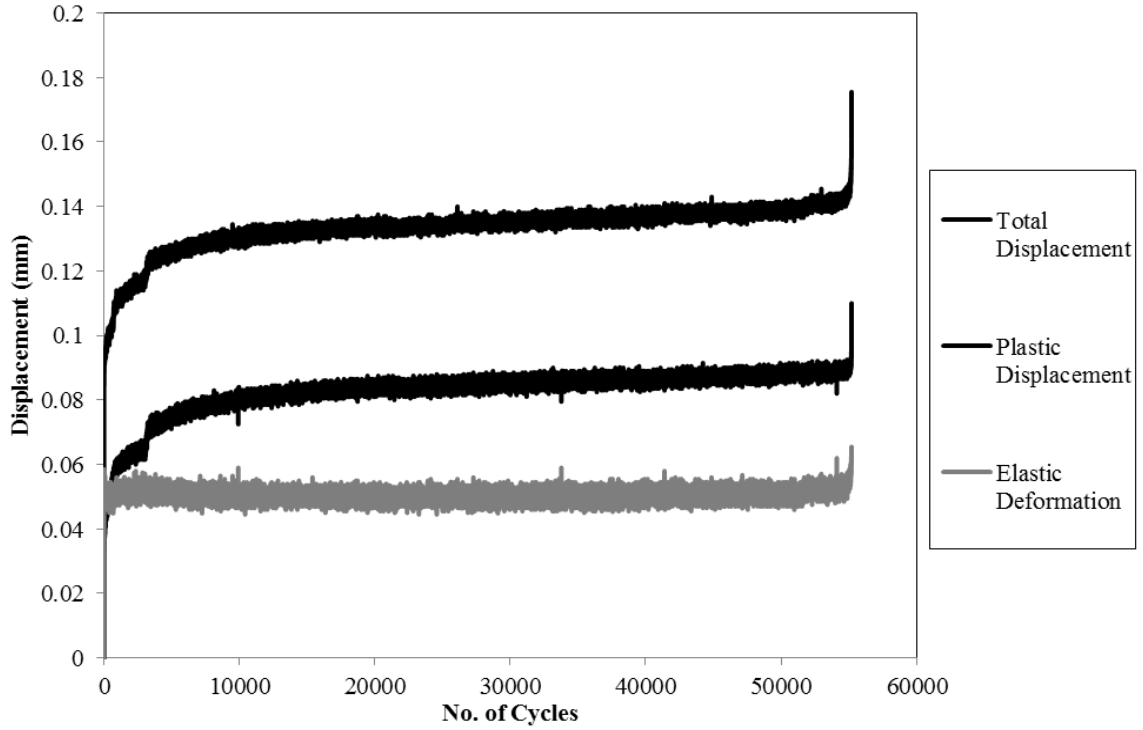

Figure C27. Displacement Variation v/s No. of Cycles in a Fatigue Test at 80% Stress Level [Sand-Cement (6%) Specimens (FT-6)]

Seven beam specimens were tested for the silt-cement beam specimens (8% binder). Table C3 shows the summary of the fatigue test results on the silt-cement beam specimens. From the silt-cement specimen fatigue curves, we can see that not all the specimen ruptured shortly after the cycles to half the initial modulus was reached. The specimens ruptured when the initial modulus reached in the range of 50% to 70%. Figures C28 to C33 shows the flexural modulus degradation curves for specimens FT-1 to FT-3 and FT-5 to FT-7 for silt-cement specimens stabilized with 8% cement.

Table C3. Summary of the Fatigue Strength Test Results on Silt-Cement Specimens (Binder Content: 8%)

SN	SL (%)	IFM (MPa)	FFM (MPa)	PFME (%)	IS (με)	N
FT-1	90	746	608	81	529	3,063
FT-2	90	1,078	939	87	498	1,996
FT-3	85	1,066	648	61	502	12,558
FT-4	85	1,076	1,013	94	414	14,396
FT-5	75	753	515	68	733	41,377
FT-6	75	1,302	1,074	83	475	30,259
FT-7	65	1,300	806	62	363	75,537

SN = Specimen Number; SL = Stress Level; IFM = Initial Flexural Modulus; FFM = Final Flexural Modulus (i.e. Flexural Modulus at the end of Fatigue Test); PFME =Percent of Flexural Modulus at the End of Test; IS = Initial Strain; N = Number of Cycles at the End of Test (i.e. Fatigue Life)

Note: *Range of Failure: 50% to 70% of IFM (Average: 60%)*

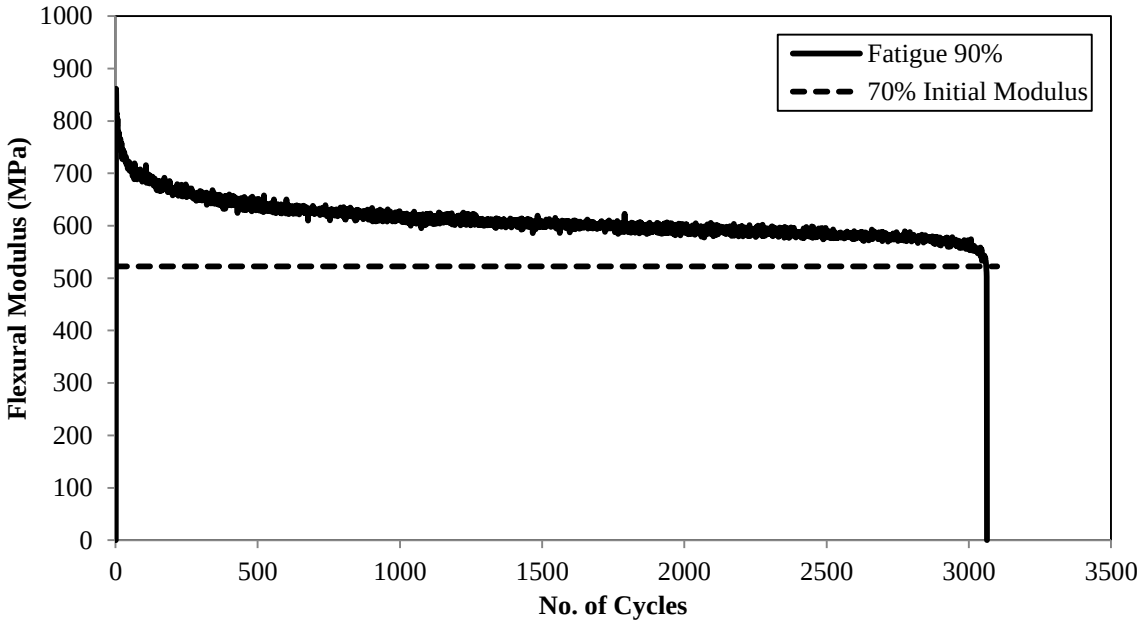

Figure C28. Typical Degradation of Flexural Modulus in a Fatigue Test at 90% Stress Level [Silt-Cement (8%) Specimens (FT-1)]

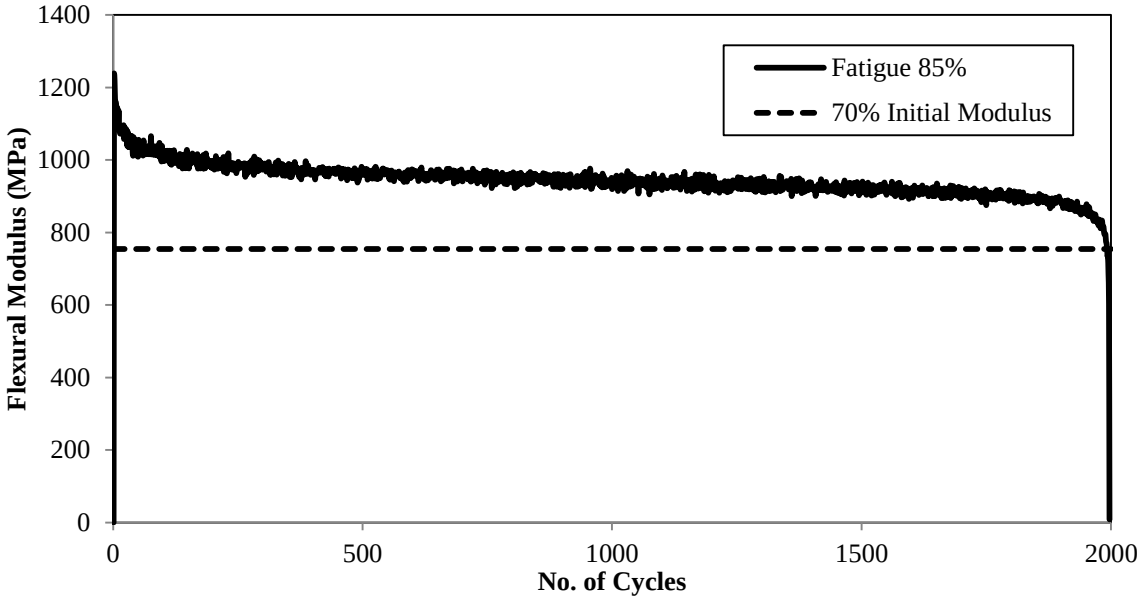

Figure C29. Typical Degradation of Flexural Modulus in a Fatigue Test at 90% Stress Level [Silt-Cement (8%) Specimens (FT-2)]

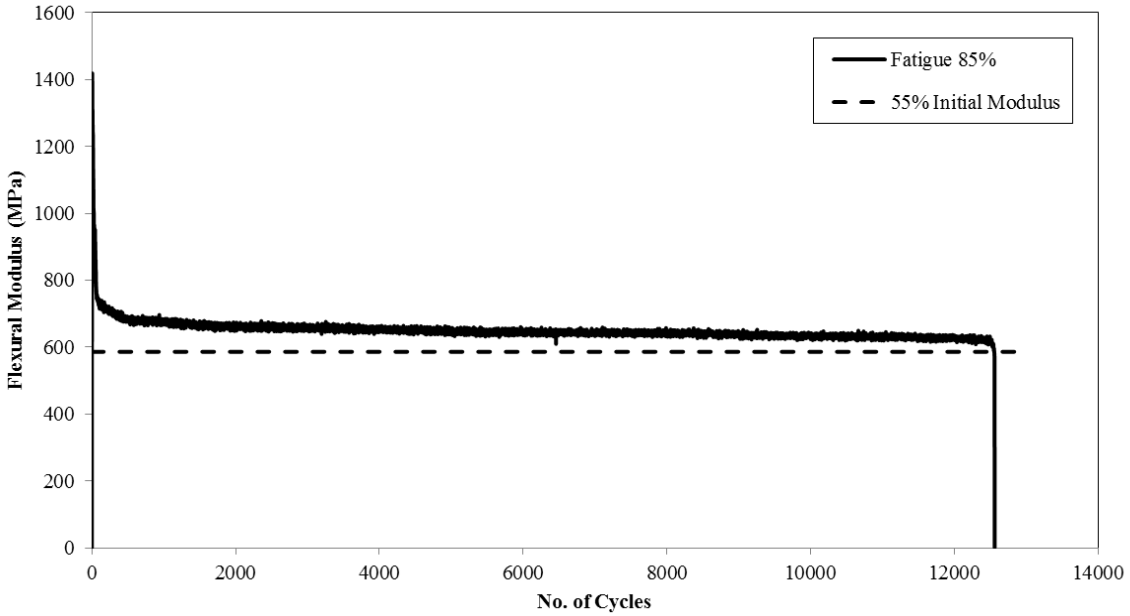

Figure C30. Typical Degradation of Flexural Modulus in a Fatigue Test at 85% Stress Level [Silt-Cement (8%) Specimens (FT-3)]

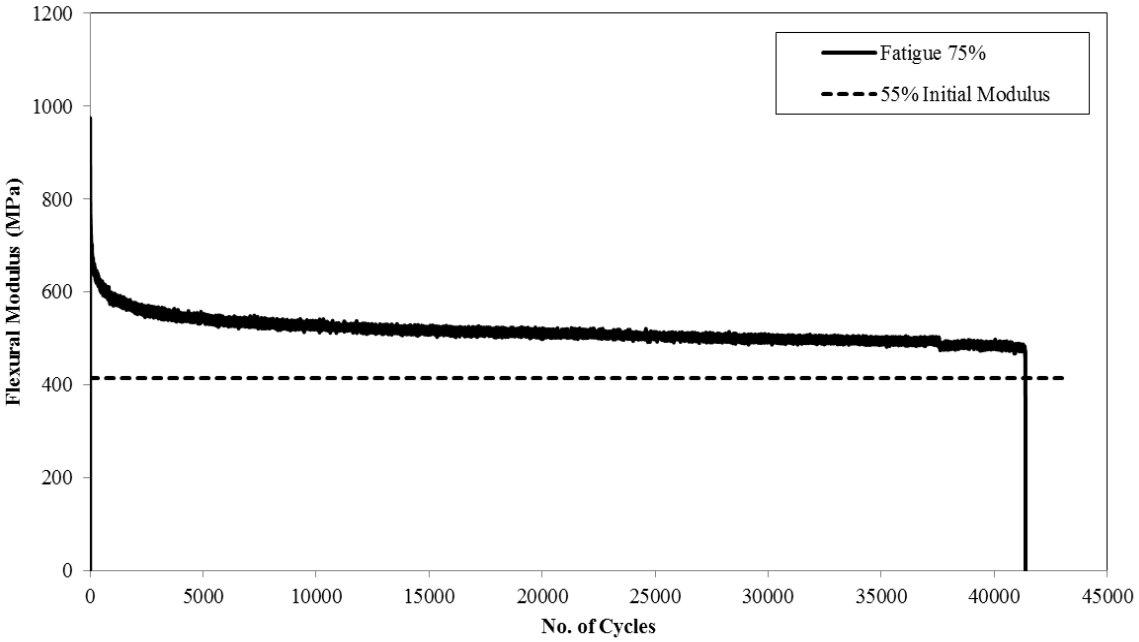

Figure C31. Typical Degradation of Flexural Modulus in a Fatigue Test at 75% Stress Level [Silt-Cement (8%) Specimens (FT-5)]

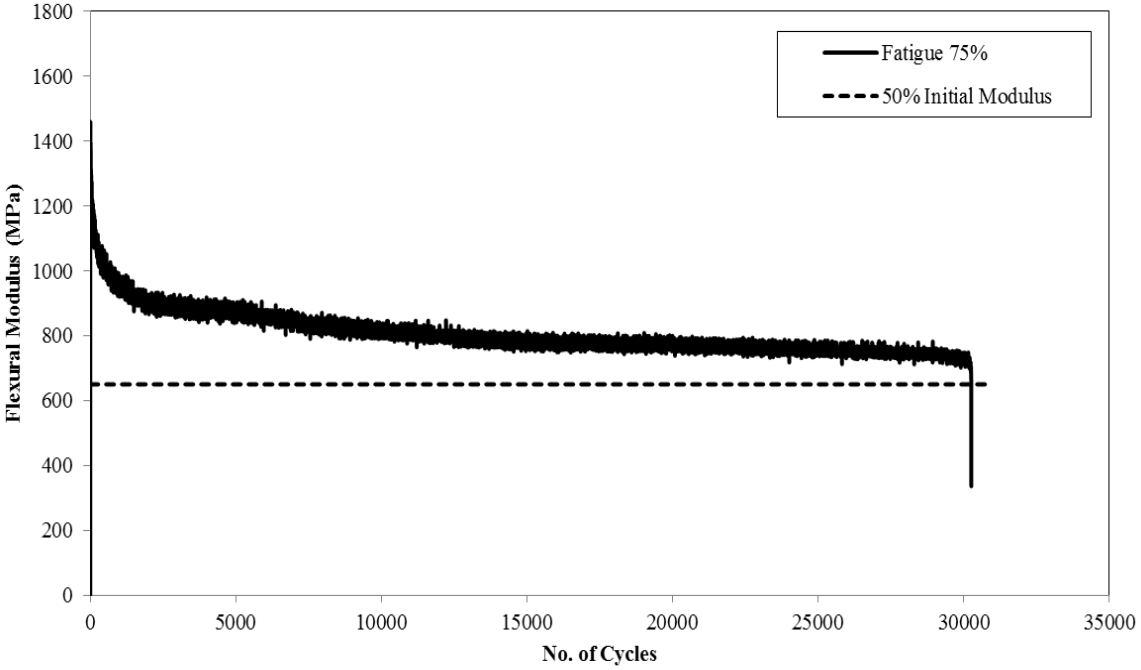

Figure C32. Typical Degradation of Flexural Modulus in a Fatigue Test at 75% Stress Level [Silt-Cement (8%) Specimens (FT-6)]

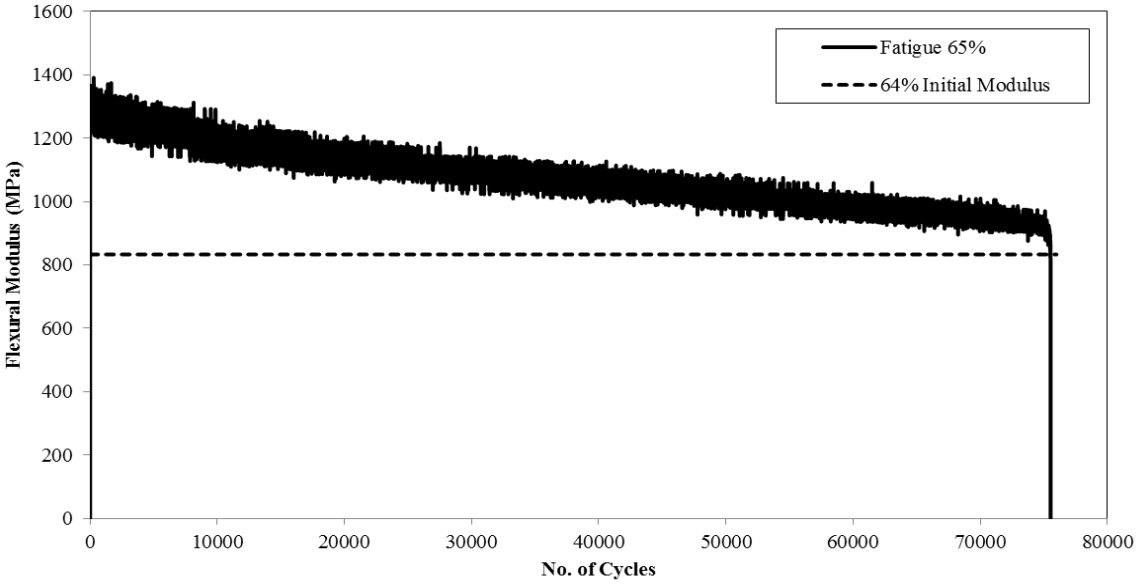

Figure C33. Typical Degradation of Flexural Modulus in a Fatigue Test at 65% Stress Level [Silt-Cement (8%) Specimens (FT-7)]

Figures C34 to C39 shows the displacement (total, plastic and elastic) variation curves for specimens FT-1 to FT-3 and FT-5 to FT-7 (from Table 4.11) for silt-cement specimens stabilized with 8% cement.

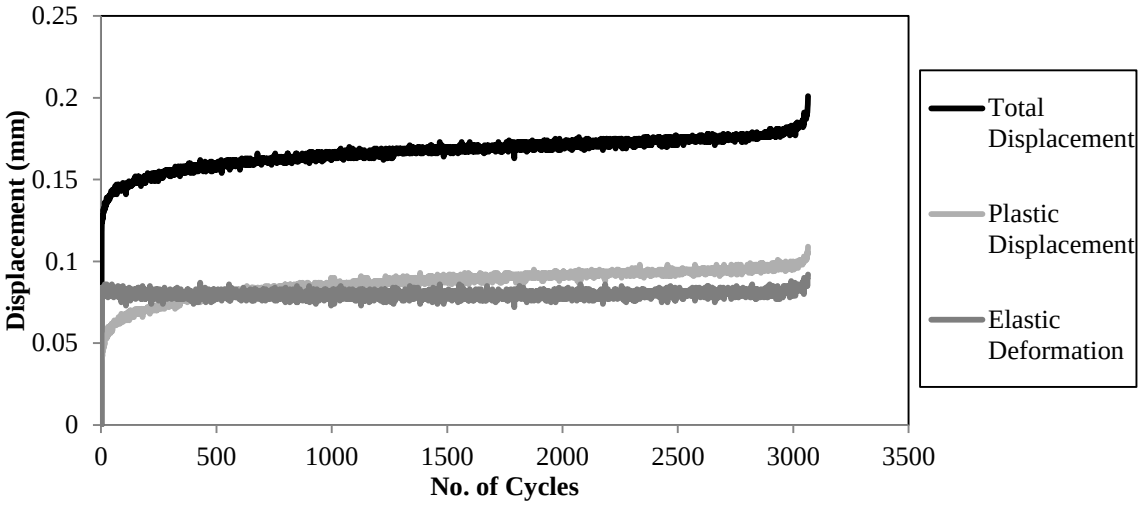

Figure C34. Displacement Variation v/s No. of Cycles in a Fatigue Test at 90% Stress Level [Sand-Cement (6%) Specimens (FT-1)]

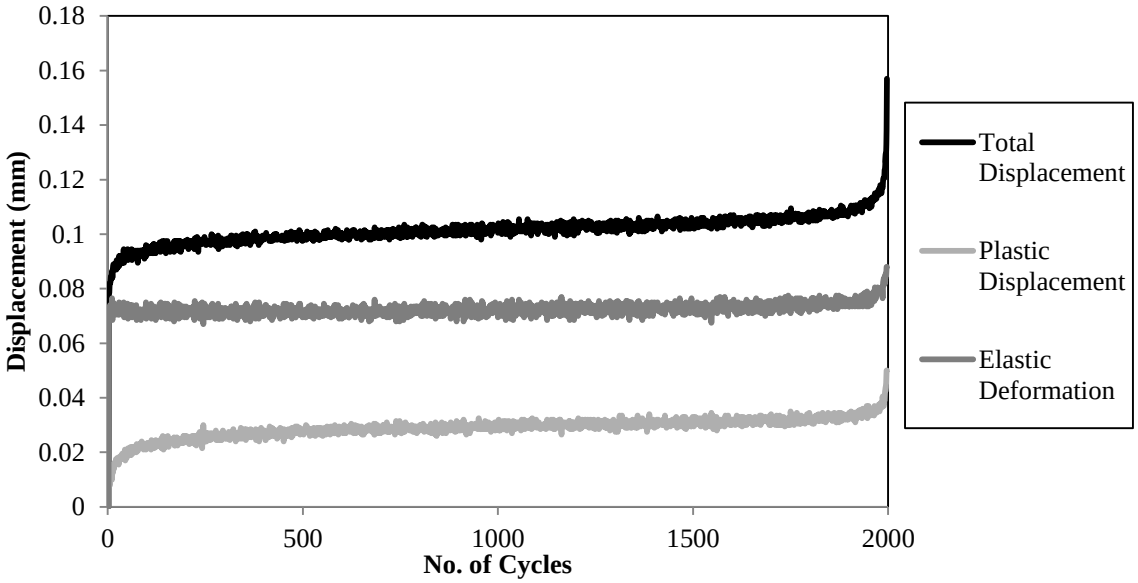

Figure C35. Displacement Variation v/s No. of Cycles in a Fatigue Test at 90% Stress Level [Sand-Cement (6%) Specimens (FT-2)]

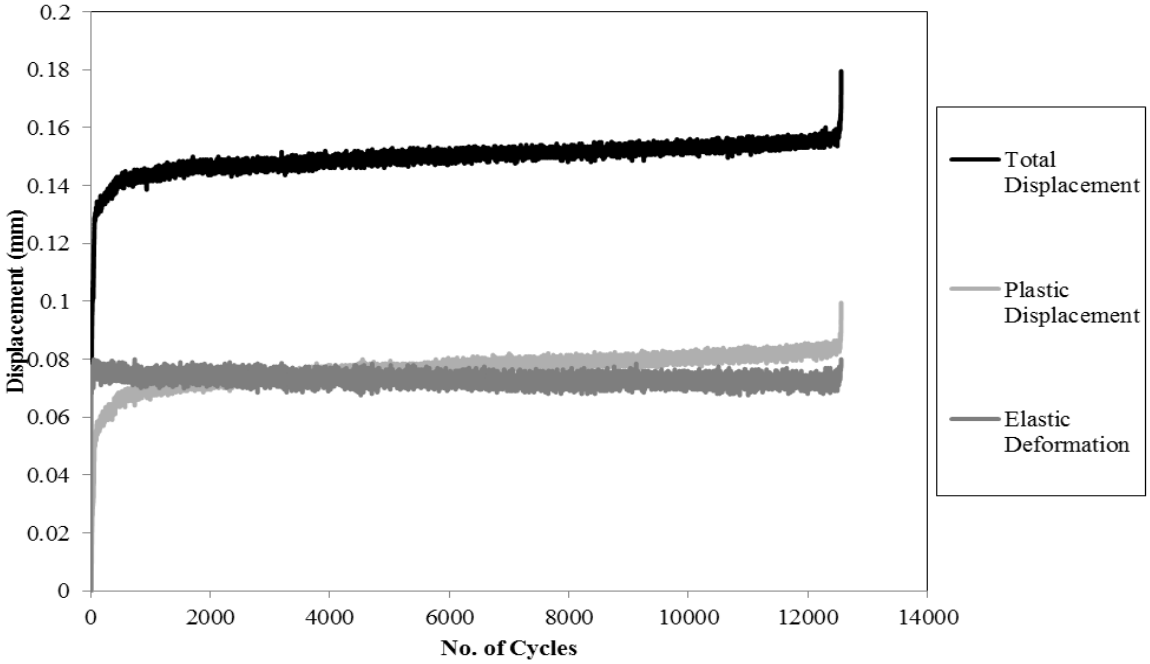

Figure C36. Displacement Variation v/s No. of Cycles in a Fatigue Test at 85% Stress Level [Sand-Cement (6%) Specimens (FT-3)]

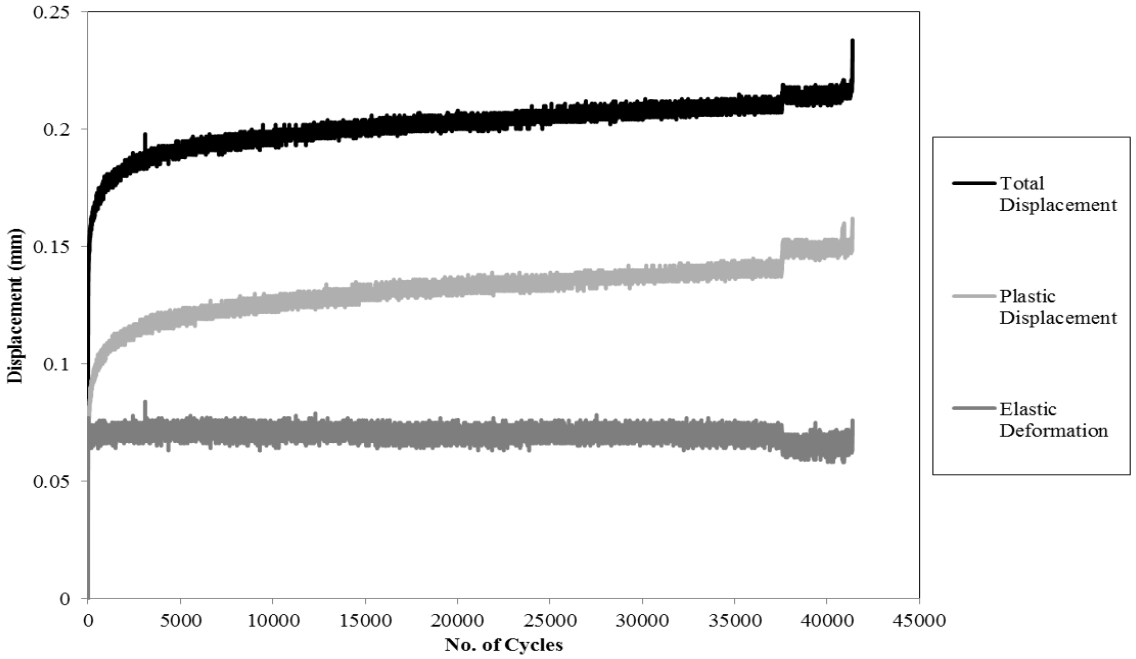

Figure C37. Displacement Variation v/s No. of Cycles in a Fatigue Test at 75% Stress Level [Sand-Cement (6%) Specimens (FT-5)]

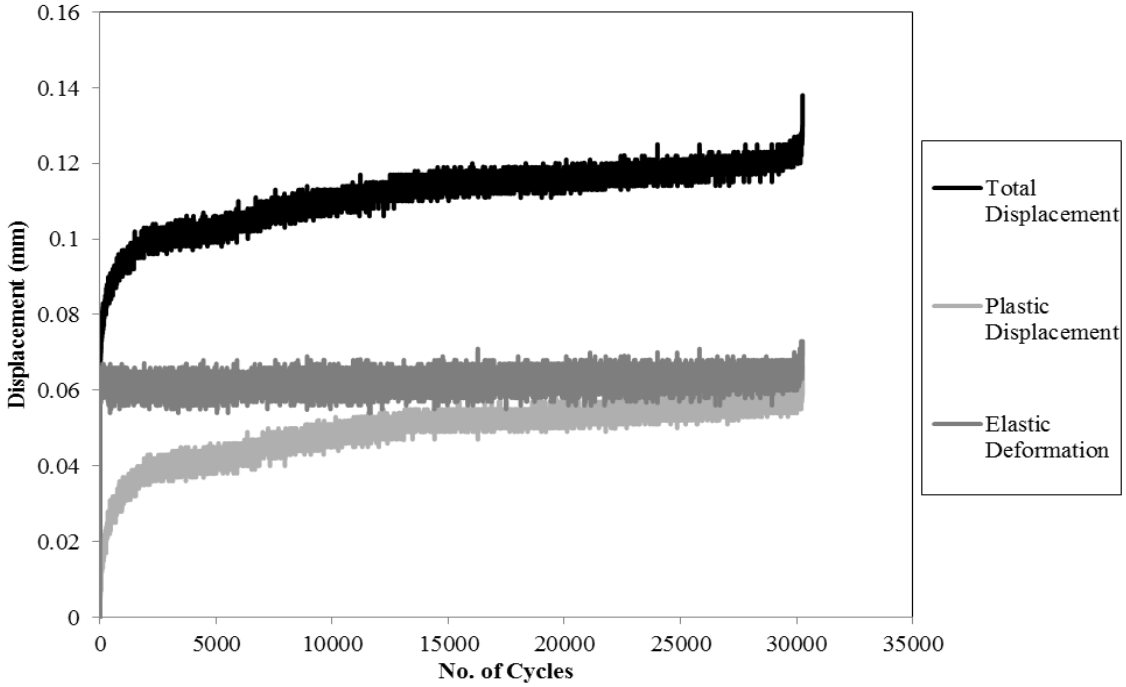

Figure C38. Displacement Variation v/s No. of Cycles in a Fatigue Test at 75% Stress Level [Sand-Cement (6%) Specimens (FT-6)]

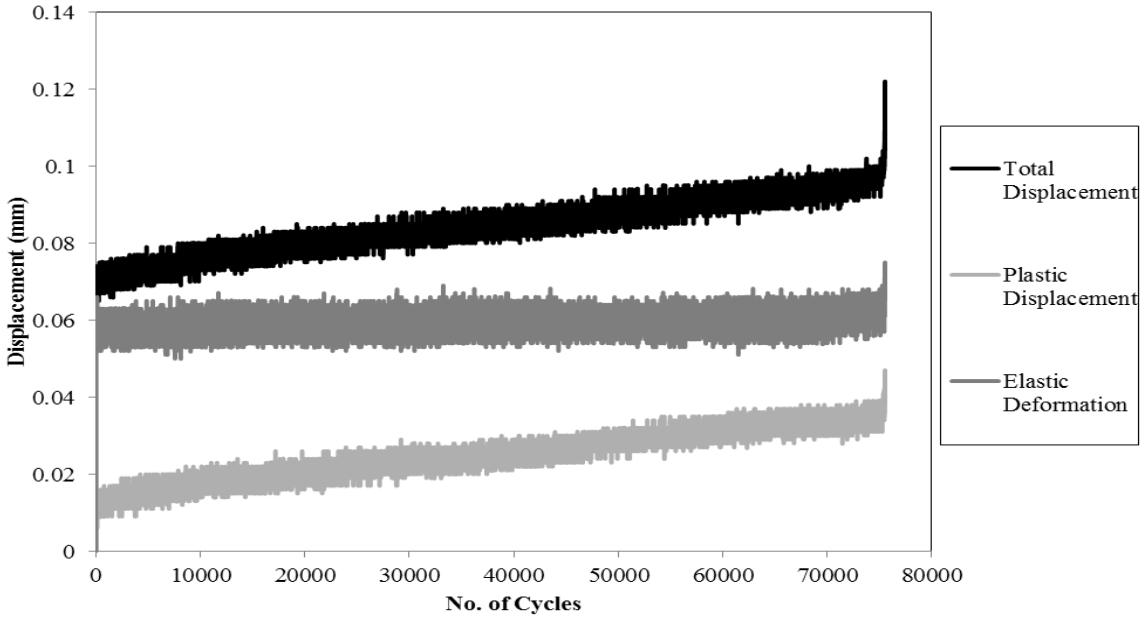

Figure C39. Displacement Variation v/s No. of Cycles in a Fatigue Test at 65% Stress Level [Sand-Cement (6%) Specimens (FT-7)]

Six beam specimens were tested for the sand-fly ash beam specimens (13% binder). Table C4 shows the summary of the fatigue test results on the sand-fly ash beam specimens. From the sand-fly ash specimen fatigue curves, we can see that not all the specimen ruptured shortly after the cycles to half the initial modulus was reached. The specimens ruptured when the initial modulus reached in the range of 40% to 48%. Specimen FT-6 did not fail after 100,000 cycles.

Table C4. Summary of the Fatigue Strength Test Results on Sand-Fly ash Specimens (Binder Content: 13%)

SN	SL (%)	IFM (MPa)	FFM (MPa)	PFME (%)	IS (με)	N
FT-1	75	-	-	-	-	9
FT-2	75	741	-	-	383	40
FT-3	65	859	450	52	310	1,855
FT-4	65	824	470	57	322	11,908
FT-5	60	788	471	60	307	64,657
FT-6*	60	964	599	62	280	>100,000

*SN = Specimen Number; SL = Stress Level; IFM = Initial Flexural Modulus; FFM = Final Flexural Modulus (i.e. Flexural Modulus at the end of Fatigue Test); PFME =Percent of Flexural Modulus at the End of Test; IS = Initial Strain; N = Number of Cycles at the End of Test (i.e. Fatigue Life); * Did not fail*

Note: *Range of Failure: 40% to 48% of IFM (Average: 44%)*

Figures C40 to C43 shows the flexural modulus degradation curves for specimens FT-2 to FT-5 for sand-fly ash specimens stabilized with 13% class C fly ash.

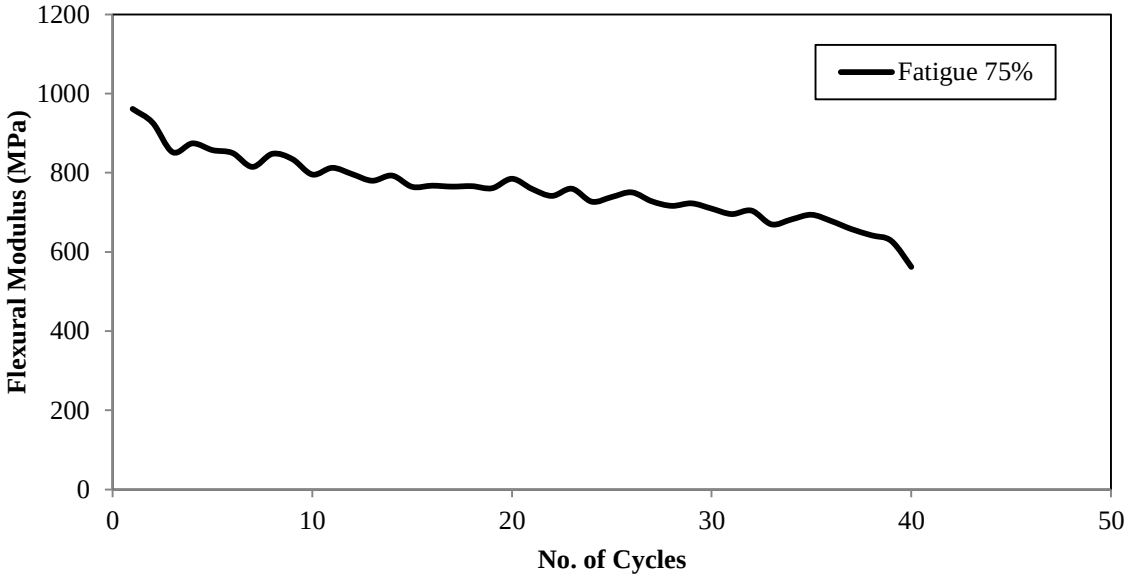

Figure C40. Typical Degradation of Flexural Modulus in a Fatigue Test at 75% Stress Level [Sand-Fly ash (13%) Specimens (FT-2)]

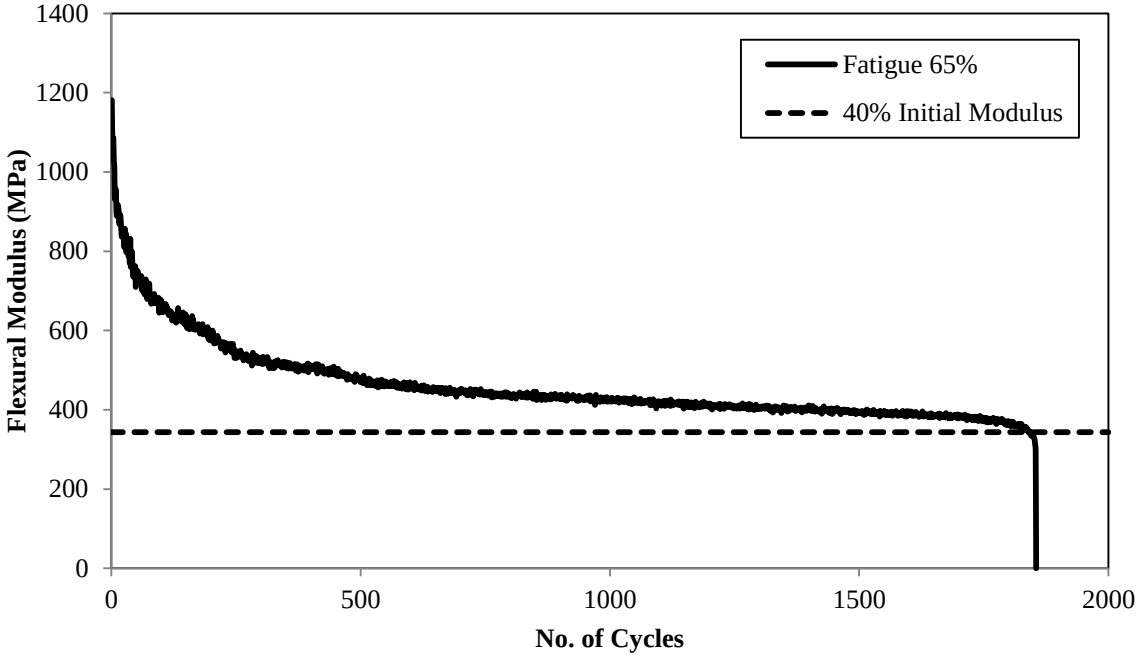

Figure C41. Typical Degradation of Flexural Modulus in a Fatigue Test at 65% Stress Level [Sand-Fly ash (13%) Specimens (FT-3)]

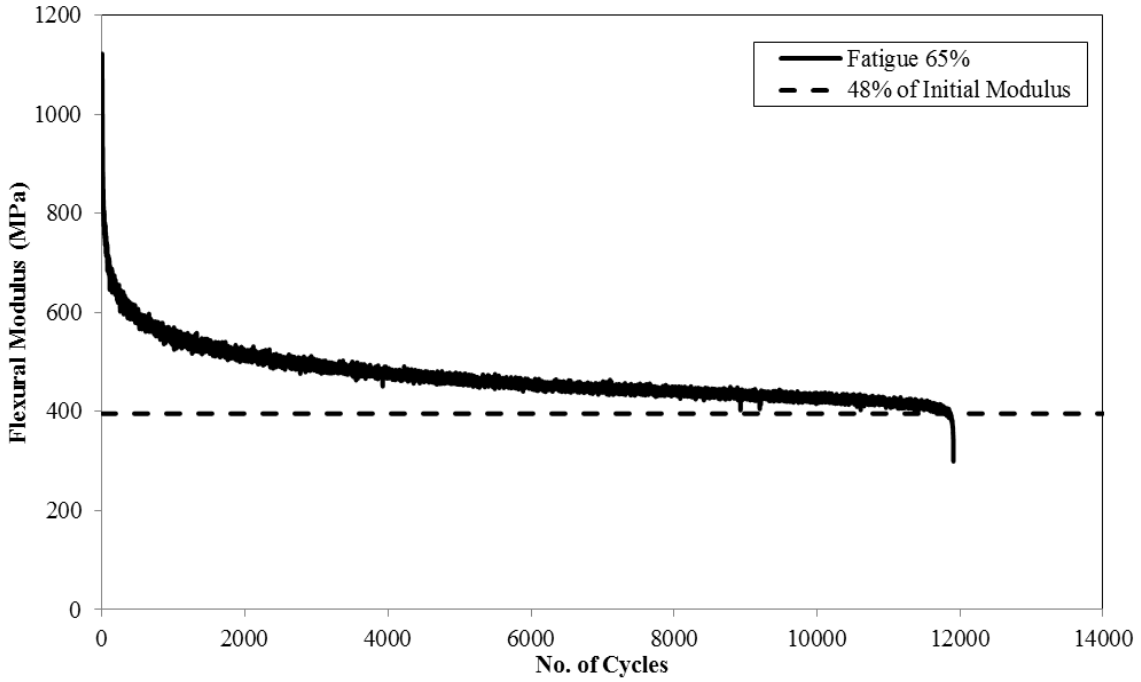

Figure C42. Typical Degradation of Flexural Modulus in a Fatigue Test at 65% Stress Level [Sand-Fly ash (13%) Specimens (FT-4)]

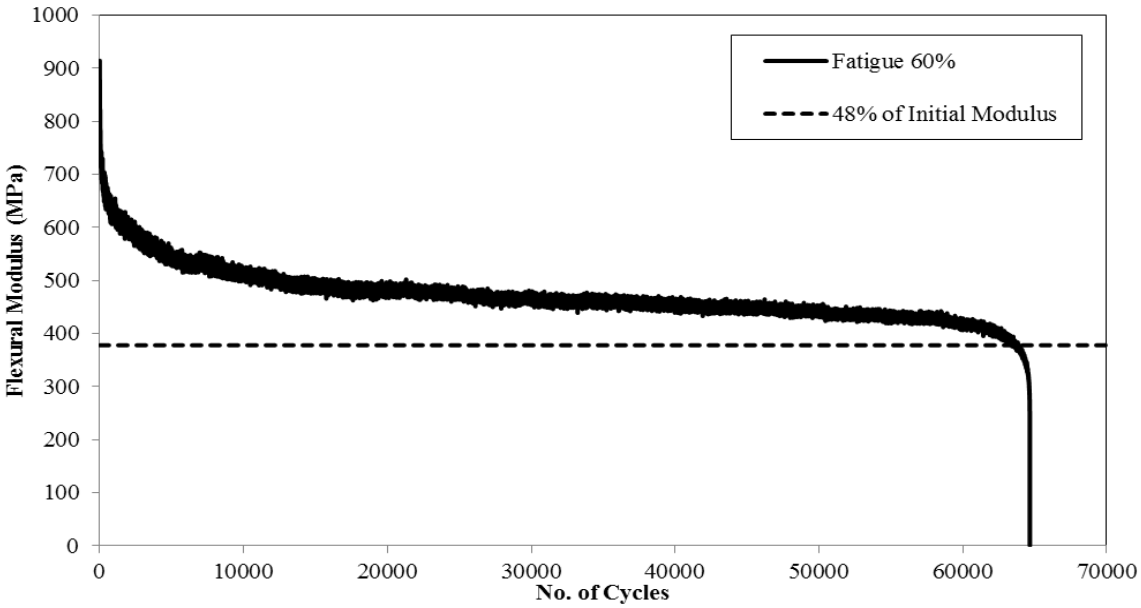

Figure C43. Typical Degradation of Flexural Modulus in a Fatigue Test at 60% Stress Level [Sand-Fly ash (13%) Specimens (FT-5)]

Figures C44 to C47 shows the displacement (total, plastic and elastic) variation curves for specimens FT-2 to FT-5 (from Table 4.12) for sand-fly ash specimens stabilized with 13% class C fly ash.

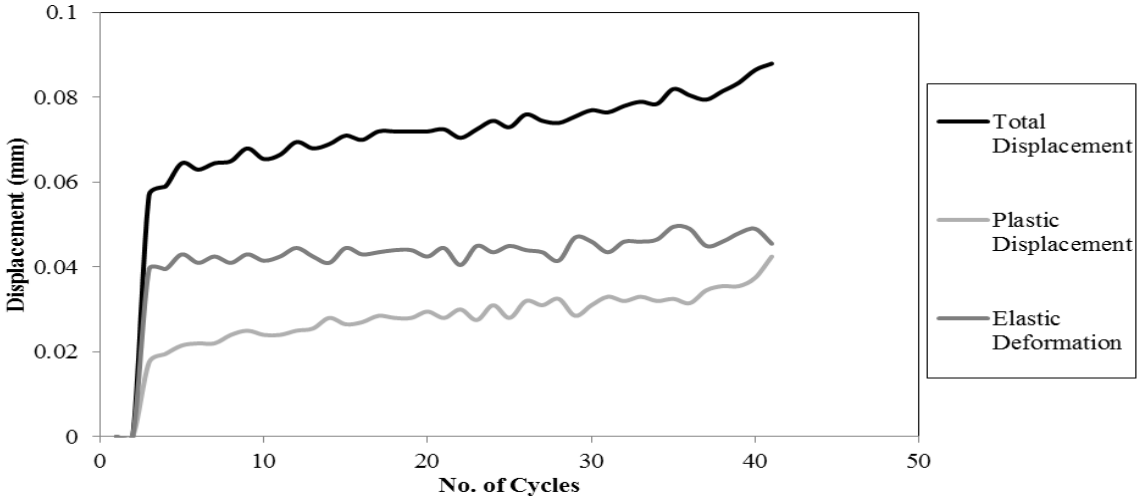

Figure C44. Displacement Variation v/s No. of Cycles in a Fatigue Test at 75% Stress Level [Sand-Fly ash (13%) Specimens (FT-2)]

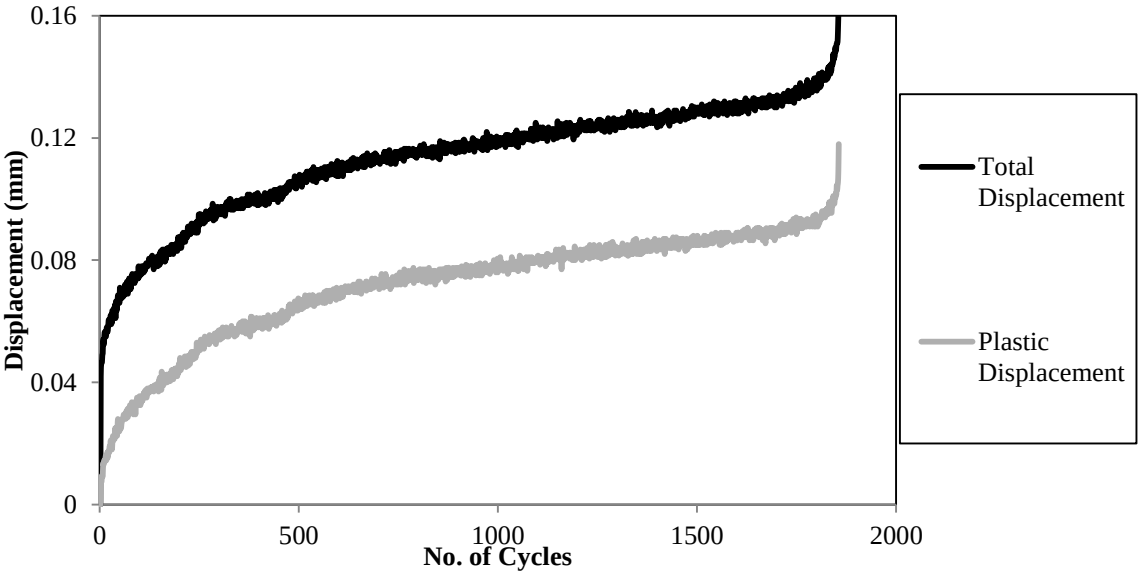

Figure C45. Displacement Variation v/s No. of Cycles in a Fatigue Test at 65% Stress Level [Sand-Fly ash (13%) Specimens (FT-3)]

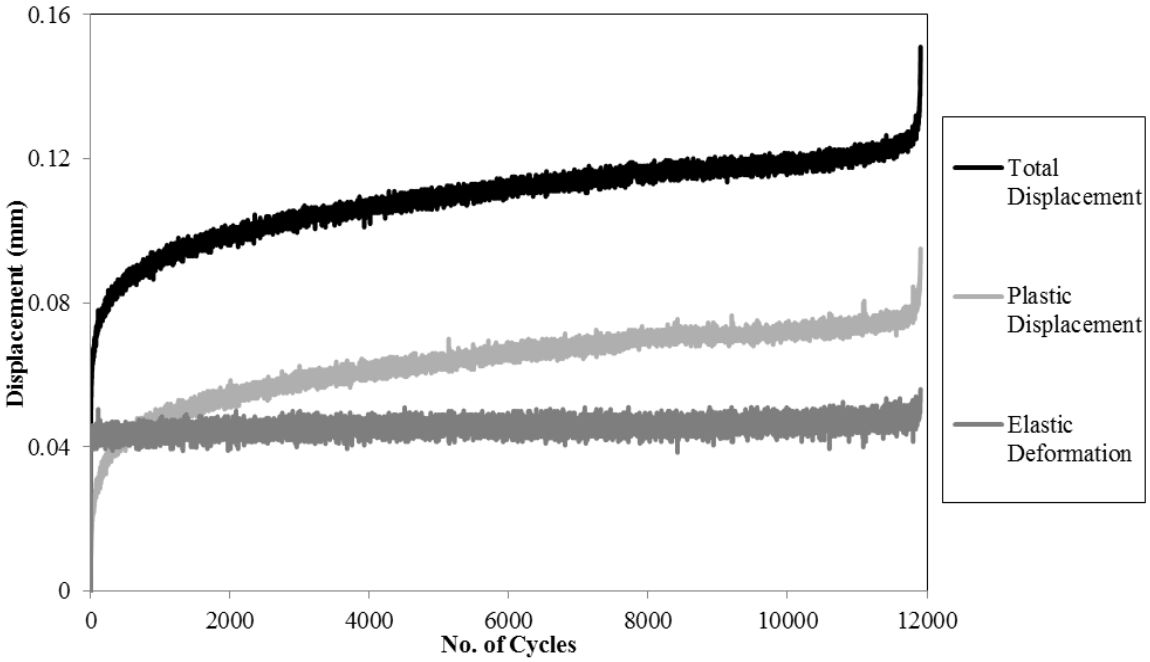

Figure C46. Displacement Variation v/s No. of Cycles in a Fatigue Test at 65% Stress Level [Sand-Fly ash (13%) Specimens (FT-4)]

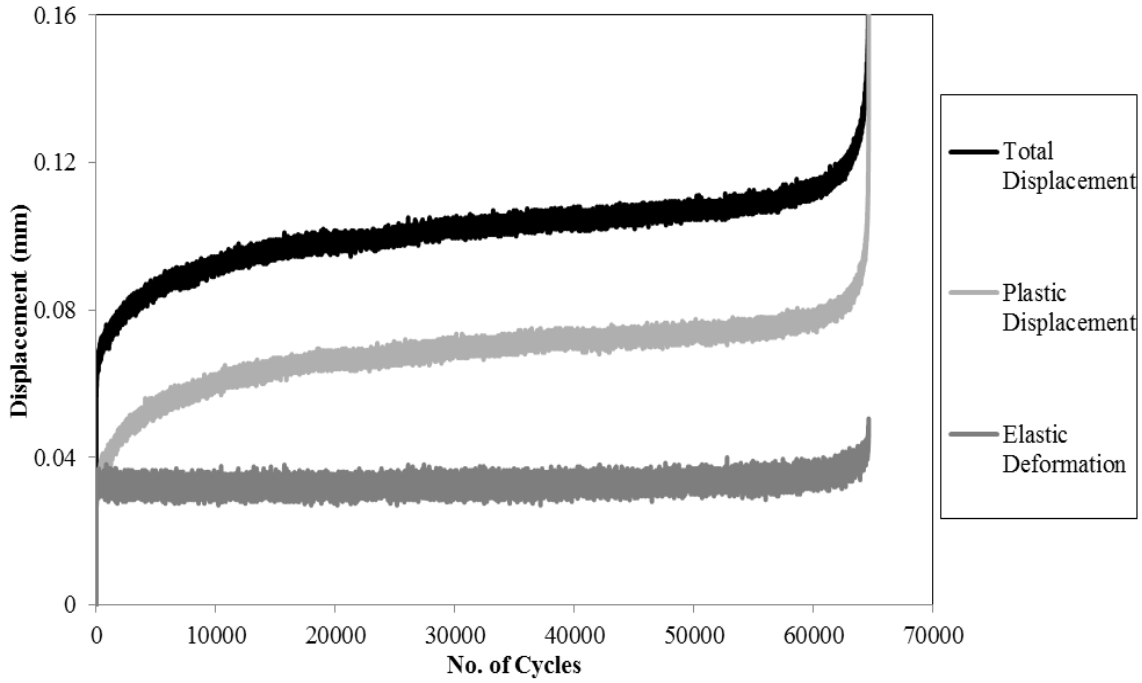

Figure C47. Displacement Variation v/s No. of Cycles in a Fatigue Test at 60% Stress Level [Sand-Fly ash (13%) Specimens (FT-5)]

Ten beam specimens were tested for the gravel-fly ash beam specimens (13% binder). Table C5 shows the summary of the fatigue test results on the gravel-fly ash beam specimens. The gravel-fly ash specimens did not perform well for the fatigue cracking test. The fatigue life of these specimens was quite less. Specimen FT-10 did not fail after 281,000 cycles of loading at 40% stress level. Only specimen FT-5 performed well as compared to the rest.

Table C5. Summary of the Fatigue Strength Test Results on Gravel-Fly ash Specimens (Binder Content: 13%)

SN	SL (%)	IFM (MPa)	FFM (MPa)	PFME (%)	IS (με)	N
FT-1	85	-	-	-	-	5
FT-2	75	-	-	-	-	2
FT-3	65	-	-	-	-	2
FT-4	65	-	-	-	-	7
FT-5	65	768	372	48	328	2,246
FT-6	65	-	-	-	-	2
FT-7	60	-	-	-	-	5
FT-8	60	-	-	-	-	4
FT-9	50					7
FT-10*	40	448	266	59	347	>281,000

*SN = Specimen Number; SL = Stress Level; IFM = Initial Flexural Modulus; FFM = Final Flexural Modulus (i.e. Flexural Modulus at the end of Fatigue Test); PFME =Percent of Flexural Modulus at the End of Test; IS = Initial Strain; N = Number of Cycles at the End of Test (i.e. Fatigue Life); * Did not fail*

Four beam specimens were tested for the silt-fly ash beam specimens (13% binder). Table C6 shows the summary of the fatigue test results on the silt-fly ash beam specimens. The silt-fly ash specimens also did not perform well for the fatigue cracking test. These specimens already failed while they were tested for the flexural modulus test.

These were the weakest among all the mixtures. Therefore, the binder content was increased to 18% and was tested for fatigue cracking, which is presented in Section 4.4.2.

Table C6. Summary of the Fatigue Strength Test Results on Silt-Fly ash Specimens (Binder Content: 13%)

SN	SL (%)	IFM (MPa)	FFM (MPa)	PFME (%)	IS (με)	N
FT-1	75	-	-	-	-	1
FT-2	70	-	-	-	-	3
FT-3	65	-	-	-	-	3
FT-4*	45	515	215	42	147	20,000**

*SN = Specimen Number; SL = Stress Level; IFM = Initial Flexural Modulus; FFM = Final Flexural Modulus (i.e. Flexural Modulus at the end of Fatigue Test); PFME =Percent of Flexural Modulus at the End of Test; IS = Initial Strain; N = Number of Cycles at the End of Test (i.e. Fatigue Life); * Did not fail; **Estimated value*

Though the specimen FT-4 did not fail after 117,626 cycles at 45% stress level, the Flexural Modulus degradation curve in Figure C48 shows that half of the initial modulus has been reached around 20,000 cycles. And as per Midgley and Yeo (2008), the cycles of load to half initial modulus were very close to the cycles of load to ultimate failure of the samples for the flexural beam fatigue test. Hence, the fatigue life at 45% stress level for specimen FT-4 was taken as 20,000 cycles.

Seven beam specimens were tested for the silt-lime-fly ash beam specimens (4% lime and 12% class F fly ash). Table C7 shows the summary of the fatigue test results on the silt-lime-fly ash beam specimens. From the silt-lime-fly ash specimen fatigue curves, we can see that not all the specimen ruptured shortly after the cycles to half the initial modulus was reached. The specimens ruptured when the initial modulus reached in the range of 55% to 69%.

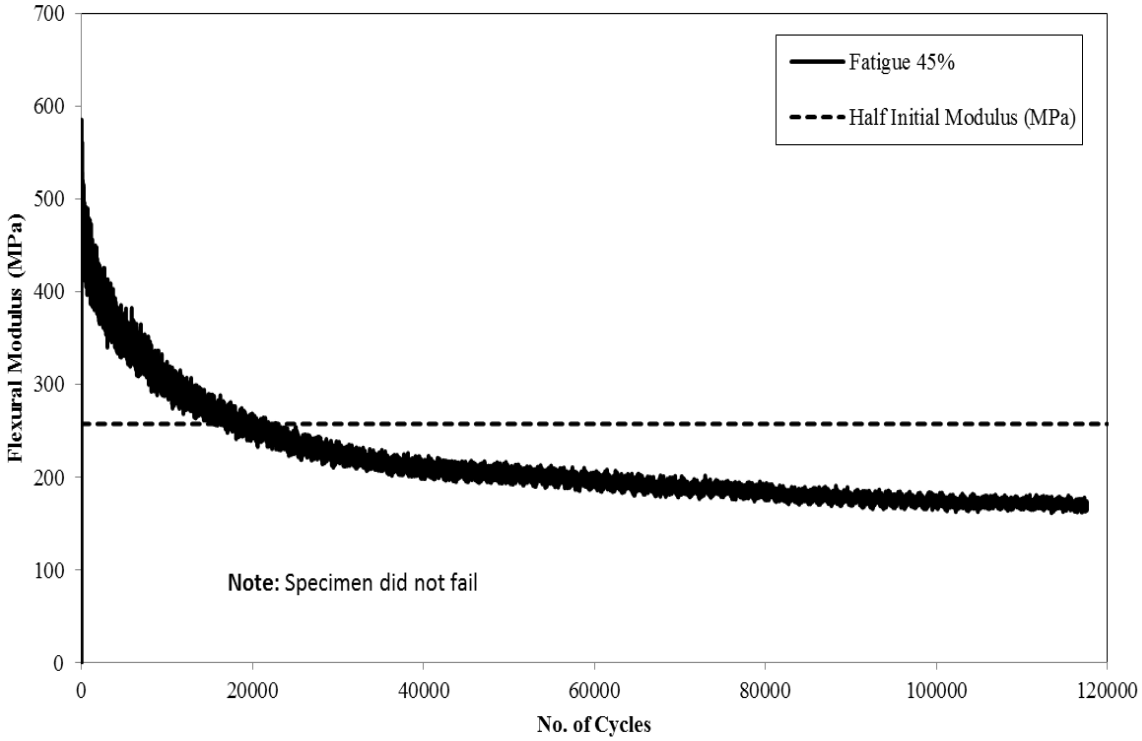

Figure C48. Typical Degradation of Flexural Modulus in a Fatigue Test at 45% Stress Level [Silt-Fly ash (13%) Specimens (FT-4)]

Three of the silt-lime-fly ash specimens (FT-5, FT-6 and FT-7) did not fail after 130,000+ cycles. As, four of the specimens failed shortly after the initial modulus reached 55%-69%, the average of the two percentages (i.e. 62%) was used to predict the fatigue life for specimens FT-5 and FT-7. From Figure C49 and C50, it can be seen that the 62% of initial modulus was reached at 11,701 and 32,199 cycles, respectively. Hence, the fatigue life for FT-5 and FT-7 was taken as 11,701 and 32,199 cycles, respectively. For specimen FT-6, the initial modulus was not reached at 62% of initial modulus (Figure C51). Hence, the upper limit (i.e. 69%) was used to predict the fatigue life; which was 21,911 cycles from Figure C51.

Table C7. Summary of the Fatigue Strength Test Results on Silt-Lime-Fly ash Specimens (Binder Content: 4/12%)

SN	SL (%)	IFM (MPa)	FFM (MPa)	PFME (%)	IS (με)	N
FT-1	85	545	482	91	297	515
FT-2	85	612	519	87	326	1,118
FT-3	80	686	562	82	537	3,465
FT-4	80	819	627	77	352	2307
FT-5*	70	1,106	620	56	250	11,701**
FT-6*	65	907	638	70	280	21,911**
FT-7*	60	1,185	710	60	191	32,199**

*SN = Specimen Number; SL = Stress Level; IFM = Initial Flexural Modulus; FFM = Final Flexural Modulus (i.e. Flexural Modulus at the end of Fatigue Test); PFME =Percent of Flexural Modulus at the End of Test; IS = Initial Strain; N = Number of Cycles at the End of Test (i.e. Fatigue Life); * Did not fail; **Estimated value*

Note: *Range of Failure: 55% to 69% of IFM (Average: 62%)*

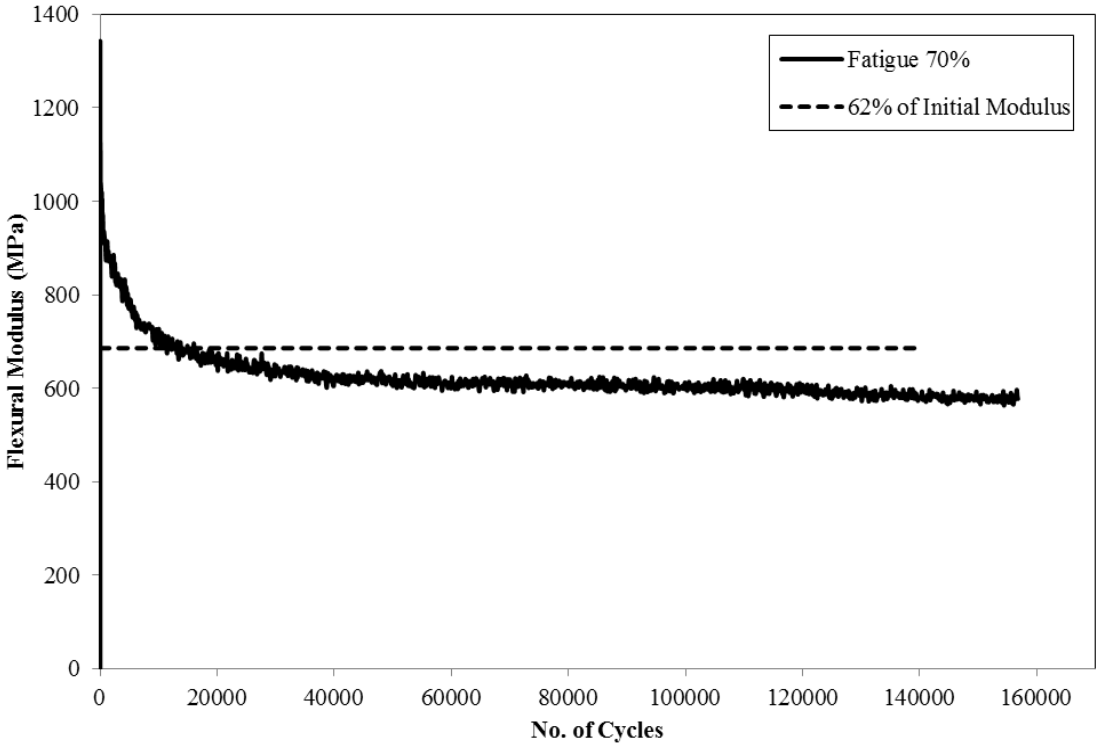

Figure C49. Typical Degradation of Flexural Modulus in a Fatigue Test at 70% Stress Level [Silt-Lime-Fly ash (4/12%) Specimens (FT-5)]

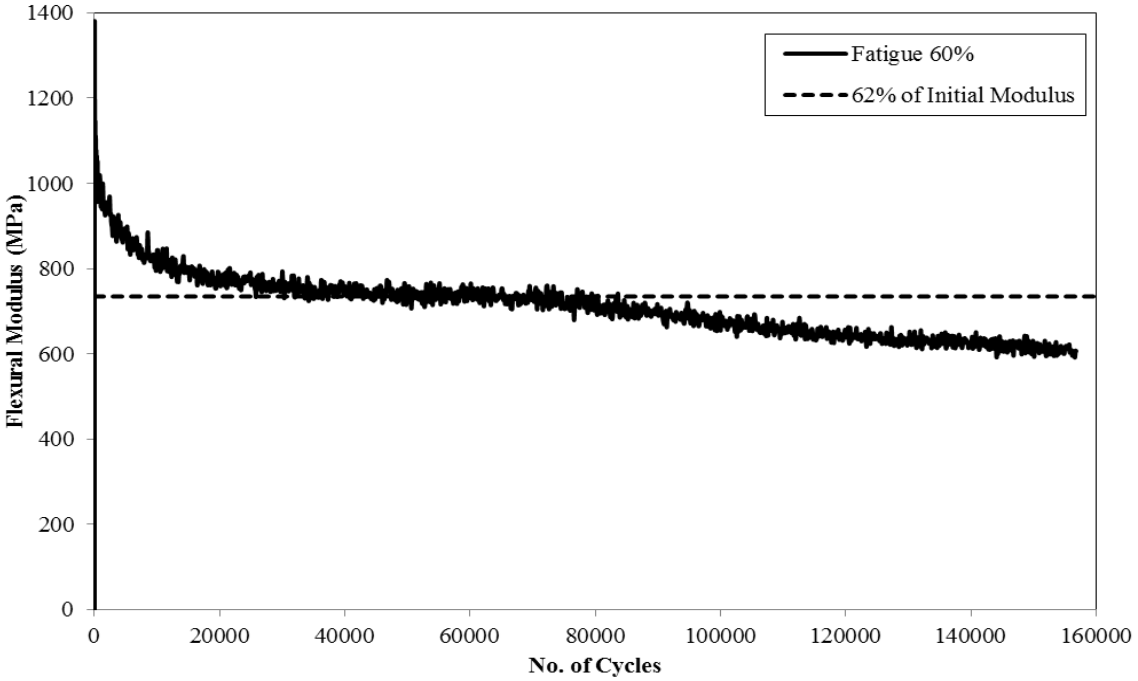

Figure C50. Typical Degradation of Flexural Modulus in a Fatigue Test at 60% Stress Level [Silt-Lime-Fly ash (4/12%) Specimens (FT-7)]

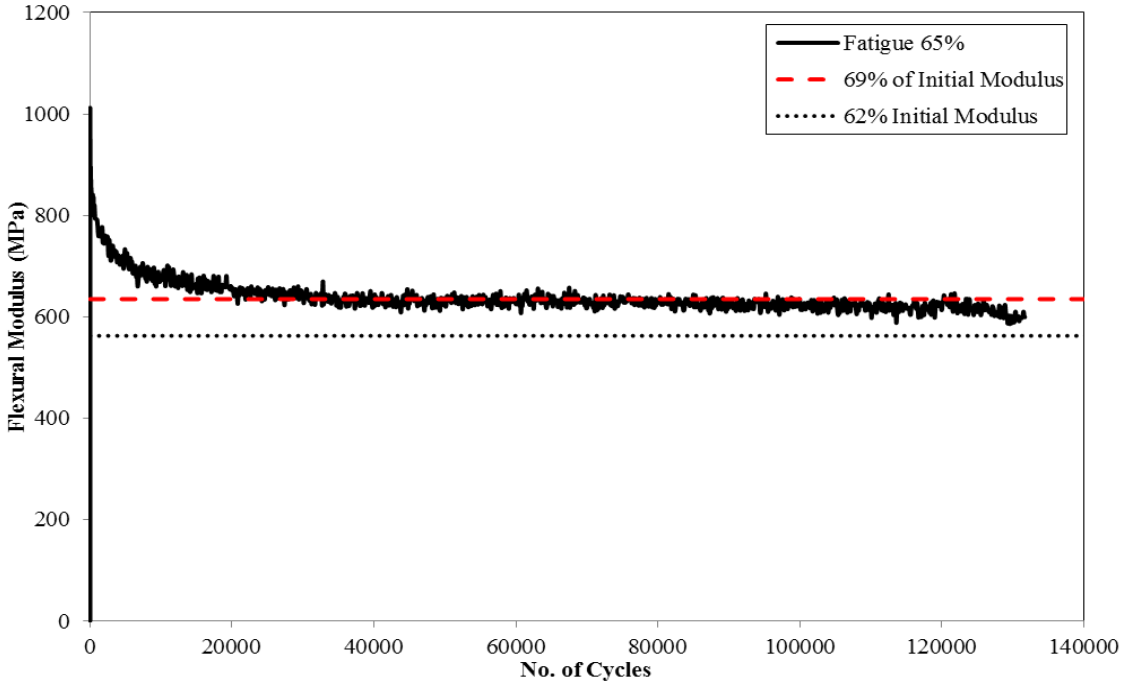

Figure C51. Typical Degradation of Flexural Modulus in a Fatigue Test at 65% Stress Level [Silt-Lime-Fly ash (4/12%) Specimens (FT-6)]

Figures C52 to C54 shows the flexural modulus degradation curves for specimens FT-2 to FT-4 for silt-lime-fly ash specimens stabilized with 4% lime and 12% class F fly ash.

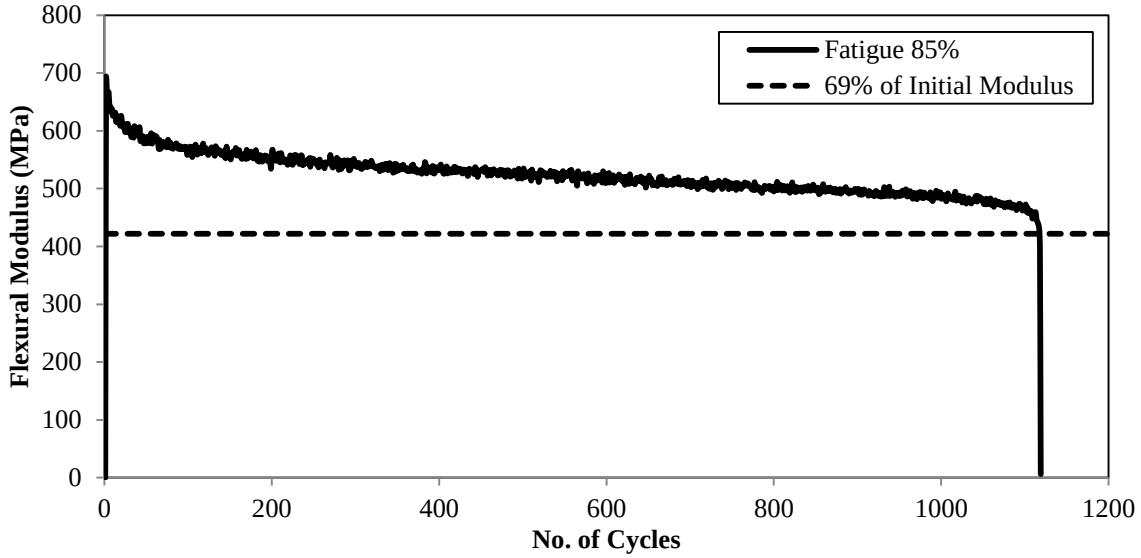

Figure C52. Typical Degradation of Flexural Modulus in a Fatigue Test at 85% Stress Level [Silt-Lime-Fly ash (4/12%) Specimens (FT-2)]

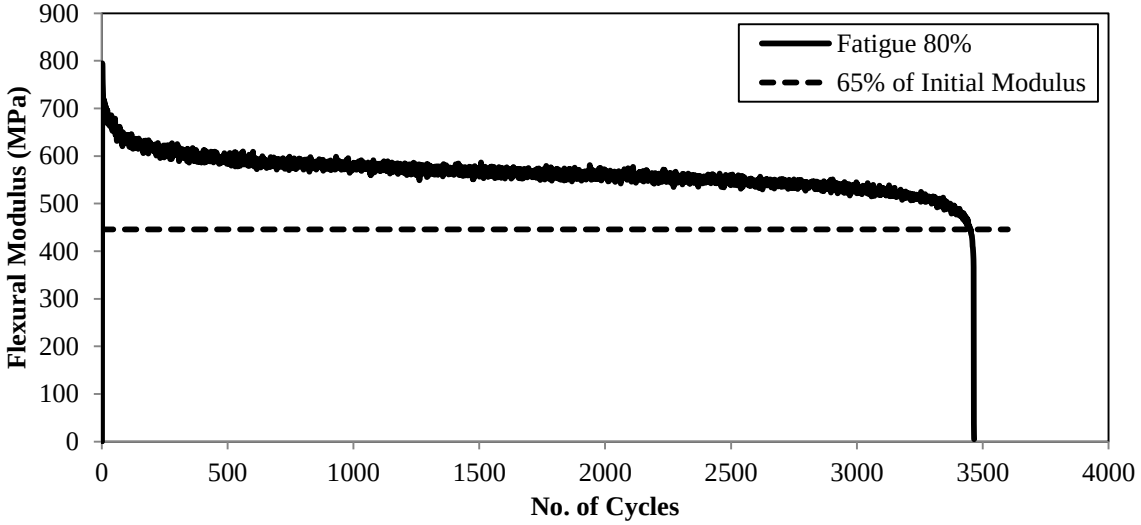

Figure C53. Typical Degradation of Flexural Modulus in a Fatigue Test at 80% Stress Level [Silt-Lime-Fly ash (4/12%) Specimens (FT-3)]

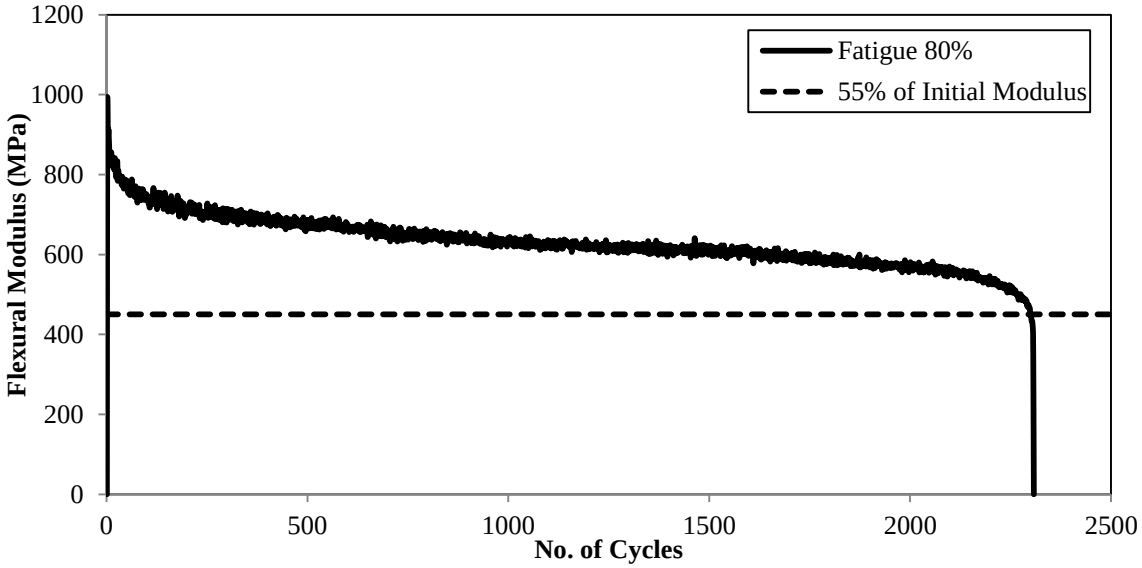

Figure C54. Typical Degradation of Flexural Modulus in a Fatigue Test at 80% Stress Level [Silt-Lime-Fly ash (4/12%) Specimens (FT-4)]

Figures C55 to C57 shows the displacement (total, plastic and elastic) variation curves for specimens FT-2 to FT-4 for silt-lime-fly ash specimens stabilized with 4% lime and 12% class F fly ash.

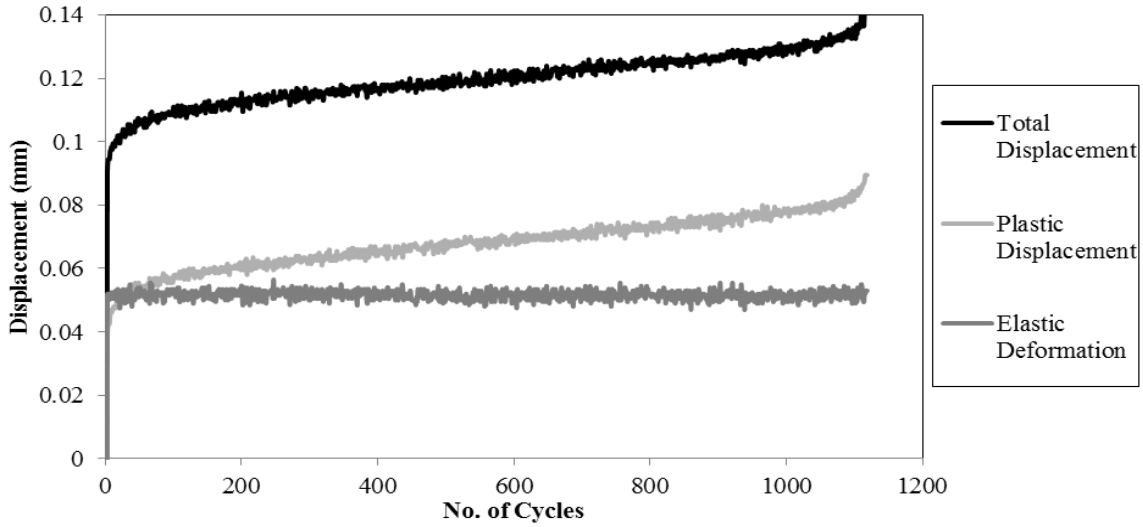

Figure C55. Displacement Variation v/s No. of Cycles in a Fatigue Test at 85% Stress Level [Silt-Lime-Fly ash (4/12%) Specimens (FT-2)]

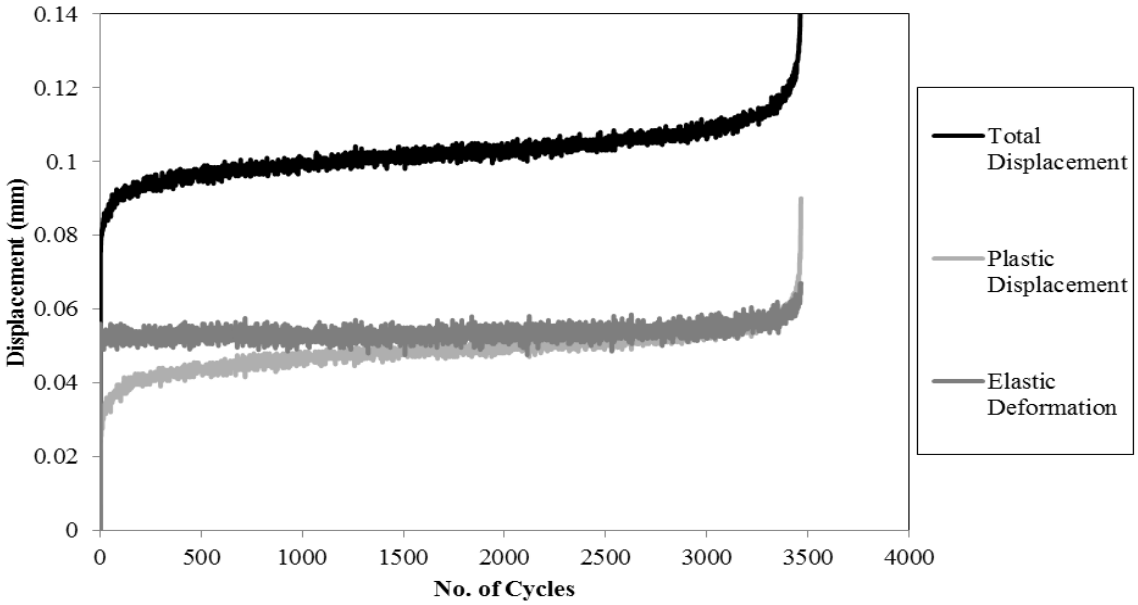

Figure C56. Displacement Variation v/s No. of Cycles in a Fatigue Test at 80% Stress Level [Silt-Lime-Fly ash (4/12%) Specimens (FT-3)]

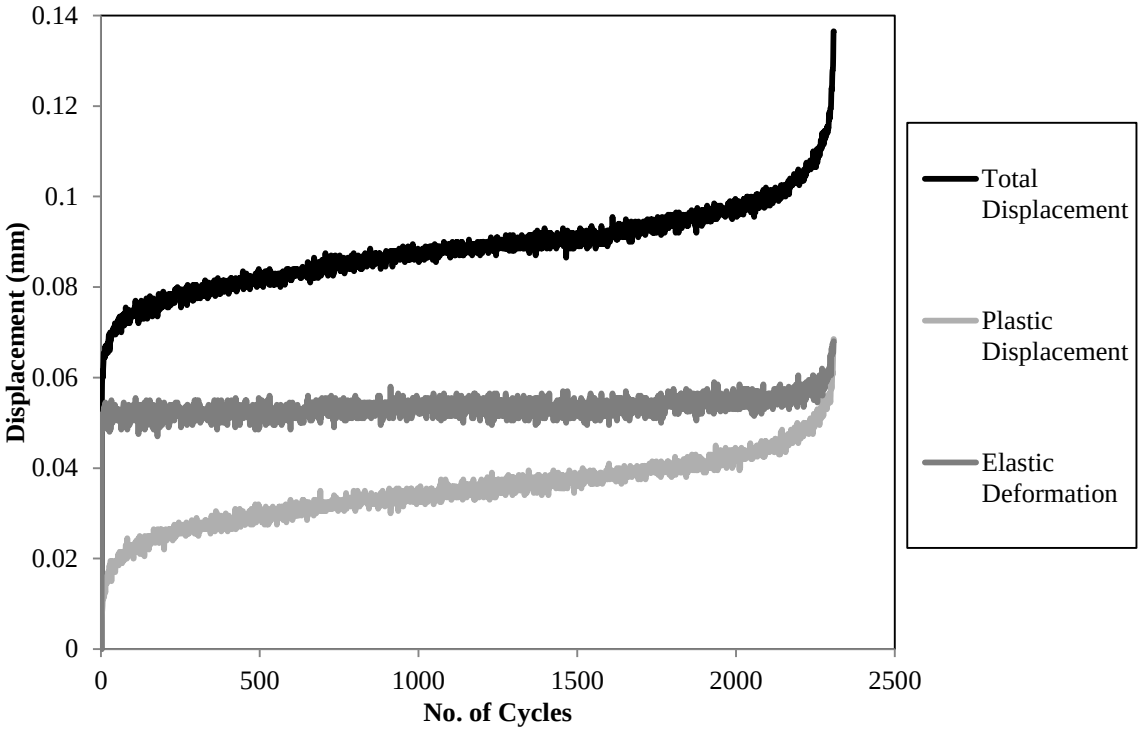

Figure C57. Displacement Variation v/s No. of Cycles in a Fatigue Test at 80% Stress Level [Silt-Lime-Fly ash (4/12%) Specimens (FT-4)]

Six beam specimens were tested for the clay-lime beam specimens (6% binder). Table C8 shows the summary of the fatigue test results on the clay-lime beam specimens. From the clay-lime specimen fatigue curve, we can see that the specimen ruptured shortly after the cycles to half the initial modulus was reached. Two of the clay-lime specimens (FT-5 and FT-6) did not fail after 120,000+ cycles. As, per Midgley and Yeo (2008), half the initial modulus was used to predict the fatigue life of these specimens. From Figure C58 and C59, the 50% of initial modulus was reached at 3,137 and 29,993 cycles, respectively. Hence, the fatigue life for FT-5 and FT-6 was taken as 3,137 and 29,993 cycles, respectively. Figures C60 shows the flexural modulus degradation curves for specimen FT-3 for clay-lime specimens stabilized with 6% lime.

Table C8. Summary of the Fatigue Strength Test Results on Clay-Lime Specimens (Binder Content: 6%)

SN	SL (%)	IFM (MPa)	FFM (MPa)	PFME (%)	IS (με)	N
FT-1	90	-	-	-	-	15
FT-2	90	-	-	-	-	14
FT-3	85	606	417	69	319	1,370
FT-4	85	401	231	58	479	4,280
FT-5*	75	667	137	20	265	3,137**
FT-6*	65	593	285	48	261	29,933**

*SN = Specimen Number; SL = Stress Level; IFM = Initial Flexural Modulus; FFM = Final Flexural Modulus (i.e. Flexural Modulus at the end of Fatigue Test); PFME =Percent of Flexural Modulus at the End of Test; IS = Initial Strain; N = Number of Cycles at the End of Test (i.e. Fatigue Life); * Did not fail; **Estimated value*

Note: *All specimens failed at 50% of IFM*

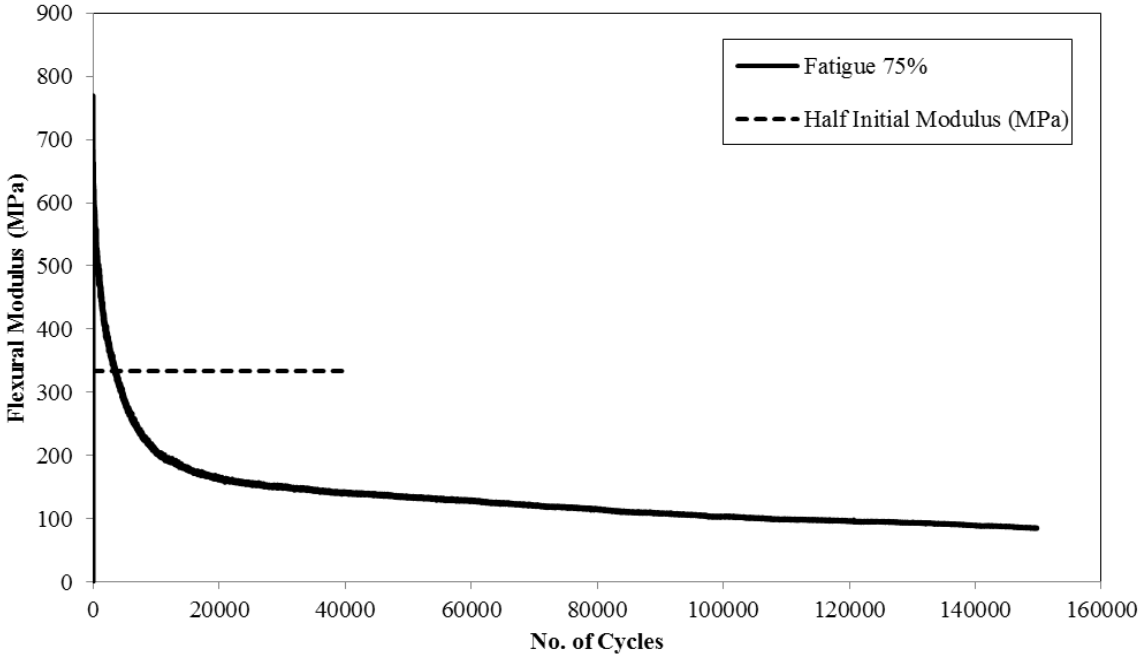

Figure C58. Typical Degradation of Flexural Modulus in a Fatigue Test at 75% Stress Level [Clay-Lime (6%) Specimens (FT-5)]

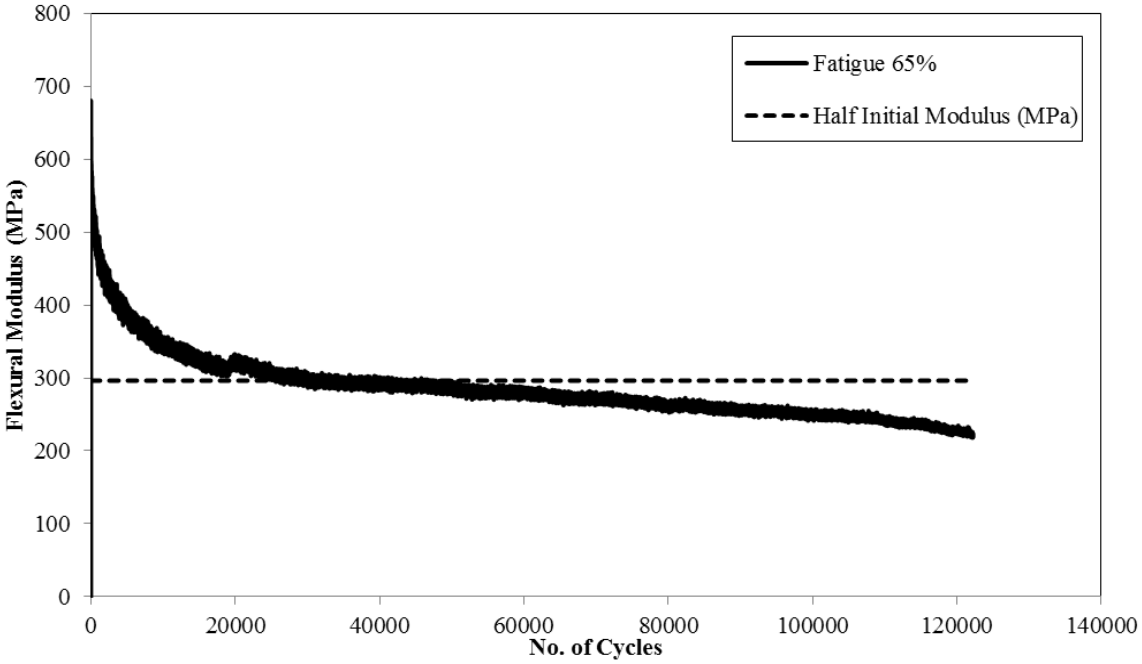

Figure C59. Typical Degradation of Flexural Modulus in a Fatigue Test at 65% Stress Level [Clay-Lime (6%) Specimens (FT-6)]

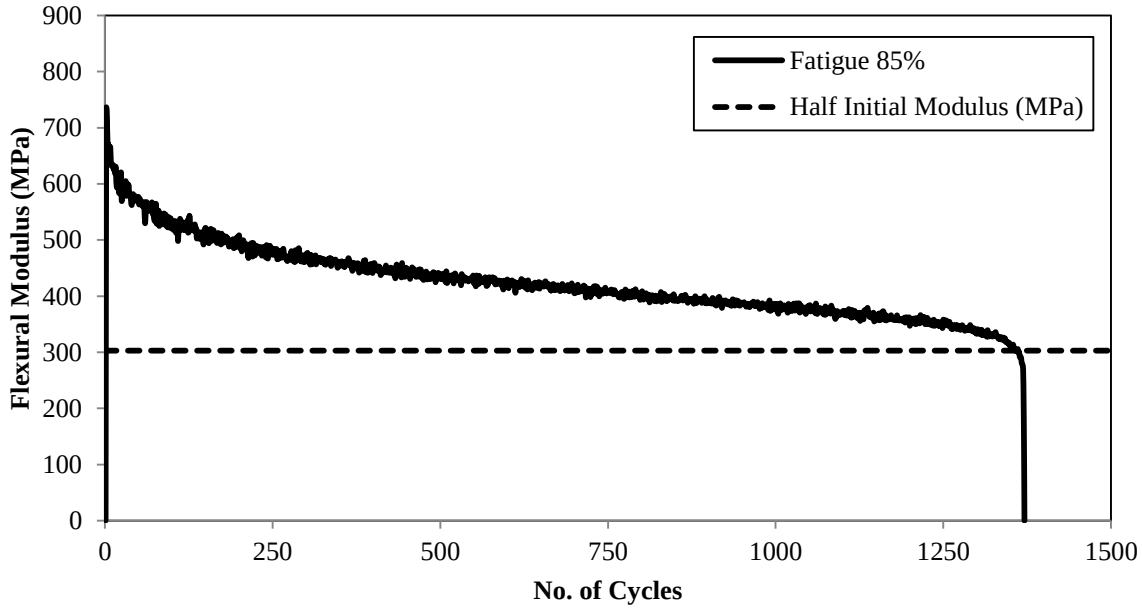

Figure C60. Typical Degradation of Flexural Modulus in a Fatigue Test at 85% Stress Level [Clay-Lime (6%) Specimens (FT-3)]

Figure C61 shows the displacement (total, plastic and elastic) variation curves for specimen FT-3 for clay-lime specimens stabilized with 6% lime.

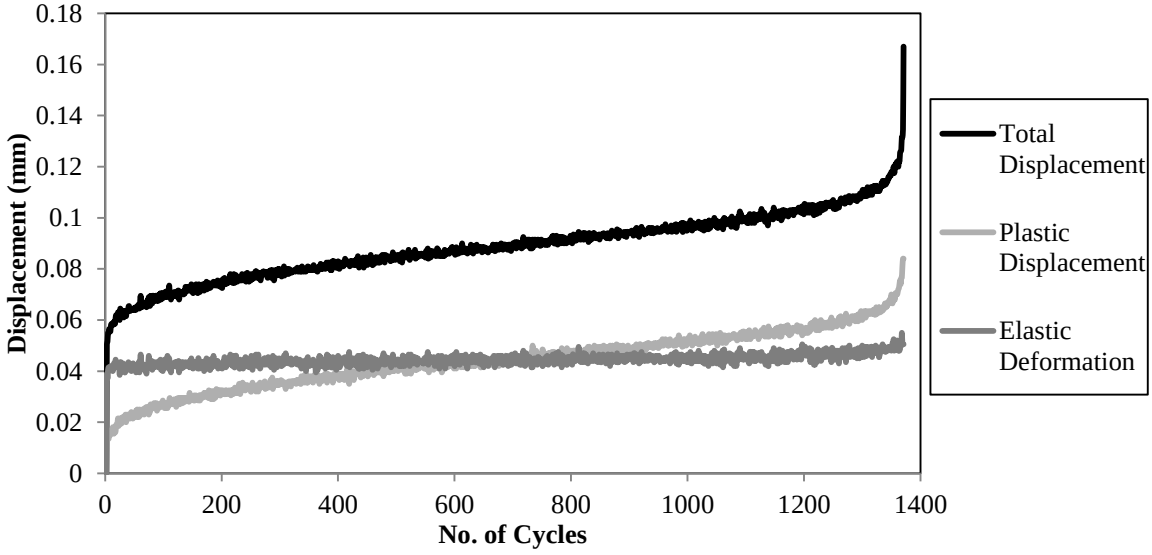

Figure C61. Displacement Variation v/s No. of Cycles in a Fatigue Test at 85% Stress Level [Clay-Lime (6%) Specimens (FT-3)]

C1. FATIGUE TESTING OF BEAM SPECIMENS WITH REDUCED DENSITY

Six beam specimens were tested for the gravel-cement beam specimens (3% binder). These specimens were compacted at about 90% of the target dry density. Table C9 shows the summary of the fatigue test results on the gravel-cement beam specimens.

The gravel-cement specimens did not perform well for the fatigue cracking test as compared to the same specimens which were compacted to the target dry density (comparing Table 4.9). The fatigue life of these specimens was quite less. Figures C62 to C64 shows the flexural modulus degradation curves for specimen FT-4, FT-5 and FT-6 for gravel-cement specimens stabilized with 3% cement and compacted to 90% dry density. From the gravel-cement specimen fatigue curves, we can see that all the specimens ruptured shortly after the cycles to half the initial modulus was reached.

Table C9. Summary of the Fatigue Strength Test Results on Gravel-Cement Specimens (Binder Content: 3%, 90% MDD)

SN	SL (%)	IFM (MPa)	FFM (MPa)	PFME (%)	IS (με)	N
FT-1	85	-	-	-	-	15
FT-2	85	-	-	-	-	8
FT-3	75	724	-	-	581	41
FT-4	75	805	621	77	450	73
FT-5	65	506	429	85	796	133
FT-6	65	1,179	941	80	401	167

SN = Specimen Number; SL = Stress Level; IFM = Initial Flexural Modulus; FFM = Final Flexural Modulus (i.e. Flexural Modulus at the end of Fatigue Test); PFME =Percent of Flexural Modulus at the End of Test; IS = Initial Strain; N = Number of Cycles at the End of Test (i.e. Fatigue Life)

Note: *All specimens failed at 50% of IFM*

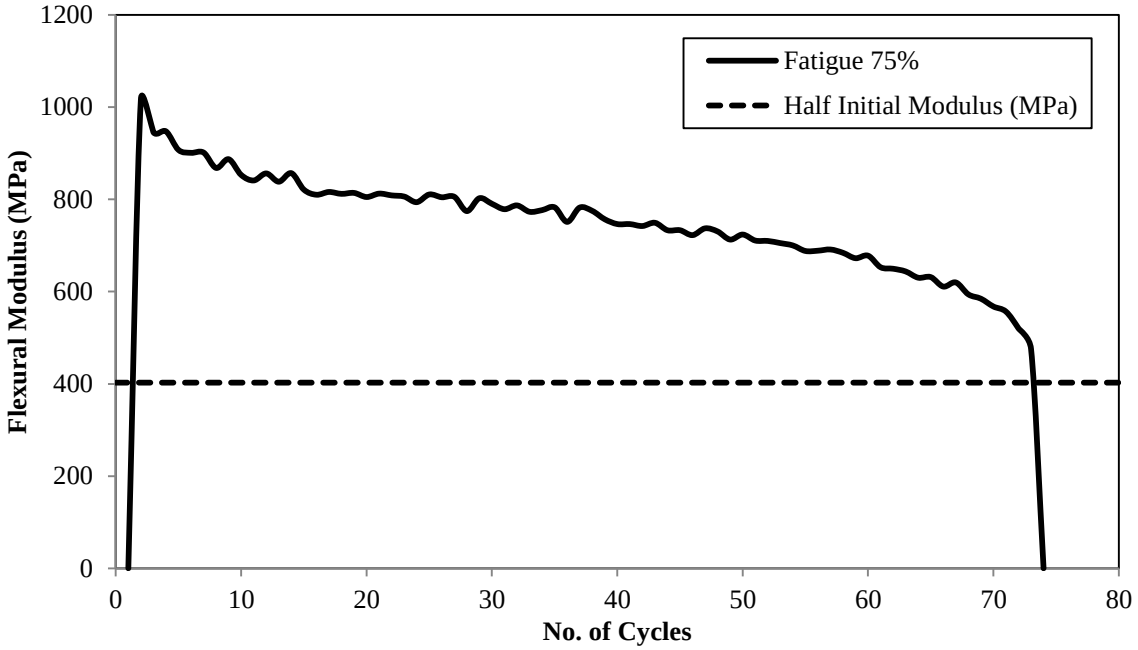

Figure C62. Typical Degradation of Flexural Modulus in a Fatigue Test at 75% Stress Level [Gravel-Cement (3%) Specimens (FT-4), 90% MDD]

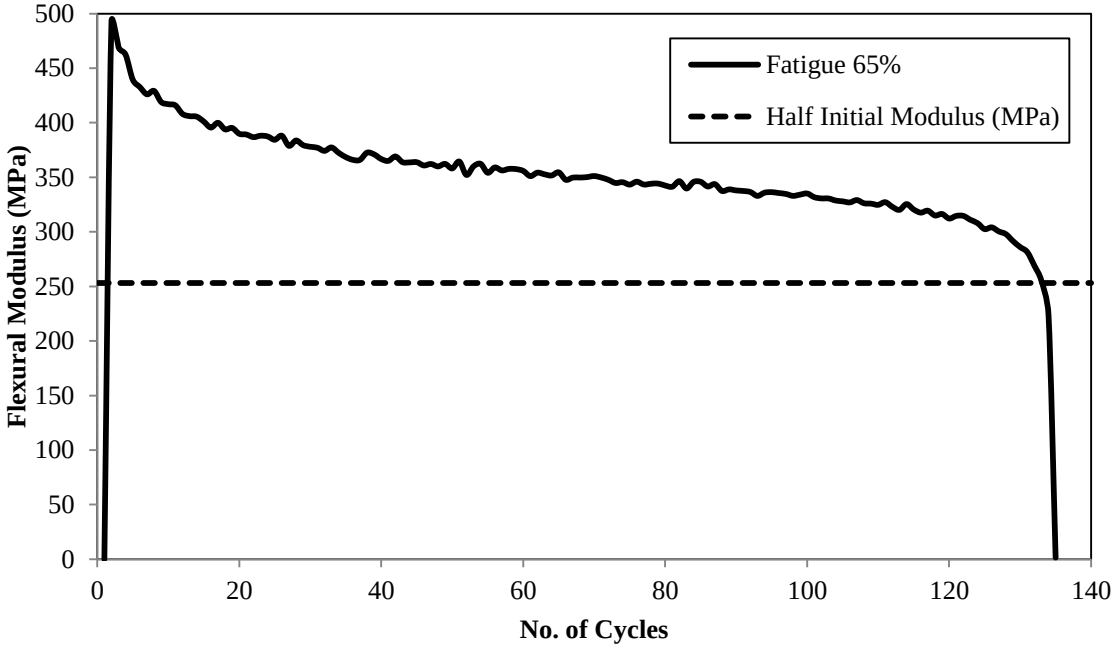

Figure C63. Typical Degradation of Flexural Modulus in a Fatigue Test at 65% Stress Level [Gravel-Cement (3%) Specimens (FT-5), 90% MDD]

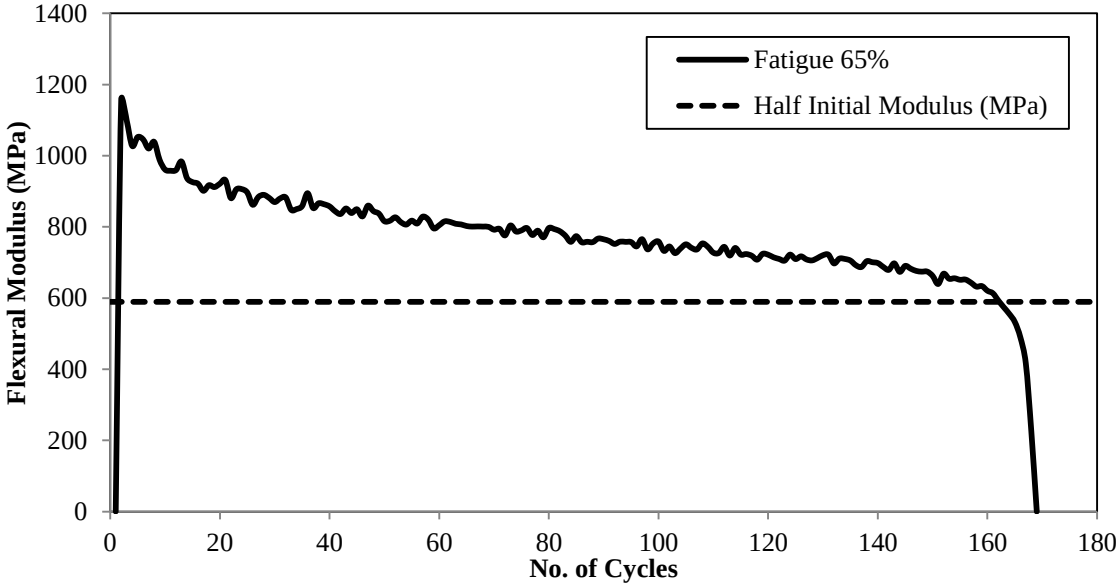

Figure C64. Typical Degradation of Flexural Modulus in a Fatigue Test at 65% Stress Level [Gravel-Cement (3%) Specimens (FT-6), 90% MDD]

Figures C65 to C67 shows the displacement (total, plastic and elastic) variation curves for specimen FT-4, FT-5 and FT-6 for gravel-cement specimens stabilized with 3% cement and compacted to 90% dry density.

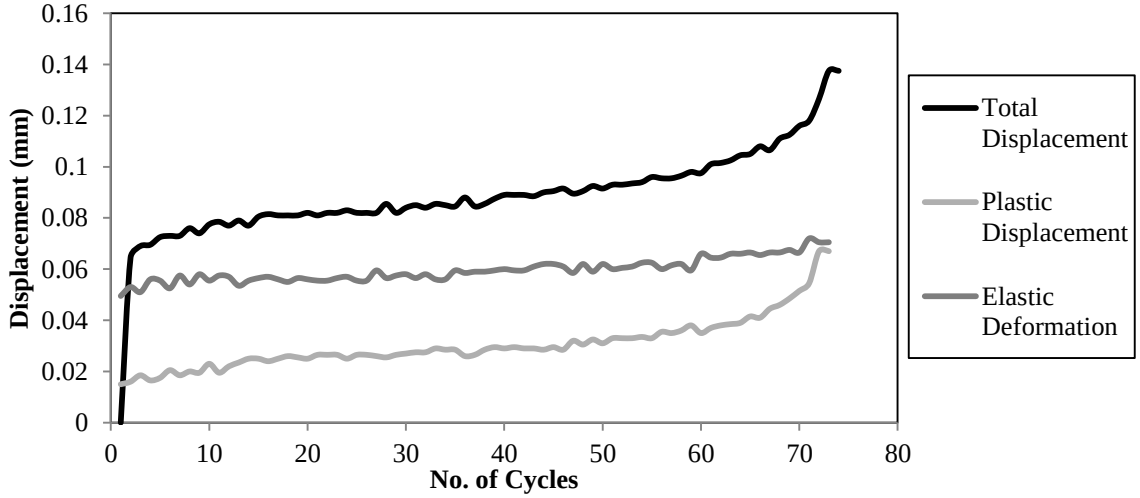

Figure C65. Displacement Variation v/s No. of Cycles in a Fatigue Test at 75% Stress Level [Gravel-Cement (3%) Specimens (FT-4), 90% MDD]

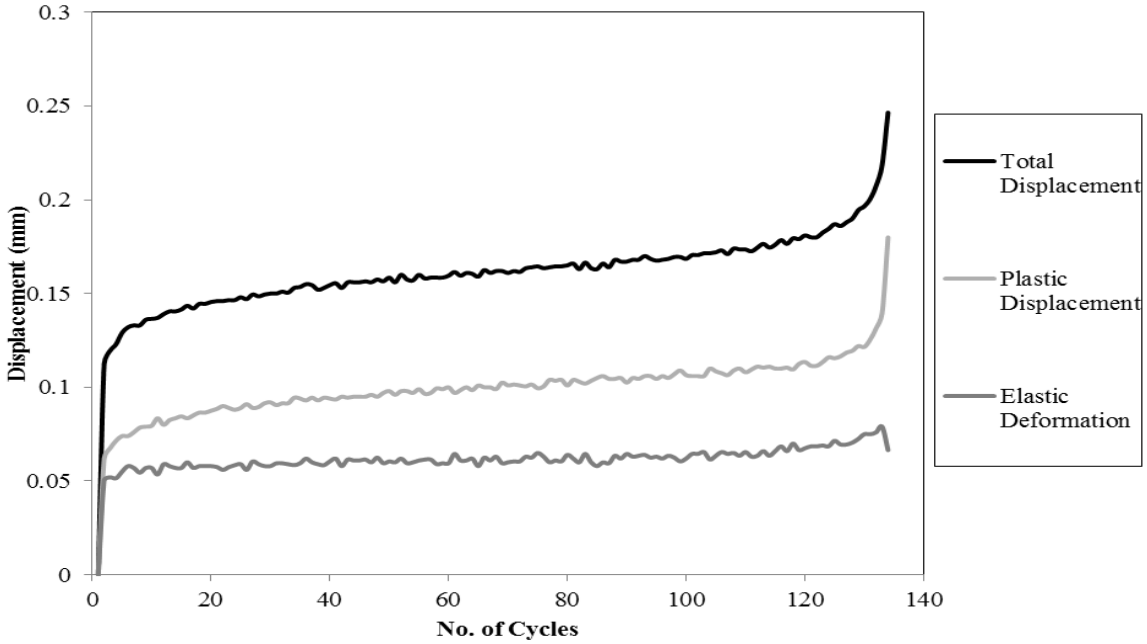

Figure C66. Displacement Variation v/s No. of Cycles in a Fatigue Test at 65% Stress Level [Gravel-Cement (3%) Specimens (FT-5), 90% MDD]

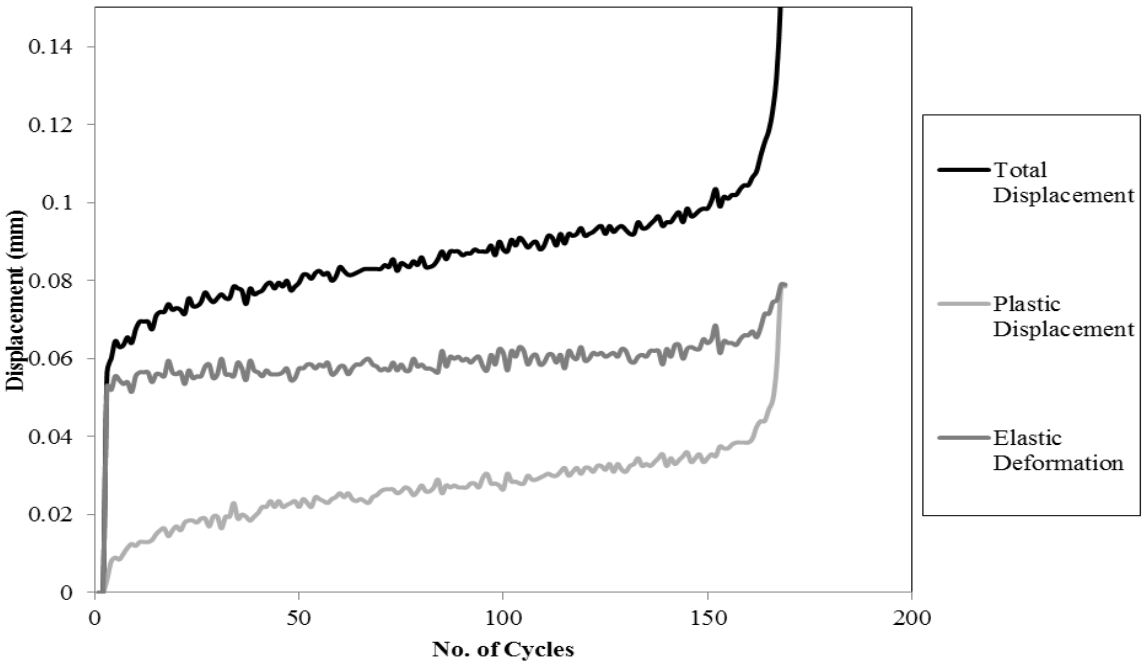

Figure C67. Displacement Variation v/s No. of Cycles in a Fatigue Test at 65% Stress Level [Gravel-Cement (3%) Specimens (FT-6), 90% MDD]

Six beam specimens were tested for the silt-cement beam specimens (8% binder). These specimens were compacted at about 90% of the target dry density. Table C10 shows the summary of the fatigue test results on the silt-cement beam specimens. From the silt-cement specimen fatigue curve, we can see that not all the specimen ruptured shortly after the cycles to half the initial modulus was reached. The specimens ruptured when the initial modulus reached in the range of 55% to 65%. Two of the silt-cement specimens (FT-5 and FT-6) did not fail after 100,000+ cycles.

Figures C68 to C70 shows the flexural modulus degradation curves for specimen FT-1, FT-2 and FT-3 for silt-cement specimens stabilized with 8% cement and compacted to 90% dry density.

Table C10. Summary of the Fatigue Strength Test Results on Silt-Cement Specimens (Binder Content: 8%, 90% MDD)

SN	SL (%)	IFM (MPa)	FFM (MPa)	PFME (%)	IS (με)	N
FT-1	90	1,061	921	87	368	141
FT-2	85	855	545	64	443	13,081
FT-3	85	1,115	833	75	364	11,015
FT-4	75	1,086	654	60	347	68,093
FT-5*	65	525	397	76	595	>220,000
FT-6*	65	734	484	66	423	>100,000

*SN = Specimen Number; SL = Stress Level; IFM = Initial Flexural Modulus; FFM = Final Flexural Modulus (i.e. Flexural Modulus at the end of Fatigue Test); PFME =Percent of Flexural Modulus at the End of Test; IS = Initial Strain; N = Number of Cycles at the End of Test (i.e. Fatigue Life); * Did not fail*

Note: *Range of Failure: 55% to 65% of IFM (Average: 60%)*

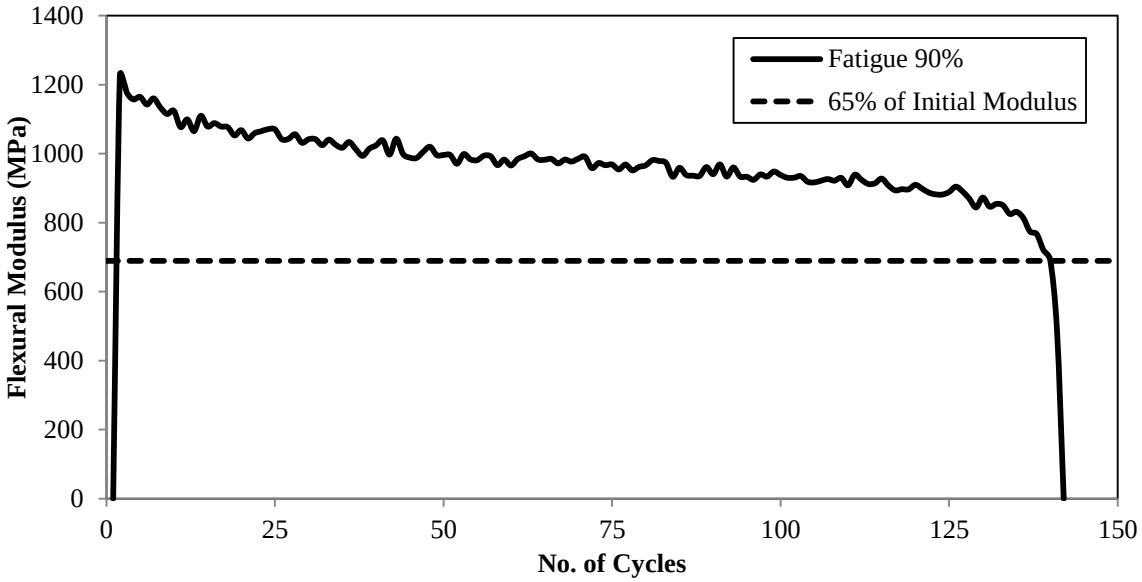

Figure C68. Typical Degradation of Flexural Modulus in a Fatigue Test at 90% Stress Level [Silt-Cement (8%) Specimens (FT-1), 90% MDD]

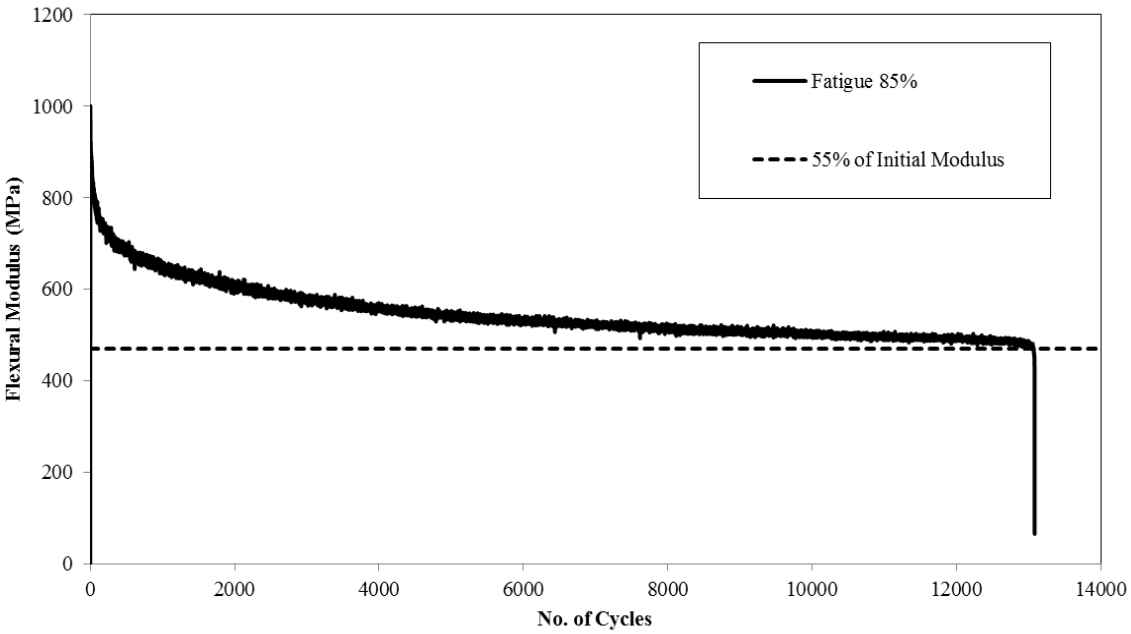

Figure C69. Typical Degradation of Flexural Modulus in a Fatigue Test at 85% Stress Level [Silt-Cement (8%) Specimens (FT-2), 90% MDD]

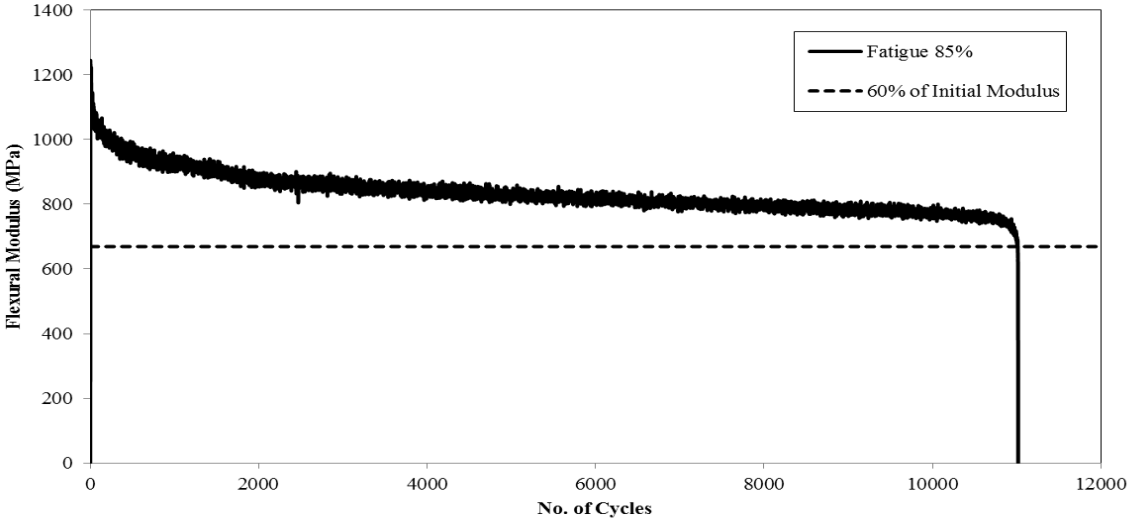

Figure C70. Typical Degradation of Flexural Modulus in a Fatigue Test at 85% Stress Level [Silt-Cement (8%) Specimens (FT-3), 90% MDD]

Figures C71 to C73 shows the displacement (total, plastic and elastic) variation curves for specimen FT- FT-1, FT-2 and FT-3 for silt-cement specimens stabilized with 8% cement and compacted to 90% dry density.

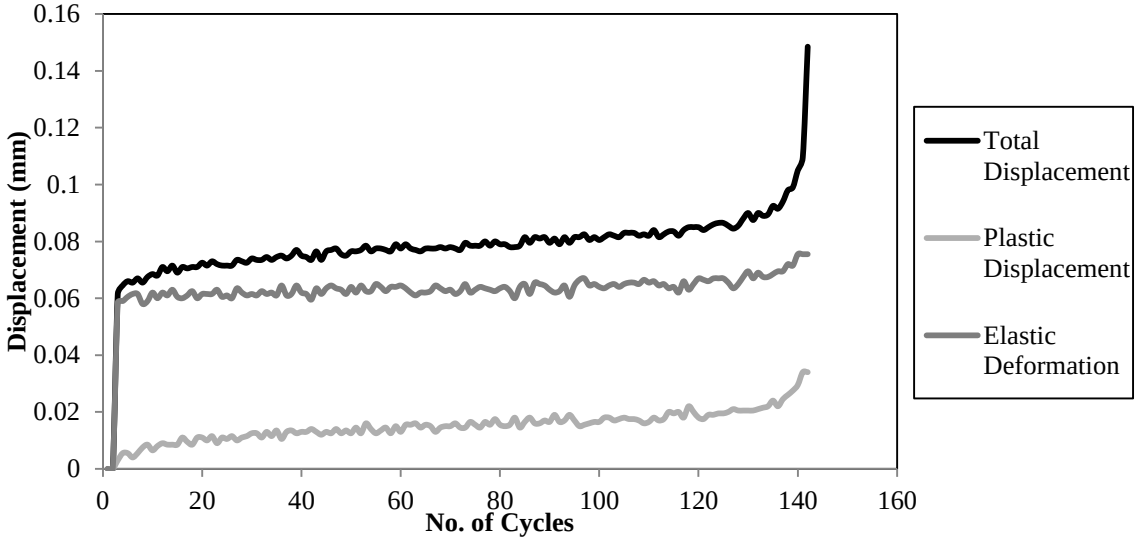

Figure C71. Displacement Variation v/s No. of Cycles in a Fatigue Test at 90% Stress Level [Silt-Cement (8%) Specimens (FT-1), 90% MDD]

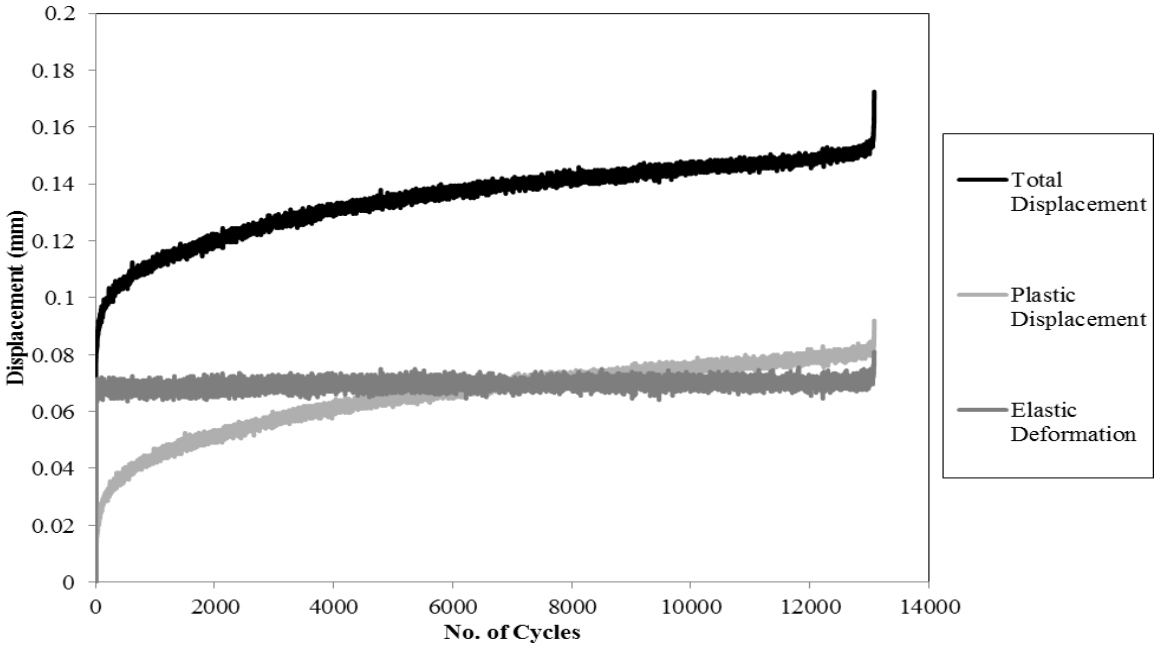

Figure C72. Displacement Variation v/s No. of Cycles in a Fatigue Test at 85% Stress Level [Silt-Cement (8%) Specimens (FT-2), 90% MDD]

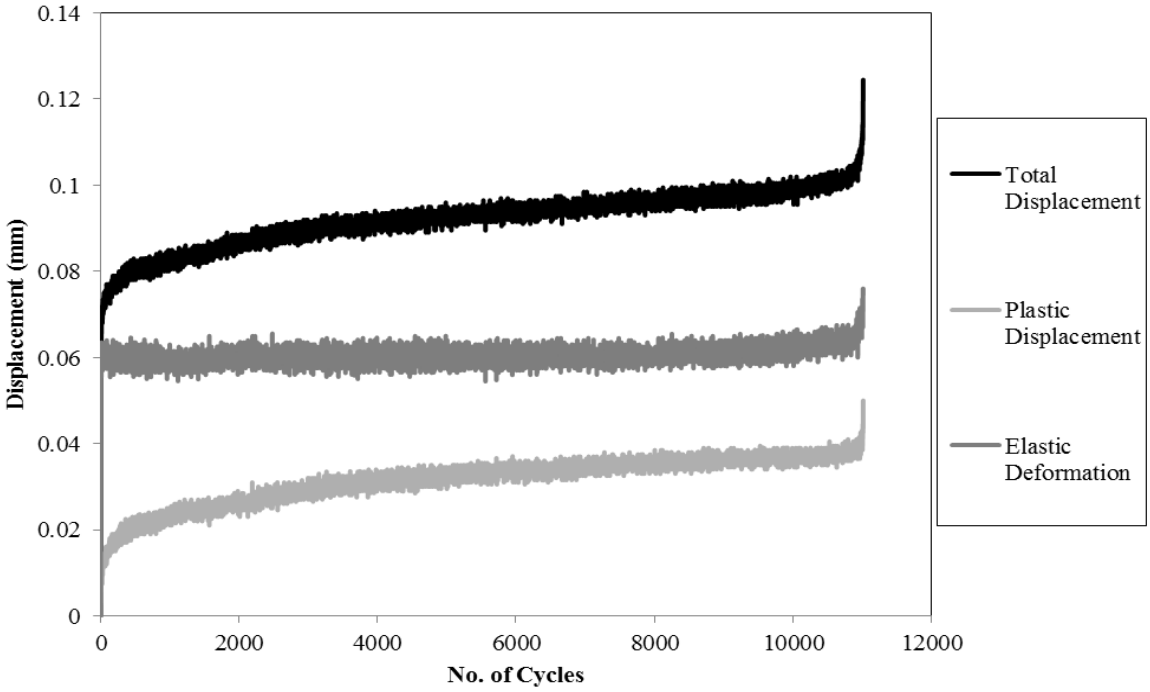

Figure C73. Displacement Variation v/s No. of Cycles in a Fatigue Test at 85% Stress Level [Silt-Cement (8%) Specimens (FT-3), 90% MDD]

C.2. FATIGUE TESTING OF BEAM SPECIMENS WITH HIGHER BINDER CONTENT

Seven beam specimens were tested for the gravel-cement beam specimens (5% binder). Table C11 shows the summary of the fatigue test results on the gravel-cement beam specimens. From the gravel-cement specimen fatigue curves, the specimens ruptured shortly after the cycles to half the initial modulus was reached.

Specimen FT-3 did not fail after 150,000 cycles, but 50% of initial modulus shows the fatigue life of the specimen to be around 1,016 cycles (Figure C74). Specimen FT-4 failed after 9,969 cycles, but half of the initial modulus line shows the failure to occur at 6,211 cycles (Figure C75). Hence, the fatigue life for specimen FT-4 was taken as 6,211 cycles. Specimen FT-7 did not fail even after 120,000 cycles.

Table C11. Summary of the Fatigue Strength Test Results on Gravel-Cement Specimens (Binder Content: 5%)

SN	SL (%)	IFM (MPa)	FFM (MPa)	PFME (%)	IS (με)	N
FT-1	75	-	-	-	-	24
FT-2	75	-	-	-	-	36
FT-3*	65	1,892	566	30	328	1,016**
FT-4	65	1,572	836	53	457	9,969
FT-5	55	1,697	1,079	64	285	11,836
FT-6	55	1,391	495	36	1465	11,026
FT-7*	50	1,187	572	48	457	>120,000

*SN = Specimen Number; SL = Stress Level; IFM = Initial Flexural Modulus; FFM = Final Flexural Modulus (i.e. Flexural Modulus at the end of Fatigue Test); PFME =Percent of Flexural Modulus at the End of Test; IS = Initial Strain; N = Number of Cycles at the End of Test (i.e. Fatigue Life); * Did not fail; **Estimated value*

Note: *All specimens failed at 50% of IFM*

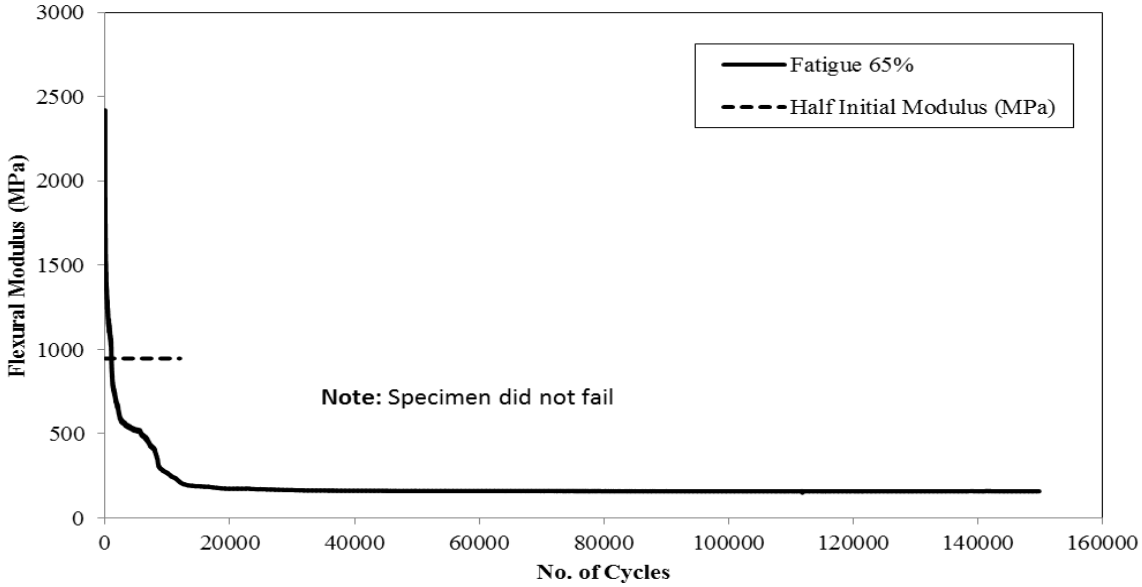

Figure C74. Typical Degradation of Flexural Modulus in a Fatigue Test at 65% Stress Level [Gravel-Cement (5%) Specimens (FT-3)]

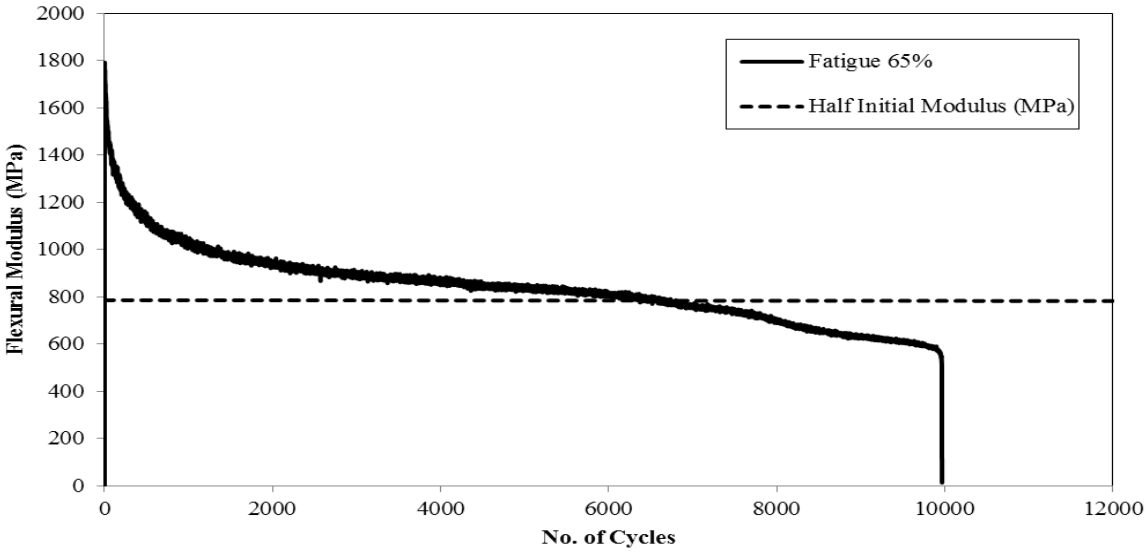

Figure C75. Typical Degradation of Flexural Modulus in a Fatigue Test at 65% Stress Level [Gravel-Cement (5%) Specimens (FT-4)]

Figure C76 shows the flexural modulus degradation curve for specimen FT-5 for gravel-cement specimens stabilized with 5% cement.

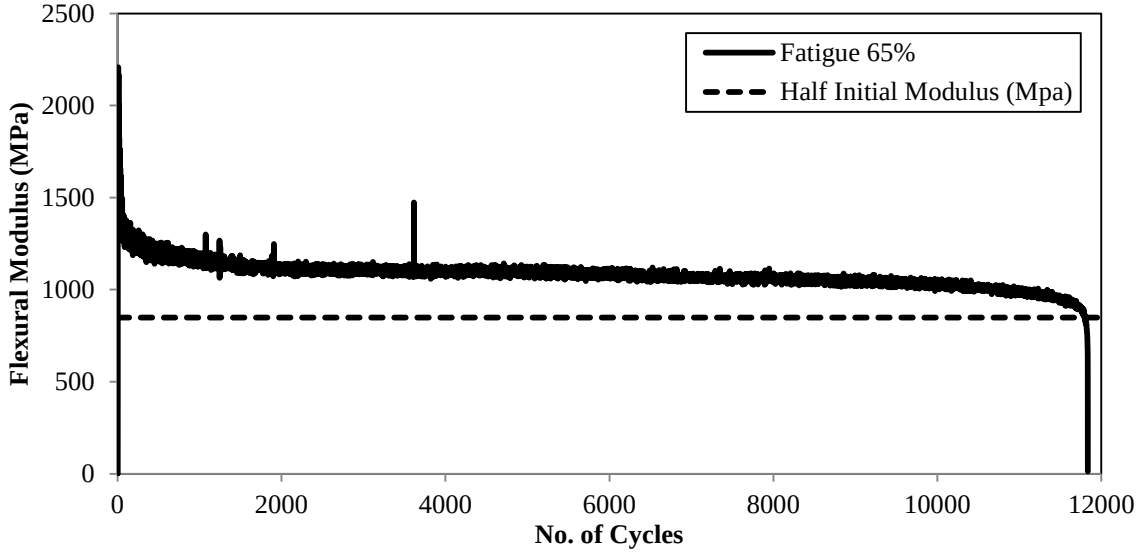

Figure C76. Typical Degradation of Flexural Modulus in a Fatigue Test at 55% Stress Level [Gravel-Cement (5%) Specimens (FT-5)]

Figure C77 shows the displacement (total, plastic and elastic) variation curve for specimen FT-5 for gravel-cement specimens stabilized with 5% cement.

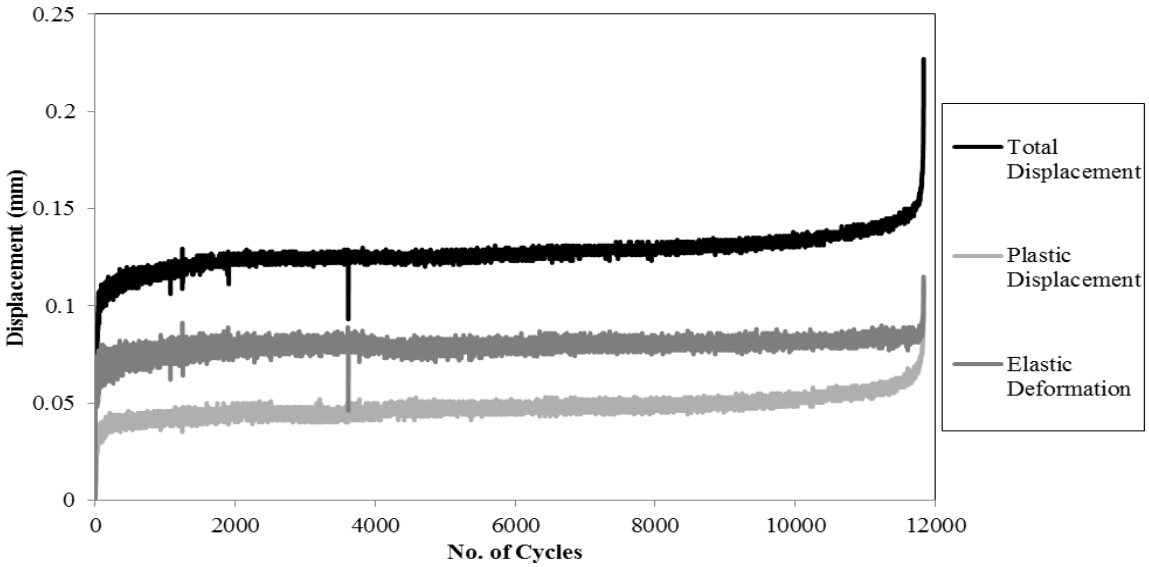

Figure C77. Displacement Variation v/s No. of Cycles in a Fatigue Test at 55% Stress Level [Gravel-Cement (5%) Specimens (FT-5)]

Six beam specimens were tested for the sand-cement beam specimens (8% binder). Table C12 shows the summary of the fatigue test results on the sand-cement beam specimens. From the sand-cement specimen fatigue curves, we can observe that the specimens ruptured shortly after the cycles to half the initial modulus was reached.

Specimen FT-6 did not fail after 185,000 cycles, but 50% of initial modulus shows the fatigue life of the specimen to be around 78,321 cycles (Figure C78).

Table C12. Summary of the Fatigue Strength Test Results on Sand-Cement Specimens (Binder Content: 8%)

SN	SL (%)	IFM (MPa)	FFM (MPa)	PFME (%)	IS (με)	N
FT-1	85	1,982	1,677	85	465	142
FT-2	85	1,243	768	62	736	1,186
FT-3	75	1,444	562	39	513	9,882
FT-4	75	1,372	323	24	466	14,633
FT-5	65	1,274	712	56	235	56,044
FT-6*	65	1,164	978	84	466	78,321**

*SN = Specimen Number; SL = Stress Level; IFM = Initial Flexural Modulus; FFM = Final Flexural Modulus (i.e. Flexural Modulus at the end of Fatigue Test); PFME =Percent of Flexural Modulus at the End of Test; IS = Initial Strain; N = Number of Cycles at the End of Test (i.e. Fatigue Life); * Did not fail; **Estimated value*

Note: *All specimens failed at 50% of IFM*

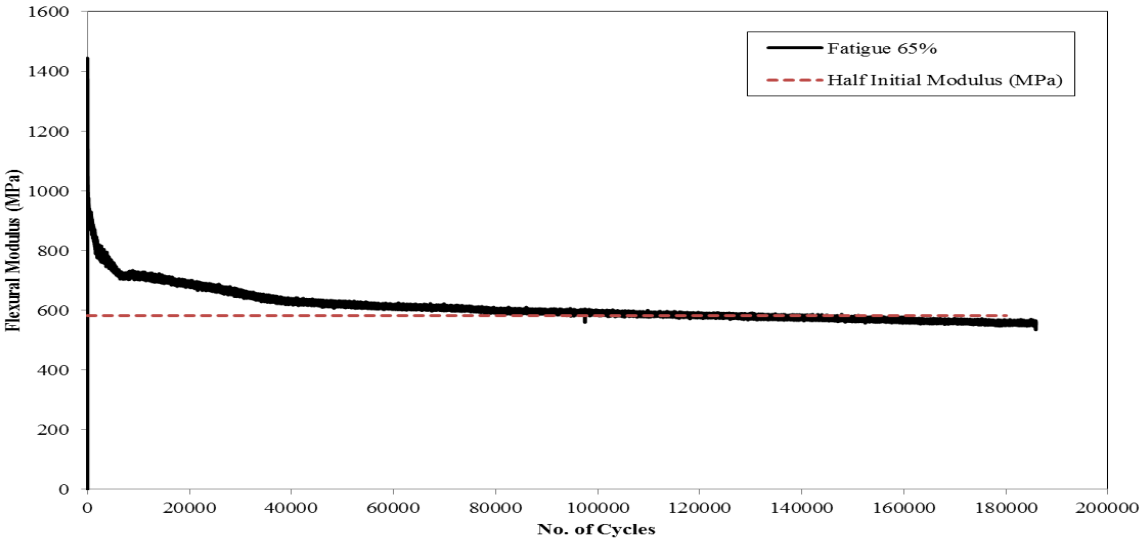

Figure C78. Typical Degradation of Flexural Modulus in a Fatigue Test at 65% Stress Level [Sand-Cement (8%) Specimens (FT-6)]

Figure C79 and C80 shows the flexural modulus degradation curve for specimens FT-1 and FT-2 for sand-cement specimens stabilized with 8% cement.

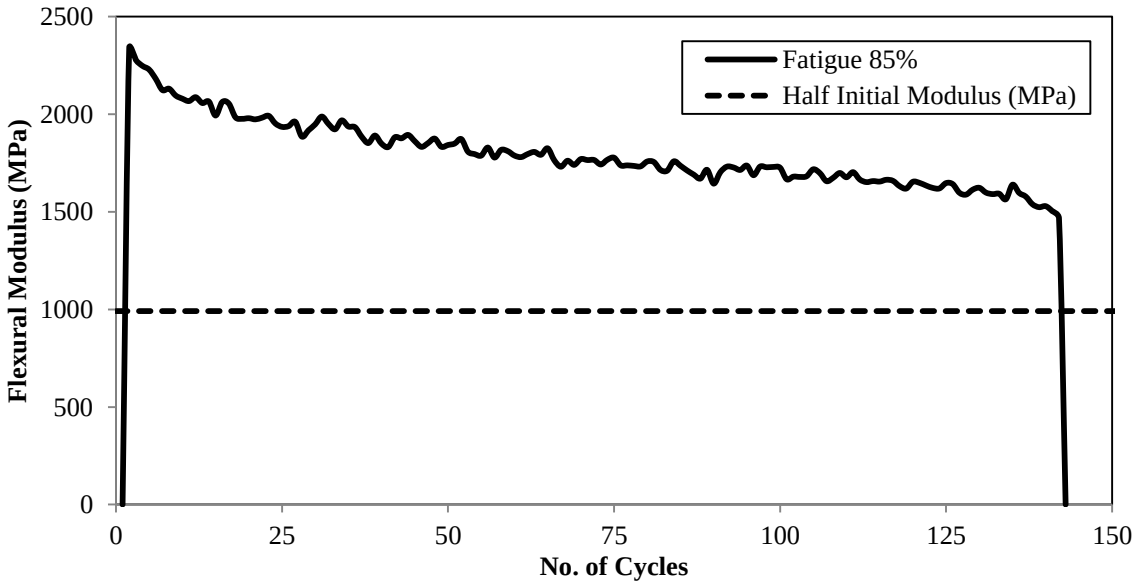

Figure C79. Typical Degradation of Flexural Modulus in a Fatigue Test at 85% Stress Level [Sand-Cement (8%) Specimens (FT-1)]

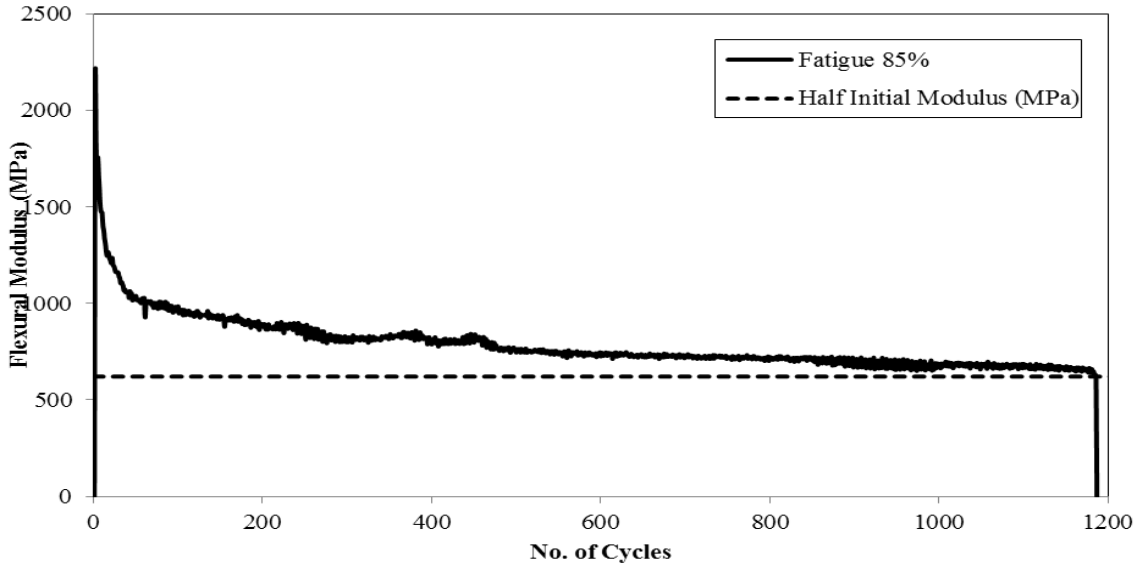

Figure C80. Typical Degradation of Flexural Modulus in a Fatigue Test at 85% Stress Level [Sand-Cement (8%) Specimens (FT-2)]

Figure C81 and C82 shows the displacement (total, plastic and elastic) variation curve for specimens FT-1 and FT-2 for sand-cement specimens stabilized with 8% cement.

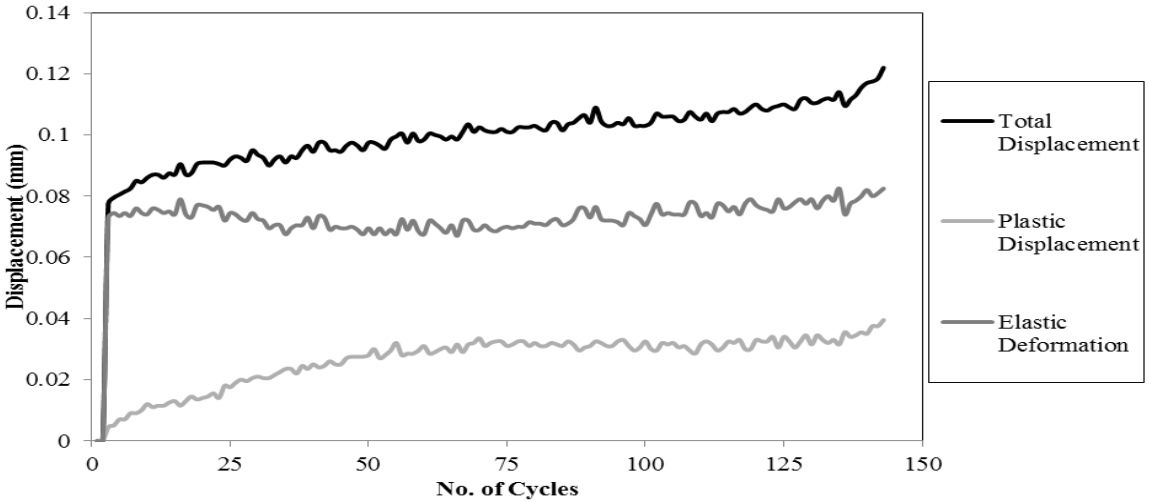

Figure C81. Displacement Variation v/s No. of Cycles in a Fatigue Test at 85% Stress Level [Sand-Cement (8%) Specimens (FT-1)]

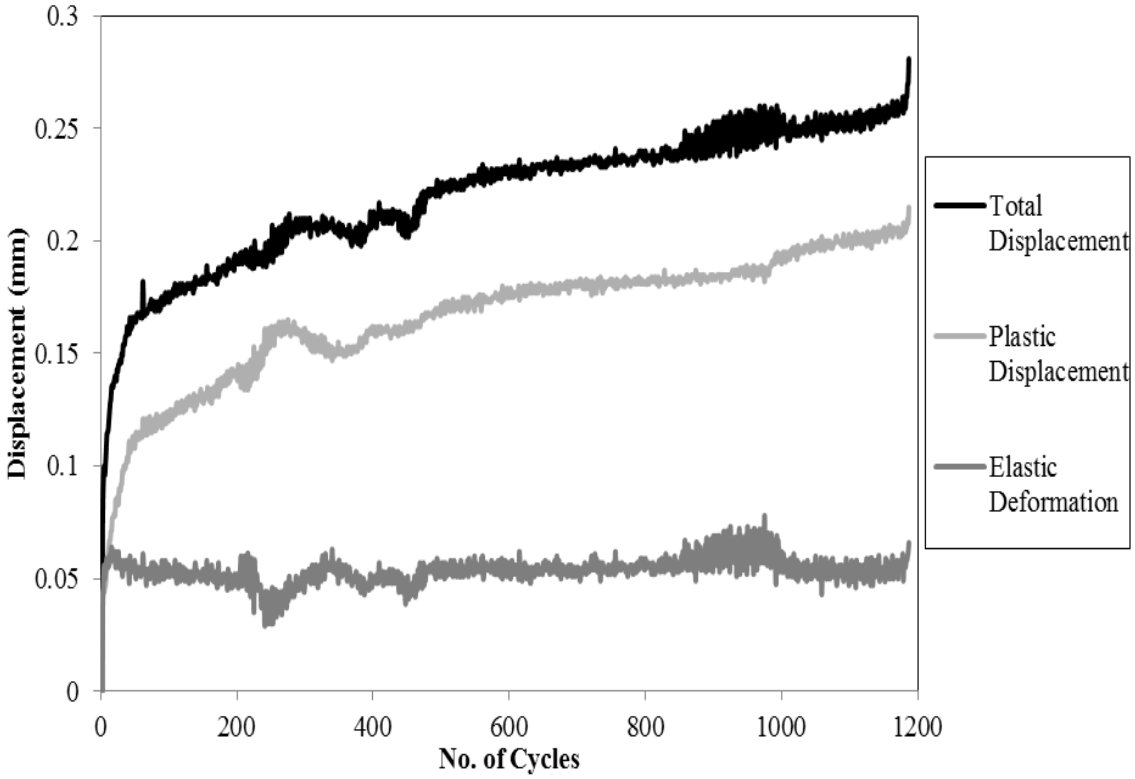

Figure C82. Displacement Variation v/s No. of Cycles in a Fatigue Test at 85% Stress Level [Sand-Cement (8%) Specimens (FT-2)]

Six beam specimens were tested for the silt-fly ash beam specimens (18% binder). Table C13 shows the summary of the fatigue test results on the silt-fly ash beam specimens. From the silt-fly ash specimen fatigue curves, we can see that the specimens ruptured shortly after the cycles to half the initial modulus was reached. Specimen FT-5 and FT-6 did not fail after 170,000 cycles, but 50% of initial modulus shows the fatigue life of the specimen to be around 2,069 and 2,783 cycles, respectively (Figure C83 and C84).

Table C13. Summary of the Fatigue Strength Test Results on Silt-Fly ash Specimens (Binder Content: 18%)

SN	SL (%)	IFM (MPa)	FFM (MPa)	PFME (%)	IS (με)	N
FT-1	80	-	-	-	-	2
FT-2	50	-	-	-	-	13
FT-3	50	-	-	-	-	17
FT-4	45	647	423	68	181	502
FT-5*	40	730	189	26	136	2,069**
FT-6*	40	619	202	33	186	2,783**

*SN = Specimen Number; SL = Stress Level; IFM = Initial Flexural Modulus; FFM = Final Flexural Modulus (i.e. Flexural Modulus at the end of Fatigue Test); PFME =Percent of Flexural Modulus at the End of Test; IS = Initial Strain; N = Number of Cycles at the End of Test (i.e. Fatigue Life); **Estimated value*

Note: *All specimens failed at 50% of IFM*

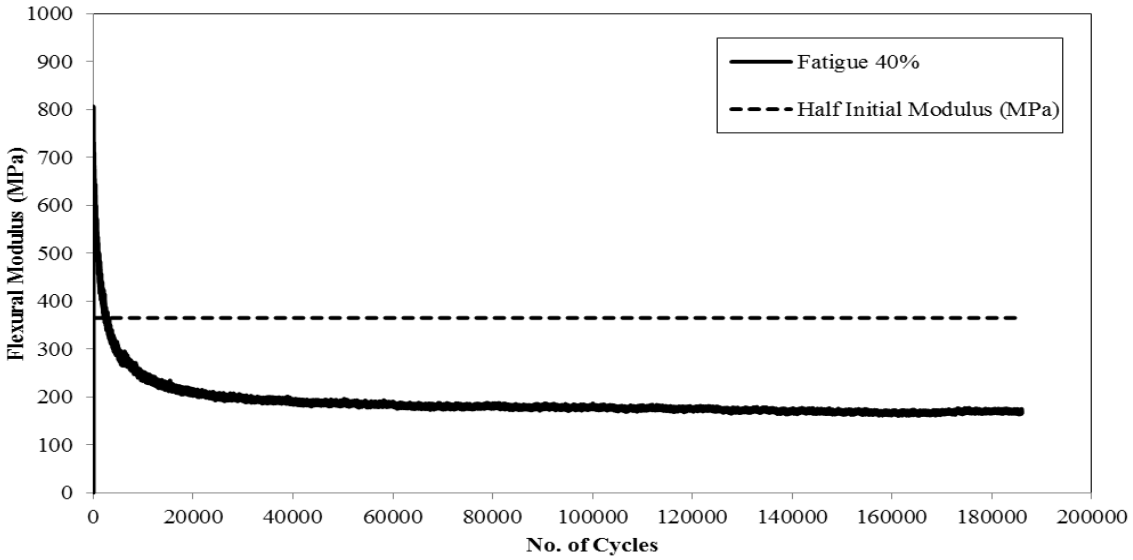

Figure C83. Typical Degradation of Flexural Modulus in a Fatigue Test at 40% Stress Level [Silt-Fly ash (18%) Specimens (FT-5)]

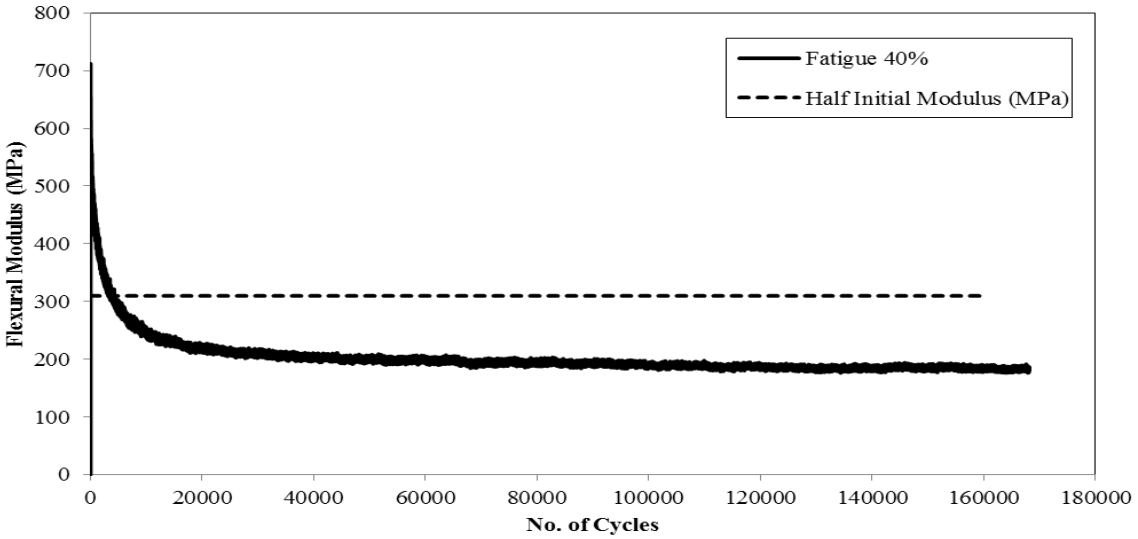

Figure C84. Typical Degradation of Flexural Modulus in a Fatigue Test at 40% Stress Level [Silt-Fly ash (18%) Specimens (FT-6)]

Figure C85 shows the flexural modulus degradation curve for specimen FT-4 for silt-fly ash specimens stabilized with 18% class C fly ash.

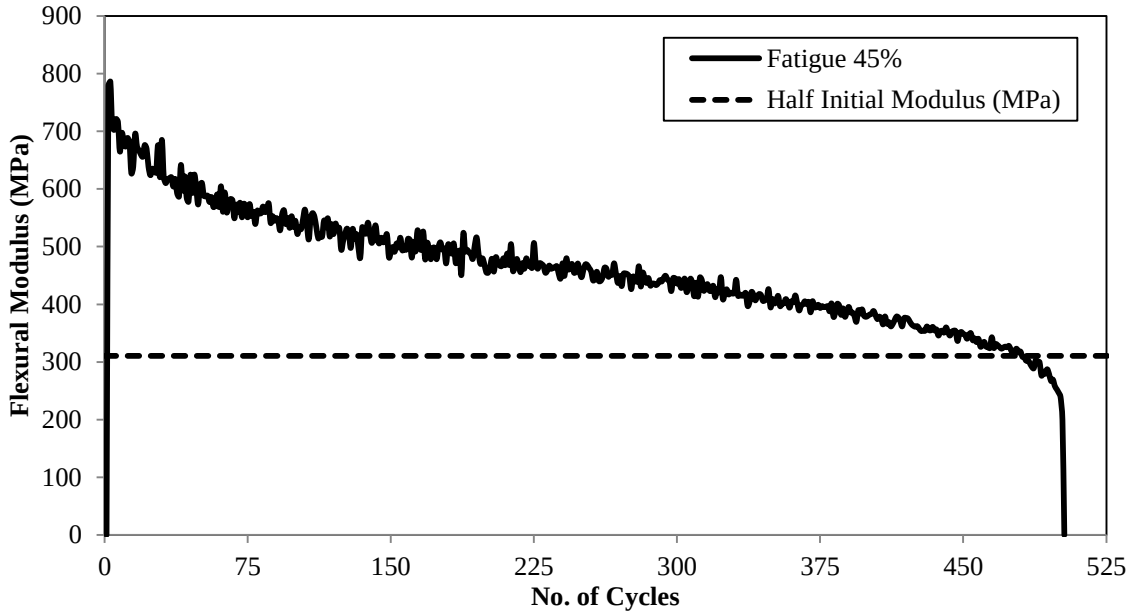

Figure C85. Typical Degradation of Flexural Modulus in a Fatigue Test at 45% Stress Level [Silt-Fly ash (18%) Specimens (FT-4)]

Figure C86 shows the displacement (total, plastic and elastic) variation curve for specimen FT-4 for silt-fly ash specimens stabilized with 18% class C fly ash.

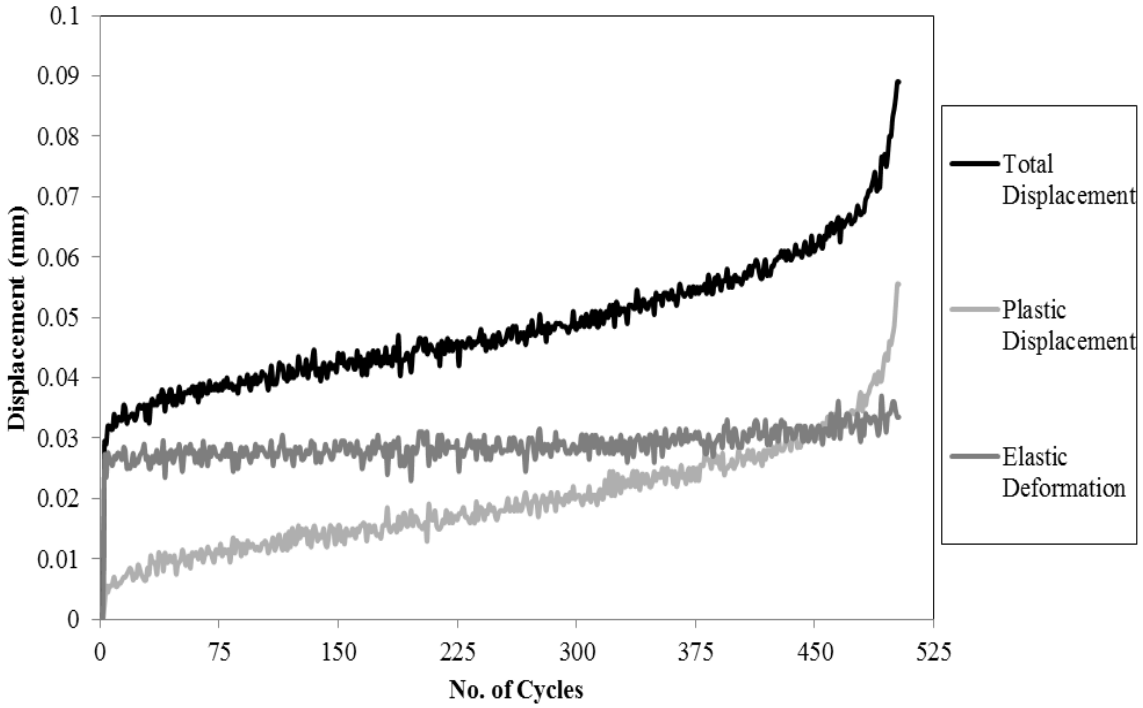

Figure C86. Displacement Variation v/s No. of Cycles in a Fatigue Test at 45% Stress Level [Silt-Fly ash (18%) Specimens (FT-4)]

APPENDIX – D: FATIGUE PERFORMANCE MODEL

This section shows the fatigue modeling for the different mixtures from our laboratory test data. This model is based on the stress ratio and the fatigue life. Figure D1 shows the relationship for clay-cement (12%) specimens. Figure D2 shows the relationship for gravel-cement (3%) specimens.

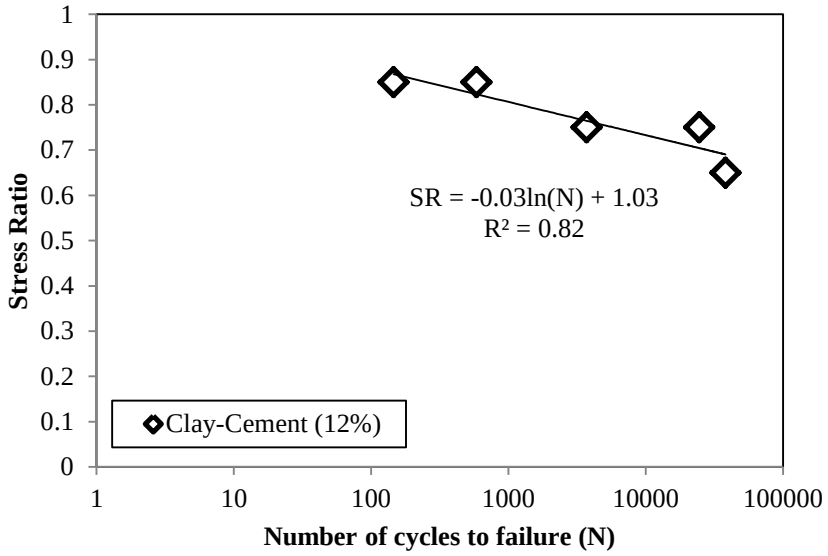

Figure D1. Fatigue Modelling for Clay-Cement (12%) Specimens

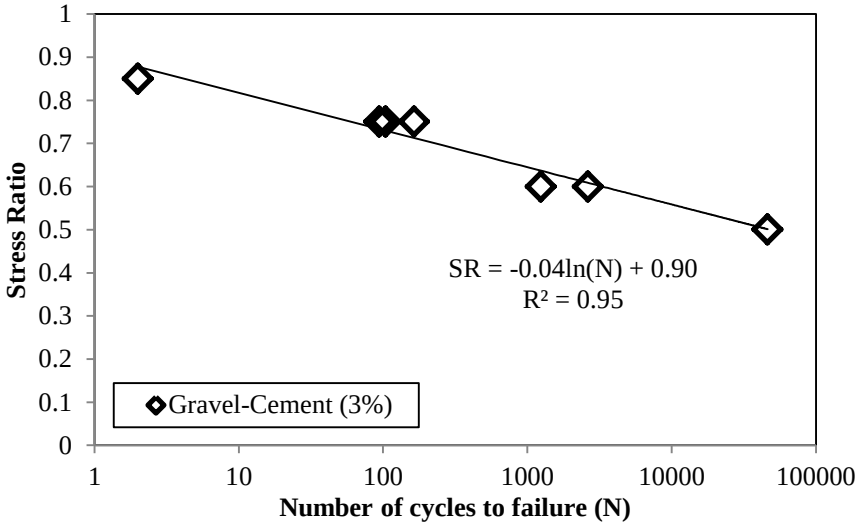

Figure D2. Fatigue Modelling for Gravel-Cement (3%) Specimens

Figure D3 shows the relationship for sand-cement (6%) specimens. Figure D4 shows the relationship for silt-cement (8%) specimens.

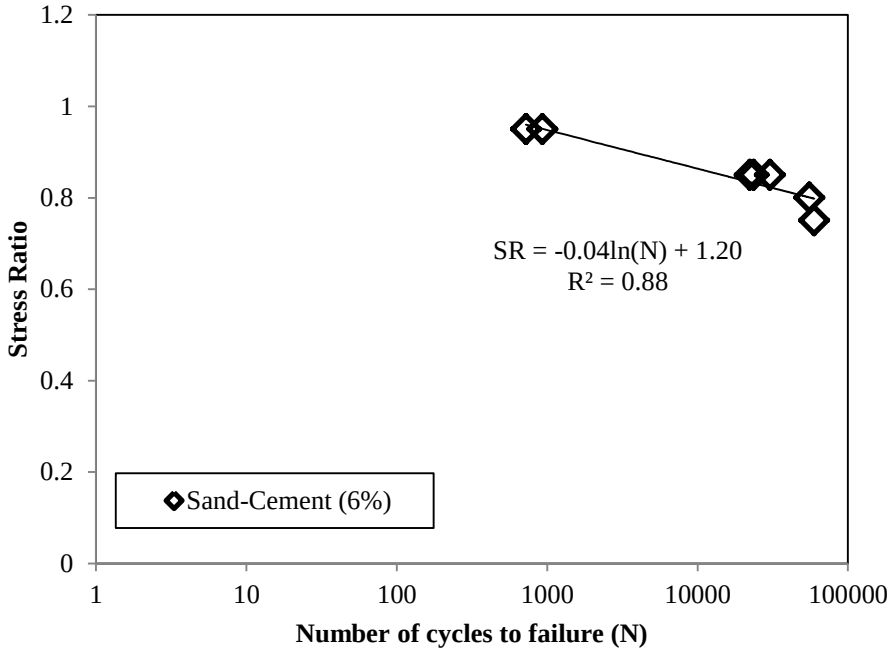

Figure D3. Fatigue Modelling for Sand-Cement (6%) Specimens

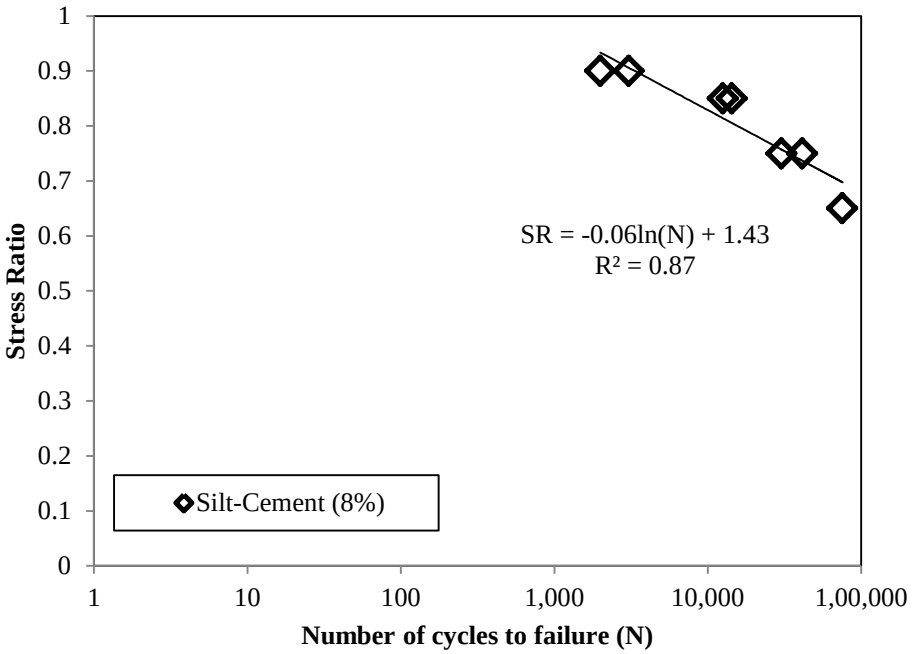

Figure D4. Fatigue Modelling for Silt-Cement (8%) Specimens

Figure D5 shows the relationship for sand-fly ash (13%) specimens. Figure D6 shows the relationship for silt-lime-fly ash (4/12%) specimens.

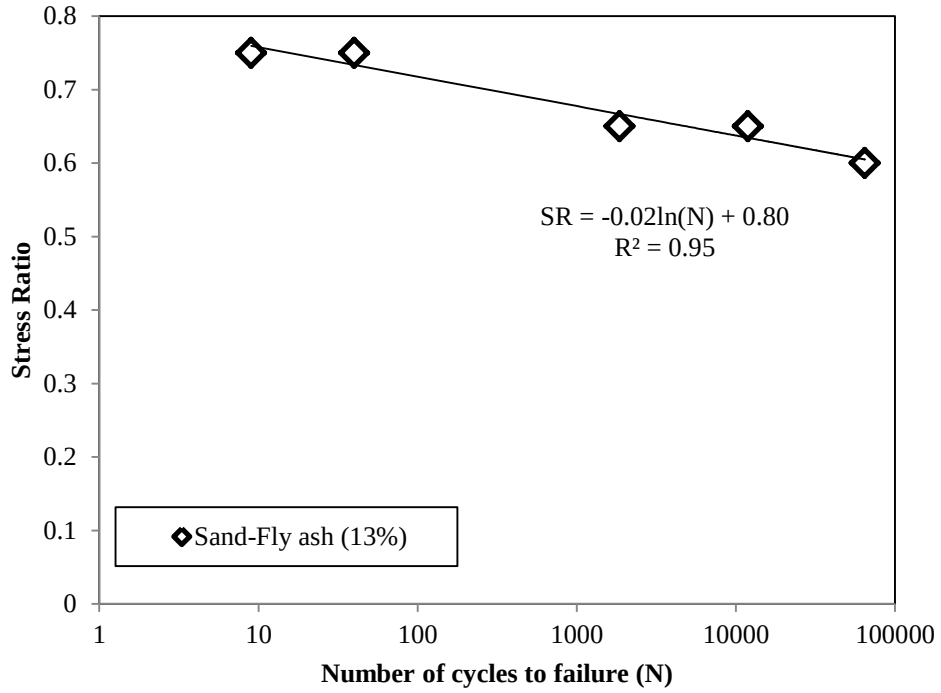

Figure D5. Fatigue Modelling for Sand-Fly ash (13%) Specimens

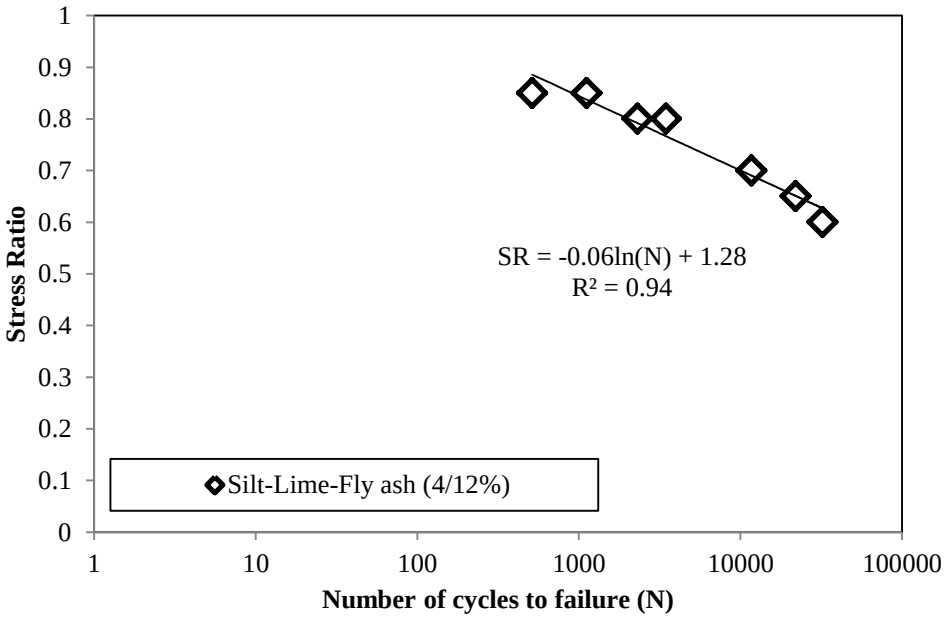

Figure D6. Fatigue Modelling for Silt-Lime-Fly ash (4/12%) Specimens

Figure D7 shows the relationship for clay-lime (6%) specimens. Figure D8 shows the relationship for gravel-cement (3%) specimens with 90% MDD.

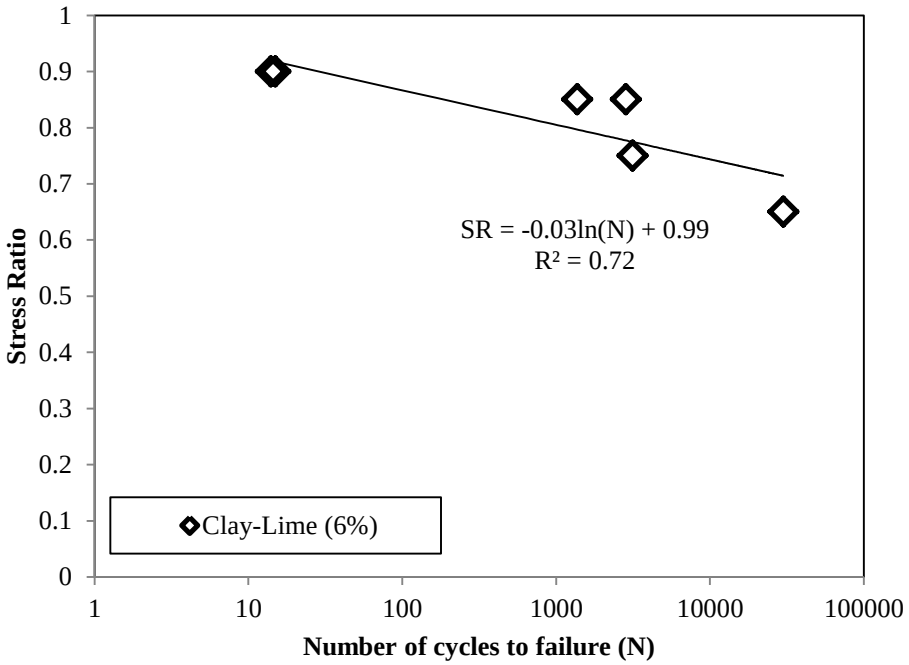

Figure D7. Fatigue Modelling for Clay-Lime (6%) Specimens

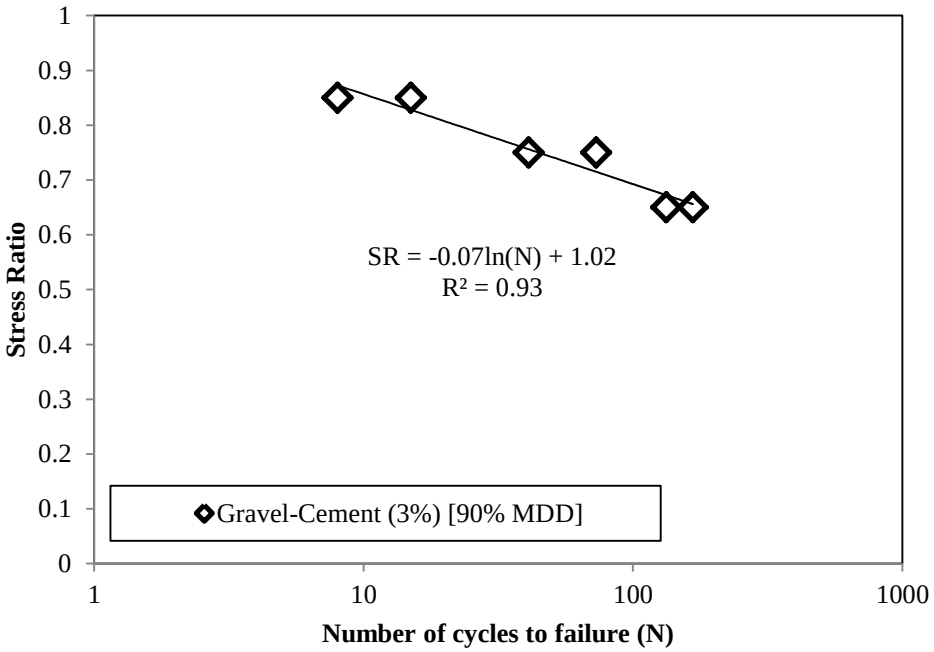

Figure D8. Fatigue Modelling for Gravel-Cement (3%) Specimens with 90% MDD

Figure D9 shows the relationship for silt-cement (8%) specimens with 90% MDD. Figure D10 shows the relationship for gravel-cement (5%) specimens.

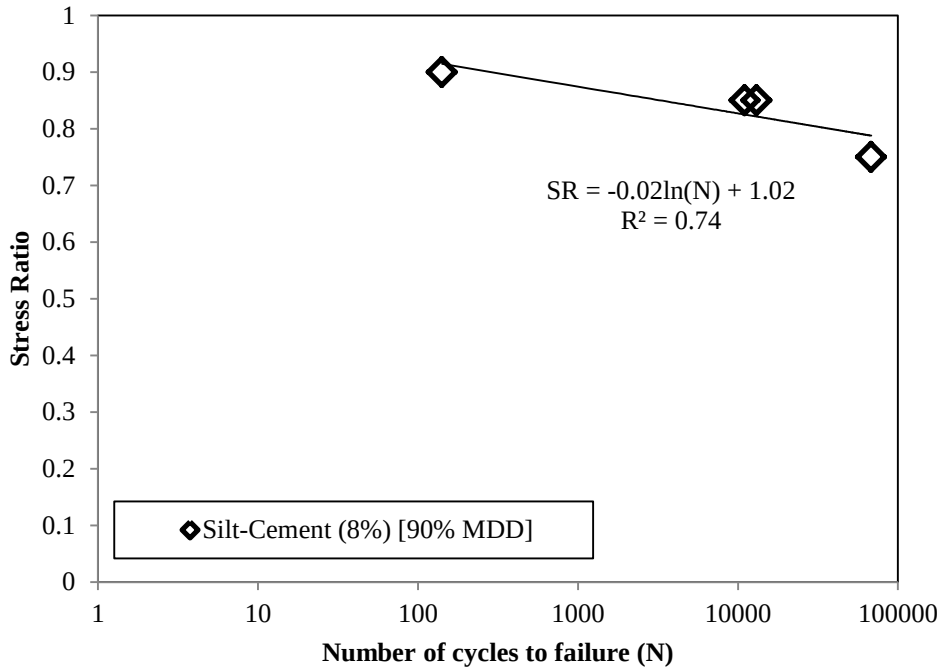

Figure D9. Fatigue Modelling for Silt-Cement (8%) Specimens with 90% MDD

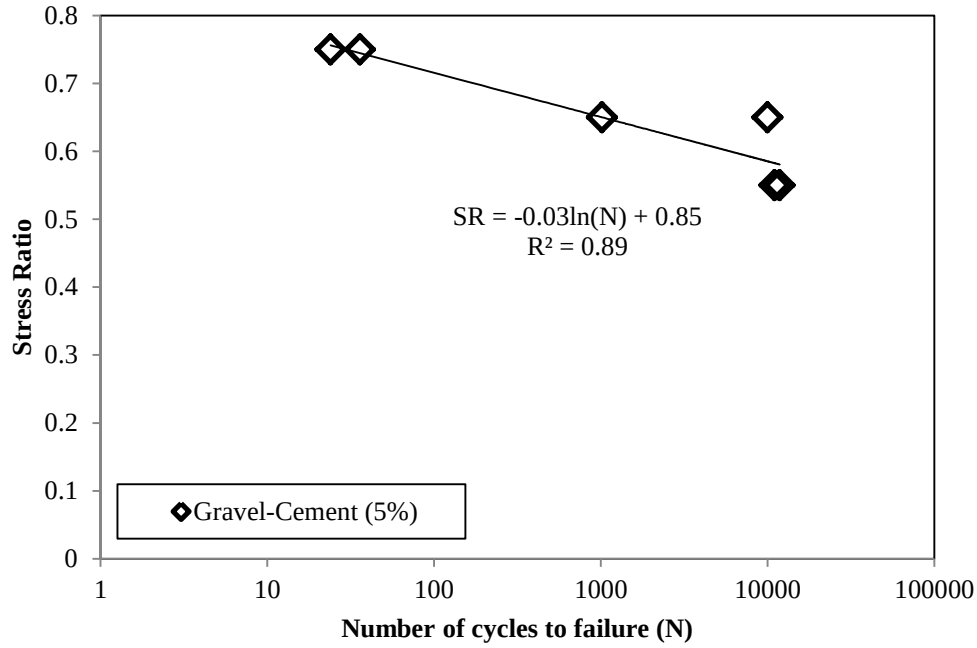

Figure D10. Fatigue Modelling for Gravel-Cement (5%) Specimens

Figure D11 shows the relationship for sand-cement (8%) specimens. Figure D12 shows the relationship for silt-fly ash (18%) specimens.

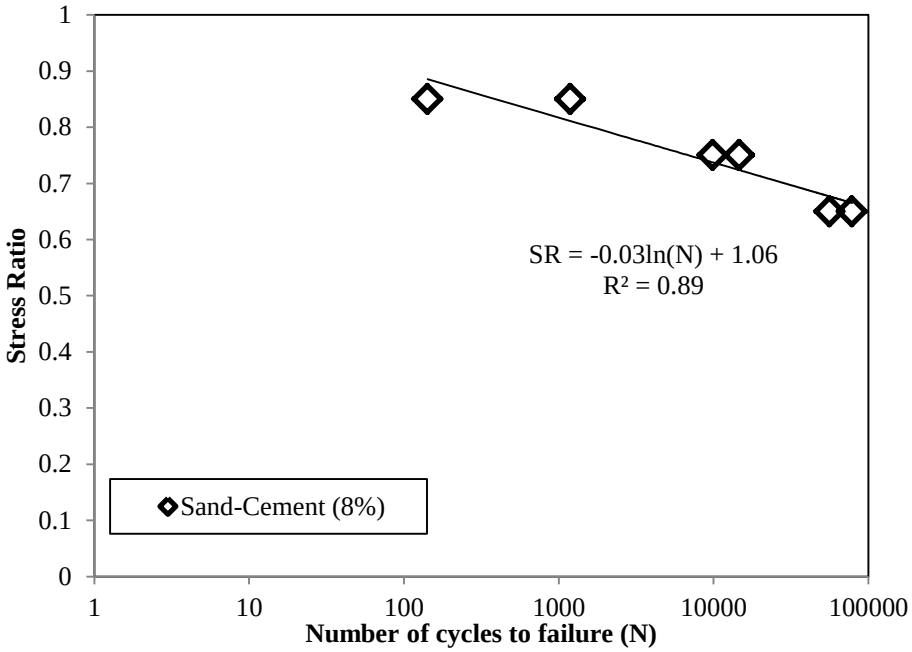

Figure D11. Fatigue Modelling for Sand-Cement (8%) Specimens

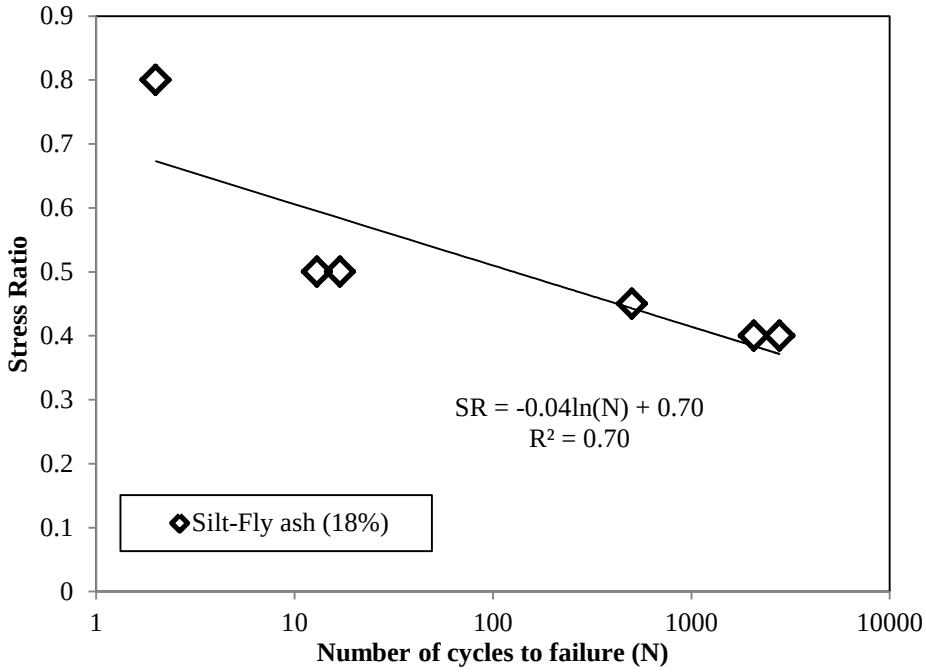

Figure D12. Fatigue Modelling for Silt-Fly ash (18%) Specimens

D.1. VALIDATION OF FATIGUE PERFORMANCE MODEL USING CONCRETE MODELS

Figure D13 shows the fatigue model validation for clay-cement (12%) specimens using the concrete models.

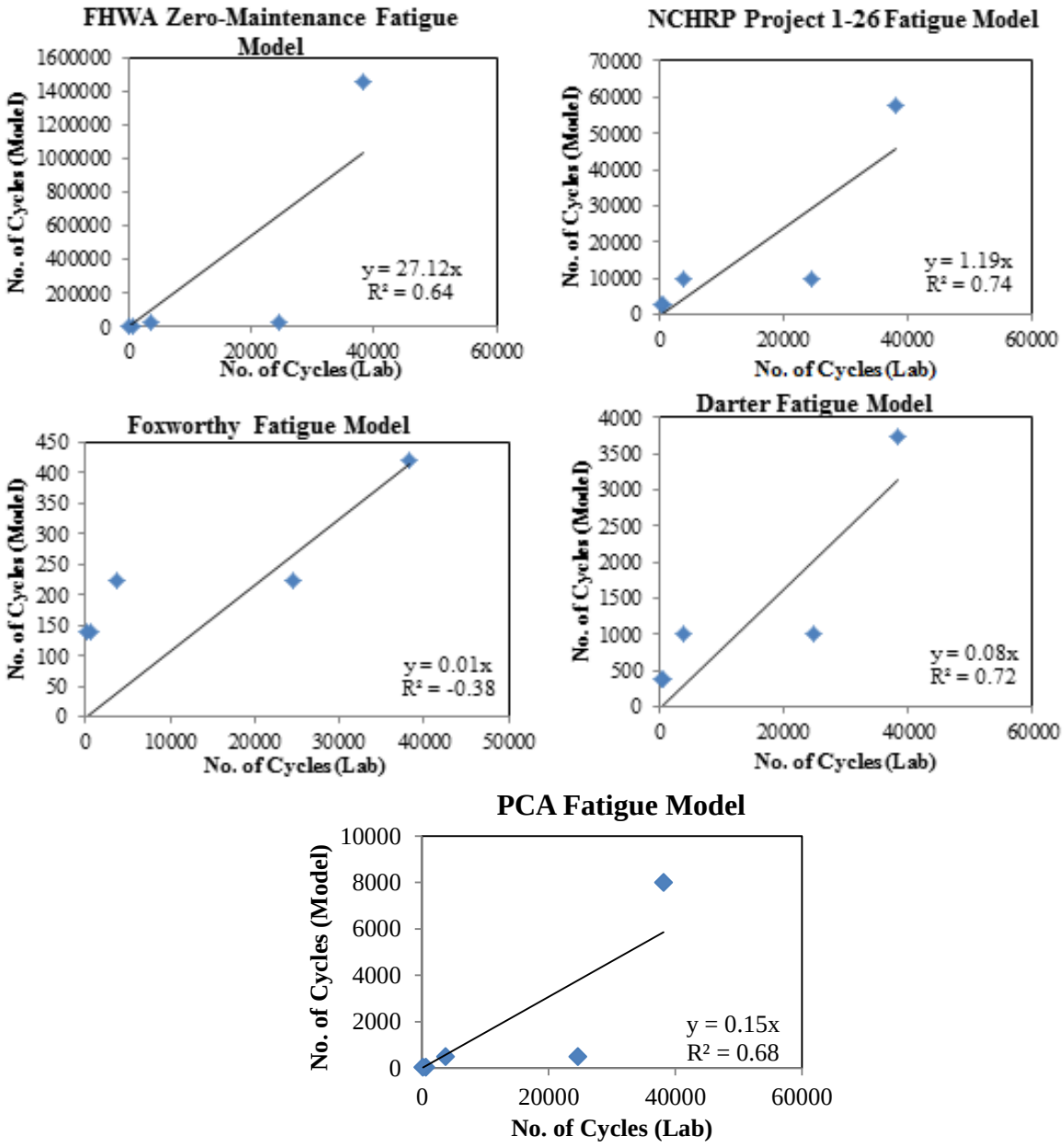

Figure D13. Validation of Clay-Cement (12%) Specimens Using Concrete Models

Figure D14 shows the fatigue model validation for gravel-cement (3%) specimens using the concrete models.

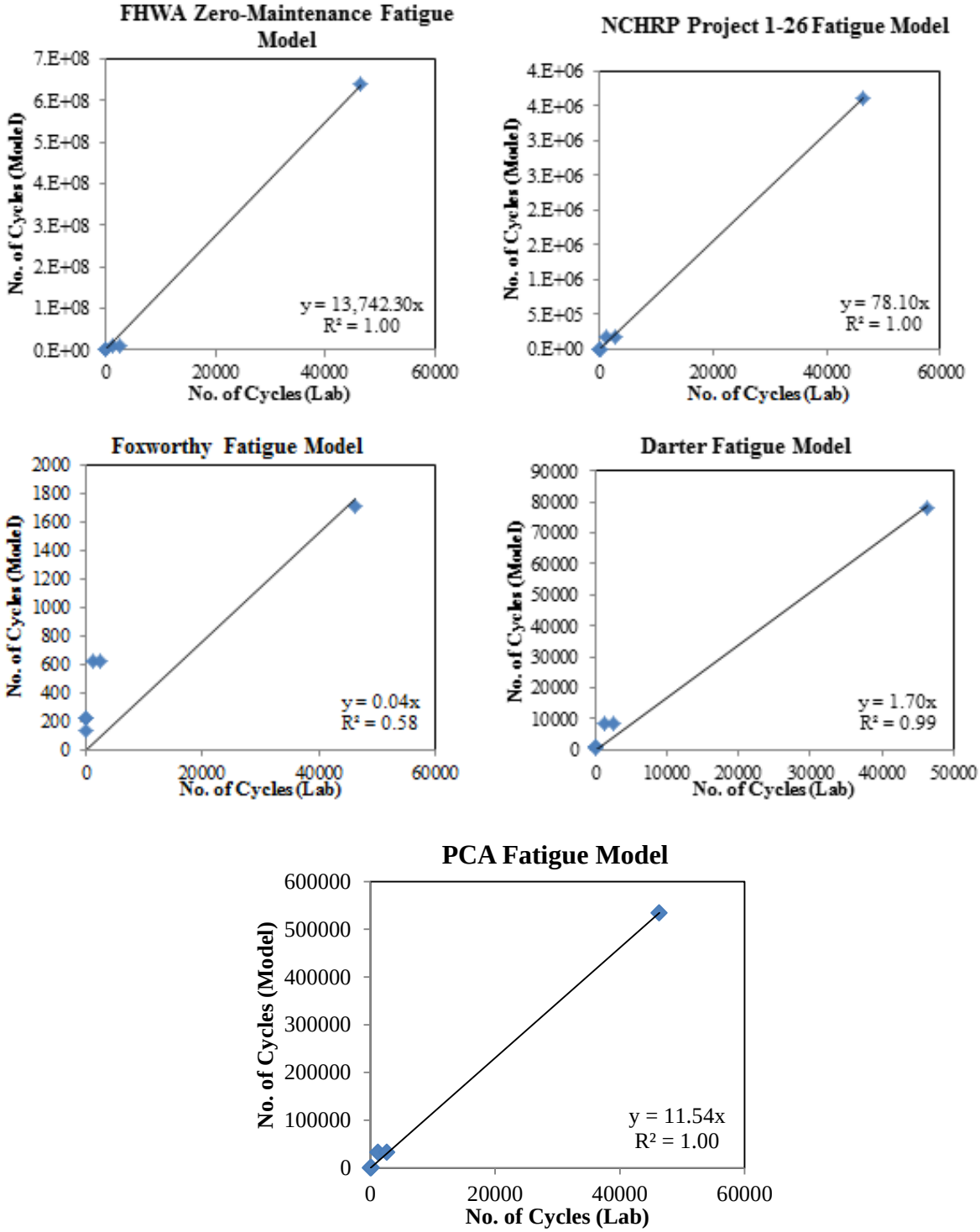

Figure D14. Validation of Gravel-Cement (3%) Specimens Using Concrete Models

Figure D15 shows the fatigue model validation for sand-cement (6%) specimens using the concrete models.

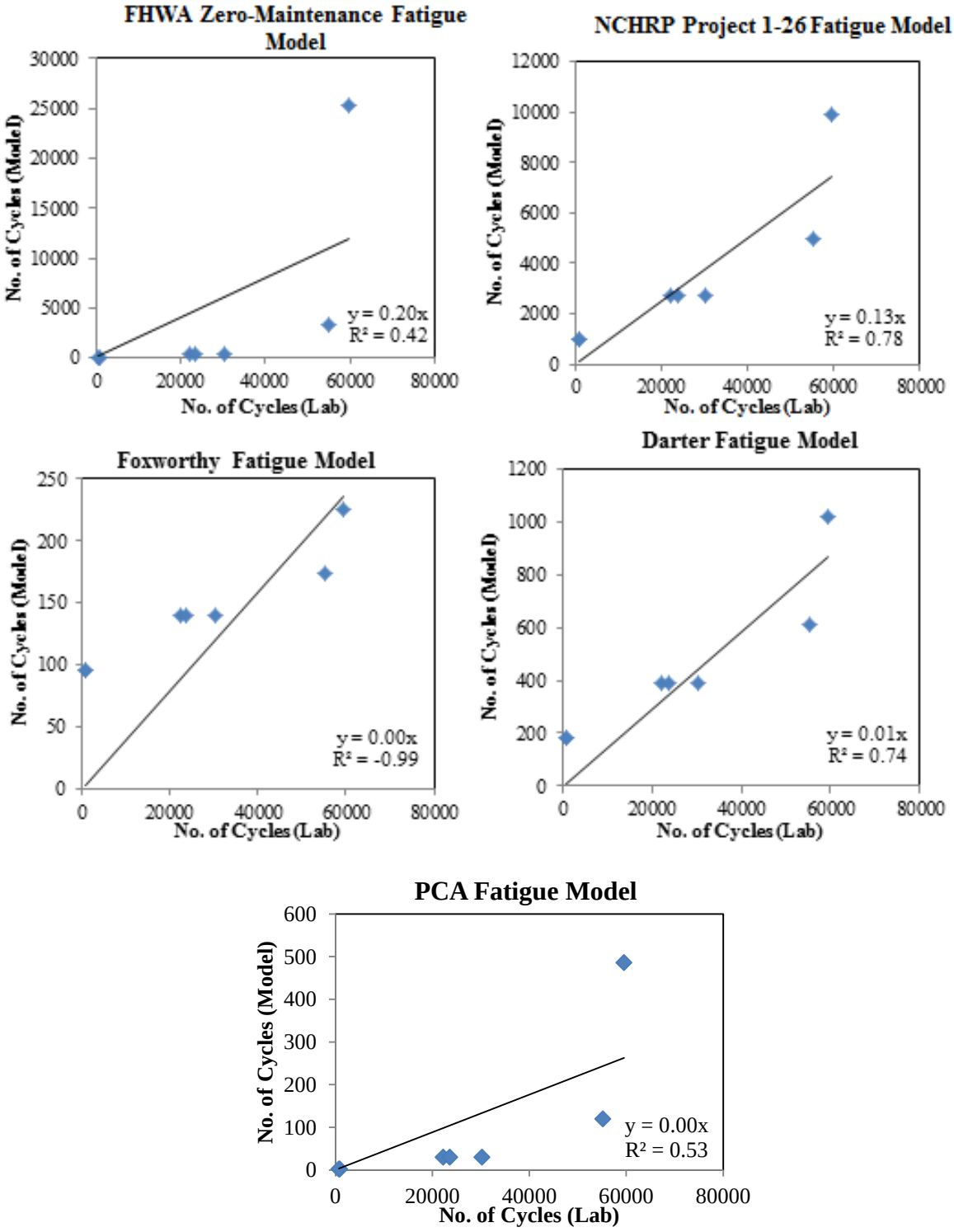

Figure D15. Validation of Sand-Cement (6%) Specimens Using Concrete Models

Figure D16 shows the fatigue model validation for silt-cement (8%) specimens using the concrete models.

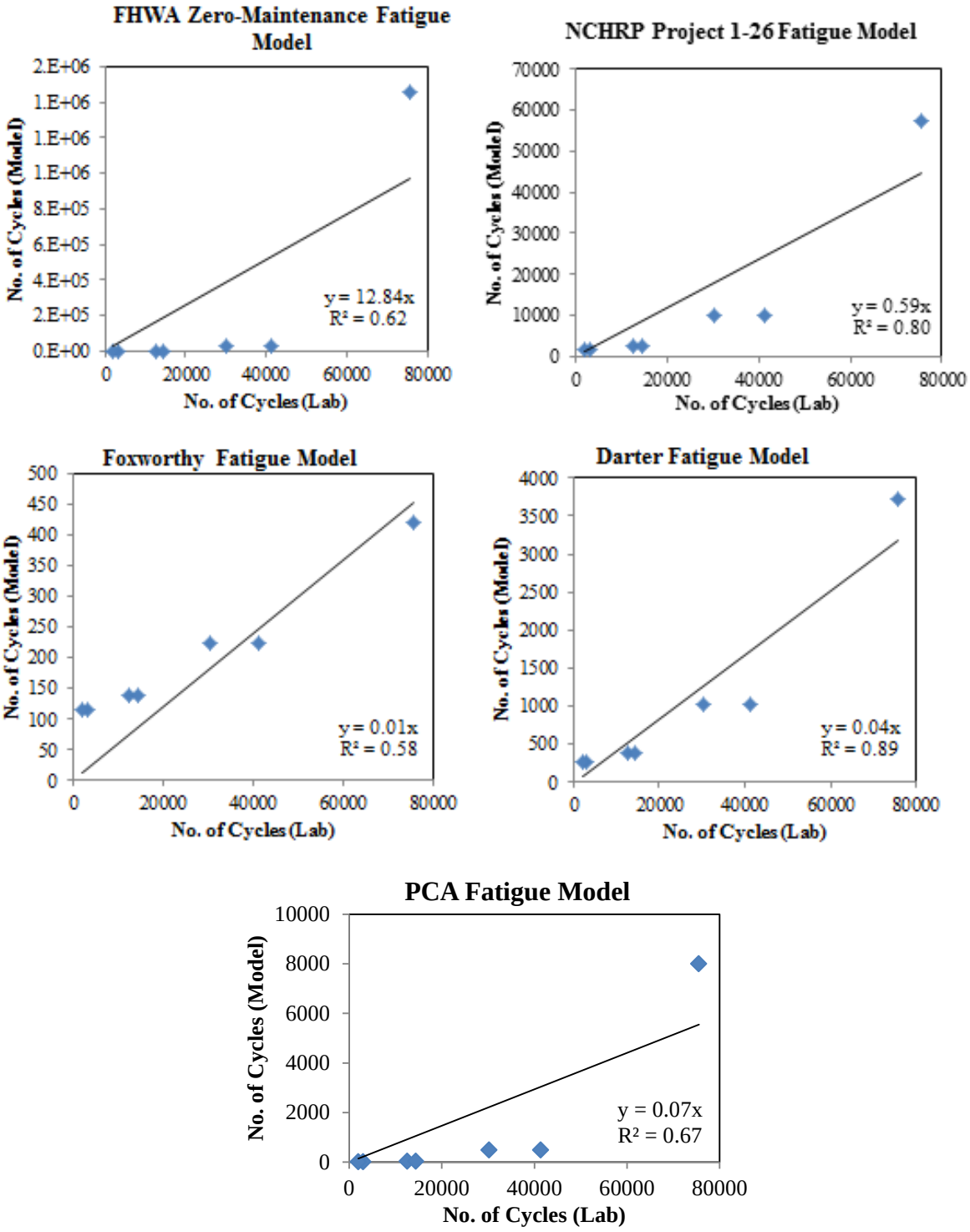

Figure D16. Validation of Silt-Cement (8%) Specimens Using Concrete Models

Figure D17 shows the fatigue model validation for sand-fly ash (13%) specimens using the concrete models.

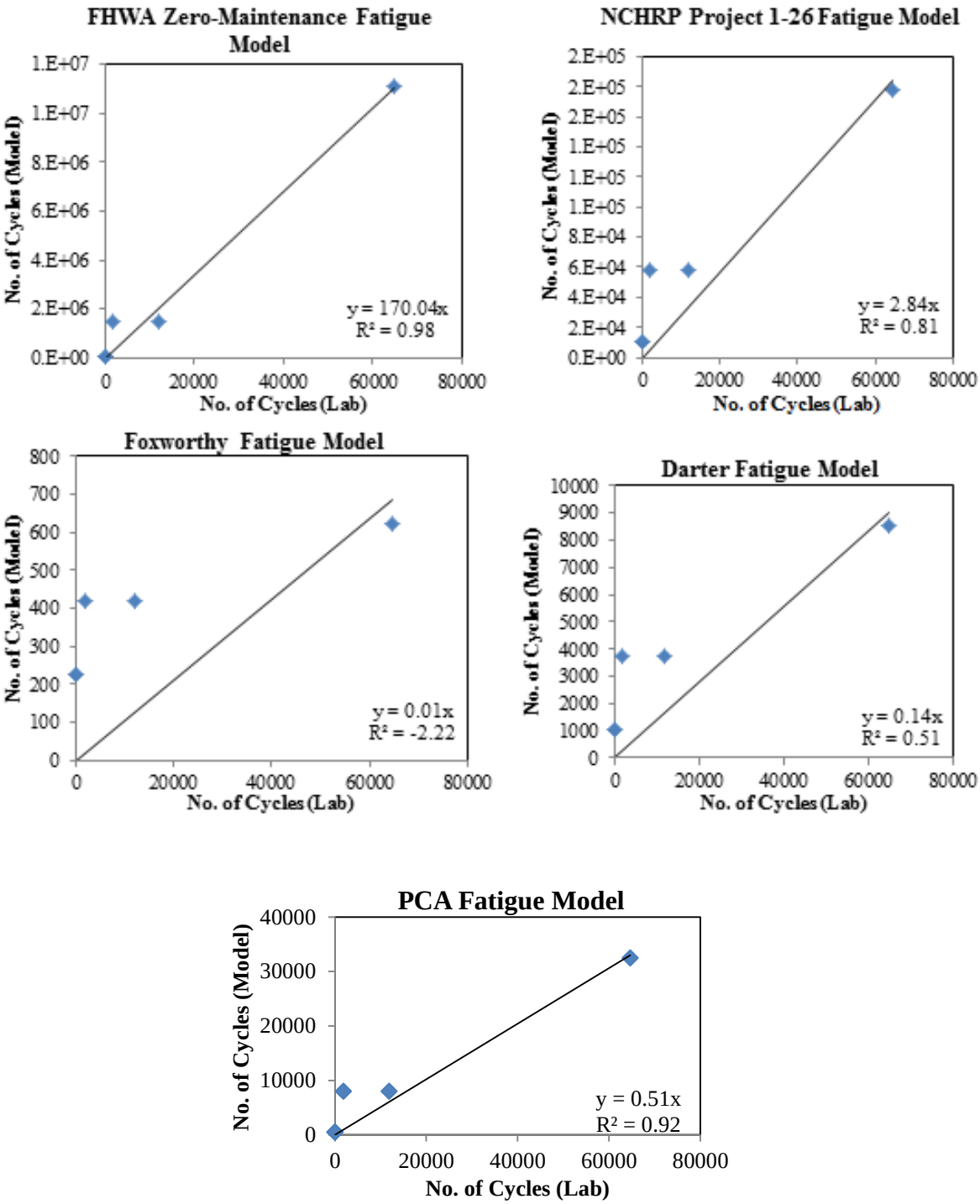

Figure D17. Validation of Sand-Fly ash (13%) Specimens Using Concrete Models

Figure D18 shows the fatigue model validation for silt-lime-fly ash (4/12%) specimens using the concrete models.

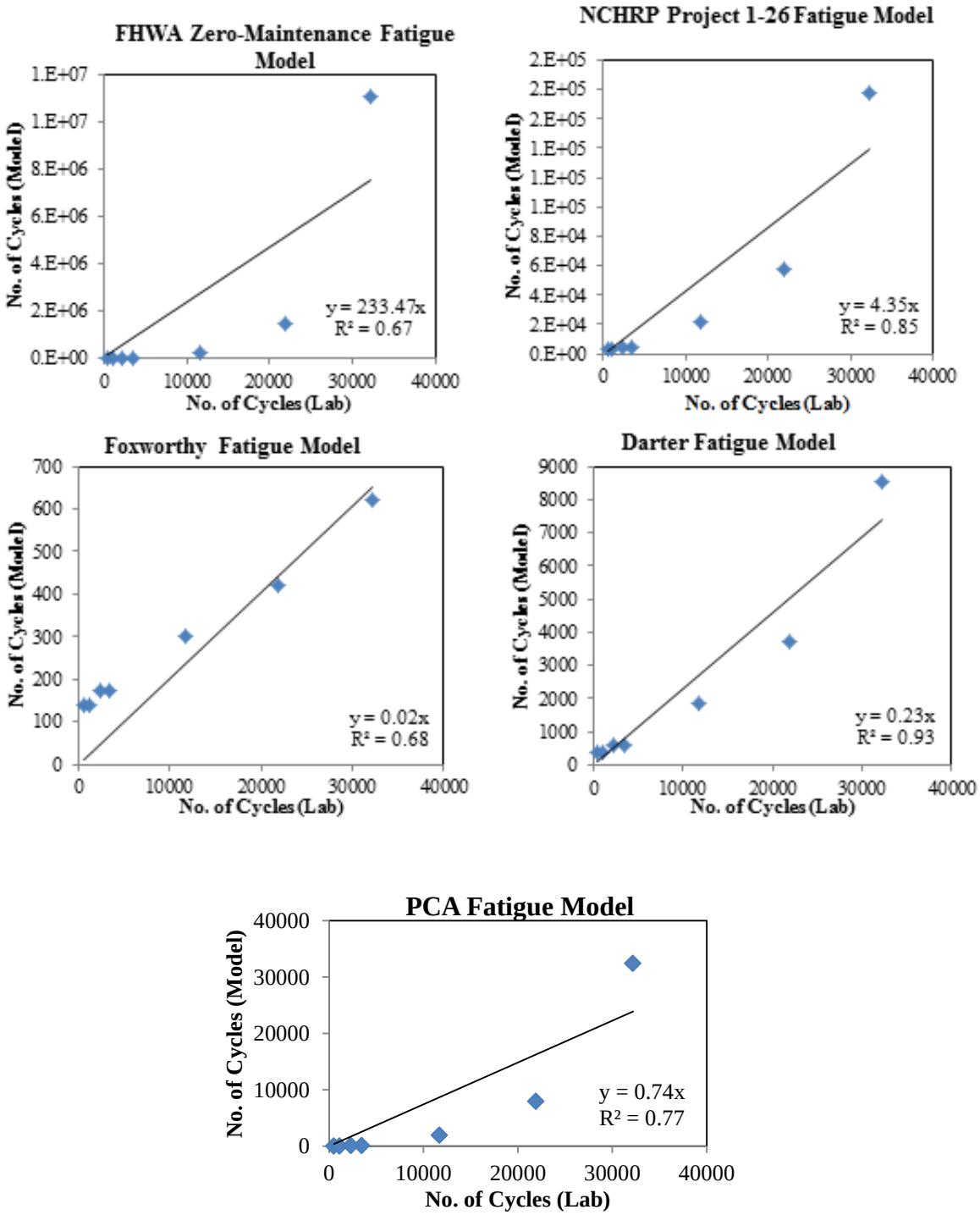

Figure D18. Validation of Silt-Lime-Fly ash (4/12%) Specimens Using Concrete Models

Figure D19 shows the fatigue model validation for clay-lime (6%) specimens using the concrete models.

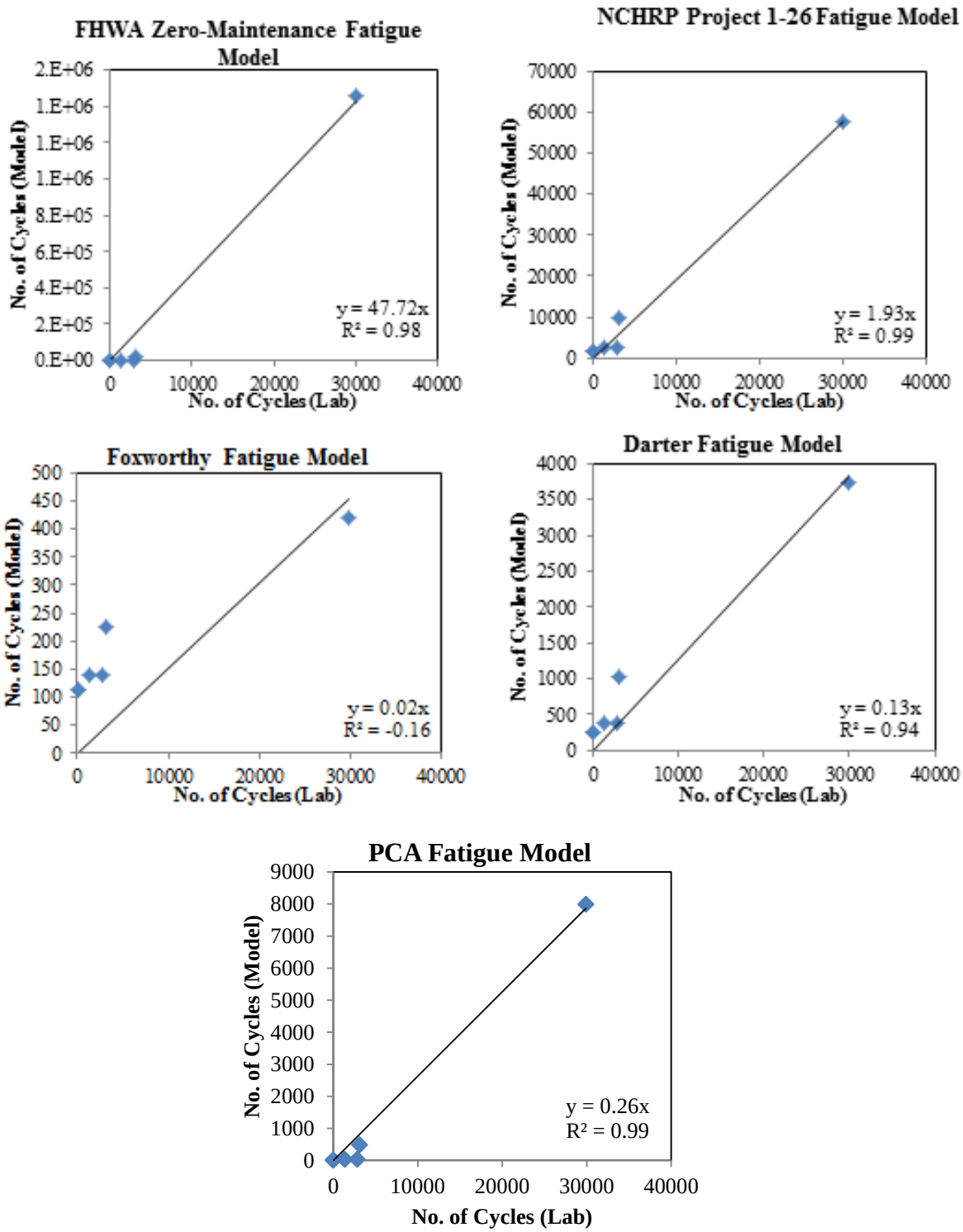

Figure D19. Validation of Clay-Lime (6%) Specimens Using Concrete Models

Figure D20 shows the fatigue model validation for gravel-cement (3%, 90% MDD) specimens using the concrete models.

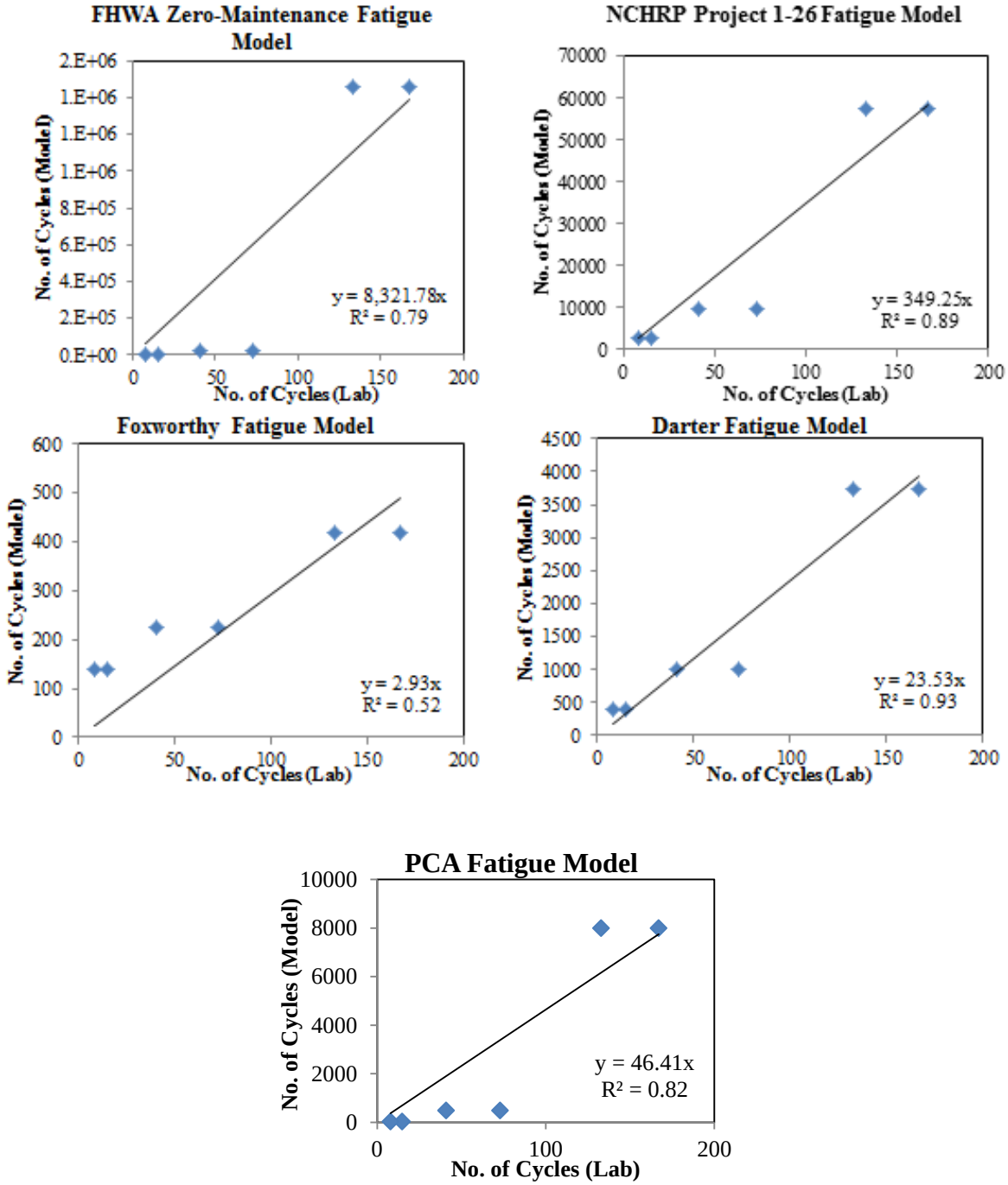

Figure D20. Validation of Gravel-Cement (3%, 90% MDD) Specimens Using Concrete Models

Figure D21 shows the fatigue model validation for silt-cement (8%, 90% MDD) specimens using the concrete models.

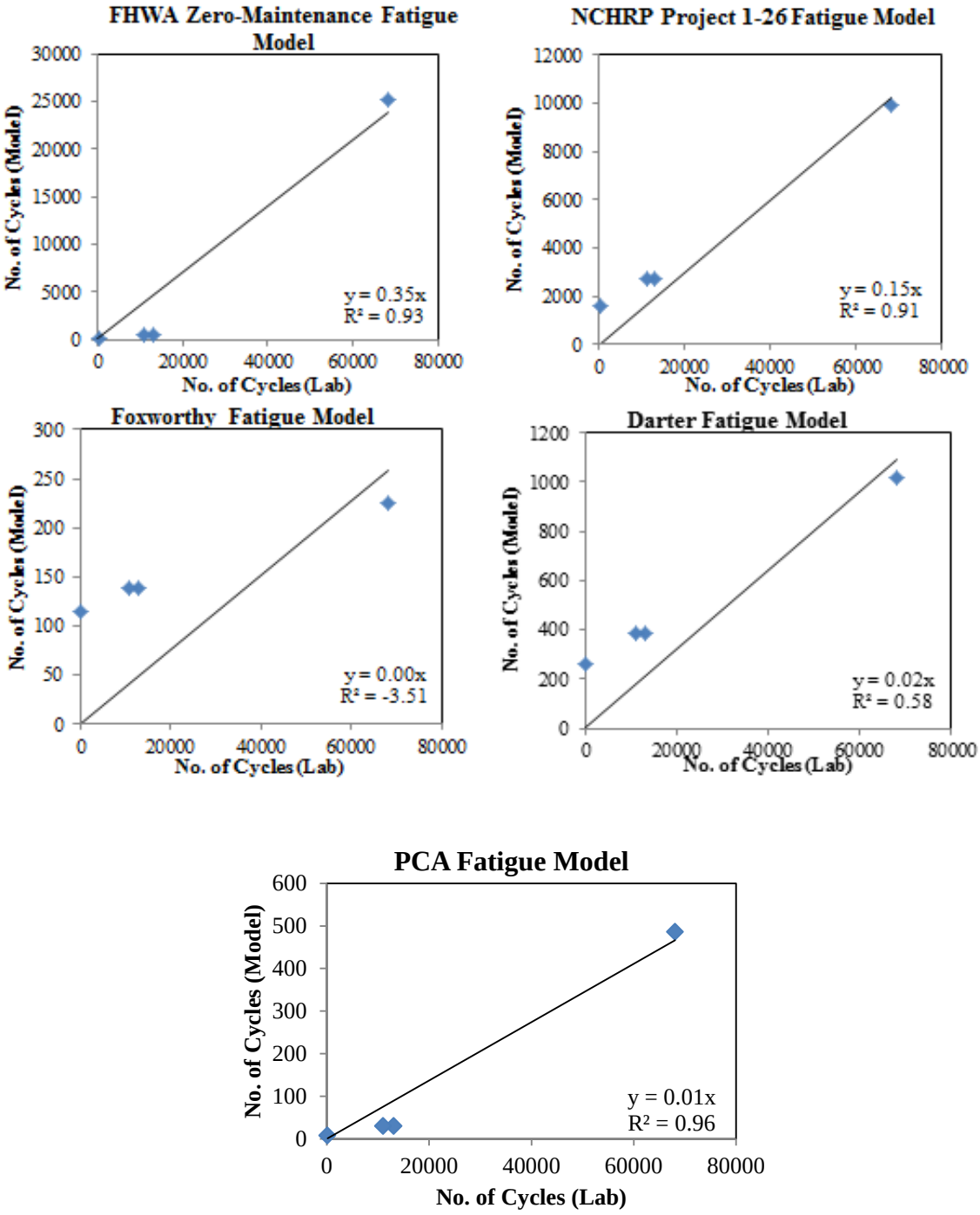

Figure D21. Validation of Silt-Cement (8%, 90% MDD) Specimens Using Concrete Models

Figure D22 shows the fatigue model validation for gravel-cement (5%) specimens using the concrete models.

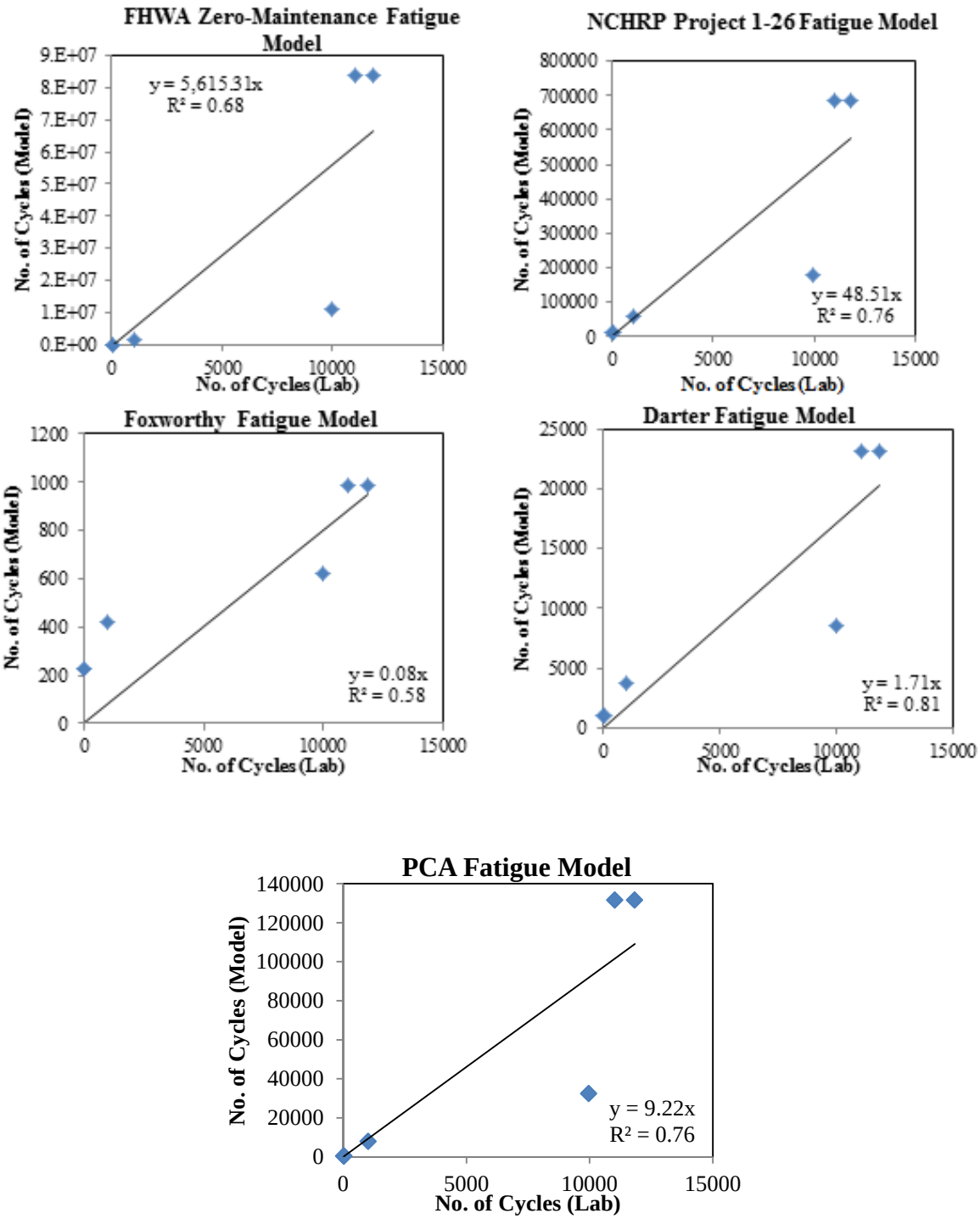

Figure D22. Validation of Gravel-Cement (5%) Specimens Using Concrete Models

Figure D23 shows the fatigue model validation for sand-cement (8%) specimens using the concrete models.

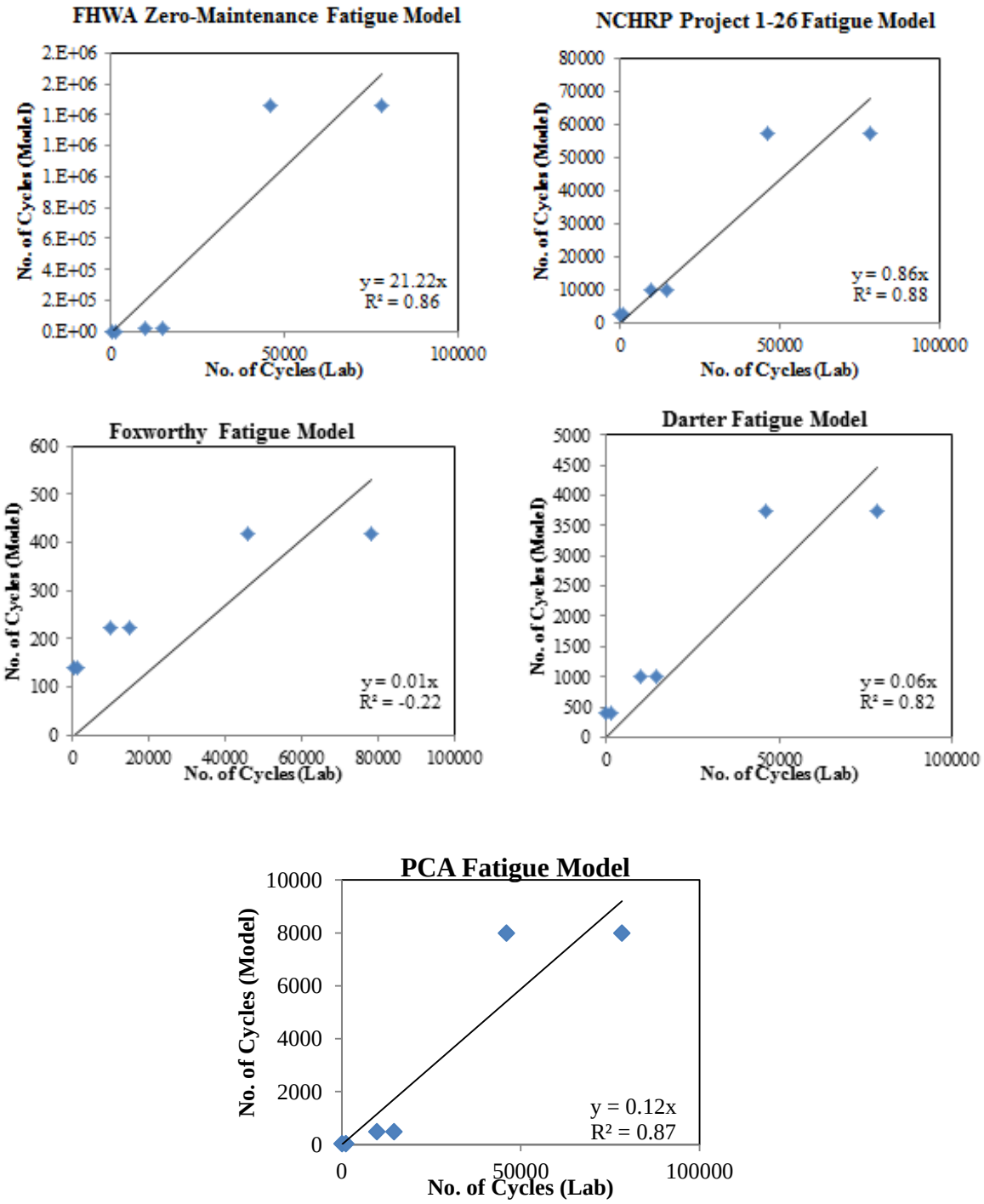

Figure D23. Validation of Sand-Cement (8%) Specimens Using Concrete Models

Figure D24 shows the fatigue model validation for silt-fly ash (18%) specimens using the concrete models.

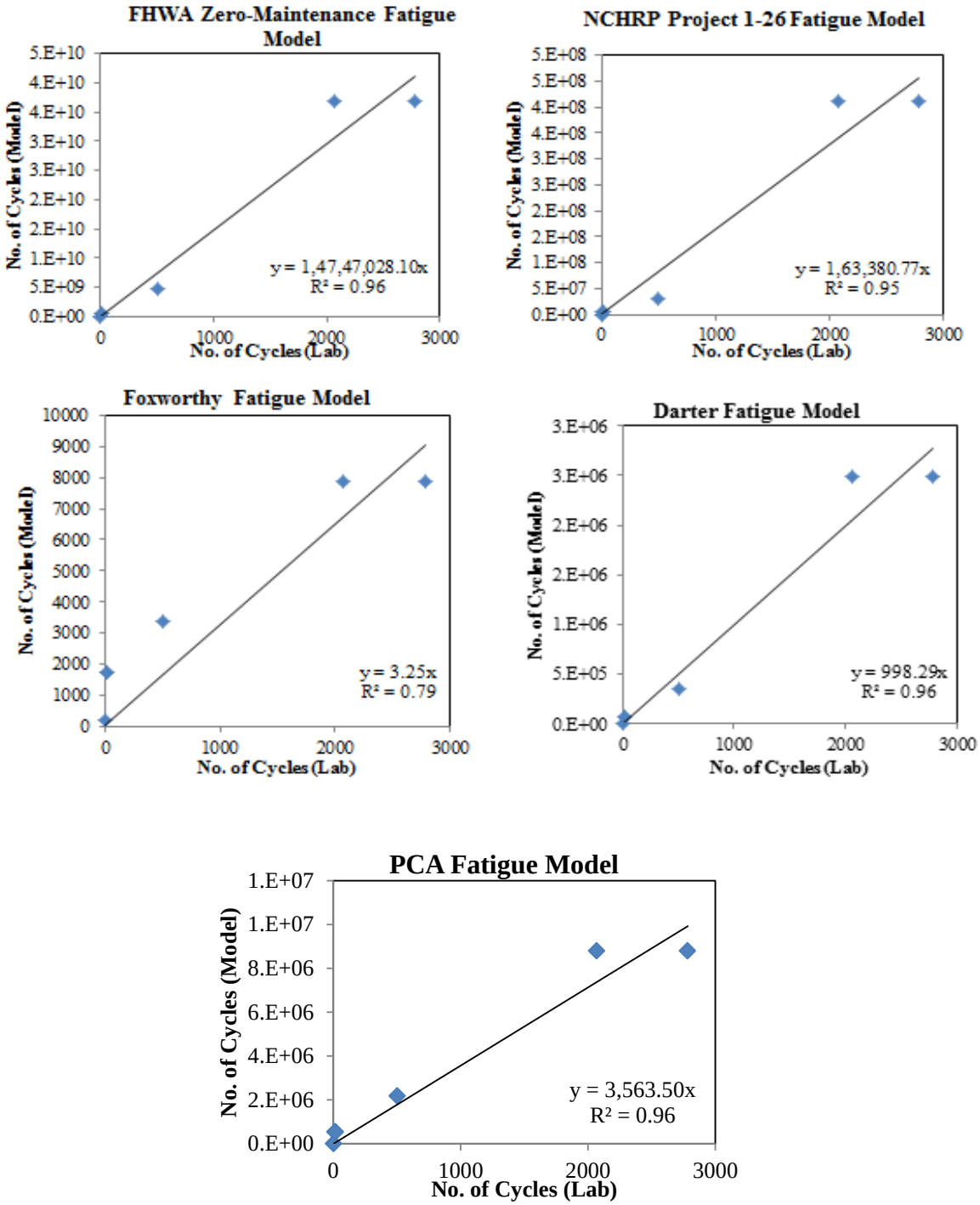

Figure D24. Validation of Silt-Fly ash (18%) Specimens Using Concrete Models

D.2. VALIDATION OF FATIGUE PERFORMANCE MODEL USING MEPDG MODEL

Figure D25 shows the fatigue model validation for cement stabilized specimens using the MEPDG model.

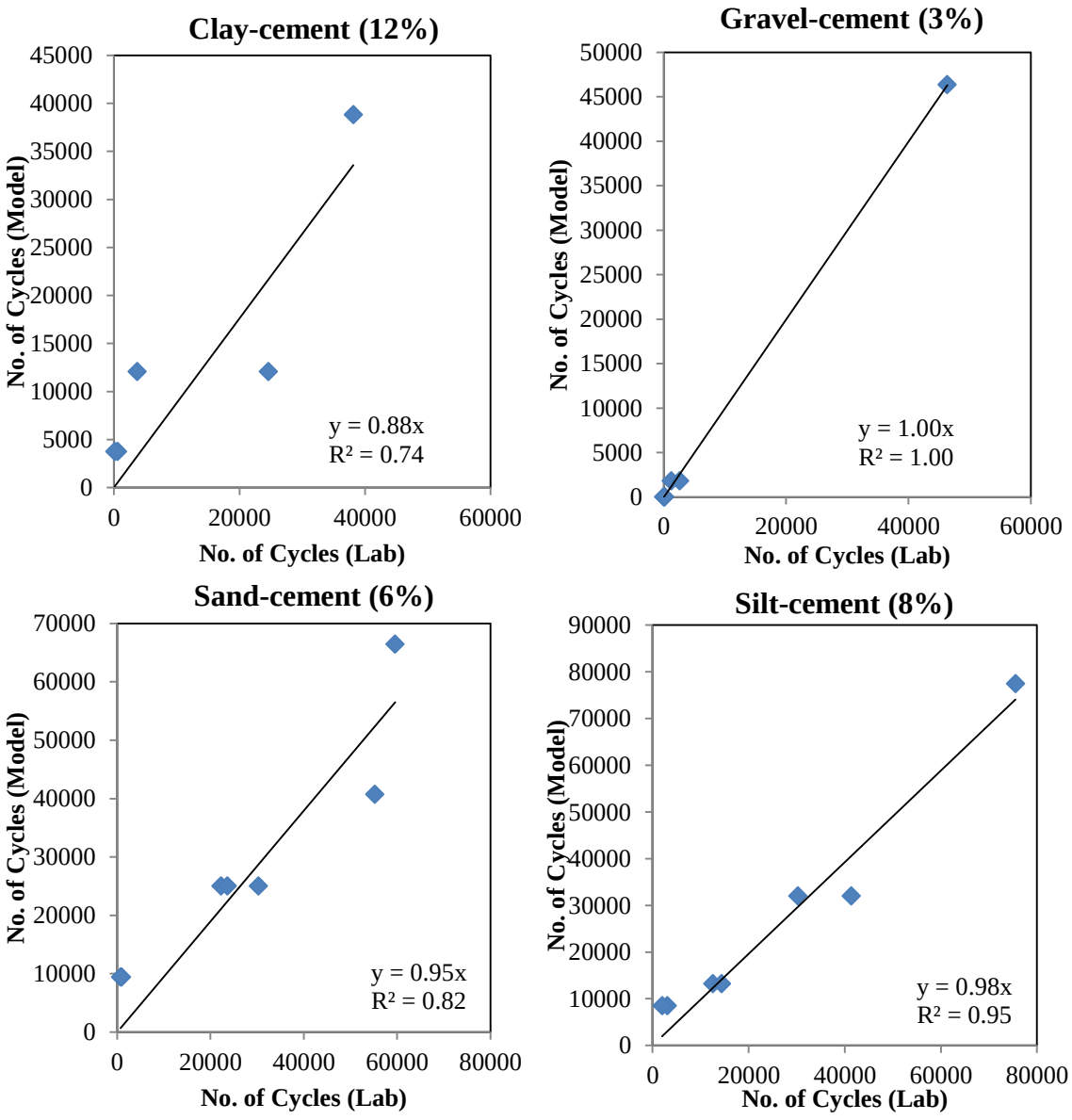

Figure D25. Validation of Cement Stabilized Specimens Using MEPDG Model

Figure D26 shows the fatigue model validation for fly ash and lime stabilized specimens using the MEPDG model.

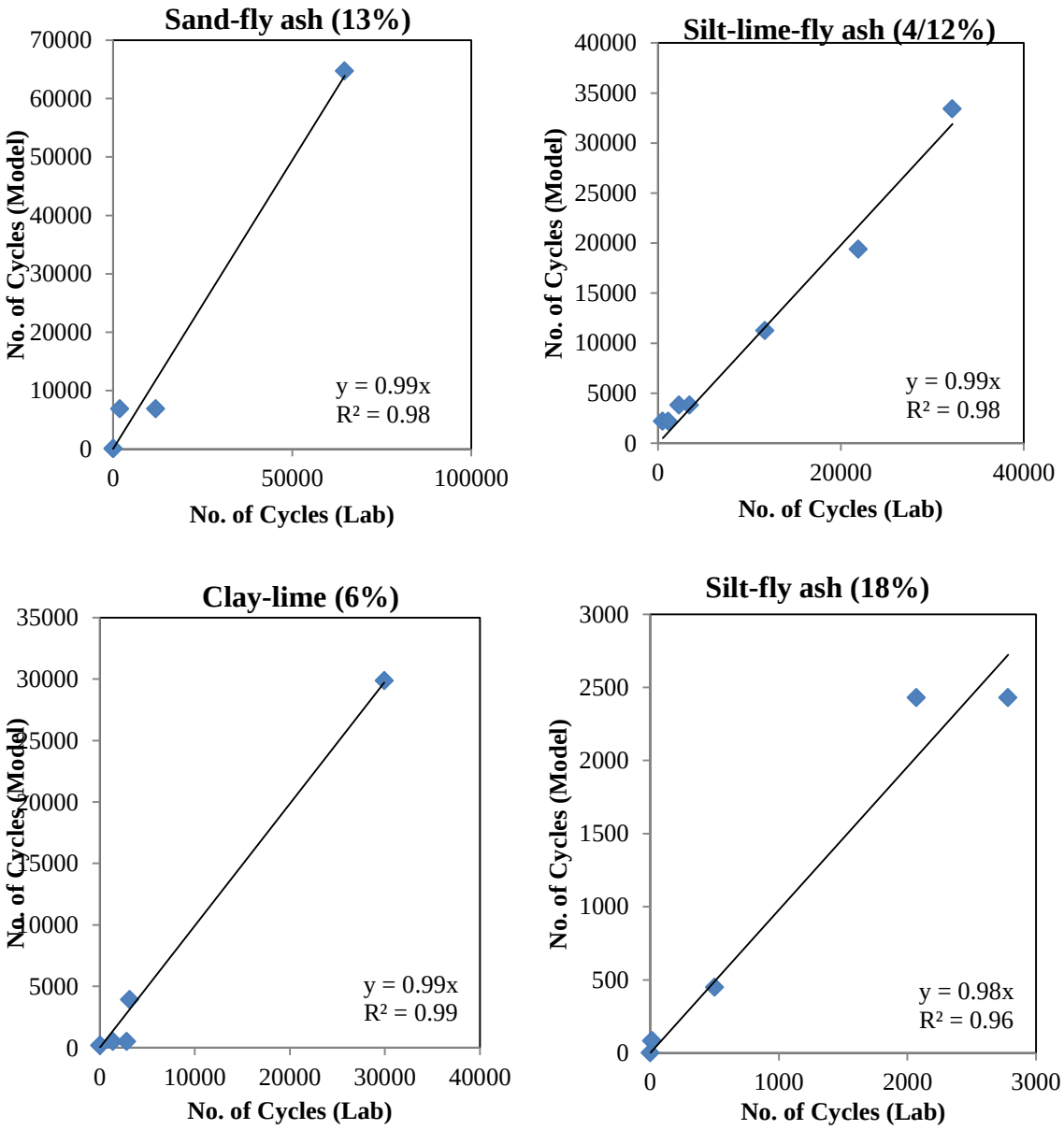

Figure D26. Validation of Fly ash and Lime Stabilized Specimens Using MEPDG Model

Figure D27 shows the fatigue model validation for gravel-cement and silt-cement specimens with reduced density using the MEPDG model. Figure D28 shows the fatigue model validation for gravel-cement and sand-cement specimens with higher binder content using the MEPDG model.

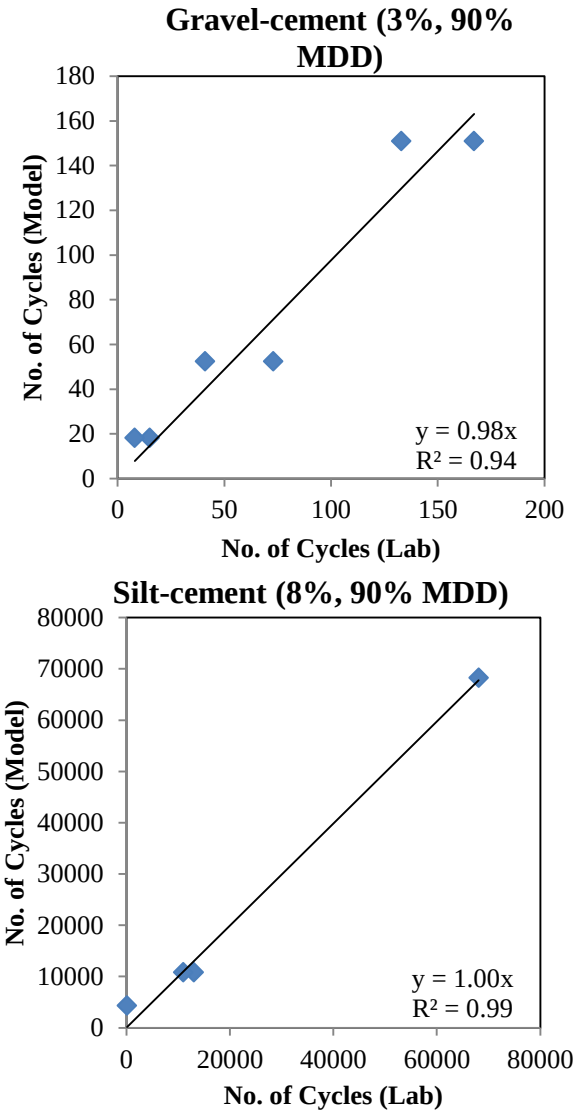

Figure D27. Validation of Reduced Density Specimens Using MEPDG Model

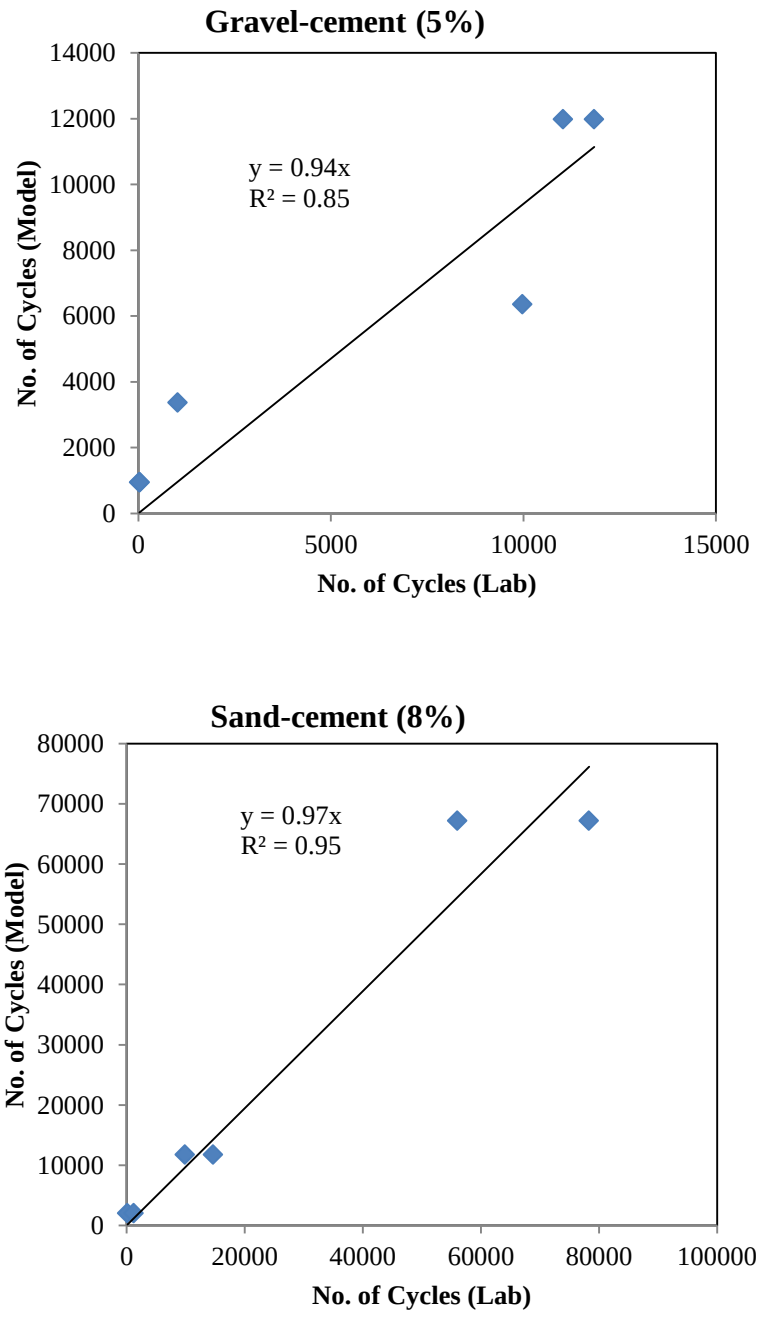

Figure D28. Validation of Higher Binder Content Specimens Using MEPDG Model

D.3. VALIDATION OF FATIGUE PERFORMANCE MODEL USING STRAIN BASED MODELS

Figure D29 to D31 shows the fatigue model validation for strain based models.

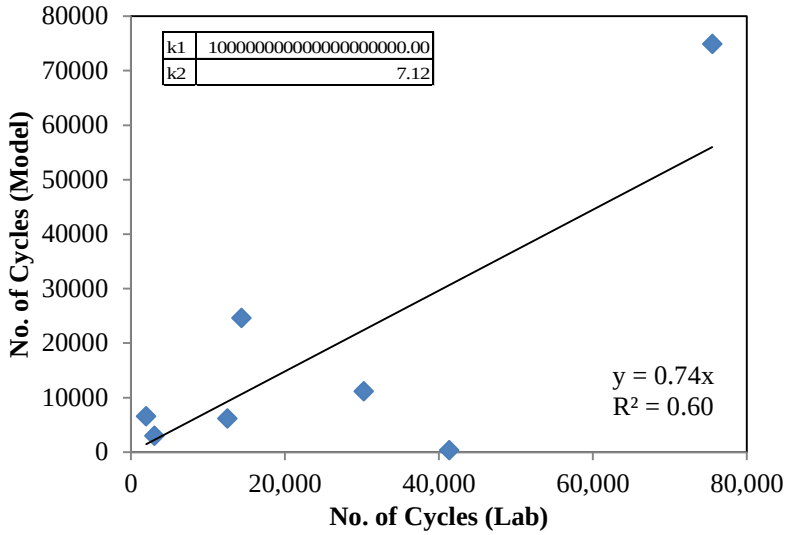

Figure D29. Validation of Silt-Cement (8%) Specimen Using Bonnaure et al. (1980) and Finn et al. (1977) models

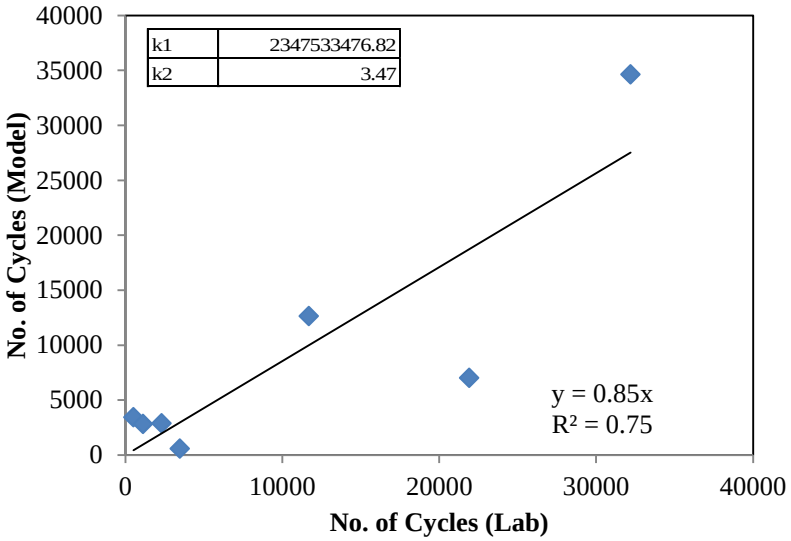

Figure D30. Validation of Silt-Lime-Fly ash (4/12%) Specimen Using Bonnaure et al. (1980) and Finn et al. (1977) models

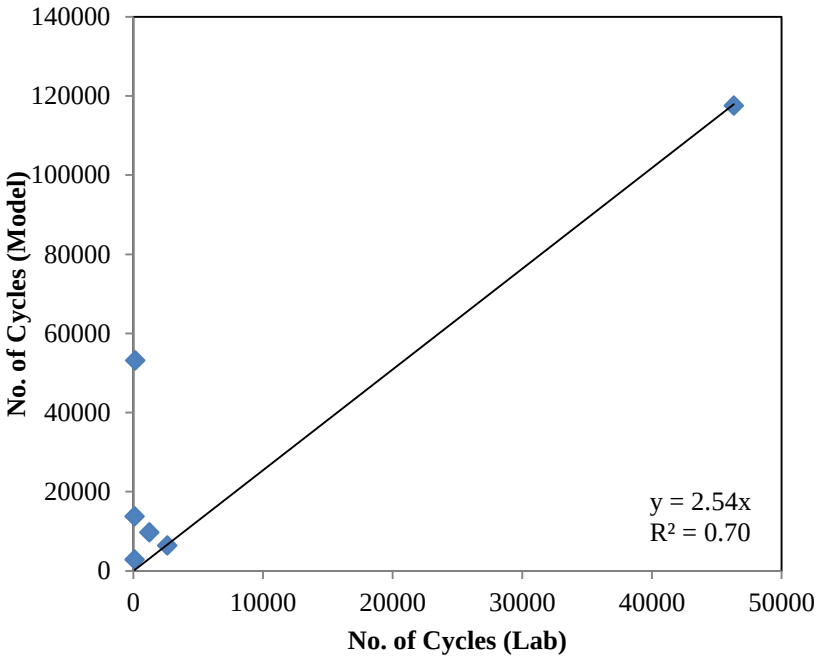

Figure D31. Validation of Gravel-Cement (3%) Specimen Using Jameson et al. (1992) model

APPENDIX – E: ULTRASONIC PULSE VELOCITY TESTING

This section shows the relationship between the flexural strength with the constrained modulus/P-wave velocity. The constrained modulus and P-wave velocity for cement-stabilized soils are presented in Table E1 to E4. The results involve all the specimens that were tested for the flexural strength involving change in density, time and binder content.

Table E1. Results of Ultrasonic Wave Velocity Tests of Sand Stabilized with Cement

Specimen	Constrained Modulus (MPa)	P-Wave Velocity (m/s)	Note
Sand-Cement (6%)	16,744	2,851	28 Days Cured
	17,224	2,880	
	17,245	2,888	
	17,729	2,929	56 Days Cured
	18,572	2,997	
	22,248	3,226	360 Days Cured
	24,176	3,362	
	23,344	3,306	
Sand-Cement (8%)	39,638	4,339	28 Days Cured
	38,342	4,330	
	38,521	4,265	

Table E2. Results of Ultrasonic Wave Velocity Tests of Silt Stabilized with Cement

Specimen	Constrained Modulus (MPa)	P-Wave Velocity (m/s)	Note
Silt-Cement (8%)	14,910	2,642	28 Days Cured
	14,809	2,683	
	14,454	2,611	
	11,550	2,398	90% MDD
	10,175	2,140	
	10,346	2,291	

Table E3. Results of Ultrasonic Wave Velocity Tests of Clay Stabilized with Cement

Specimen	Constrained Modulus (MPa)	P-Wave Velocity (m/s)	Note
Clay-Cement (12%)	10,357	2,311	28 Days Cured
	10,404	2,281	
	9,733	2,225	
	5,814	1,778	90% MDD
	4,913	1,633	
	25,455	3,540	360 Days Cured
	25,401	3,509	
	27,938	3,670	

Table E4. Results of Ultrasonic Wave Velocity Tests of Gravel Stabilized with Cement

Specimen	**Constrained Modulus (MPa)**	**P-Wave Velocity (m/s)**	**Note**
Gravel-Cement (3%)	20,729	3,017	28 Days Cured
	19,353	2,935	
	20,189	3,056	
	19,039	2,944	92% MDD
	18,648	2,935	
	39,641	4,078	360 Days Cured
	38,760	4,009	
Gravel-Cement (5%)	23,038	3,334	28 Days Cured
	24,515	3,252	
	24,515	3,252	

The constrained modulus and P-wave velocity for the class C fly ash-stabilized and lime-stabilized soils are presented in Table E5 and E6, respectively; and for the lime and class F fly ash-stabilized soils are presented in Table E7.

Table E5. Results of Ultrasonic Wave Velocity Tests on Class C Fly Ash-Stabilized Soils

Specimen	Constrained Modulus (MPa)	P-Wave Velocity (m/s)	Note
Silt-Fly ash (13%)	7,536	1,942	7 Days Cured
	6,391	1,797	
	6,453	1,802	
	1,173	796	90% MDD
	1,061	761	
	1,341	850	
Silt-Fly ash (18%)	8,246	2,000	7 Days Cured
	8,853	2,073	
	7,998	1,980	
Sand-Fly ash (13%)	9,718	2,159	7 Days Cured
	8,894	2,071	
	8,687	2,049	
Gravel-Fly ash (13%)	10,786	2,239	7 Days Cured
	8,168	1,936	
	11,540	2,261	

Table E6. Results of Ultrasonic Wave Velocity Tests of Lime-Stabilized Soils

Specimen	**Constrained Modulus (MPa)**	**P-Wave Velocity (m/s)**	**Note**
Clay-Lime (6%)	5,288	1,660	7 Days Cured
	5,006	1,667	
	5,357	1,687	
	4,806	1,640	
	675	642	84% MDD
	697	654	

Table E7. Results of Ultrasonic Wave Velocity Tests on Lime and Class F Fly Ash-Stabilized Soils

Specimen	**Constrained Modulus (MPa)**	**P-Wave Velocity (m/s)**	**Note**
Silt-Lime-Fly ash (4/12%)	9,728	2,213	7 Days Cured
	10,939	2,290	
	9,114	2,101	
	4,976	1,666	88% MDD
	2,942	1,273	
	3,060	1,311	

Figure E1 and E2 shows the relationship between the constrained modulus and flexural strength for coarse and fine-grained soils; respectively.

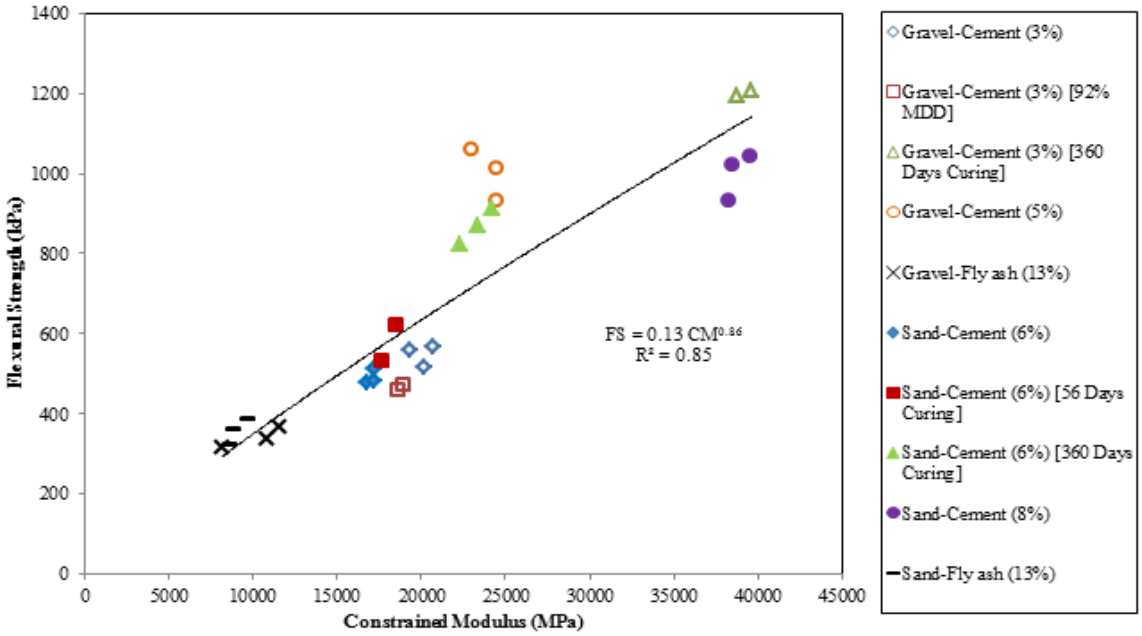

Figure E1. Relationship between the Constrained Modulus and Flexural Strength for Coarse-Grained Soils

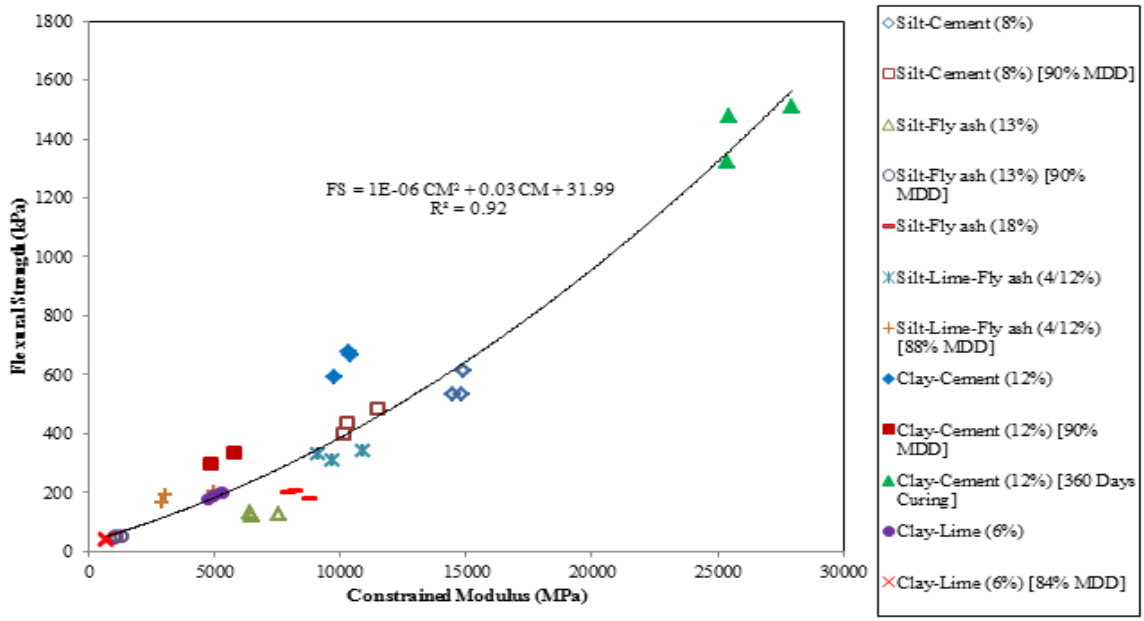

Figure E2. Relationship between the Constrained Modulus and Flexural Strength for Fine-Grained Soils

Figure E3 and E4 shows the relationship between the P-wave velocity and flexural strength for coarse and fine-grained soils; respectively.

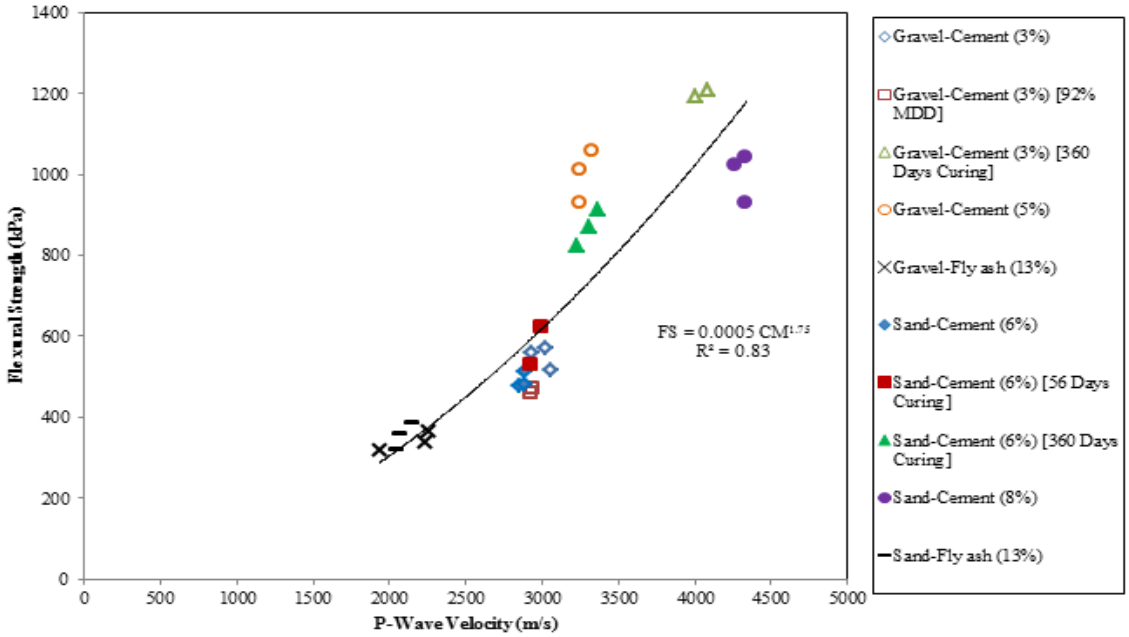

Figure E3. Relationship between the P-Wave Velocity and Flexural Strength for Coarse-Grained Soils

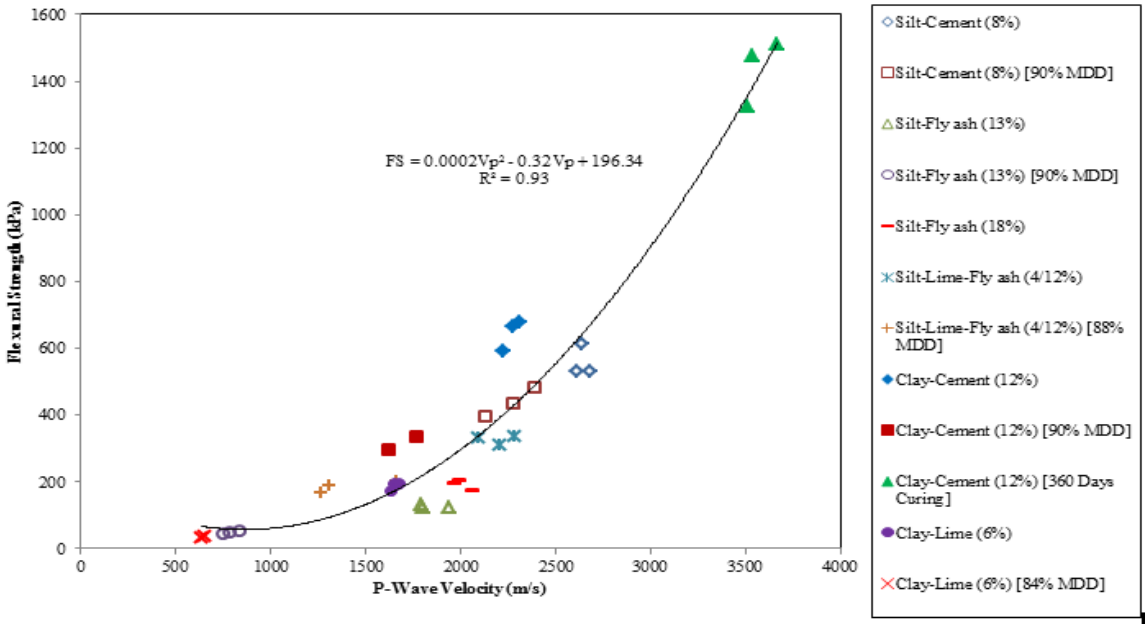

Figure E4. Relationship between the P-Wave Velocity and Flexural Strength for Fine-Grained Soils

Figure E5(a) and E5(b) shows the relationship between the constrained modulus and P-wave velocity with flexural strength, respectively for the silt stabilized with binders.

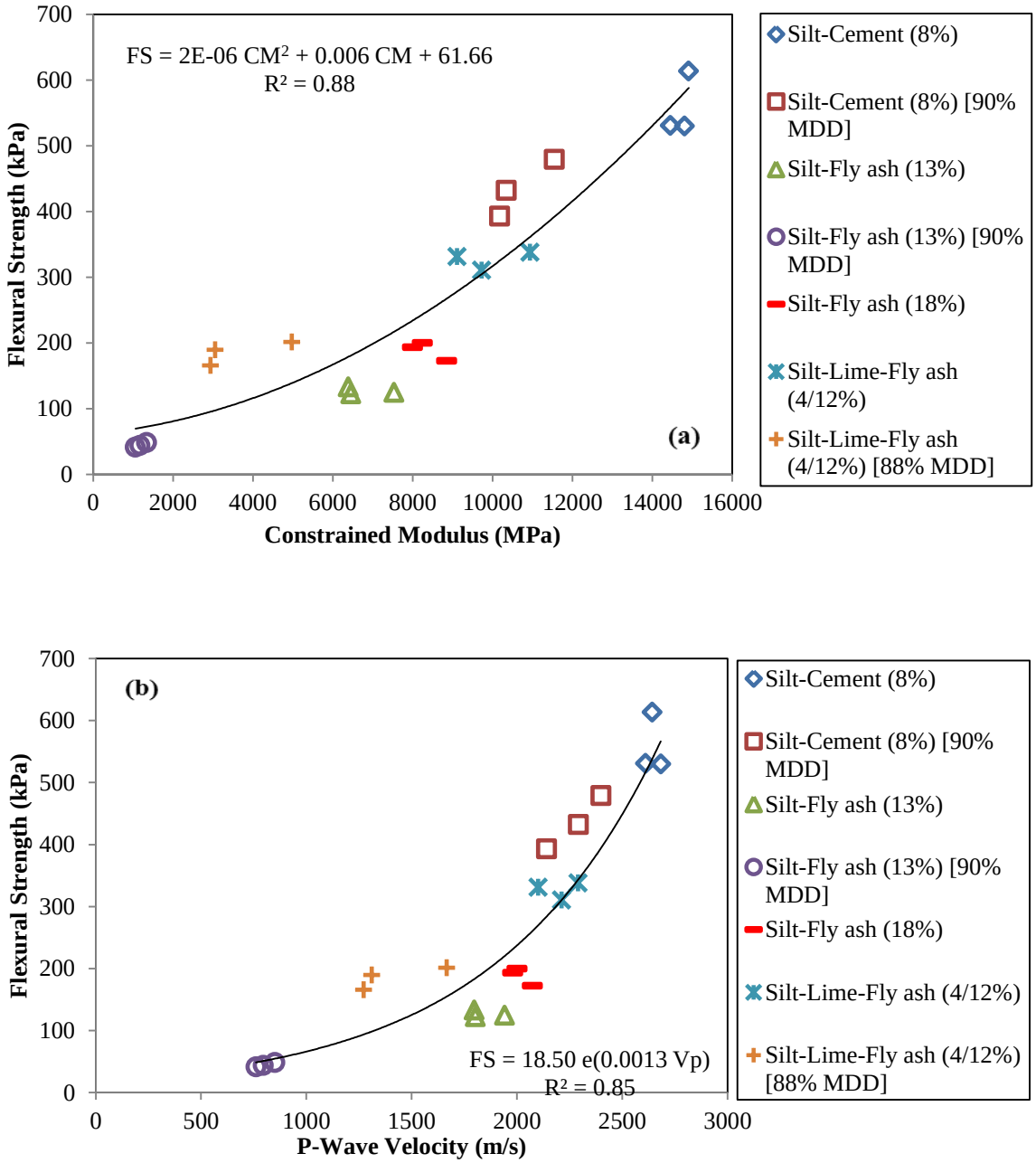

Figure E5. Relationship between the Constrained Modulus/P-Wave Velocity and Flexural Strength for Silt Stabilized with Binders

Figure E6(a) and E6(b) shows the relationship between the constrained modulus and P-wave velocity with flexural strength, respectively for the clay stabilized with binders.

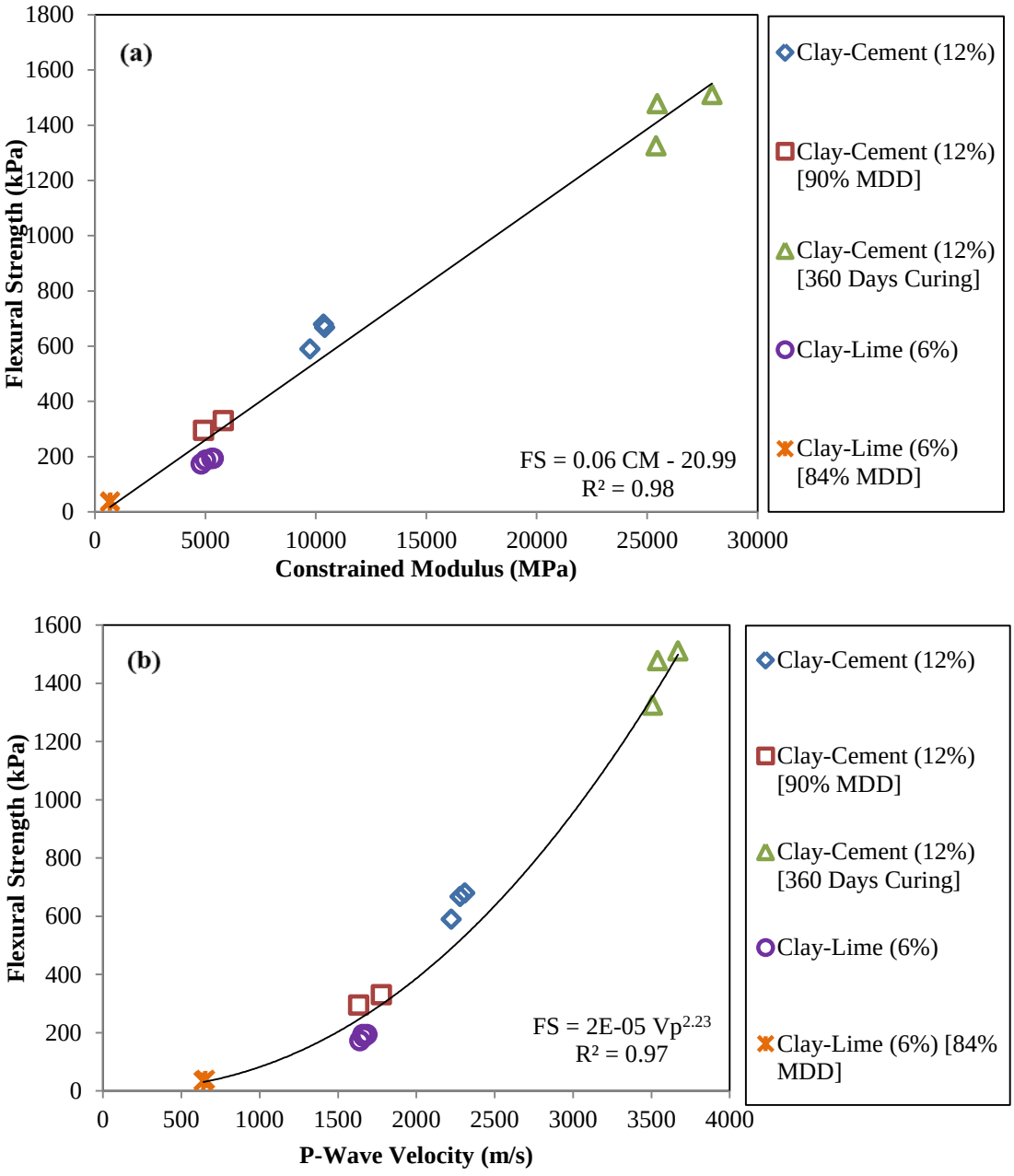

Figure E6. Relationship between the Constrained Modulus/P-Wave Velocity and Flexural Strength for Clay Stabilized with Binders

Figure E7(a) and E7(b) shows the relationship between the constrained modulus and P-wave velocity with flexural strength, respectively for the sand stabilized with binders.

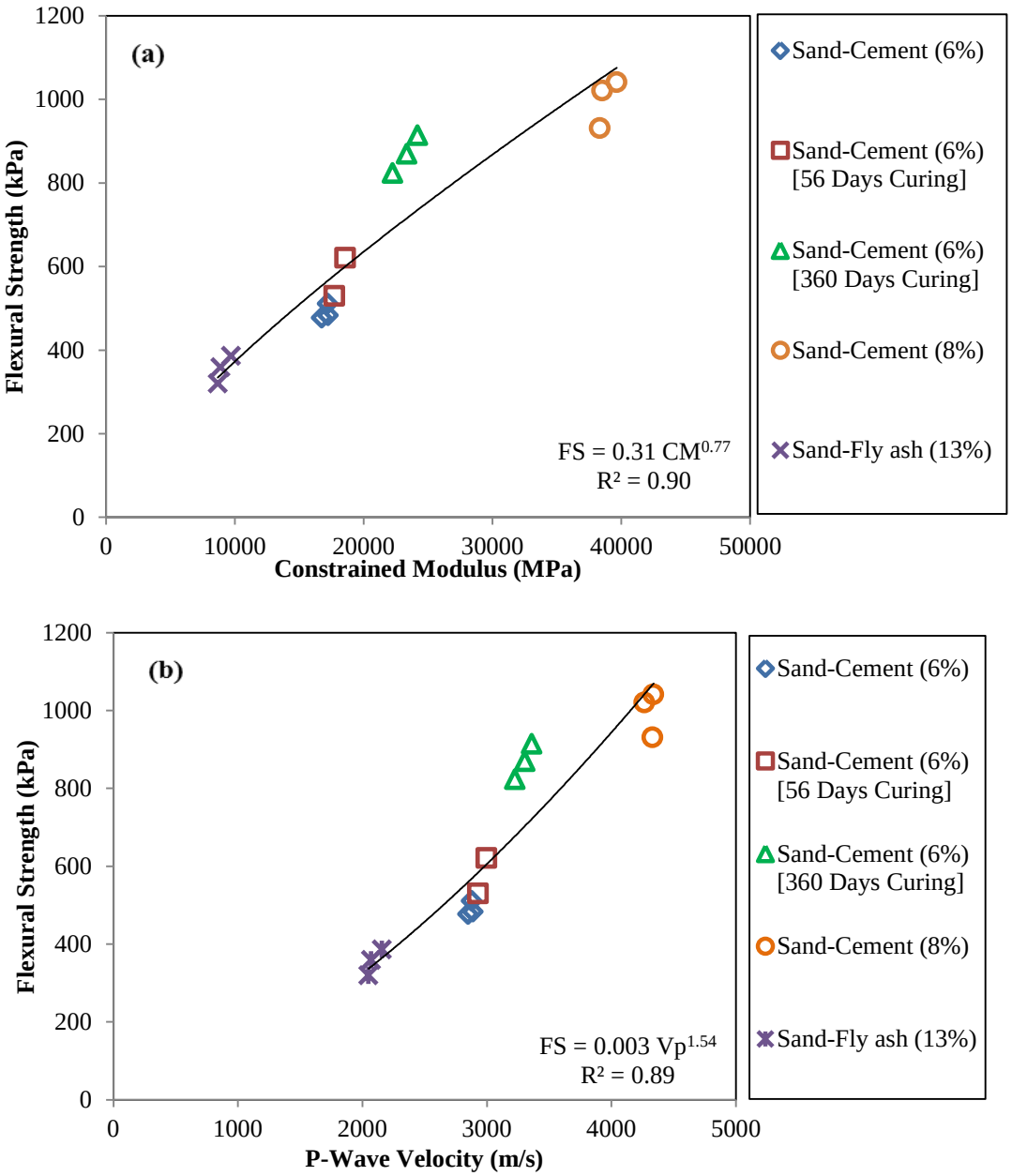

Figure E7. Relationship between the Constrained Modulus/P-Wave Velocity and Flexural Strength for Sand Stabilized with Binders

Figure E8(a) and E8(b) shows the relationship between the constrained modulus and P-wave velocity with flexural strength, respectively for the gravel stabilized with binders.

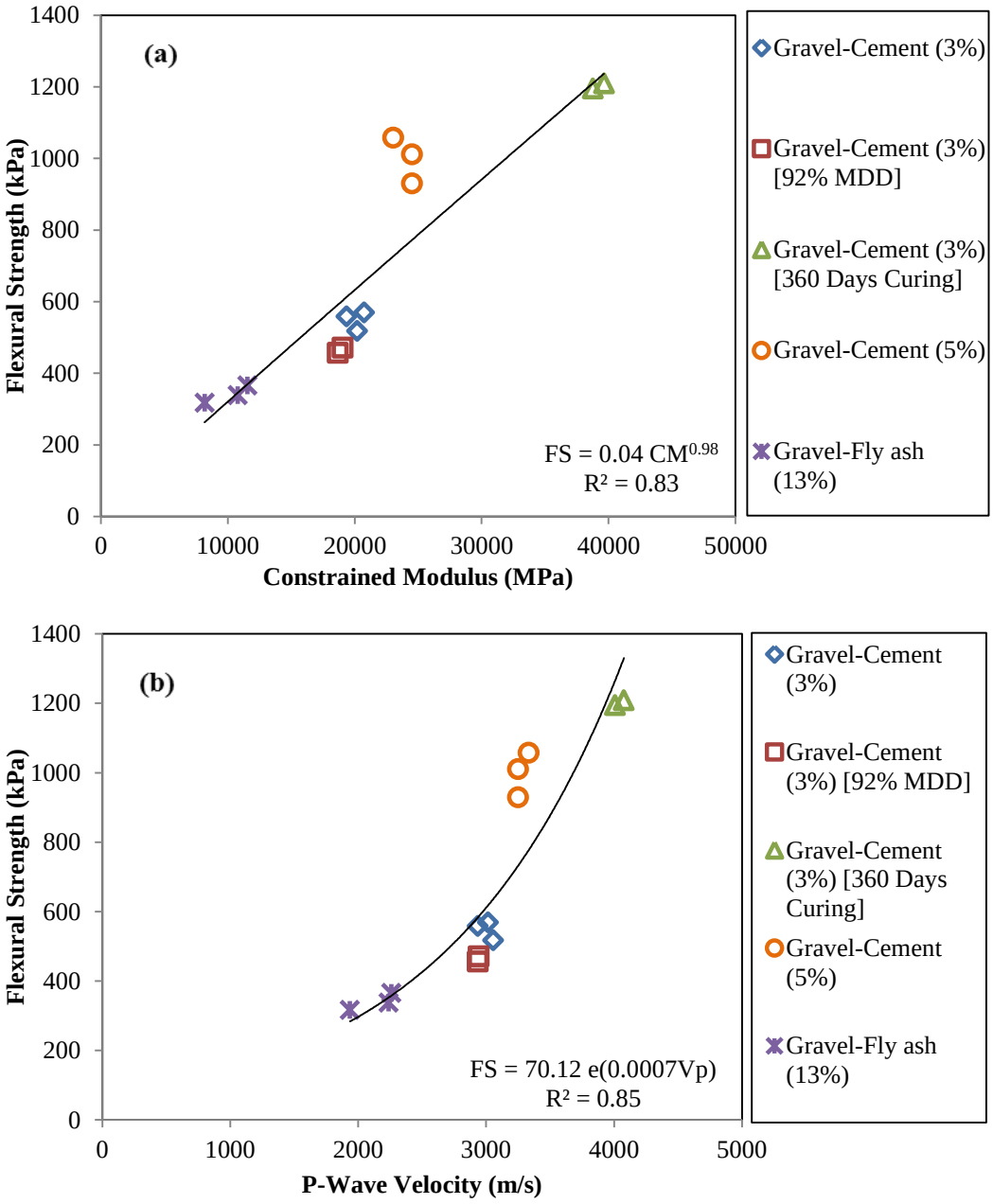

Figure E8. Relationship between the Constrained Modulus/P-Wave Velocity and Flexural Strength for Gravel Stabilized with Binders

Figure E9(a) and E9(b) shows the relationship between the constrained modulus and P-wave velocity with flexural strength, respectively for the cement-stabilized soils.

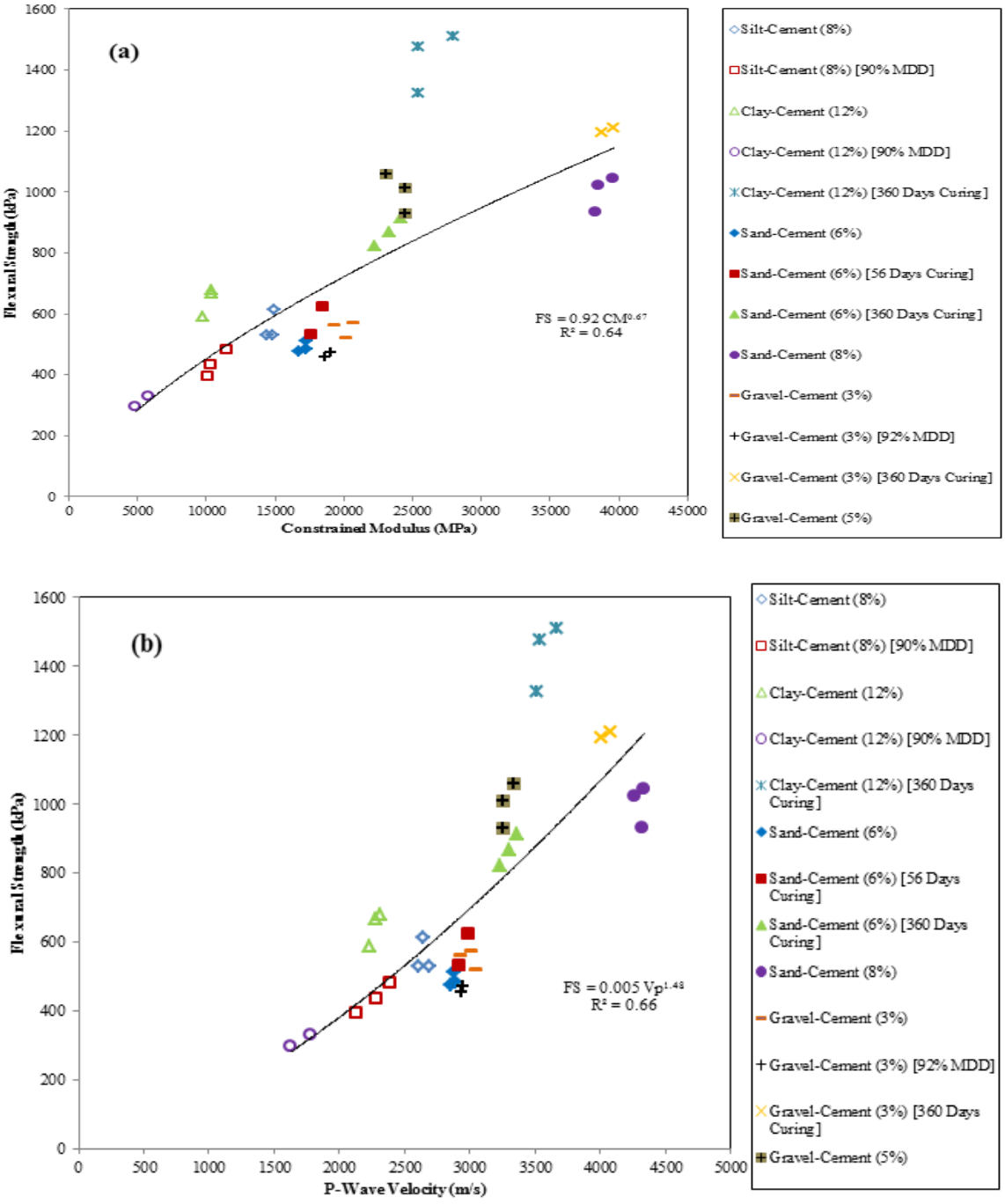

Figure E9. Relationship between the Constrained Modulus/P-Wave Velocity and Flexural Strength for Cement-Stabilized Soils

Figure E10(a) and E10(b) shows the relationship between the constrained modulus and P-wave velocity with flexural strength, respectively for the class C fly ash-stabilized soils.

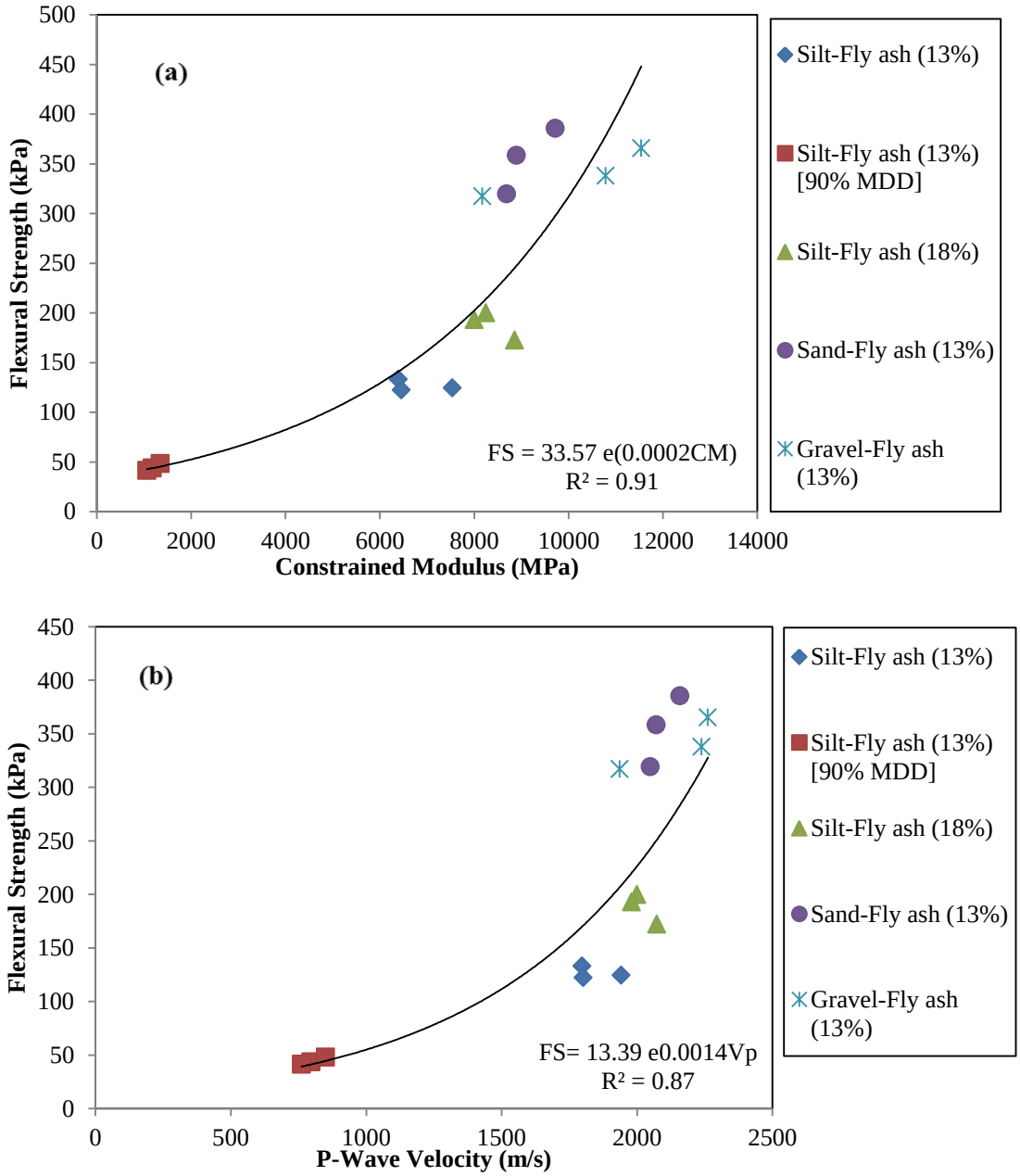

Figure E10. Relationship between the Constrained Modulus/P-Wave Velocity and Flexural Strength for Class C Fly Ash-Stabilized Soils

Figure E11(a) and E11(b) shows the relationship between the constrained modulus and P-wave velocity with flexural strength, respectively for the lime/class F fly ash-stabilized soils.

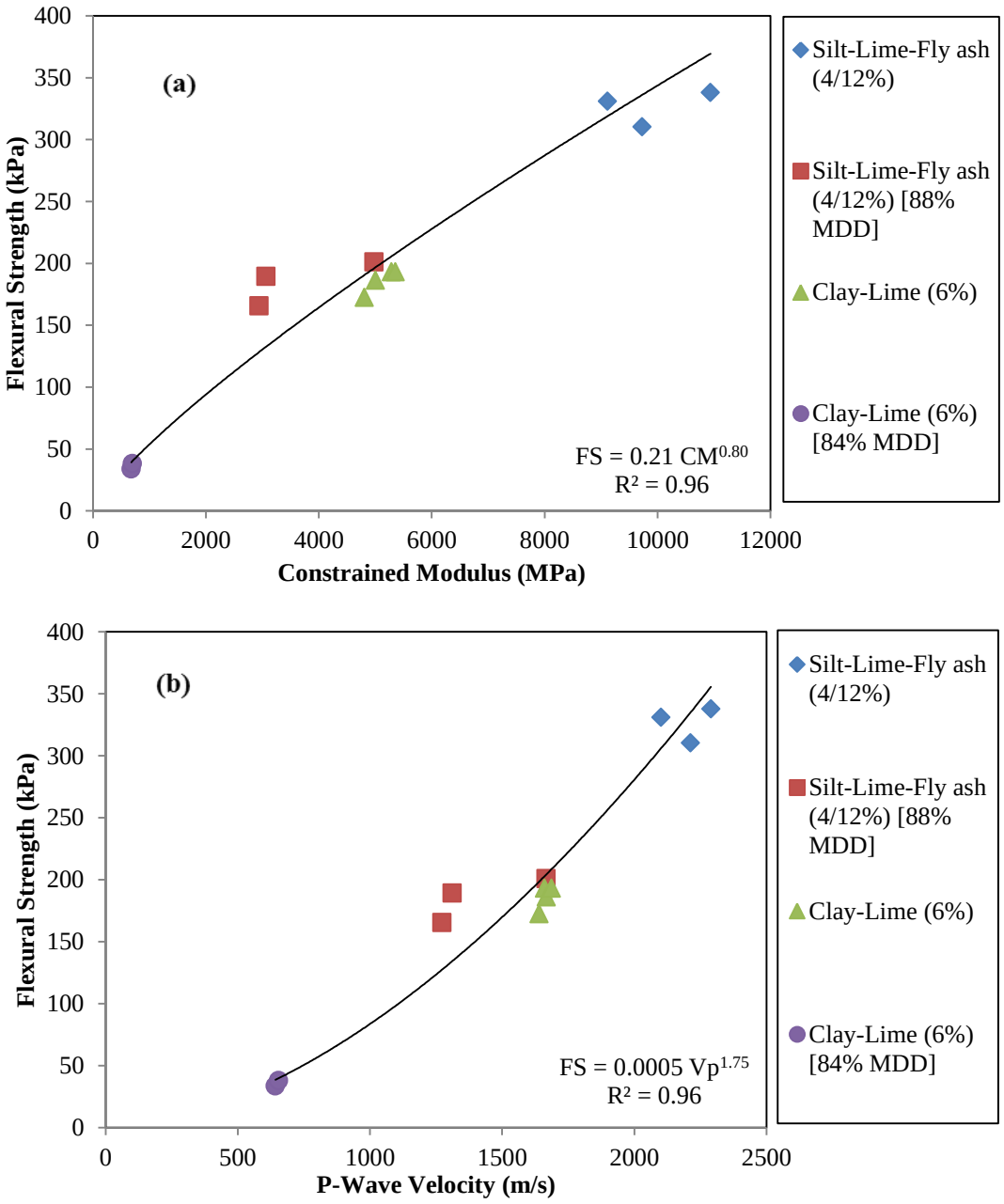

Figure E11. Relationship between the Constrained Modulus/P-Wave Velocity and Flexural Strength for Lime/Class F Fly Ash-Stabilized Soils

APPENDIX – F: MODULUS GROWTH TESTS

F.1. FLEXURAL MODULUS TESTS

This chapter presents results from the flexural and constrained moduli testing of gravel-cement, sand-cement, silt-cement and clay-cement beam specimens. Table F1 shows the flexural modulus of gravel-cement specimens for each specimen at different curing period.

Table F1. Summary of Flexural Modulus Growth over time (Gravel—Cement Specimens)

Days Cured	Flexural Modulus (MPa)				COV (%)
	Specimen # 1	Specimen # 2	Specimen # 3	Average	
28	474	726	688	630	22
56	715	814	1087	872	22
90	1127	940	1191	1086	12
120	930	1099	791	940	16
150	1017	1297	838	1050	22
180	1739	1315	1239	1431	19

Table F2 and F3 shows the flexural modulus of sand-cement and clay-cement specimens for each specimen at different curing period, respectively.

Table F2. Summary of Flexural Modulus Growth over time (Sand—Cement Specimens)

Days Cured	Flexural Modulus (MPa)				COV (%)
	Specimen # 1	Specimen # 2	Specimen # 3	Average	
28	828	735	597	720	16
56	854	888	621	787	18
90	1109	1422	1234	1255	13
120	1173	1109	814	1032	19
150	1485	1273	895	1218	25
180	1692	1571	681	1315	42

Table F3. Summary of Flexural Modulus Growth over time (Clay—Cement Specimens)

Days Cured	Flexural Modulus (MPa)				COV (%)
	Specimen # 1	Specimen # 2	Specimen # 3	Average	
28	649	583	575	602	7
56	872	734	846	817	9
90	704	761	939	802	15
120	874	946	975	931	6
150	1025	1013	910	982	6
180	879	1325	966	1056	22

Table F4 shows the flexural modulus of silt-cement specimens for each specimen at different curing period.

Table F4. Summary of Flexural Modulus Growth over time (Silt—Cement Specimens)

Days Cured	Flexural Modulus (MPa)				COV (%)
	Specimen # 1	Specimen # 2	Specimen # 3	Average	
28	743	669	794	735	9
56	826	861	1205	964	22
90	1099	891	776	922	18
120	1634	684	1201	1173	41
150	1638	951	854	1147	37

F.2. CONSTRAINED MODULUS TESTS

Figure F1 shows the constrained modulus for each specimen of silt-cement specimens at different curing period.

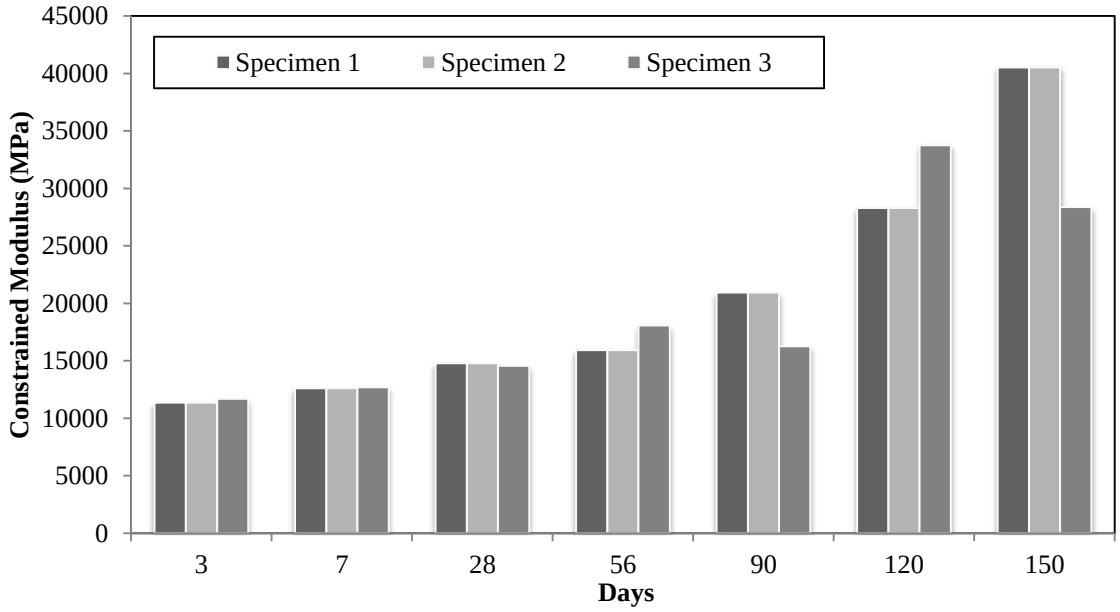

Figure F1. Summary of Constrained Modulus Growth over time (Silt-Cement Specimens)

Figure F2 and F3 shows the constrained modulus for each specimen of sand-cement and clay-cement specimens at different curing period, respectively.

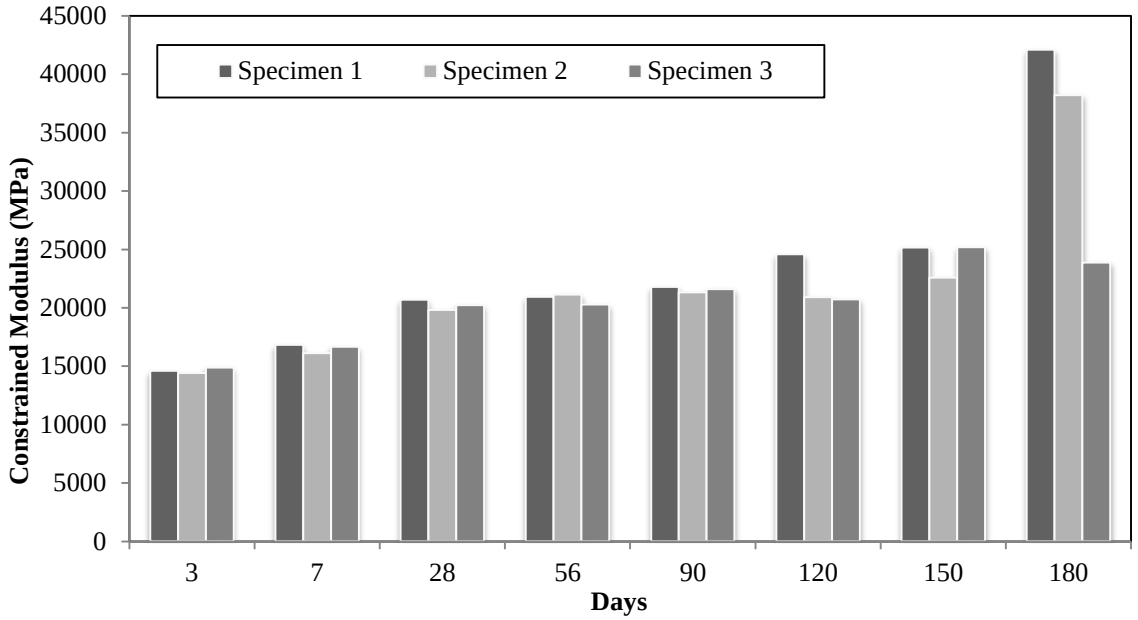

Figure F2. Summary of Constrained Modulus Growth over time (Sand-Cement Specimens)

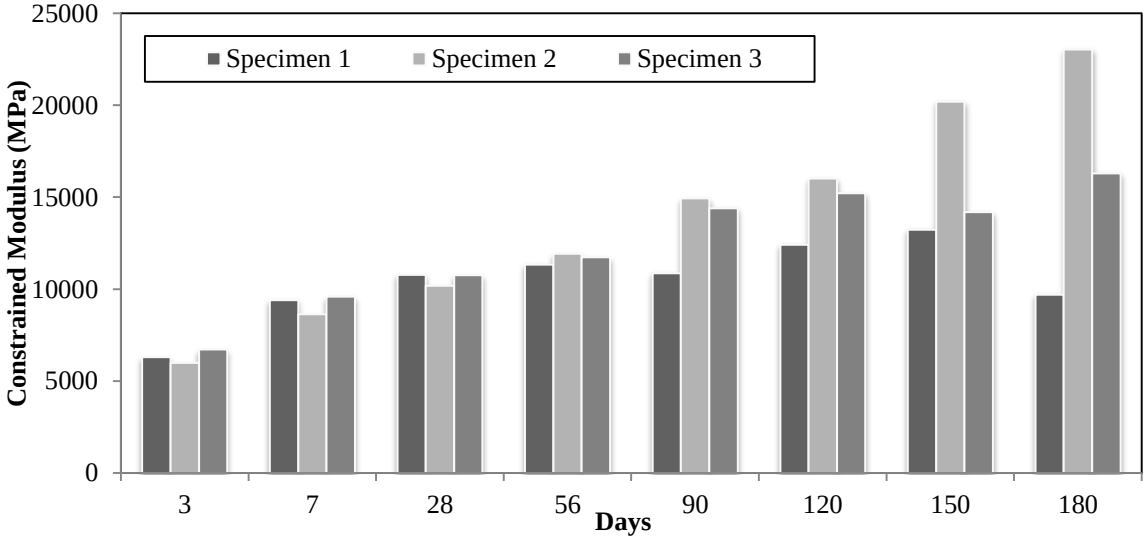

Figure F3. Summary of Constrained Modulus Growth over time (Clay-Cement Specimens)

Figure F4 and F5 shows the constrained modulus for each specimen of gravel-cement and gravel-fly ash specimens at different curing period, respectively.

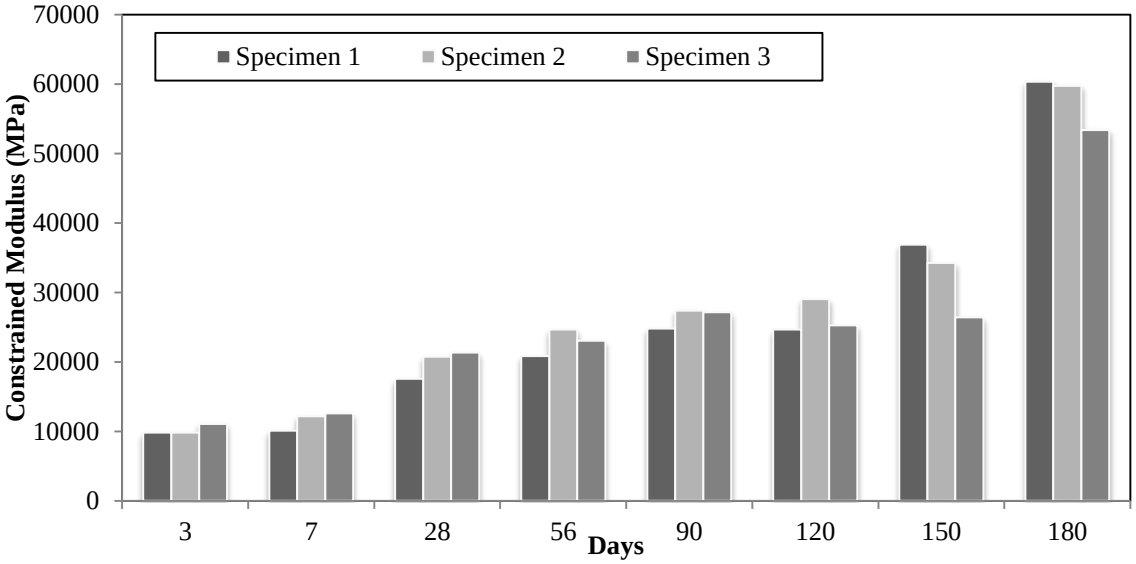

Figure F4. Summary of Constrained Modulus Growth over time (Gravel-Cement Specimens)

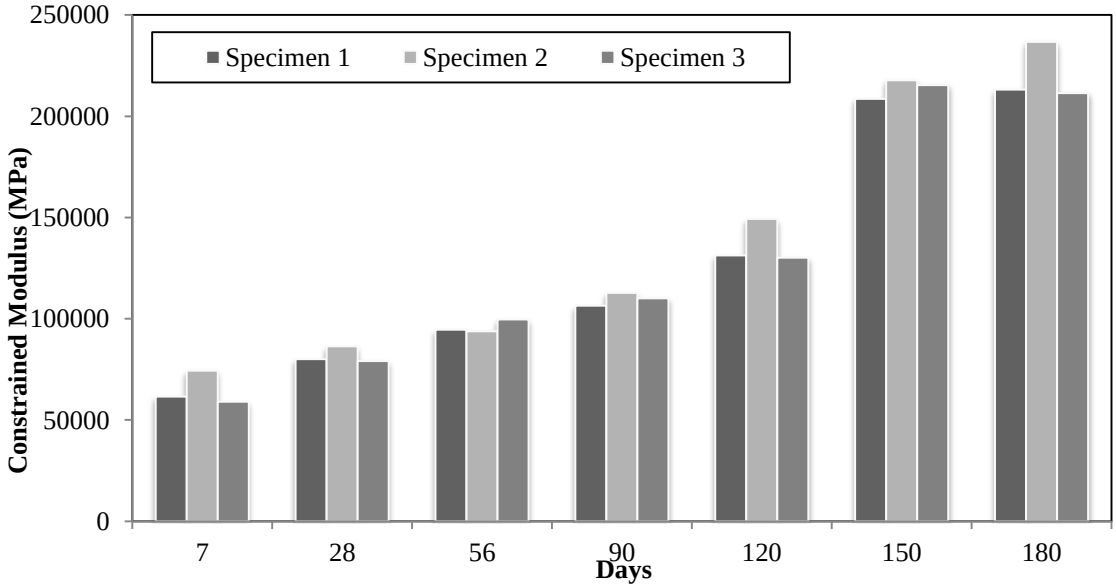

Figure F5. Summary of Constrained Modulus Growth over time (Gravel-Fly ash Specimens)

Figure F6 and F7 shows the constrained modulus for each specimen of silt-lime-fly ash (class F) and clay-lime specimens at different curing period, respectively.

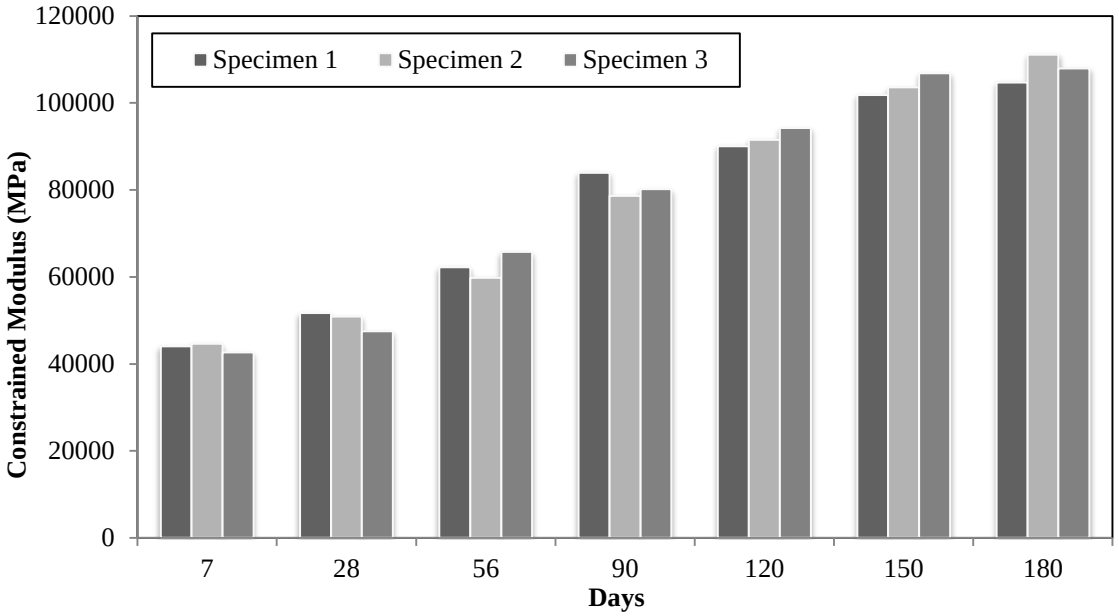

Figure F6. Summary of Constrained Modulus Growth over time (Silt-Lime-Fly ash Specimens)

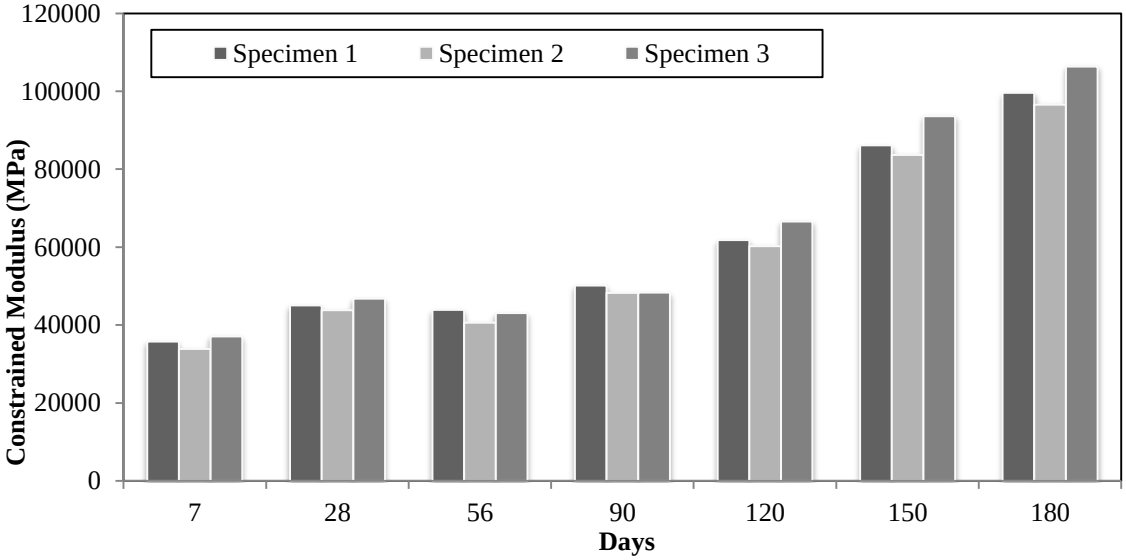

Figure F7. Summary of Constrained Modulus Growth over time (Clay-Lime Specimens)

F.3. RESILIENT MODULUS TESTS

Figure F8 and F9 shows the internal and external resilient modulus, respectively for the gravel-fly ash specimen at different curing periods.

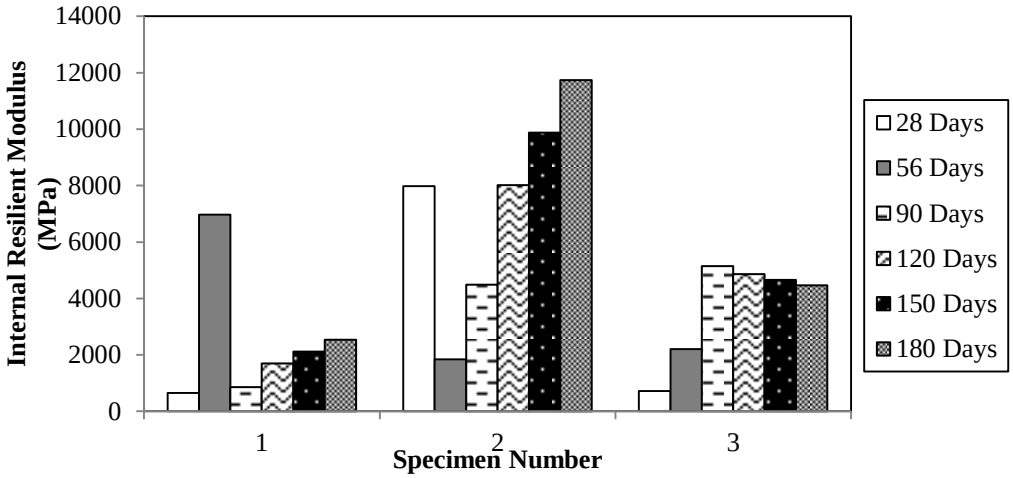

Figure F8. Summary of Internal Resilient Modulus Growth over time (Gravel-Fly ash Specimens)

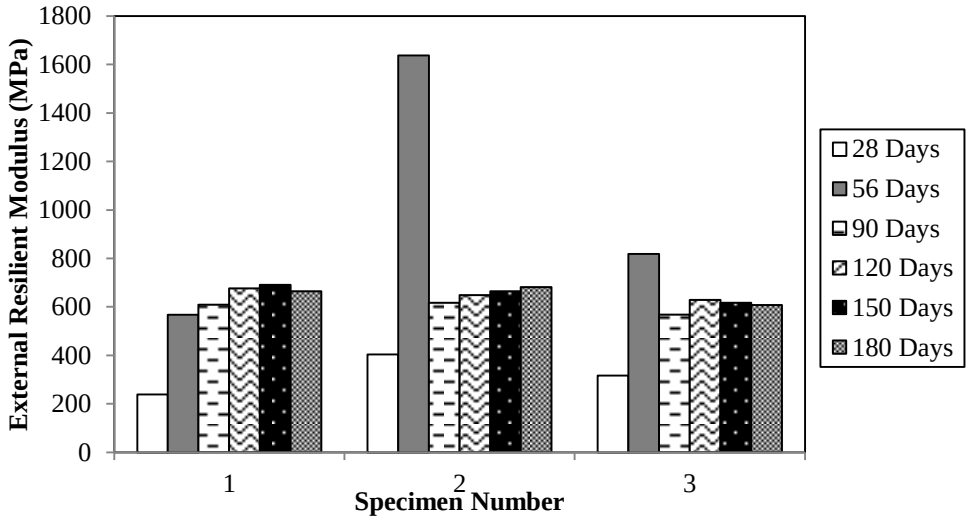

Figure F9. Summary of External Resilient Modulus Growth over time (Gravel-Fly ash Specimens)

Figure F10 and F11 shows the internal and external resilient modulus, respectively for the silt-lime-fly ash specimen at different curing periods.

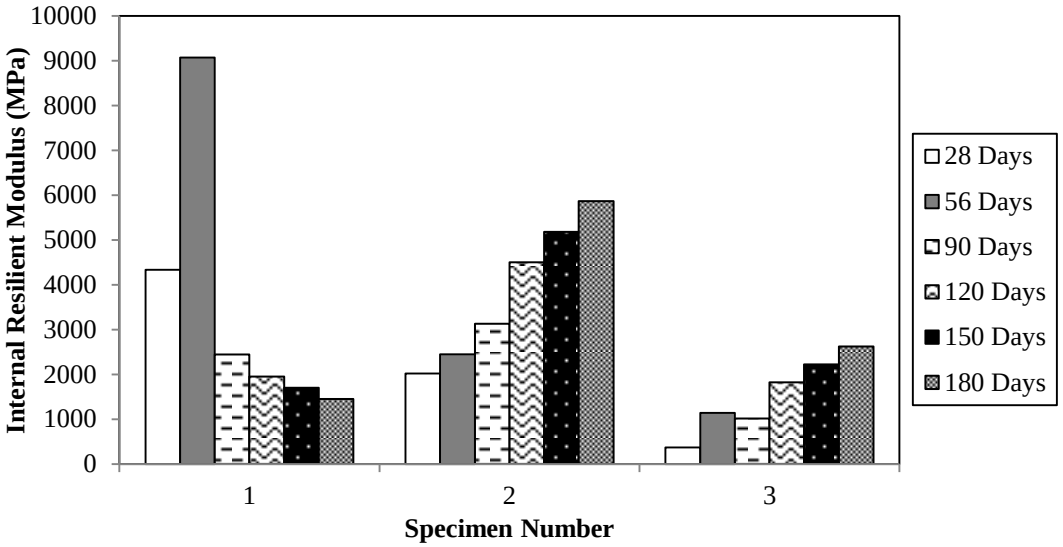

Figure F10. Summary of Internal Resilient Modulus Growth over time (Silt-Lime-Fly ash Specimens)

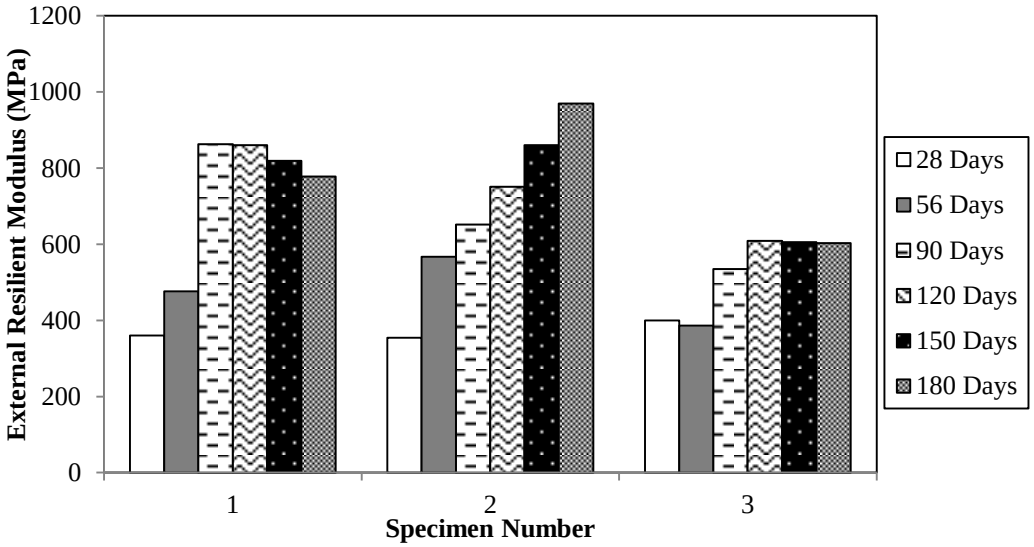

Figure F11. Summary of External Resilient Modulus Growth over time (Silt-Lime-Fly ash Specimens)

Figure F12 and F13 shows the internal and external resilient modulus, respectively for the clay-lime specimen at different curing periods.

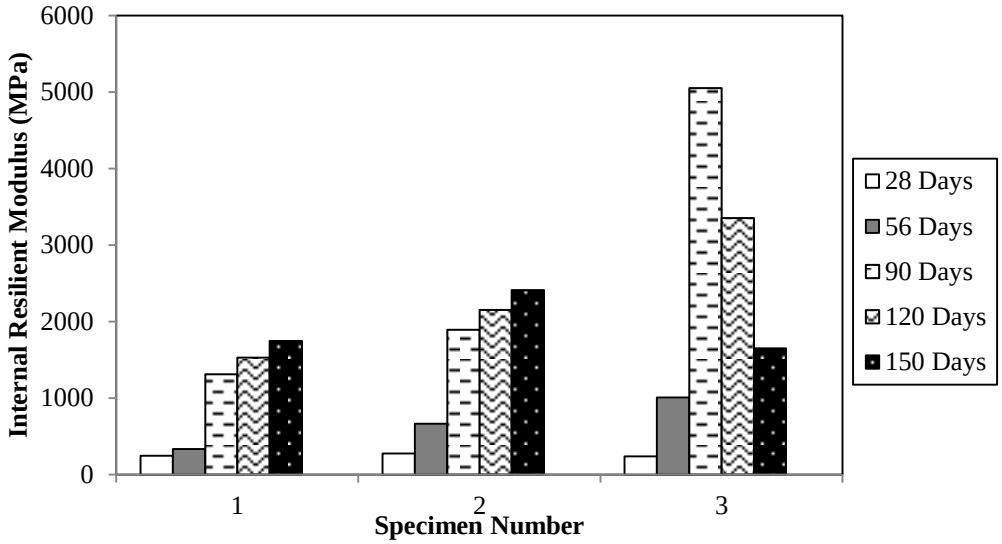

Figure F12. Summary of Internal Resilient Modulus Growth over time (Clay-Lime Specimens)

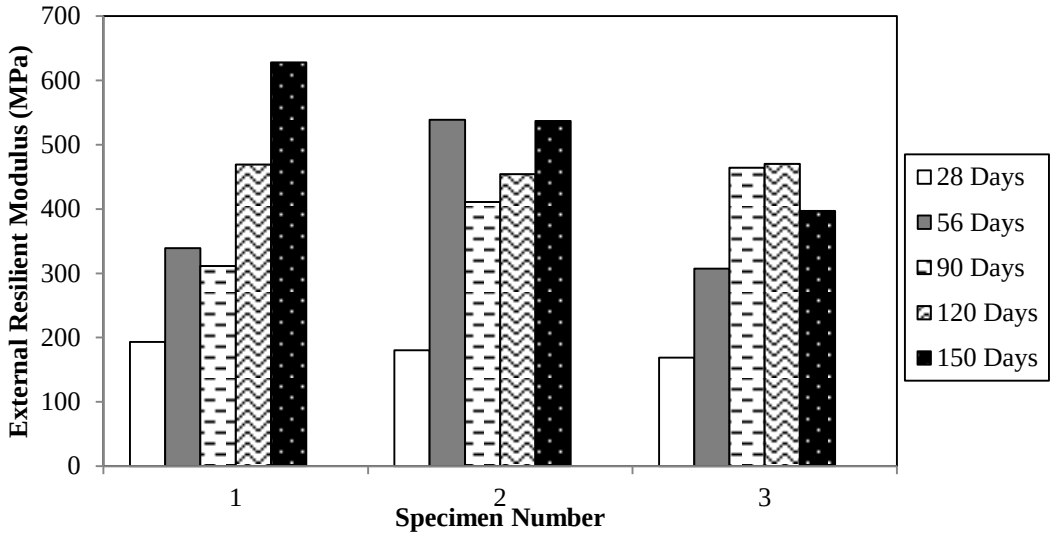

Figure F13. Summary of External Resilient Modulus Growth over time (Clay-Lime Specimens)